

TOPOLOGICAL EXCITATIONS AND SPIN DYNAMICS IN MAGNETIC SYSTEMS IN LOW DIMENSIONS

Thesis submitted for the degree of

Doctor of Philosophy (Sc.)

In **Physics (Theoretical)**

by

Subhajit Sarkar

Department of Physics

University of Calcutta

2016

To
the memory of my father

Acknowledgments

I express my heartfelt gratitude to both of my Ph. D. supervisors, Dr. Ranjan Chaudhury and Dr. Samir Kumar Paul with whom any kind of discussions, academic or non academic, was a pleasure to take part. I am indebted to CSIR, Government of INDIA, for providing financial support under grant no. **09/575(0089)/2010-EMR-I** during first five years of my tenure, and to the Director of S. N. Bose National Centre For Basic Sciences (SNBNCBS) providing me an extension for one more year.

I thank all my fellow students. They always stood by my side asking over and over again. I am especially thankful to Arindam, Victor and Tanmoy. Discussions with Arghya Da (Arghya Dutta), Aslam, Rakesh were a great pleasure. I would also like to acknowledge the helpful attitude of the non-academic staff members of SNBNCBS.

I am thankful to Dr. Saptarshi Mandal of IOP Bhubaneswar for providing me opportunity for an academic visit to IOP. Discussions with Prof. Mukunda P. Das, Prof. Prasanta Panigrahi and Dr. Manoranjan Kumar on various occasions are gratefully acknowledged.

Finally, I convey my sincere gratitude to my family members, my mother, my wife, my sister and my in-laws for their constant support. This journey would not have been possible without their immense help.

List of publications

1. “Theoretical analysis of neutron scattering results for quasi-two dimensional ferromagnets,” **Subhajit Sarkar**, Samir K. Paul, and Ranjan Chaudhury, Eur. Phys. J. B **85**, 380 (2012); arXiv:1203.3069v2 [cond-mat.str-el].
2. “The connection between vortex-like topological excitations and conventional excitations in quantum spin systems on two dimensional lattice and their stability,” **Subhajit Sarkar**, Ranjan Chaudhury, and Samir K. Paul, Int. J. Mod. Phys. B, **Vol. 29**, No. 29 (2015) 1550209 (22 pages); arXiv:1410.5921v3 [cond-mat.str-el]; Erratum, Int. J. Mod. Phys. B, Vol. 29, No. 31 (2015) 1592004 (1 page).
3. “Semi-phenomenological analysis of neutron scattering results for quasi-two dimensional quantum anti-ferromagnet,” **Subhajit Sarkar**, Ranjan Chaudhury, and Samir K. Paul, arXiv:1506.06856v3 [cond-mat.str-el] (2016), communicated.

This thesis is based on all the above mentioned papers whose reprints/preprints are attached at the end of the thesis.

TOPOLOGICAL EXCITATIONS
AND SPIN DYNAMICS
IN MAGNETIC SYSTEMS
IN LOW DIMENSIONS

Contents

Contents	5
1 Introduction	7
1.1 Brief review of quasi-two dimensional magnetic systems: theoretical and experimental results	22
1.2 Motivations	27
1.3 Outline of the Thesis	28
2 Spin Dynamics In Quasi-two Dimensional Ferromagnets: A Semi-Classical Approach	31
2.1 Introduction	31
2.2 Spin dynamics in presence of topological excitations	33
2.2.1 Convolutd In-Plane Dynamical Structure Function	37
2.2.2 Convolutd Out-of-Plane Dynamical Structure Function	38
2.2.3 Estimation of Contributions from Spin-Wave Like Modes	38
2.2.4 Bound Meron Contribution	38
2.2.5 Total Dynamical Structure Function (Spin-Spin Correlation)	39
2.3 Relevant information on K_2CuF_4	40
2.4 Calculation of dynamical structure function and comparison with experimental results	42
2.5 Summary	49
3 Spin Dynamics In Quasi-two Dimensional Anti-ferromagnets: A Semi-classical Approach	52
3.1 Introduction	52
3.2 Spin dynamics in presence of topological excitations	55

3.3	Relevant information on La_2CuO_4	57
3.4	Calculations of the integrated intensities	60
3.5	Summary	69
4	Microscopic description of quantum spin vortices and anti-vortices	72
4.1	Introduction	72
4.2	Construction of quantum spin vortex and anti-vortex	74
4.3	Connection between the vortex and magnons	79
4.4	Quantum mechanical stability of the vortex/anti-vortex state	80
4.4.1	Single charge 1 vortex	81
4.4.2	Finite density of charge 1 vortices	84
4.5	Higher charged vortices	87
4.6	Summary and Discussion	90
5	Summary and Outlook	93
	Appendices	98
A	Windsor factor	99
B	Magnons and Magnon-Magnon interaction	101
B.1	One Magnon States	101
B.2	Two magnon states	102
B.3	Higher magnon states	103
C	The Tukey and the modified Tukey function	106
D	Dependence Of The Physical Range On The Magnitude Of The Value Of Spin	108
	Bibliography	110

Chapter 1

Introduction

Investigations on the magnetic properties of low-dimensional (low-d) systems are long standing important research problems of modern condensed matter physics. The physics of magnetic systems in this restricted dimensionality is very interesting owing to the occurrence of several unusual magnetic properties observed in experiments. Such a restricted dimensionality, d is defined as an object which is infinite only in one or two spatial directions and therefore, corresponds to $d = 1$ (1d) or $d = 2$ (2d). The common intrinsic features of low-dimensionality make inherent parallelism between widely different phenomena in condensed matter physics along with characteristics shared between them. The initiative on the theoretical studies of low dimensional (both one and two dimensional) magnetism can be traced back to some eighty years or so which started with the invention of the one-dimensional classical Ising model and the Bethe ansatz formulation of the one dimensional quantum Heisenberg model [1, 2]. This was followed by the famous Onsager solution of $2d$ Ising magnets [3]. During the last four decades a considerable effort is being made on the experimental studies of such low-d magnetic systems where in almost all the cases the system being studied happens to be a quasi-low-d system [4]. In the quasi-low-d systems the Intra-chain or intra-layer coupling is typically $10^3 - 10^6$ times the inter-chain or inter-layer coupling. These are very close approximation to pure 1d or 2d systems in a certain temperature range. Magnets in these restricted dimensions have a natural realization since they exist as real bulk crystals, although with spatially anisotropic exchange interactions, leading to the magnetic coupling being much stronger in one or two spatial dimensions than the remaining ones. Such low dimensional magnetic materials often have all the advantages of bulk materials in providing sufficient intensity for experimental measurements of thermal properties, e.g. specific heat, as well as static and dynamic magnetic properties via, e.g. neutron scattering

techniques [5]. With the discovery of layered copper oxide compounds possessing a considerably high superconducting temperature, the applicability of the physics of low-d magnetic systems has achieved a new impetus [6]. The parent compound being a layered anti-ferromagnet (AFM) is an approximation to 2d AFM upto a high degree of accuracy [7, 8]. By now it is clear that the magnetic properties of these materials are also crucial for the superconductivity.

The most important contribution of the low-d magnetism to the fundamental physics is in the field of phase transitions and critical phenomena. The studies of the effects of the reduced dimensionality of the lattice, the symmetry of the Hamiltonian and quantum mechanical nature of the spins on the critical properties of magnetic systems had an immense impact on the field of solid state physics. In contrast to the three-dimensional (3d) systems, the possibility of long range ordering is significantly restricted in the low-d systems. The long range ordering of spins in the low-d systems is unstable against the spontaneous formation of low energy excitations. In this regard the Mermin-Wagner theorem states that at any non-zero temperature, a 1d or 2d isotropic spin ‘‘S’’ Heisenberg model with finite range exchange interaction cannot exhibit any long range ferromagnetic order (implying $T_c = 0$) or anti-ferromagnetic order (implying $T_N = 0$) [9, 10]. However, real materials exhibit finite ordering temperature owing to the existence of weak inter-chain (quasi-1d) or inter-layer (quasi-2d) couplings. These excitations can be both topological and non-topological in character. In particular, in the two spatial dimensions the vortex/meron type topological excitations play a crucial role in bringing out a non-conventional phase transition widely known as the Berezinskii-Kosterlitz-Thouless (BKT) transition [11]. This transition is driven by the unbinding processes of vortex-anti-vortex bound pairs at a critical temperature T_{BKT} [12, 13].

To make a brief review of the low-d magnetism in this thesis let me start with a brief overview of the physics of 1d and quasi-1d magnetic systems, especially the corresponding quantum spin systems. Then the 2-d and quasi-2d magnetic systems shall be reviewed in a way to fit into the purpose.

One dimensional spin systems: The field of one dimensional (1d) magnetism is vast and is still developing rapidly. The 1d spin systems are quite accurately realizable in quasi-1d magnetic materials. In the 1d quantum systems the quantum effects are strong and very often lead to new phases with non-trivial ground state properties. Furthermore, the presence of

frustration leads to more interesting behaviours. In this regard, quantum spin model involving both the nearest-neighbour and next-nearest-neighbour interactions, viz., the Majumdar - Ghosh model in one dimensional lattice has attracted a great deal of research interests [14]. Many of the models in 1d can be solved exactly (the so-called “exactly solvable”) by several analytical methods, e.g. Bethe Ansatz technique, spin fermion mapping and application of quantum field theoretical methods, perturbational approaches via series expansion methods, and many more [15]. Moreover, large variety of numerical approaches such as exact diagonalization (ED), density matrix renormalization group (DMRG) and Quantum Monte Carlo (QMC) calculations have contributed immensely in understanding the quantum phases and quantum phase transitions (QPT) [16]. The quantum effects have been investigated in quasi-1d materials mostly having either Cu^{2+} - ions which realize spin- $\frac{1}{2}$ or Ni^{2+} - ions which realize spin-1 [17,18]. Spin-1 chain-like material $CsNiF_3$ has served as a reference material for the demonstration of non-linear excitations [19]. The Fourier transform of the spin-spin correlation function i.e., the dynamical structure function (DSF) $S(\mathbf{q}, \omega)$ determines the cross section in a scattering experiment as well as the line-shapes corresponding to the nuclear magnetic resonance (NMR) and electron spin resonance (ESR) experiments. This DSF most efficiently serves as a bridge between the theory and the experiments. The most important model describing the interaction between the localized moments in magnetic insulators is,

$$\mathcal{H} = -J \sum_n (S_n^x S_{n+1}^x + S_n^y S_{n+1}^y + \lambda S_n^z S_{n+1}^z) - g\mu_B \sum_n \mathbf{S}_n, \quad (1.1)$$

where only the nearest neighbour interaction has been taken into account and the last term signifies the presence of external magnetic field. J is the exchange interaction; for $J > 0$ the model is ferromagnetic and for $J < 0$ anti-ferromagnetic. When $\lambda = 1$ the model represents a 1d Heisenberg model and $\lambda = 0$ corresponds to the XY model in 1d. The anisotropy is XY type for $\lambda < 1$ and is Ising type for $\lambda > 1$.

The 1d quantum spin chains are divided into two classes based on the value of spin. First one corresponds to the case of spin $S = \frac{1}{2}$ and the other one corresponds to the case of spin $S > \frac{1}{2}$. Let me first discuss spin chains with $S = \frac{1}{2}$. In this case, depending on the values of J or λ the model shows the occurrences of various phases which are characterized by very interesting properties of the ground state and the excited states.

In the Ising-anisotropic case corresponding to $\lambda > 1$ and $J > 0$ the ground state is doubly degenerate fully polarized *ferromagnetic state*. Only the application of an external magnetic field in the z-direction lifts the degeneracy. The low lying excited states are the states of one spin-deviation or collectively the magnons. The excitation spectrum is gapped (in the limit $q \rightarrow 0$) with a gap $(\lambda - 1)J$ (expressed in the unit of energy). The spectrum becomes gapless in the limit of the isotropic Heisenberg model corresponding to $\lambda = 1$. In this very limit the Mermin-Wagner theorem holds and the spin-spin correlation decays exponentially at any finite temperature. Similarly the two magnon bound states can be found in this model below the scattering continuum and these are intimately related to the concept of 2 domain walls corresponding to two broken bonds [20,21]. However, the one magnon excitation energy is not affected by the presence of the two magnon bound states.

For $J < 0$ with $\lambda > 1$ the above model is in the *anti-ferromagnetic Ising phase* and the doubly degenerate Néel state turns out to be lowest energy state. In this state although $S_{tot}^z = 0$ there exist a finite sublattice magnetization and long range order (LRO) in the corresponding correlation. Unlike the case of ferromagnet, however, in this case quantum fluctuations prevent the order from being complete since the sublattice magnetization does not commute with the above Hamiltonian. The states corresponding to the elementary excitations are described starting from the Néel state [22]. The low energy excitations are described in terms of magnons, and the domain wall picture corresponding to the state of two simultaneous spin deviations remains valid. In the anti-ferromagnetic Ising phase the elementary excitations are known to form a continuum with the relative momentum of the two domain walls serving as an internal degree of freedom [23].

On the other hand when the anisotropy is XY type i.e. corresponding to $\lambda < 1$ the model possesses a gapless excitation continuum. This model on a 1d chain can be solved by both Bethe ansatz as well as by mapping of $S = \frac{1}{2}$ spin operators into spin less fermion via nonlocal Jordan-Wigner transformation. For strictly $S = \frac{1}{2}$ systems the nonlocal Jordan-Wigner transformation makes the XXZ Hamiltonian an interacting fermion Hamiltonian in 1d. In the pure XY limit corresponding to $\lambda = 0$ the fermion chain becomes non-interacting system. In this very limit both transverse and longitudinal correlation show power law decay and the low temperature behaviour of specific heat is linear in T [24,25]. For $\lambda \neq 0$ the interacting Fermion Hamiltonian can be treated both in perturbation theory and by Bethe ansatz. Correlations functions still

show power law behaviour. The XY regime of the Heisenberg chain thus stays in a critical phase which is equivalent to the Tomonaga-Luttinger liquid. The low energy excitations are either dressed particles obtained by adding or removing a Fermion (and thereby changing S_{tot}^z by one unit), or particle-hole pair which do not change S_{tot}^z .

In the limit $\lambda = 1$ for $J < 0$ the model (1.1) becomes 1d *isotropic Heisenberg antiferromagnetic model*. The ground state energy of this model is given by, $\mathcal{E}_0 = \frac{NJ}{2} - 2JN \ln 2$ and the elementary excitations form a particle-hole continuum; $\omega(q, k) = \epsilon(q + k) - \epsilon(k)$. This excitation continuum is obtained from the dispersion relation corresponding to a more fundamental excitation and the dispersion is given by, $\epsilon(k) = \frac{\pi}{2} J |\sin k|$ ($-\pi \leq k \leq \pi$). These excitations which have topological character, are usually called spinons [26]. The low lying excitation spectrum is a combination of two spinons [27]. Spinons are spin 1/2 objects and a combination two spinons gives rise to spin 1 as well as spin 0 states. In the Heisenberg model the spinons are non-interacting only in the thermodynamic limit corresponding to $N \rightarrow \infty$ limit. Spinons get de-localized in to spin-waves throughout the lattice via exchange interaction. In a system with even number of lattice sites the total spin is always integer and the spins are always excited in pairs. However, the presence of next nearest neighbour interaction in the AFM isotropic Heisenberg model makes the physics more interesting [14]. The Hamiltonian takes the form,

$$\mathcal{H} = -J \sum_n (\mathbf{S}_n \cdot \mathbf{S}_{n+1} + \alpha \mathbf{S}_n \cdot \mathbf{S}_{n+2}), \quad (1.2)$$

where $J < 0$ and which for $\alpha > 0$ exhibits frustration because of competing interaction. For $\alpha = 1/2$ one arrives at the Majumdar-Ghosh limit where the exact form of the ground state is known to be a product of singlets (dimers) [14]. The ground state is doubly degenerate with energy $\mathcal{E}_0^{MG} = -\frac{3JN}{8}$ and the long range order (LRO) is absent in the ground state. However, perfect ordering of singlets exists as the Majumdar-Ghosh ground state forms dimer crystal. Quantitatively this is identified from the finite value of four-spin correlation function (exhibiting off diagonal LRO). For arbitrary values of α the excitation spectrum is gapless for $0 < \alpha < \alpha_c (\approx 0.2411)$ [28, 29]. At $\alpha = \alpha_c$ a phase transition occurs to a dimerized state characterized by (two fold degenerate) singlet ground state with doubled lattice constant and a gap appears. Bosonization approach on the other hand gives $\alpha_c \approx 1/6$ [28, 29]. It is worthwhile to mention that models with explicit or spontaneous dimerization are particularly relevant in the spin-Peierls chains, i.e., the spin chains which dimerize due to spin phonon interaction. Inorganic spin-Peierls material $CuGeO_3$ stimulated the research in the field of dimerized spin

chains although it is still controversial whether a spin only model can capture the physics of real spin-Peierls materials [30, 31].

Let me discuss the spin chains with $S > 1/2$. In this regard, spin chains with AFM exchange interaction becomes most interesting. The behaviour of AFM spin chain with integer and half-integer values of spin is very different from each other. This was first discovered by Haldane [32]. The ground state of integer spin - S Heisenberg AFM chain possesses a finite spectral gap which is very surprising in the sense that this gap appears in spite of the presence of rotational invariance in the Hamiltonian. The gap, given by $\Delta_{Haldane} = JS e^{-\pi S}$, is called Haldane gap and the ground state is disordered, and this phase is called the Haldane phase. The lowest order excitation turns out to be three fold degenerate. However, for half-odd-integer spins the partition function contains a non trivial phase factor $e^{-2\pi i S Q}$ where ‘Q’ is called the topological charge/Pontryagin index. The interference between different topological configurations at the end leads to the absence of gap in this case. In this regard, the Lieb-Schultz-Mattis (LSM) theorem states that a half integer spin S chain with short range exchange interaction and translationally (by lattice constant) and rotationally (rotation around z-axis) invariant Hamiltonian either has gapless excitation spectrum or has degenerate ground states corresponding to spontaneously broken translational symmetry [24]. This theorem is valid only for half-integer spin systems. In Cu-doped NENP the occurrence of Haldane phase has been confirmed via electron spin resonance (ESR) experiment [33].

Spin chains with alternating exchange interactions, frustrated spin chains with anisotropy and spin ladders consisting of two or more coupled spin chains are being investigated very actively and the field still possesses loads of unsolved issues [34]. However, in this thesis a review of frustrated one dimensional and quasi-one dimensional spin systems is out of scope. Hence in the following I shall review only 2d and quasi-2d spin systems.

Two dimensional spin systems: There is a plethora of insulating magnetic materials including organic layered compounds, layered transition metal compounds, layered perovskites, graphite intercalation compounds and many more, which serve as very good 2d spin systems in certain ranges of temperature (depending on different physical properties of the material). The insulating magnetic systems are generally described by the Heisenberg model and its variants. Although the spin- S isotropic Heisenberg model in 2d does not exhibit a long range order at any finite

temperature and therefore does not exhibit a phase transition (in the conventional sense), the XXZ and the XY models in 2d exhibit the topological phase transition widely known as BKT transition [9, 10, 12, 13]. In this thesis, I shall concentrate on 2d models with nearest neighbour interaction only. There are several models with next and/or next-to-next nearest neighbour interactions and models involving special geometric structure of the underlying lattices which supports frustrations [35]. Such models are outside my consideration here.

The Hamiltonian describing the interaction between the local spin moments in a magnetic insulator is given by,

$$\mathcal{H} = - \sum_{\mathbf{r}, \delta} (J_x S_{\mathbf{r}}^x S_{\mathbf{r}+\delta}^x + J_y S_{\mathbf{r}}^y S_{\mathbf{r}+\delta}^y + J_z S_{\mathbf{r}}^z S_{\mathbf{r}+\delta}^z) - g\mu_B \sum_{\mathbf{r}} \mathbf{S}_{\mathbf{r}}, \quad (1.3)$$

where $(\mathbf{r} + \delta)$ is the position of nearest neighbour point of \mathbf{r} on a 2d lattice. The last term, $g\mu_B \sum_{\mathbf{r}} \mathbf{S}_{\mathbf{r}}$ in the above Hamiltonian signifies the presence of an external magnetic field. Depending on the spin dimensionality ‘ n ’ and different combination of the exchange interactions, the following classification of models emerges (See Table 1.1). One of the most spectacular achieve-

Spin-dimensionality n	interactions	models
$n = 3$ and	$J_x = J_y = J_z$	Isotropic Heisenberg model
$S_x^2 + S_y^2 + S_z^2 = S(S+1)$	$J_x = J_y \gg J_z$	XY anisotropic (XXZ) model
	$J_z \gg J_x = J_y$	Ising anisotropic model
$n = 2$ and $S_x^2 + S_y^2 = S(S+1)$	$J_x = J_y$	Planar model
$n = 1$ and $S_z^2 = S(S+1)$	$J_z \neq 0$	Ising model

Table 1.1: Classification of spin models.

ments in the theoretical and experimental investigations on magnetic systems is a thorough understanding on how the spin dimensionality ‘ n ’ and the lattice dimensionality ‘ d ’ influence the critical behaviour of a many body system. Regardless of the spin dimensionality, transition temperature T_c has always non zero positive values in 3d systems. Whereas, the 1d systems always have $T_c = 0$. For example, in the 1d Ising-type ferromagnetic system the long range order (LRO) is unstable for kink type thermal excitations [36]. Kink, in this case is an excitation that separates the spin-up and spin-down regions.

The 2d magnetic systems, being on the borderline between ordering and non-ordering systems, are the most important. Onsager had showed that the 2d Ising model has an LRO in the conventional sense in the absence of magnetic field [3]. On the other hand Isotropic Heisenberg model on 2d lattices do not possess any LRO. It is the XY and the XY anisotropic Heisenberg model (XXZ model) which turn out to be most interesting because these support quasi-LRO, and the phase transition from the paramagnetic phase to quasi-LRO is the well known topological phase transition. Kosterlitz and Thouless and Berezinskii independently have investigated the low temperature phase of 2d XY model and put forward the concept of topological phase transition [11–13]. The topological order below a certain finite temperature T_{BKT} comprises of pairs of vortex and anti-vortex spin arrangements. The transition is marked by unbinding of vortex anti-vortex pairs. Subsequently the BKT theory has been extended to describe melting in solids [11]. The XXZ model has also been shown to exhibit such a topological phase transition and the topological excitations in this model are called merons [37–42]. For this model the spin dynamics induced by the merons above T_{BKT} is very special owing to the occurrence of a central peak (in constant \mathbf{q} scan) in the dynamical structure function (DSF).

It is worthwhile to mention that the mean field (MF) theory fails badly in 2d (and in general in low-d) magnetic systems whereas the 3d magnetic systems are very well described by it. The MF theory becomes exact when the dimensionality (Euclidean) d of the system becomes greater than certain critical value d_u [43] where the of d_u depends on the model under consideration. This is called the *upper critical dimension* (UCD) above which the mean field theory gives best and accurate results. To be more specific if one takes the example of the isotropic Heisenberg model, the UCD for this model is $d_u = 4$ when only the static properties are considered, whereas UCD for the same is $d_u = 6$ when the dynamic properties are concerned [44]. In 1d magnetic systems there is no transition to LRO for all the available models viz., Ising, XY and Heisenberg models, whereas in 2d XY and Heisenberg models do not possess any LRO but the 2d Ising model does. However the MF theory predicts the existence of LRO irrespective of the lattice dimensionality and the value of the transition temperature depends on the lattice dimensionality only through the number of nearest neighbours ‘ z ’ [45].

In the following I shall describe briefly and purposefully the topological phase transition in the 2d classical XY model (where the spins are constrained to lie in the plane) and the same corresponding to the 2d classical XXZ model will be described in the subsequent chapters. Here

by classical XY model it is meant that the spins in the Hamiltonian are classical vectors having magnitude S on a two dimensional lattice.

Magnets with easy plane anisotropy come into the XY universality class owing to the fact that the underlying symmetry is the O_2 symmetry [46]. The corresponding order parameter that indicates the breakdown of this symmetry, is a two dimensional vector $\langle \mathbf{S} \rangle = S(\cos\theta, \sin\theta)$ where θ is the phase angle. The Hamiltonian is given by,

$$\mathcal{H} = -J \sum_{\langle i,j \rangle} (S_i^x S_j^x + S_i^y S_j^y) = -J \sum_{\langle i,j \rangle} \cos(\theta_i - \theta_j), \quad (1.4)$$

where $\langle i, j \rangle$ denotes that the interaction is between the nearest neighbours only. It is well known from the Mermin-Wagner theorem that the long wavelength phase fluctuations destroy the phase correlation at long distances and therefore, true LRO is impossible in 2d [9, 10]. However a new type of excitations called vortices (and anti-vortices) had been found in this model [11–13]. These are localized topological excitations characterized by a so called winding number, ‘ Q ’ defined by, $\oint \nabla\theta(\mathbf{r}) \cdot d\mathbf{l} = 2\pi Q$ where the closed integral is taken along a contour surrounding the center of the excitation. The continuum limit has been considered in the above mentioned definition by supposing that all the length scales in the systems are much larger than the lattice spacing ‘ a ’. For vortex configuration ‘ Q ’ is a positive integer and for anti-vortex configuration ‘ Q ’ is a negative integer. A schematic picture of spin vortex with $Q = 1$ and anti-vortex with $Q = -1$ are shown in Figure 1.1 One important quantity corresponding to the model(1.4) is the spin-wave stiffness/helicity modulus, ρ_s . This describes how much free energy it costs to apply an in-plane twist or gradient to the spins and at $T = 0$ its value is given by, $\rho_s = zS^2J/4$, where z is the coordination number. Energy (strictly speaking the free energy) of an isolated vortex configuration is given by, $E_V = E_c + \pi Q^2 \rho_s \ln(L/a)$, where ‘ L ’ is the size of the system, ‘ a ’ stands for lattice spacing as mentioned earlier and E_c is the energy of the vortex core [11,47]. Hence, in a macroscopically large system the vortex excitation energy diverges and therefore isolated vortex configuration is not feasible. However a vortex-anti-vortex bound pair can exist for which the energy can be shown to be given by $E_{V-AV} = 2E_c + \pi Q_i Q_j \rho_s \ln(R/a)$, where Q_i and Q_j are the topological charges of vortex and anti-vortex respectively, E_c is the vortex core energy and R is the mutual separation [11, 47]. Considering a long enough path enclosing both the vortex and the anti-vortex, one finds the net topological charge to be zero and the energy of the pair does not diverge with the sample size. It is worthwhile to mention that the vortex core happens to be the region corresponding to $r \leq a$ where the continuum

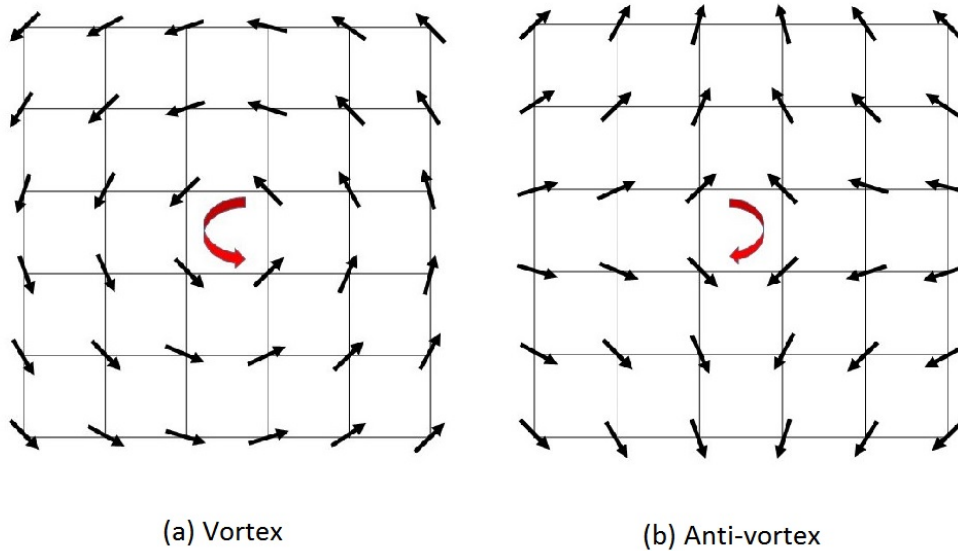


Figure 1.1: (a) $Q=1$ classical vortex, (b) $Q=-1$ classical anti-vortex.

approximation turns out to be invalid because the angle θ varies very rapidly from one lattice point to the other. The lattice spacing therefore, can be regarded as a short distance cutoff. If the two excitations have opposite topological charge only then the interaction will be attractive i.e. vortices and anti-vortices form stable pair, otherwise they repel each other.

The long distance behaviour of the spin-spin correlation function for the 2d XY model is given by $\langle \mathbf{S}(\mathbf{r}) \cdot \mathbf{S}(\mathbf{0}) \rangle \approx (\frac{r}{L})^{-\eta}$ where $\eta = T/2\pi J$. This shows that the correlation function decays algebraically with the distance and the corresponding exponent η varies continuously with temperature. The free energy corresponding to the presence of a single vortex is, $F \approx (\pi\rho_s Q^2 - 2K_B T) \ln(L/a)$ where the entropy of the configuration is approximately $2k_B \ln(L/a)$. The free energy changes sign at a temperature $k_B T_{BKT} = (\pi/2)\rho_s Q^2$ and precisely at this temperature the vortex-anti-vortex bound pair starts dissociating. It is the logarithmic interaction between the topological excitations combined with the entropy in 2d which allows the subtleties of the vortex-anti-vortex unbinding transition at T_{BKT} . The most remarkable thing happens to be the universal value of the renormalized (due to the thermal excitations) spin-wave stiffness, ρ_s^R below T_{BKT} suddenly turns out to be zero just above T_{BKT} . More precisely, $\rho_s^R(T_{BKT}^-)/T_{BKT} = 2/\pi$ just below T_{BKT} and $\rho_s^R(T_{BKT}^+) = 0$ just above T_{BKT} and this is referred to as universal jump. For T above T_{BKT} a truly disordered phase with effectively non-interacting vortex-anti-

vortex gas develops and the spin - spin correlation function decays exponentially with the spatial separation which is in contrast to the power law dependence in the regime $T < T_{BKT}$ [see Figure 1.2].

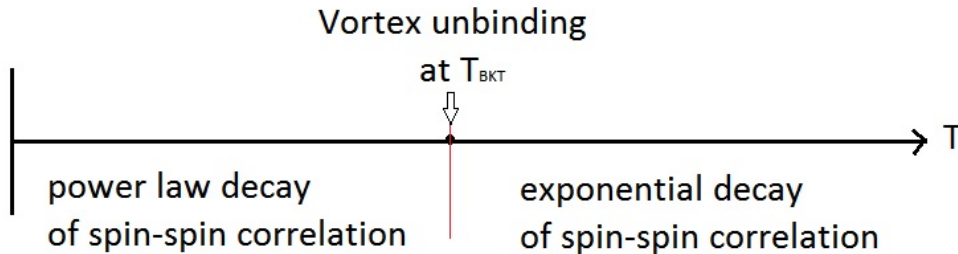


Figure 1.2: *Schematic of BKT transition.*

From the renormalization group analysis, it can be shown that the correlation length becomes exponentially divergent near T_{BKT} and it is given by, $\xi \approx ae^{b/\sqrt{\tau}}$, where $\tau = \frac{T-T_{BKT}}{T_{BKT}}$ [47, 48]. The value of b is typically around 1.5. The correlation length further sets the length scale for the density of unbound vortices. The vortices are actually correlated within an area $\sim (2\xi)^2$ and therefore the density of free vortices becomes $n_v \sim (2\xi)^{-2}$. Since the free energy density in the high temperature phase above T_{BKT} is of the order of ξ^{-2} , the specific heat c_v obtained from this free energy possesses a very weak essential singularity which is practically unobservable in the experiment. However, there exists an anomalous jump in c_v near T_{BKT} because of the entropy liberated due to the unbinding of vortex-anti-vortex pairs [47, 48].

Three dimensional magnetism: Our knowledge of the three dimensional models of magnetic insulators are mainly based on certain approximate methods. One such method is the high temperature series expansion. On the other hand, the low temperature behaviour of the magnetic systems are generally described by considering possible low energy excitations [21]. These are spin waves, quantized as magnons and are constructed from the exact ground state for simple ferromagnetic materials or the classical lowest energy state (Neel state) for anti-ferromagnetic materials. The thermodynamic properties are calculated by considering a perfect fluid of magnons (linear spin waves). Magnon-magnon interactions are described in the low density (of magnons)

limit by an approximate Boson Hamiltonian containing quartic terms [21]. This Hamiltonian is obtained via the Holstein-Primakoff transformation. A reasonably detailed discussion on the magnons and multi-magnon states (occur due to magnon-magnon interactions) is given in the Appendix B.

Neutron scattering theory: Neutron scattering is the most powerful and versatile experimental tool for studying the microscopic properties of magnetic materials. The critical properties of magnetic systems are fantastically probed by neutrons. In the critical phenomena, the behaviour of pair correlation function of the order parameter in space and time is of considerable interest and therefore experimental studies (via scattering experiments) of the same can be performed if the probe couples with order parameter itself. Furthermore, the wave length associated with the probing particle must be of the same order as the correlation length (in case of spatial correlation) and the frequency of the corresponding wave (actually the de' Broglie wave associated with the probing particle) must be of the same order as the inverse correlation time (in the case of temporal correlation). All these conditions are well satisfied by neutrons [49, 50].

Elastic and inelastic neutron scattering experiments provide us with an extraordinarily detailed access to spin structures, magnetic-excitation spectra, soft-modes and critical dynamics at magnetic phase transitions, because neutrons interact with the local electronic/atomic magnetic moments present inside a solid state material. In the magnetic neutron scattering the spin-spin correlation function is measured and this can clearly distinguish between the phases of different symmetry. Given a sufficient instrumental resolution (to be discussed in due course), there exists no ambiguity in determining any ordered or disordered phase in a magnetic system because signatures of these phases in the neutron scattering experiments are radically different. In the neutron scattering, one measures neutron count, which is proportional to the differential scattering cross section. Furthermore, in any scattering experiment one always measures the properties of the incident (i) and final (f) neutron beams and infers the momentum and energy transferred to/from the sample. Here thermal neutrons are generally used because they have energies similar to those of many excitation processes of interest in solids. In the following, let me briefly describe the theoretical aspects of the neutron scattering technique.

A diffraction or a scattering experiment is governed by the laws of momentum and energy conservation, viz., $\mathbf{Q} = \mathbf{k}_i - \mathbf{k}_f$ and $\omega = E_i - E_f$ respectively. In the elastic scattering experiment,

the initial and the final momentum remain unchanged i.e., $|\mathbf{k}_i| = |\mathbf{k}_f| = \frac{2\pi}{\lambda}$ where λ is the wavelength of the wave associated with the neutron beam. In this case it turns out that $|\mathbf{Q}| = 2|\mathbf{k}_i|\sin\theta_s$ where the angle $2\theta_s$ is the angle between the incident and the final beam. When the $|\mathbf{Q}| = |\mathbf{G}|$ where \mathbf{G} is the reciprocal lattice vector, the well known Bragg condition is satisfied. The magnitude of $|\mathbf{Q}|$ can be controlled by adjusting the angle $2\theta_s$. Thus the elastic scattering experiment does figure out the magnetic lattice structure of the sample [50].

A more complicated situation occurs in the inelastic neutron scattering (INS) experiments. In this case the initial and final momentum do not remain same i.e., $|\mathbf{k}_i| \neq |\mathbf{k}_f|$ and both energy and momentum transfer occur to/from the sample. For a single-crystal sample, energies become dependent only on the relative momentum \mathbf{q} measured with respect to a reciprocal lattice vector and therefore, the momentum transfer \mathbf{Q} is expressed as, $\mathbf{Q} = \mathbf{G} + \mathbf{q}$. In the INS experiment a constant \mathbf{q} measurement is performed by varying \mathbf{k}_f as well as the scattering angle and the relative orientation of the crystal with respect to \mathbf{k}_i . When $\mathbf{k}_i > \mathbf{k}_f$ energy is transferred from the sample to the neutron and in the opposite case energy is transferred to the sample [50]. The quasi-elastic neutron scattering is generally looked upon as a limiting case of INS where the energy transfer is very small compared to the incident or final energy. Quasi-elastic scattering is characterized by energy transfer peaks centred at zero energy (with finite widths) whereas in the Inelastic scattering peaks can occur at any energy be it finite or zero.

The rate at which the neutrons are scattered by a sample is given by the product $\phi(k_i)\sigma$, where $\phi(k_i)$ and σ are the incident neutron flux and the scattering cross section respectively. In a typical neutron scattering experiment it is more important to figure out the rate at which neutrons are scattered into a given solid angle $d\Omega_f$, in the direction of the wave vector \mathbf{k}_f , with a final energy between ω_f and $(\omega_f + d\omega_f)$. For a fixed initial neutron beam with a fixed incident flux $\phi(k_i)$ this rate is proportional to the double-differential cross section, $\frac{d^2\sigma}{d\Omega_f d\omega_f}$. In general, the double differential scattering cross section (or scattering cross section in short) is a sum of coherent and incoherent part, i.e., $\frac{d^2\sigma}{d\Omega_f d\omega_f} = \frac{d^2\sigma}{d\Omega_f d\omega_f}|_{coh} + \frac{d^2\sigma}{d\Omega_f d\omega_f}|_{inc}$, where the coherent part provides information about the cooperative effects among different atoms, such as elastic Bragg scattering or inelastic scattering by phonons or magnons in the long range ordered phase. The incoherent part on the other hand, is proportional to the time correlation of an atom with itself and provides information about the motion of individual particles. This part provides the full contribution to the cross-section in the paramagnetic or short range ordered phase. Since

neutrons act as weak perturbation and therefore, do not modify the states within the systems, the scattering cross-section can be obtained from the Fermi's Golden rule and it can be shown to be,

$$\frac{d^2\sigma}{d\Omega_f d\omega_f} = N \left(\frac{k_f}{k_i}\right) \bar{b}^2 S(\mathbf{q}, \omega) \quad (1.5)$$

where $S(\mathbf{q}, \omega)$ is the dynamical structure function and \bar{b} is the scattering length [50].

In magnetic systems, to understand the static and dynamic properties of elementary excitations one filters out the incoherent part of the inelastic scattering data. Then the remaining coherent differential scattering cross-section just delivers us with the dynamical structure function (DSF) corresponding to the order parameter correlation function in general and spin-spin correlation function in particular in spin systems. The neutrons with magnetic dipole moment $-\gamma\mu_N\sigma$, where $\gamma = 1.913$ is the gyromagnetic ratio, μ_N is the nuclear magneton, and σ is the spin operator for neutron, interact with the net magnetic moment of the atoms inside the sample via magnetic dipole interaction. The expression for the differential scattering cross-section corresponding to a magnetic system is given by,

$$\frac{d^2\sigma}{d\Omega_f d\omega_f} = N \left(\frac{k_f}{k_i}\right) e^{-2W(\mathbf{q})} p^2 \sum_{\alpha, \beta} (\delta_{\alpha, \beta} - q_\alpha q_\beta / q^2) S^{\alpha\beta}(\mathbf{q}, \omega). \quad (1.6)$$

The quantity $S^{\alpha\beta}(\mathbf{q}, \omega)$, the dynamical structure function (DSF), contains all the information on the static and dynamic properties of a spin system. The expression for the dynamical structure function is given by,

$$S(\mathbf{q}, \omega) = \frac{1}{(2\pi)^2} \int dt \sum_m e^{i(\mathbf{q}\cdot\mathbf{r}_m - \omega t)} \langle S_0^\alpha(0) S_m^\beta(t) \rangle \quad (1.7)$$

where $\langle \dots \rangle$ represents the configuration (thermal) average. In the expression (1.6) p represents the scattering amplitude and is given by $\frac{\gamma r_0}{2} g f(\mathbf{q})$, where $\gamma r_0 = 1.348$ fm is the strength of the dipolar neutron-electron interaction, g is the Lande g factor. The quantity $f(\mathbf{q})$ is the magnetic form factor, which originates from the overlap of neutron wave function with the wave function of unpaired electrons in the real space, and e^{-2W} is the Debye-Waller factor. In a theoretical study one has to calculate the expression (1.7) to compare it with the experimental data for INS which quote the differential scattering cross-section [21, 50].

The neutron scattering method is distinct from the other scattering methods owing to the fact that the neutron beam has a finite angular divergence. The main advantage of this fact

is that one can work with a much larger numbers of neutrons and thus is able to probe bulk properties of the sample. However, the disadvantage one faces with this finite beam divergence is that the energy and the momentum of neutrons do not remain well defined. A finite resolution width always exists. Then one needs to incorporate the distribution profile of neutrons in the experiment. Therefore, one has to look upon the experimental data as the convolution of the instrumental resolution function and the scattering function/ the DSF. The following equation is needed to be used,

$$S_{conv}(\mathbf{q}, \omega) = \int d\mathbf{q}' \int d\omega' R(\mathbf{q} - \mathbf{q}', \omega - \omega') S(\mathbf{q}', \omega'), \quad (1.8)$$

where $R(\mathbf{q} - \mathbf{q}', \omega - \omega')$ is the instrumental resolution function. The shape of the resolution function depends on the spectrometer configuration. During the constant \mathbf{q} scans, the shape of the resolution function varies with the energy transfer, ω . However, the momentum and the energy resolution remain coupled in the expression for the form of the function R , but this is an unwanted characteristic in the hope to tune both resolutions independently. This is best achieved by sacrificing the \mathbf{q} -resolution in favour of luminosity. The so-called monochromatic direct space focussing is the most used and effective way to achieve this [51]. Once achieved the above formula reduces to the following,

$$S_{conv}(\mathbf{q}, \omega) = \int d\omega' R(\omega - \omega') S(\mathbf{q}, \omega'). \quad (1.9)$$

Therefore, the DSFs obtained from a theoretical calculation should also be convoluted with a proper resolution function using the above expression. In this case, it is customary to choose a suitable spectral window function to mimic the instrumental resolution function. Fortunately enough, there are several spectral window functions available in the literature on spectral analysis [52, 53].

Furthermore, the DSF always obeys the principle of detailed balance. Detailed balance principle is responsible for maintaining a macroscopic steady state in a quantum mechanical system in thermal equilibrium. The principle of detailed balance is formulated for kinetic systems which can be decomposed into systems evolving through elementary processes such as collisions, elementary reactions. It states that in thermal equilibrium, each elementary process should be totally compensated by its reverse process i.e. the total rate of forward transition (in our case, say creation of excitations) and that of backward transition (annihilation of excitations) are

equal [54]. Once the detailed balance condition is incorporated the DSF corresponding to forward scattering process and the backward scattering process are connected via the following relation,

$$S^{\alpha\beta}(-\mathbf{q}, -\omega) = e^{-\frac{\hbar\omega}{k_B T}} S^{\alpha\beta}(\mathbf{q}, \omega) \quad (1.10)$$

and for centro-symmetric systems $S^{\alpha\beta}(-\mathbf{q}, -\omega) = S^{\alpha\beta}(\mathbf{q}, -\omega)$ [50]. In this thesis the detailed balance condition has been incorporated in the calculation of DSF via the Windsor factor which is discussed in the Appendix A.

In the following, I shall present a brief review of the existing theoretical and experimental results for quasi-two dimensional magnetic systems.

1.1 Brief review of quasi-two dimensional magnetic systems: theoretical and experimental results

The BKT transition and the topological order below T_{BKT} with zero order parameter have been verified experimentally in the thin film of super-fluid and superconductors, and in Josephson junction arrays [55, 56]. However, in spite of the fact that the BKT theory was originally proposed in 2d XY model of magnets, the evidences of the BKT transition are often very subdued in the real magnetic systems. In real magnetic systems, it is impossible to get a pure 2d critical behaviour owing to their layered structure. Furthermore, the real magnetic materials are mostly described by anisotropic Heisenberg Hamiltonian. Nevertheless, in a considerable number of magnetic materials possessing easy plane anisotropy, even if quite weak, the signatures of BKT transition have been found. These materials in a certain regime of physical parameters, such as temperature, behave as 2d systems. In this regime, the weak interlayer coupling breaks down but very often it becomes difficult to extract a pure 2d XY behaviour in terms of signatures in the thermodynamic quantities such as the universal jump in the renormalized spin-wave stiffness near T_{BKT} or the anomalous jump in c_v just above T_{BKT} . It is because the 2d critical behaviour is masked by the onset of the 3d ordering (due to the presence of interlayer coupling). As a consequence, in most of the layered materials with easy plane anisotropy the above mentioned jump in the c_v have not been observed in experiments. Apart from the thermodynamic signatures, the most important and interesting signature is the occurrence of a central peak (in the constant \mathbf{q} scan) above T_{BKT} in the INS experiments. This peak is widely believed to be associated with

the dynamics of the mobile topological excitations occurring in these type of layered materials.

It is worthwhile to mention that in the paramagnetic phase of pure 3d magnetic systems a central peak in the INS data has also been observed but this is followed by the occurrence of two finite frequency peaks [57]. This central peak has origin which is totally different from what has been considered here [58].

With the availability of improved crystal growing techniques and refined experimental set-ups, investigations on the layered (quasi-two dimensional) magnetic materials have been at the forefront of active research during last four decades. The INS experimental technique has been serving as the primary and most used tool due to its added advantages as mentioned earlier. Beside this, the electron spin resonance (ESR) and the nuclear magnetic resonance (NMR) both being local probes, are also being used these days.

Layered materials with weak easy plane anisotropy such as $BaM_2(XO_4)_2$ ($M = Co, Ni$; $X = P, As$) compounds, K_2CuF_4 , La_2CuO_4 , Intercalated graphite compounds (GIC) and many more, have been investigated via INS experiment. All these materials have been modelled by the XXZ Hamiltonian quite successfully [59]. In $BaM_2(XO_4)_2$, the exchange interaction within the layers takes place via the direct $M - M$ exchange and via $M - O - X - O - M$ super-exchange, while the interlayer exchange occurs via long bonds of $M - O - X - O - O - X - O - M$ involving many intermediate ions. The presence of planar anisotropy introduces a preference for the moments to lie within the plane.

For example, in $BaNi_2(PO_4)_2$, a spin 1 Honeycomb lattice AFM, the elastic neutron scattering data shows that the 3d ordering temperature $T_N \sim (23.5 \pm 0.5)$ [59]. For this material, the behaviour of the correlation length ξ as a function of temperature has been well fitted with the exponential expression of ξ corresponding to the 2d XY model. The critical exponent corresponding to the correlation length turned out to be $\eta = 0.31$ which is very close to theoretically obtained value of $\eta = 0.25$. However, fitting with a power law behaviour of ξ ($\sim (T/T_N - 1)^{-\nu}$) has not provided a good matching of the value of exponent between theory and experiment. Thus, the behaviour of the correlation length indicates a strong possibility of the dynamics of topological excitations in this material above T_N ($T_{BKT} = 0.98T_N$). In the INS experiment, this has been supported by the presence of the so-called central peak (in the constant \mathbf{q} scan) and

also by the sudden disappearance of the long wavelength excitations. Furthermore, a strong λ type anomaly in the specific heat c_v just above T_N has also been observed. A point to be noted is that for small values of q the BKT theory predicts a discontinuous decrease in the spin wave energy [60–62].

Qualitatively similar behaviour have been observed in $BaNi_2(AsO_4)_2$ (a spin 1 planar anti-ferromagnetic material) and in $BaCo_2(AsO_4)_2$ (a spin 1/2 ferromagnetic material). The existence of strong 2d magnetic correlations have been confirmed by the quasi-elastic neutron scattering experiments. Similar central peaks have been observed in these materials also. A strong λ type anomaly in c_v , very similar to what has been observed in $BaNi_2(PO_4)_2$, is also present in these materials. This occurs just above the 3d ordering temperature [59]. However, the occurrence of such a strong λ type anomaly in c_v corresponding to these materials is in contrast to the specific heat corresponding to the 3d isotropic Heisenberg model which are typically composed of Schotkky type bump, followed by a very weak λ type anomaly [63]. On the contrary, $BaCo_2(PO_4)_2$ have not shown any strong 2d XY behaviour [59].

In K_2CuF_4 , a spin 1/2 square lattice ferromagnet and in La_2CuO_4 , a spin 1/2 square lattice anti-ferromagnet (the parent compound of the high T_c Cuprate superconductor) similar central peaks in constant \mathbf{q} scan have been observed [7, 8, 64, 65]. In this thesis, we shall consider these two materials as the reference materials for comparison of theoretical results with the respective experimental results. The reason for this choice is that these are square lattice layered magnetic materials and therefore theoretical calculations have turned out to be not so complicated because of its simple lattice structure. Moreover, these are spin 1/2 systems and quantum effects are expected to be quite strong. The experimental details corresponding to these materials shall be described in subsequent chapters.

The Graphite intercalation compounds (GICs) also have provided themselves as very interesting systems for the experimental studies of the phase transitions in 2D magnetism even in spite of several difficulties regarding the preparation of good quality samples. However, the occurrences of vortex like topological excitations and their dynamics in these GICs have proved to be controversial [59]

The spin dynamics in 2d triangular Chromium lattice AFMs have been investigated via ESR measurements. In ESR measurements, the presence of spin vortices make an impact on the spin relaxation in the critical region. This has been shown recently via the analysis of ESR linewidth broadening for various quasi-two dimensional triangular and honeycomb lattices. Free movement of the spin vortices above T_{BKT} increase the spin relaxation and thereby lead to a decorrelation in the excited spins. This makes the linewidth of ESR to be proportional to the inverse of the correlation length. The divergence of the temperature dependent ESR linewidth has been well described in terms of the BKT scenario exhibiting vortex-anti-vortex unbinding mechanism. Based on the analysis of the spin relaxation via ESR method, it has been argued that the correlation length follows the BKT predicted form with a modified value of the critical exponent around 0.37 [66]. Recently, ESR measurements have been reported for the spin 1 quasi-two-dimensional honeycomb lattice anti-ferromagnet $BaNi_2(VO_4)_2$ and the planar anisotropic properties have been confirmed via investigations on the angular dependence of the resonance field and the linewidth. The divergence of the temperature-dependent linewidth on approaching T_N from above has been described in terms of the BKT transition, where $T_{BKT} = 0.9T_N$ with $T_N = 50$ K [67]. Various square lattice spin 1/2 ferromagnetic materials possessing frustration have also been investigated via the above mentioned local probes and similar line width divergence has been observed [68].

Since the XXZ (corresponding to $J_x = J_y = J$ and $J_z = \lambda J$; λ being the anisotropy parameter in the equation (1.3)) model on two dimensional lattices suits best in describing the critical properties of layered magnetic systems possessing easy plane anisotropy, theoretical as well as numerical investigations on this model have attracted a great deal of interest during last three decades. Attempts have been made in the past to describe the dynamics of mobile topological excitations corresponding to XXZ models assuming that these topological excitations constitute a classical ideal gas. Both ferromagnetic and anti-ferromagnetic models have been considered. Spins on two dimensional lattices have been assumed as classical vectors. In the XXZ model the spin profile of the topological excitations are meronic in character [42]. The projection of the classical spins corresponding to a meron on the xy-plane has the profile of a vortex as shown in Figure 1.1. On the other hand the cross-sectional view of the spin profile looks like the following Figure 1.3. This phenomenological theory (hereafter recognized as vortex-gas phenomenology) along with Monte Carlo Molecular Dynamics (MCMD) simulations have suggested that the exis-

tence of the central peak in the dynamical structure function is due to the scattering of neutrons from the above mobile topological excitations [37–41]. Furthermore, the root mean square (rms)



Figure 1.3: z -axis projection of the spin profile of meron (*i.e.* the cross-sectional view of meron).

velocity of the merons have been calculated by Huber considering the meron velocity autocorrelation function [37]. In this calculation it has been assumed that the merons do not interact with the spin waves. The vortex-gas phenomenology has further established that out-of-plane component of the static spin-spin correlation remain exponential function both below and above T_{BKT} which is in contrast to the general expectation of algebraic decay of correlation below T_{BKT} . However, the in-plane component of the spin-spin correlations has been found to be algebraic function below T_{BKT} and exponentially decaying above T_{BKT} , in commensurate with the general expectation. Therefore, vortex-gas phenomenology for XXZ model can clearly distinguish between the effects of the in-plane and the out-of-plane components of spins. MCMD simulation have further pointed out that the out-of-plane correlation function becomes dominating above a critical value of the anisotropy parameter $\lambda = \lambda_c = 0.8$. While the vortex-gas phenomenology does not account for the interaction between the spin-waves (collective modes) and the topological excitations, the behaviour of the collective modes like spin waves in the presence of a single vortex/meron corresponding to two-dimensional easy plane classical Heisenberg ferromagnet have been investigated using approximate analytical treatment in the continuum limit and numerical diagonalization techniques. It has been found that the renormalized spin wave modes show a strong localization of their amplitudes near the vortex core [69–71].

Incidentally, a rather different approach has been put forward to explain the origin of the central peak in the dynamical structure function $S(\mathbf{q}, \omega)$ corresponding to XY-anisotropic classical Heisenberg ferromagnetic model in two spatial dimensions. In this theory, the occurrence of the peak has been attributed to the fluctuations of the density of the topological excitations

due to local diffusion and creation-annihilation of merons and anti-merons [72]. However, such a theory based on diffusion mechanism seems to be more appropriate for $T \gg T_{BKT}$ because diffusive processes are expected to become dominant in this temperature regime, whereas most of the experimental data available are at temperatures which are just above T_{BKT} [38].

On the other hand, there are quite a few spin 1/2 layered materials available on which extensive INS experiment have been performed as has been mentioned earlier. In these spin systems, the quantum effects are expected to be dominating. The question of existence of the topological excitations, namely, vortices and merons in two-dimensional quantum XY and XXZ spin systems have been explored both numerically and analytically [73–79]. It has been determined numerically that in this case, the vortex-anti-vortex pair density is non-zero even at $T = 0$ [73]. In a pure quantum mechanical treatment, it has been found that almost all the vortices and anti-vortices are bound in pairs on square lattice and the number of isolated free vortices per site vanishes for $T < T_{BKT}$ [73]. Monte Carlo simulations have also been performed on quantum XY model on two-dimensional lattices. The validity of the BKT transition for this model has been confirmed [74, 75]. A full-fledged quantum treatment has also been performed based on the application of path integral techniques using the coherent state basis, for XY-anisotropic Heisenberg ferromagnet on a square lattice [76–79]. The partition function for the above quantum spin model has been expressed in terms of an effective action containing a topological part (Wess Zumino term) which contains a genuine topological term as a charge-measuring object for the vortices/merons (anti-vortices/anti-merons) alongside a non-topological term. It has been shown that in the very large anisotropy limit (corresponding to $J_x = J_y = J$ and $J_z = \lambda J; \lambda \rightarrow 0$ in the equation (1.3)) the topological term can characterize the topological excitations viz, vortices and anti-vortices [76–79]. In this formalism, the topological term arises from the path integral formulation of the quantum partition function in contrast to the situation where the vorticity operator has been introduced heuristically [73].

1.2 Motivations

In spite of a lot of studies on the anisotropic Heisenberg models, in particular the XXZ model on two dimensional lattices, the contributions of the topological excitations to the spin dynamics in these models are still not completely understood and especially the theoretical explanation of the available experimental data have largely been based on the vortex-gas phenomenology. However,

the results of the vortex-gas phenomenology and numerical simulation was shown to lead to an anomaly in the case of layered magnetic systems having very low spin values ($S=1/2$). Strikingly enough, the value of the T_{BKT} obtained from the Renormalization group analysis and numerical calculations turns out to be four (4) times the value of T_{BKT} calculated from the classical expression obtained by Kosterlitz and Thouless [80]. This particular anomaly motivates us to apply the vortex-gas phenomenology to specific spin 1/2 layered magnetic materials so that the origin of such anomaly can be clearly identified. Furthermore, such a task would examine how far the vortex-gas phenomenology is applicable in low spin magnetic systems.

Moreover, past attempts which have been made towards the understanding of the interaction between the collective excitations and the topological excitations below T_{BKT} led to a renormalization of the spin-wave modes. Such a renormalization of the spin-wave modes occur within the vortex core, typical core radius being of the order of few lattice spacing. It was found that certain spin-wave mode drives a crossover in the static vortex structure from purely in-plane vortex to a vortex with purely well-defined localized out-of-plane components. This happens when the value of the anisotropy parameter λ exceeds certain threshold value. This amounts to a development of meron character in the vortex [81, 82]. However, the existing theory have not come up with any explicit form of the spin-wave-meron interaction. These facts motivate us to investigate in this thesis the explicit form of the quantum state representing a meron like topological excitation.

In the following I shall describe the outline of my thesis.

1.3 Outline of the Thesis

This thesis is divided into two parts. In the first part in chapters 2 and 3, a semi-phenomenological analysis is performed in search for the understanding of the spin dynamics induced by the topological excitations in the layered magnetic systems with easy plane anisotropy. In the second part in 4, the microscopic aspects of the topological excitations are described.

In chapter 2, I shall describe our semi-phenomenological studies on analysing the available results from the INS experiment performed on a quasi-two dimensional spin 1/2 ferromagnetic material K_2CuF_4 [83]. Our formalism is based on a conventional semi-classical a model of an

ideal gas of mobile merons and anti-merons, built on the background of the fully polarized classical ferromagnetic spin configuration corresponding to an XY- anisotropic Heisenberg ferromagnet on a square lattice. The methodology involves an extension of existing vortex gas phenomenology by incorporating several experimental factors such as instrumental resolution function along with the incorporation of the detailed balance condition. The incorporation of detailed balance condition allows us to extract out the semi-classical DSF from the classical one using Windsors prescription (described in the Appendix A). The instrumental resolution function is mimicked by using a suitably chosen spectral window function. The semi-classical DSFs are calculated in two different temperatures which are chosen in accordance with temperatures at which the experimental data are available. In this chapter, I shall also describe the key outcomes of our investigations.

In chapter 3, I shall describe our semi-phenomenological studies on analysing the available results from the INS experiment performed on a quasi-two dimensional spin 1/2 anti-ferromagnetic (AFM) material La_2CuO_4 [84]. The methodology is quite similar to the previous one. However, this time in the anti-ferromagnetic system, the merons and anti-merons are built on the background of the Neel state, using a bipartite classical spin configuration. In this chapter, I shall describe our calculation of the integrated intensities corresponding to DSFs in several different temperatures. This is again in accordance with temperatures at which the experimental data are available [84]. The key outcomes of our investigations on the above mentioned AFM system are also described.

In chapter 4, I shall describe the microscopic aspects of the topological excitations in the extreme anisotropy limit ($\lambda \rightarrow 0$) [85]. In this limit, the merons become flattened and can be looked upon as vortices. In this chapter, we perform a critical analysis of the quantum state representing a vortex/anti-vortex. We present a scheme for the construction of quantum states of vortex like topological excitations corresponding to spin - 1/2 strongly XY-anisotropic nearest neighbour Heisenberg ferromagnet on two-dimensional lattice. The procedure involving Pauli spin basis states is carried out corresponding to both infinite dilute limit and finite density limit of vortex/anti-vortex. The particulars of the above mentioned limits are clearly defined in this chapter.

Chapter 5 sums up the conclusions of our investigations in this thesis and provides some future outlook. In Appendix A, I shall describe Windsor's prescription and the Windsor factor. A detailed derivation of this factor is also given. In Appendix B, magnons and interactions between them shall be described briefly. In Appendix C, I shall describe the Tukey and Modified Tukey function which are used in this thesis for mimicking the instrumental resolution. Appendix D describes how the DSF behaves when the value of the spin changes. Here, we consider a simple case corresponding to the DSF obtained in the classical spin-wave theory. From the outcome of this task we have inferred the dependence of the value of DSFs corresponding to the spin dynamics induced by the topological excitations on the value of the spin.

Chapter 2

Spin Dynamics In Quasi-two Dimensional Ferromagnets: A Semi-Classical Approach

2.1 Introduction

Two-dimensional (2d) magnetic models possess a variety of properties depending on the symmetry of the spin space and that of the lattice on which the spins are located, the range of interactions between the spins, quantum nature of spins, and the temperature at which the experimental measurement is done. In most of the cases an ideal 2d magnetic system can not be realized, rather the existence of a small inter-layer coupling makes the system layered/quasi-two dimensional (quasi-2d). Close to the critical point, all the magnetic systems behave either like an Ising system if the Hamiltonian contains an Ising anisotropy even if very small, or like an XY system if the Hamiltonian contains small planar anisotropy. Such a general property, widely known as the “universality”, is quite remarkably observed in the 2d and quasi-2d systems. More importantly, spin dynamics corresponding to the quasi-2d magnetic systems with planar anisotropy are interesting owing to existence of both topological and conventional (spin wave) excitations. It is in this ‘two spatial dimensions’ that magnetic systems exhibit a topological phase transition, viz., the Berezinskii-Kosterlitz-Thouless (BKT) transition [11–13]. The main idea of the BKT transition is that the vortices/merons and anti-vortices/anti-merons remain as bound pairs below a certain temperature T_{BKT} and above this temperature they start moving

freely. The spin dynamics induced by the movement of these excitations (above T_{BKT}) have been investigated through inelastic neutron scattering techniques as well as theoretical analysis [38–41, 59]. In quasi-two dimensional systems a central peak (peak corresponding to $\hbar\omega = 0$) has been found in the dynamical structure function when the latter is plotted in constant “ \mathbf{q} ” scan. Inelastic neutron scattering (INS) experiments performed on $BaCo_2(AsO_4)_2$, Rb_2CrCl_4 and K_2CuF_4 have indeed shown the occurrences of such central peaks [59].

The existence of topological phase transition and consequently the dynamics of topological excitations were proposed long ago for a spin-1/2 XY-anisotropic layered ferromagnet K_2CuF_4 [64, 65]. Extensive experimental studies of spin-dynamics in this layered ferromagnet have been carried out using INS technique. Their results exhibit a central peak (at $\omega = 0$) in the plot of “neutron count vs. energy transfer ($\hbar\omega$)” at a fixed value of the wave-vector \mathbf{q} . Subsequent developments of approximate analytical theories and Monte Carlo Molecular Dynamics (MCMD) calculations have suggested that the existence of such a central peak in these layered magnetic systems is a potential signature of the dynamics of freely moving merons and anti-merons [38]. In the corresponding phenomenological scenario the freely mobile merons and anti-merons are considered to be forming a classical ideal gas obeying the Maxwell velocity distribution [38].

In this chapter, I shall explain our detailed theoretical study which has been carried out to analyse more critically the available results from the inelastic neutron scattering experiment performed on K_2CuF_4 . This material is of particular interest here because it is a spin- 1/2 system and therefore, the quantum effects are expected to be strong. The material further possesses an easy plane anisotropy and hence falls into the XY universality class. On the other hand, since this is a ferromagnetic spin system the quantum mechanical ground state is well defined. Moreover, the lattice on which the spins are situated is a square lattice, unlike the other available quasi-2d ferromagnetic materials possessing honeycomb lattice structures. Therefore, the formalism described here can be applied in a straightforward manner to K_2CuF_4 . Our formalism is based on a conventional semi-classical-like treatment involving a model of an ideal gas of merons/anti-merons corresponding to an XY-anisotropic Heisenberg ferromagnet on a square lattice [83]. This incorporates the realistic instrumental resolution function which is modelled by a suitably chosen spectral window function. Furthermore and more importantly, the detailed balance condition has also been incorporated via the Windsor factor. The results for semi-classical DSFs for our model corresponding to spin- 1/2 , show occurrence of negative

values in a large range of energy transfer even encompassing the experimental range, when convoluted with a realistic spectral window function. This result strongly indicates failure of the conventional theoretical framework to be applicable to the experimental situation corresponding to low spin systems. The range over which the semi-classical DSFs remain positive depends on the value of the spin [83]. Based on the analysis presented in the Appendix D this issue has been discussed in this chapter.

Before we proceed let me describe the organization of this chapter. In Section 2.2, the classical theory of mobile vortices and anti-vortices is described briefly. In the same section I have explained our mathematical formulations in detail. In Section 2.3, a brief description of the different properties of the material K_2CuF_4 has been provided in order to fit the purpose. In Section 2.4 the formalism developed in 2.2 has been applied to calculate the semi-classical DSFs. In Section 2.5 the conclusions of our investigation is explained and a possible scheme for calculation of full quantum mechanical DSF and the quantum-BKT scenario are sketched out.

2.2 Spin dynamics in presence of topological excitations

The dynamics of mobile topological excitations in a two dimensional ferromagnetic system with easy plane anisotropy (XXZ anisotropy) has been treated both analytically and numerically by assuming an ideal gas of unbound merons/anti-merons above T_{BKT} . Such a phenomenological theory is called the vortex-gas phenomenology. In this chapter, I shall describe, when the experimental situations are taken into account how far the ideal vortex-gas phenomenology fits in explaining the experimental results corresponding to the spin dynamics and the phase transition in a layered spin - 1/2 ferromagnet with easy plane anisotropy. In dealing with the physical phenomena related to a single layer the simplest form of the Hamiltonian is given by,

$$\mathcal{H} = -J \sum_{\langle ij \rangle} (S_i^x S_j^x + S_i^y S_j^y + \lambda S_i^z S_j^z), \quad (2.1)$$

where (i, j) label the nearest neighbour sites on a 2d square lattice, J is the coupling constant and the classical spin vector is $\mathbf{S}_i \equiv (S_i^x, S_i^y, S_i^z)$. This is an anisotropic Heisenberg Hamiltonian which, for $J > 0$, represents a ferromagnetic system. The quantity λ is the anisotropy parameter whose XY and isotropic Heisenberg limit correspond to $\lambda = 0$ and 1 respectively. The general

time dependent spin configuration in spherical polar coordinate system is given by,

$$\begin{aligned} S_x &= S \cos\phi(\mathbf{r}, t) \sin\theta(\mathbf{r}, t), \\ S_y &= S \sin\phi(\mathbf{r}, t) \sin\theta(\mathbf{r}, t), \\ S_z &= S \cos\theta(\mathbf{r}, t), \end{aligned} \quad (2.2)$$

with $\mathbf{r} = (x, y)$. In the continuum description the above Hamiltonian can be rewritten as,

$$\mathcal{H} = \frac{JS^2}{2} \int d^2r ([\lambda + m^2(1 - \lambda)] \frac{(\nabla m)^2}{(1 - m^2)} + (1 - m^2)(\nabla\phi(\mathbf{r}, t))^2 + 4(1 - \lambda)m^2), \quad (2.3)$$

where $m = \sin\theta(\mathbf{r}, t)$ and the pair (m, ϕ) constitutes the canonically conjugate variables [39].

The equations of motion therefore are given by, $\dot{\phi} = \frac{\partial h}{\partial m}$ and $\dot{m} = -\frac{\partial h}{\partial \phi}$ where h is the Hamiltonian density corresponding to the continuum Hamiltonian (2.3). The static solutions corresponding to the above mentioned equations of motion can be obtained by following the formulation of Hikami and Tsuneto, and the solutions are given by [86],

$$\begin{aligned} \phi &= \pm \arctan\left(\frac{y}{x}\right) \\ \theta &= \frac{\pi}{2}(1 \pm e^{-r/r_v}) \quad \text{for } r \gg r_v, \\ &= 0 \text{ or } \pi \quad r \rightarrow 0, \end{aligned} \quad (2.4)$$

for single vortex centred at $\mathbf{r} = (0, 0)$, where (2.4) describes the asymptotic behaviour of θ . Here vortex core radius is given by, $r_v = \frac{a}{2} \sqrt{\frac{\lambda}{(1-\lambda)}}$ [86]. This type of spin configuration defines a ‘meronic’ type of the spin vortex.

In a magnetic system the spin dynamics induced by different excitations is captured from the form of the dynamical structure function (DSF). The DSF is the Fourier transform of the spin-spin correlation function and is defined by the relation,

$$S(\mathbf{q}, \omega) = \frac{1}{(2\pi)^2} \int d\mathbf{r} dt e^{i(\mathbf{q}\cdot\mathbf{r} - \omega t)} S(\mathbf{r}, t), \quad (2.5)$$

which is the continuum version of (1.7). The spin-spin correlation function $S(\mathbf{r}, t)$ is given by,

$$\begin{aligned} S(\mathbf{r}, t) &= \langle \mathbf{S}(\mathbf{r}, t) \cdot \mathbf{S}(\mathbf{0}, 0) \rangle \\ &= \langle S^x(\mathbf{r}, t) S^x(\mathbf{0}, 0) \rangle + \langle S^y(\mathbf{r}, t) S^y(\mathbf{0}, 0) \rangle + \langle S^z(\mathbf{r}, t) S^z(\mathbf{0}, 0) \rangle, \end{aligned} \quad (2.6)$$

where $\langle \dots \rangle$ representing the thermal average. In the case of classical gas of ideal merons the thermal average has to be taken by using Maxwell’s velocity distribution function. Here $S^{xx}(\mathbf{r}, t) = \langle S_x(\mathbf{r}, t) S_x(\mathbf{0}, 0) \rangle$ and $S^{yy}(\mathbf{r}, t) = \langle S_y(\mathbf{r}, t) S_y(\mathbf{0}, 0) \rangle$ are in-plane correlation functions and $S^{zz}(\mathbf{r}, t) = \langle S_z(\mathbf{r}, t) S_z(\mathbf{0}, 0) \rangle$ is the out-of-plane correlation function.

The in-plane spin-spin correlation can be analytically calculated by analyzing the change in the value of the spin field $S_x = S \cos\phi(\mathbf{r}, t) \sin\theta(\mathbf{r}, t)$ due to movement of a vortex/meron [38]. Every time a meron passes with its centre between the origin ($\mathbf{0}$) (chosen as a reference point) and an arbitrary point \mathbf{r} , the value of $\cos\phi(\mathbf{r}, t)$ changes by a factor of -1 , i.e. it changes its sign independent of the direction of the movement. The $\theta(\mathbf{r}, t)$ field contributes to the correlation by disallowing such sign change in an abrupt manner; in fact it allows the change only over a distance $2r_v$. *When the length scale is much larger than r_v , the dominant effect of the mobile merons is the above-mentioned change in sign.* Thus the in-plane correlation function turns out to be,

$$S^{xx}(\mathbf{r}, t) = S^2 \langle \cos^2\phi \rangle \langle (-1)^{N(\mathbf{r}, t)} \rangle, \quad (2.7)$$

where $N(\mathbf{r}, t)$ is the number of merons which passes through an arbitrary non-intersecting contour connecting $(\mathbf{0}, 0)$ and (\mathbf{r}, t) ; the average $\langle \cos^2\phi \rangle$ being $\frac{1}{2}$, *when a random spin configuration is assumed outside of the meron core.* Then it remains to find out the average, $\langle (-1)^{N(\mathbf{r}, t)} \rangle$ and in this step *the assumption of ideal gas of mobile merons* is incorporated in the calculation. Assuming that the merons are obeying the Maxwell's velocity distribution, it can be shown that

$$\langle (-1)^{N(\mathbf{r}, t)} \rangle = \exp\left[-\int_0^\infty \left(\frac{|r-ut|}{2\xi} + \frac{|r+ut|}{2\xi}\right) \mathcal{P}(u) du\right], \quad (2.8)$$

where the velocity distribution $\mathcal{P}(u)$ is given by, $\mathcal{P}(u) = \frac{2u}{\bar{u}^2} \exp[-(\frac{u}{\bar{u}})^2]$, \bar{u} being the root-mean squared velocity of the merons. In this derivation the density of free merons is assumed to be homogeneous on the average; locally however it is random [38]. From the above equation the effective analytical expression for the in-plane correlation function turns out to be,

$$S^{xx}(\mathbf{r}, t) = \frac{S^2}{2} \exp\left\{\left[\frac{r^2}{\xi^2} + \gamma^2 t^2\right]^{1/2}\right\}, \quad (2.9)$$

with $\gamma = \frac{\sqrt{\pi}\bar{u}}{2\xi}$, where \bar{u} is the root mean square velocity. Here $\xi = \xi_0 e^{b/\sqrt{\tau}}$ is the vortex-vortex correlation length. The root-mean squared velocity of the merons were first calculated by Huber as,

$$\bar{u} = \sqrt{b\pi} \frac{JS(S+1)a^2}{\hbar} \sqrt{n_v^f \tau^{-1/4}}, \quad (2.10)$$

where n_v^f is the density of free merons at $T > T_{BKT}$ [37]. In the conventional formalism corresponding to the calculation of \bar{u} , spin waves and merons are assumed to be decoupled. The Fourier transform of $S^{xx}(\mathbf{r}, t)$ in (2.9), gives rise to the in-plane dynamical structure function which is given by,

$$S^{xx}(\mathbf{q}, \omega) = \frac{S^2}{2\pi^2} \frac{\gamma^3 \xi^2}{[\omega^2 + \gamma^2(1 + \xi^2 q^2)]^2}. \quad (2.11)$$

This is a squared Lorentzian, peaked at $\omega = 0$, with q dependent width,

$$\Gamma = \frac{1}{2} \{ \pi(\sqrt{2} - 1) \}^{1/2} \left(\frac{\bar{u}}{\xi} \sqrt{1 + \xi^2 q^2} \right). \quad (2.12)$$

Exactly same results holds for $S^{yy}(\mathbf{q}, \omega)$ also because of the underlying O_2 symmetry in the spin space [38]. In the following let us discuss the form of the out-of-plane DSF.

An arbitrary configuration of the field $\theta(\mathbf{r}, t)$ corresponding to $S_z (= S \cos\theta(\mathbf{r}, t))$ can be considered to be a sum of contributions from all the merons, provided the merons do not interact with each other. Considering only incoherent scattering from non-interacting merons present in a dilute gas containing a total of N_v merons it can be shown that,

$$S_z = S \sum_{\nu=1}^{N_v} \cos\theta(\mathbf{r} - \mathbf{R}_\nu - \mathbf{u}_\nu t), \quad (2.13)$$

where \mathbf{R}_ν is the instantaneous position and \mathbf{u}_ν is the instantaneous velocity of unbound merons [38]. From the definition of $S^{zz}(\mathbf{r}, t)$ using the above equation the out-of-plane correlation function turns can be shown to be,

$$S^{zz}(\mathbf{r}, t) = n_v^f S^2 \int \int d^2R d^2u P(\mathbf{u}) \cos\theta(\mathbf{r} - \mathbf{R} - \mathbf{u}t) \cos\theta(\mathbf{R}), \quad (2.14)$$

where $P(\mathbf{u})$ is the Maxwell velocity distribution function. Performing first the spatial Fourier transform and then the temporal Fourier transform, it can be shown that, the out-of-plane dynamical structure function has the form [38],

$$S^{zz}(\mathbf{q}, \omega) = \frac{S^2}{4\pi^{5/2}} n_v^f \frac{|f(q)|^2}{\bar{u}q} \exp\left(-\frac{\omega^2}{\bar{u}^2 q^2}\right). \quad (2.15)$$

Here $|f(q)|$ is the velocity independent meron form factor and it has the form $f(\mathbf{q}) = \int d^2\mathbf{r} \cos\theta(\mathbf{r}) e^{-i\mathbf{q}\cdot\mathbf{r}}$. The form of $S^{zz}(\mathbf{q}, \omega)$ as in (2.15) exhibits a central peak at $\omega = 0$. The width of the central peak is $\Gamma_z = \bar{u}q$ i.e., linear in q .

In a typical inelastic neutron scattering experiment the count rate is proportional to the dynamical structure function (DSF),

$$I(\mathbf{q}, \omega) \propto S(\mathbf{q}, \omega). \quad (2.16)$$

This has been discussed in chapter 1. In order to compare theory with experiment one has to convolute the theoretical expression, obtained from a model under consideration, by the resolution function. The convoluted DSF $S_{conv.}(\mathbf{q}, \omega)$ given by, (1.9) The resolution function is

generally chosen to be the Fourier transform of a suitable spectral window function while plenty of them are being available in the literature of spectral analysis [83]. Thus equation (1.9) can be rewritten as,

$$S_{conv.}(\mathbf{q}, \omega) = \int dt \int d^2r R(t) S(\mathbf{r}, t) e^{i(\mathbf{q}\cdot\mathbf{r} - \omega t)}. \quad (2.17)$$

One of the most commonly used window function is the Tukey window function. A brief description of the Tukey function is given in the Appendix C.

The semi-classical DSF denoted by $S^{SC}(\mathbf{q}, \omega)$ is recovered by the relation ,

$$S^{SC}(\mathbf{q}, \omega) = \frac{2}{1 + \exp(\frac{-\hbar\omega}{k_B T})} S_{conv}(\mathbf{q}, \omega), \quad (2.18)$$

where the factor $\frac{2}{1 + \exp(\frac{-\hbar\omega}{k_B T})}$ is called the Windsor factor (See Appendix A) [87]. This factor incorporates the detailed balance condition, as required by the thermal equilibrium. The most important advantage of the use of Windsor factor is that this estimates the semi-classical DSF from the values of the DSF obtained from a classical theory [83].

2.2.1 Convolved In-Plane Dynamical Structure Function

In our formulation for the in-plane dynamical structure function we take into account the Tukey window function (see equation (C.2)) [83]. Using (2.17) and (C.2) we compute the Fourier transform of in-plane spin-spin correlation,

$$S_{conv.}^{xx}(\mathbf{q}, \omega) = \frac{1}{(2\pi)^{3/2}} \int d^2r \int_{-\frac{t_m}{2}}^{\frac{t_m}{2}} dt S^{xx}(\mathbf{r}, t) R(t) \times e^{i(\mathbf{q}\cdot\mathbf{r} - \omega t)}, \quad (2.19)$$

where $S^{xx}(\mathbf{r}, t)$ is given by (2.9). Now, $\int d^2r e^{i\mathbf{q}\cdot\mathbf{r}} = \int_0^\infty r dr \int_0^{2\pi} d\theta e^{iqr \cos\theta} = \int_0^\infty r dr J_0(qr)$, where $J_0(qr)$ is Bessel function of order zero. The spatial integration is performed from zero to a certain radius R_0 [83]. A final expression for the convolved in-plane dynamical structure function takes the form,

$$S_{conv}^{xx}(\mathbf{q}, \omega) = \frac{1}{(2\pi)^{1/2}} \int_0^{R_0} dr \int_{-\frac{t_m}{2}}^{\frac{t_m}{2}} dt S^{xx}(\mathbf{r}, t) \times r J_0(qr) R(t) \cos(\omega t). \quad (2.20)$$

Since, $S^{xx}(\mathbf{r}, t)$ and $R(t)$ (see equation (C.2)) are both even function in t , only $\cos(\omega t)$ contributes to the temporal part of the integration. The values of Y component, $S_{conv}^{yy}(\mathbf{q}, \omega)$ and X

component, $S_{conv}^{xx}(\mathbf{q}, \omega)$ of the in-plane dynamical structure functions are equal. This is because of the fact that the underlying symmetry is O_2 . Let us note that in the above analysis the formulation holds only for $T > T_{BKT}$. For $T < T_{BKT}$ the correlation length ξ is not defined and hence the formalism can't be extrapolated below T_{KT} . The above integration has been computed numerically [83].

2.2.2 Convoluted Out-of-Plane Dynamical Structure Function

The working formula for the convoluted out-of-plane dynamical structure function is given by,

$$S_{conv}^{zz}(\mathbf{q}, \omega) = \int \tilde{R}(\omega - \omega') S^{zz}(\mathbf{q}, \omega') d\omega', \quad (2.21)$$

where $\tilde{R}(\omega - \omega')$ is the Fourier transform of $R(t)$ (see (C.3)). The reason for taking (2.21) as the expression for convoluted out-of-plane dynamical structure function is that, unlike (2.9), an analytical expression for $S^{zz}(\mathbf{r}, t)$ can't be evaluated from (2.14) and hence we start from (2.15) in this formulation [83]. The integral in (2.21) has also been computed numerically.

2.2.3 Estimation of Contributions from Spin-Wave Like Modes

The $S_{conv}^{zz}(\mathbf{q}, \omega)$ defined here corresponds only to the mobile merons; whereas the experimental data contain the contributions from meron-anti-meron bound pairs as well as fragile *spin wave like* modes. The fragile *spin wave like* modes are the largely decaying modes above the Curie temperature (T_c). The fragile mode contribution has been subtracted by taking the fragile mode contribution above transition temperature to be same as the pure spin wave contribution just below transition temperature [83]. This is valid as long as the temperatures considered here are not far below or above the Curie temperature. This enables the processed experimental data to be free from any contributions due to fragile modes; however, contributions from meron-anti-meron bound pairs (or frozen pairs) still remain. Hence in the following we shall look into a method for estimating the contributions from the bound/frozen meron-anti-meron pairs [83].

2.2.4 Bound Meron Contribution

In order to compare with the experimental observations, one has to extract the mobile meron contribution from the experimental data. This can be done by subtracting the frozen meron-anti-meron pairs contribution from the experimental data [83]. To find the approximate analytical

expression for $S^{zz}(\mathbf{q}, \omega)$ due to bound meron contribution, the limiting value of \bar{u} is taken as $\bar{u} \rightarrow 0$ in (2.15). Then from (2.15) it easy to find an expression for $S_{bound}^{zz}(\mathbf{q}, \omega)$ namely,

$$S_{bound}^{zz}(\mathbf{q}, \omega) = \frac{S^2}{4\pi^2} n_v^b |f(q)|^2 \delta(\omega), \quad (2.22)$$

where n_v^b is the bound vortex/meron density. Since, the system has no net topological charge the number of merons and anti-merons present in the system must be equal and we can take $n_v^f + n_v^b = \frac{1}{2}$ assuming square lattice structure [83]. This is correct as long as the temperature is just below T_{BKT} where all the merons are frozen but once the temperature crosses T_{BKT} some of the bound merons become mobile and the bound vortex density can be approximated as,

$$n_v^b \approx \left(\frac{1}{2} - n_v^f\right), \quad (2.23)$$

where, n_v^b is in the units of inverse of plaquette size (a^2). Since, $n_v^f \sim \xi_0^{-2} \exp(-2b/\sqrt{\tau})$, n_v^b given by (2.23) is temperature dependent. Here ξ_0 is of the order of lattice parameter. Using (2.22) and (2.23) the bound vortex contribution has to be subtracted carefully from the experimentally observed count [83].

It is worthwhile to point out that the above procedure to extract out bound meron contributions can not be applied in the case of in-plane dynamical structure function (see Section 2.2.1) [83].

2.2.5 Total Dynamical Structure Function (Spin-Spin Correlation)

The general expression for the total dynamical structure function is,

$$S(\mathbf{q}, \omega) = \frac{1}{(2\pi)^{3/2}} \int d^2r \int dt S(\mathbf{r}, t) R(t) e^{i(\mathbf{q}\cdot\mathbf{r} - \omega t)}, \quad (2.24)$$

where the total spin-spin correlation is $S(\mathbf{r}, t)$ is defined by (2.6). So, the total dynamical structure function is $S(\mathbf{q}, \omega) = S^{xx}(\mathbf{q}, \omega) + S^{yy}(\mathbf{q}, \omega) + S^{zz}(\mathbf{q}, \omega)$. Since, X and Y components of the spins are symmetric we have, $S^{xx}(\mathbf{q}, \omega) = S^{yy}(\mathbf{q}, \omega)$ and the total dynamical structure function takes the form,

$$S(\mathbf{q}, \omega) = 2S^{xx}(\mathbf{q}, \omega) + S^{zz}(\mathbf{q}, \omega). \quad (2.25)$$

Here, we would consider (2.25) only for mobile vortices [83].

It is worthwhile to emphasize the fact that the formalism explained above incorporates the Windsor factor and the presence of \hbar in the quantum expression of magnetic moment corresponding to the spins constituting a meron. In this sense our combined theoretical approach can be termed as ‘semi-classical like’ [83]. It is very important to point out that in this chapter and in the next the name vortex and meron are used in the same sense to represent the same physical object, although they are different objects originally. It is only in chapter 4 these two objects shall be clearly distinguished based on the value of the anisotropy parameter (λ).

2.3 Relevant information on K_2CuF_4

In this thesis the formalism developed in Section 2.2 has been applied on a real material K_2CuF_4 for which extensive neutron scattering experiments have been performed [64, 65]. Let us now discuss briefly some properties of K_2CuF_4 which are particularly useful in our analysis. This material is a quasi-two-dimensional spin $\frac{1}{2}$ ferromagnet, where the interaction is mainly Heisenberg type with only 1% XY anisotropy. The spin Hamiltonian relevant to the above material is given by,

$$\mathcal{H} = \underbrace{\left(-J \sum_{\langle i,j \rangle} \mathbf{S}_i \cdot \mathbf{S}_j + J_A \sum_{\langle i,j \rangle} S_i^z S_j^z\right)}_{\text{intra-layer part}} - \underbrace{J' \sum_{\langle i,k \rangle} \mathbf{S}_i \cdot \mathbf{S}_k}_{\text{inter-layer part}} \quad (2.26)$$

where $\langle i, j \rangle$ represents the intra-layer nearest neighbour interaction and $\langle i, k \rangle$ represents the inter-layer nearest neighbour interaction. In the above Hamiltonian, $J(> 0)$ is the isotropic part of the intra-layer exchange coupling, J_A is anisotropic part of the intra-layer exchange coupling, and $J'(> 0)$ is the inter-layer exchange coupling. Though the system is nearly Heisenberg type, the presence of a small XY anisotropy causes the system’s low temperature behaviour to be XY-like, and this is in connection with the concept of “universality”. The phase transition in this material is close to BKT type with slight modification due to near-isotropic Heisenberg interaction. The magnetic lattice structure for K_2CuF_4 is approximately a body centred tetragonal lattice i.e., a lattice composed of stacking of 2D square lattices [64, 65]. The physical parameters are given in the Table 2.3, which have been used throughout the calculation.

From the inelastic neutron scattering experiments performed on K_2CuF_4 it has been found that there are two threshold values of q , namely $q_1 = 0.06$ and $q_2 = 0.01$, where for $q > q_1$ the system behaves like 2d Heisenberg system and for $q < q_2$ the system behaves as 3d XY system.

parameter	magnitude
exchange coupling (J)	11.93 K
lattice parameter (a)	4.123 Å
'b'	1.5
' T_{BKT} '	5.5 K
' T_c '	6.25 K

Table 2.1: Relevant parameters for K_2CuF_4 [65]

For $q_2 < q < q_1$ the system behaves as 2d XY system. This has been obtained by analysing the spin wave dispersion curve. The plot of temperature dependence of the spin wave excitation energy (or simply spin wave frequency) for this quasi-2d system, shows a sharp decrease in the frequency when the temperature approaches T_c (the Curie temperature) from below [65]. Smaller the values of q steeper the changes occur. This indicates a sudden disappearance of the long wave-length excitations. This phenomena is often attributed to the signature of a BKT transition. More importantly, the jump in the spin-wave stiffness constant (stiffness for in-plane twisting of the spins) at T_{BKT} is very difficult to observe when a finite (even if small) inter-layer coupling is present. In such a situation the study of the temperature dependence of the spin wave frequency i.e., the stiffness for transverse twisting of the spins becomes the best alternative [59]. In an ideal 2d XY system, the spin-wave frequency at a properly small value of q should retain a constant value up to T_{BKT} and then should drop to zero suddenly at T_{BKT} . However, in K_2CuF_4 the presence of a small interlayer coupling modifies the situation and such a steep drop of spin wave frequency has been observed near T_c for $q_2 < q < q_1$ [88].

In the following section, I shall elaborate the computation of the semi-classical DSFs which are performed numerically corresponding to two different temperatures viz., 6.25 K and 6.75 K, for $q(\text{planar}) = 0.04$ reciprocal lattice units (in the units of $\frac{\pi}{a}$), experimentally $\hbar q$ being the momentum transfer [83]. It is at these two temperatures where the occurrences of central peak have been reported in constant \mathbf{q} -scan measurements [65].

2.4 Calculation of dynamical structure function and comparison with experimental results

In this section, we are going to look into the calculations of the semi-classical DSF for the material K_2CuF_4 using the formalism developed in the Section 2.2 and compare the results with the corresponding experimental data. Let us start with by calculating the in-plane DSF $S^{xx}(\mathbf{q}, \omega)$. The radius R_0 in (2.21) is $(\sqrt{100^2 + 100^2})a$ for a 100×100 lattice, where a is the lattice parameter. We have varied the energy transfer $\hbar\omega$ from -0.3 meV to +0.3 meV, which includes the range -0.2 meV to +0.2 meV as used in experiment [65]. The value of t_m can be set according to the experimental resolution width (0.01 meV) [65]. The convoluted in-plane

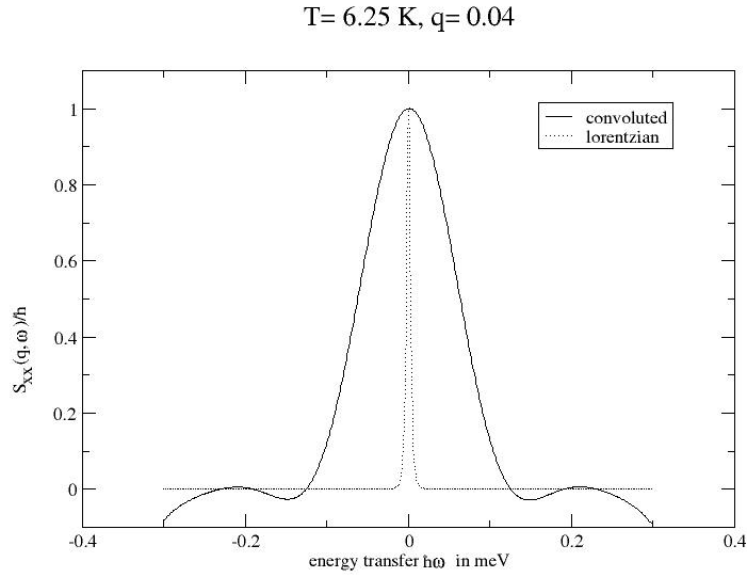


Figure 2.1: Comparison between the convoluted in-plane dynamical structure function $S_{conv}^{xx}(\mathbf{q}, \omega)$ (2.21) and unconvoluted in-plane dynamical structure function $S^{xx}(\mathbf{q}, \omega)$ (2.11) at $T = 6.25$ K and $q = 0.04$. Solid line is for convoluted theoretical expression and dotted line is for unconvoluted theoretical expression (squared Lorentzian). $\xi = 58.09a$, $\bar{u} = 0.0614 \frac{a}{t_{nat}}$, and width $\Gamma_{xx} = 0.0012 \text{ meV}$ for squared Lorentzian at $T = 6.25$ K [83].

DSF is plotted in Figures 2.1 and 2.2, where $t_{nat} = \frac{\hbar}{J\sqrt{S(S+1)}}$ is the natural time unit for the system/material (in our case K_2CuF_4). These figures indicate that after convoluting with the Tukey window function, the in-plane DSF no longer remains squared Lorentzian, though in both

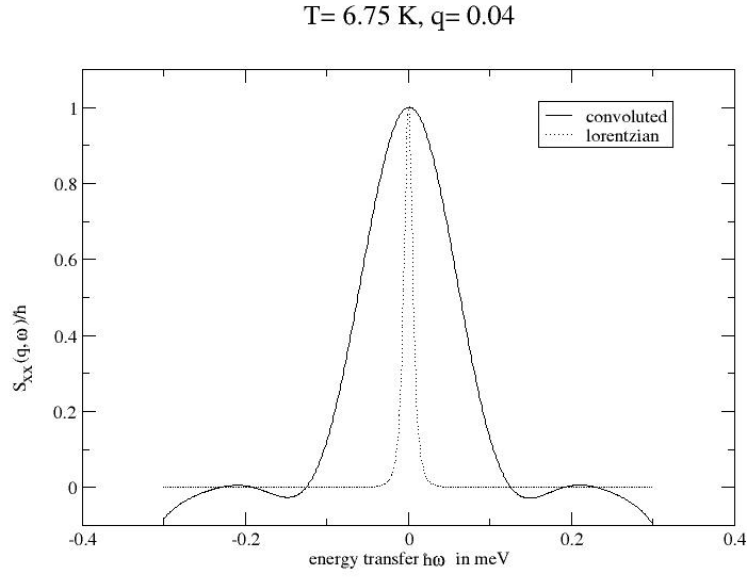


Figure 2.2: Comparison between the convoluted in-plane dynamical structure function $S_{conv}^{xx}(\mathbf{q}, \omega)$ (2.20) and unconvoluted in-plane dynamical structure function $S^{xx}(\mathbf{q}, \omega)$ (2.11) at $T = 6.75$ K and $q = 0.04$. Solid line is for convoluted theoretical expression and dotted line is for unconvoluted theoretical expression (squared Lorentzian). $\xi = 22.25a$, $\bar{u} = 0.1352 \frac{a}{t_{nat}}$ and width $\Gamma_{xx} = 0.0035 \text{ meV}$ for squared Lorentzian at $T = 6.25$ K [83].

the cases central peaks persist. The width of the $S_{conv}^{xx}(\mathbf{q}, \omega)$ curve is much larger than that of the squared Lorentzian [83]. We further notice that the convoluted in-plane DSF function $S_{conv}^{xx}(\mathbf{q}, \omega)$ becomes negative for $|\omega|$ just above 0.1 meV! These striking occurrences of negative magnitudes of the DSF have been dwelt on in great in details in Section 2.5 and also in Appendix D. Again comparing Figures 2.1 and 2.2 we find that the width of the squared Lorentzian increases with the increase of temperature whereas, that of the $S_{conv}^{xx}(\mathbf{q}, \omega)$ does not undergo any change [83]. Later, we will present a comparison of the convoluted total dynamical structure function with the experimental one(See Figures 2.5 and 2.6).

We now evaluate the out-of-plane DSF $S_{conv}^{zz}(\mathbf{q}, \omega)$ for two different temperatures, *viz.*, 6.25 K and 6.75 K, for $q(\text{planar}) = 0.04$ r.l.u, using (2.18). The expression for $\tilde{R}(\omega - \omega')$ is,

$$\tilde{R}(\omega - \omega') = \frac{1}{4\pi} \sin \left[\frac{(\omega - \omega')t_m}{2} \right] \left[\frac{2}{\omega - \omega'} - \frac{1}{\omega - \omega' + 2\pi/t_m} - \frac{1}{\omega - \omega' - 2\pi/t_m} \right]. \quad (2.27)$$

We use the same value of t_m as used for $S_{conv}^{xx}(\mathbf{q}, \omega)$. Here also the reasons for the choice of temperatures and $q(\text{planar})$ are same as that for the in-plane dynamical structure function. In Figures 2.3 and 2.4 we have plotted the out-of-plane correlation, $S_{conv}^{zz}(\mathbf{q}, \omega)$. We have varied the ω' from $-\frac{\pi}{t_m}$ to $\frac{\pi}{t_m}$ in (2.20), where t_m is estimated from the resolution width as before [83].

In this case the bound vortex contribution has been subtracted carefully, using (2.22) and (2.23), from the observed count at 6.25 K to obtain the effective contribution from mobile topological excitations. The methodology for extracting the mobile vortex contributions from the experimental data has been explained in Section 2.2. As long as the counts at 6.75 K are concerned, the fragile ‘spin wave like’ modes are highly decaying so that it can’t be assumed to be the same as the true spin wave modes observed just below T_c . So bound vortex contribution has been subtracted at 6.25 K only. The normalization factors, required for the quantitative comparison between the theoretical and the experimental results, have been estimated from the neutron count extracted from the experiment on K_2CuF_4 [65].

We again find that the out-of-plane DSFs also turn out to be negative within the resolution width(see Figures 2.3 and 2.4)! Hence, out-of-plane DSFs may not possess well defined widths. Moreover experimental peaks are out side the resolution width, while the peaks corresponding to the $S_{conv}^{zz}(\mathbf{q}, \omega)$ are at $\omega = 0$.

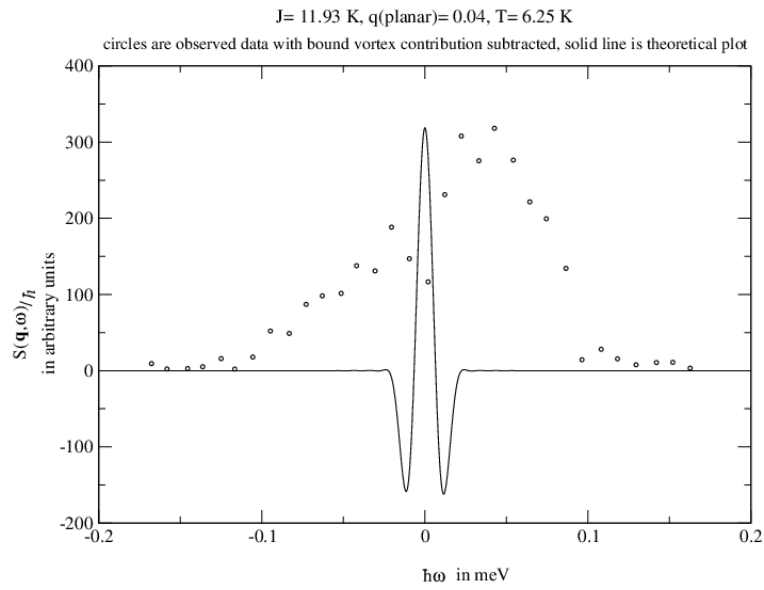


Figure 2.3: circles are observed (experimental) data, where contributions from the fragile modes as well as the bound vortex contributions have been subtracted & solid line is the plot of properly convoluted out-of-plane dynamical structure function $S^{zz}(\mathbf{q}, \omega)$ (theoretical). $\xi = 58.09a$, $\bar{u} = 0.0614 \frac{a}{t_{nat}}$ [83].

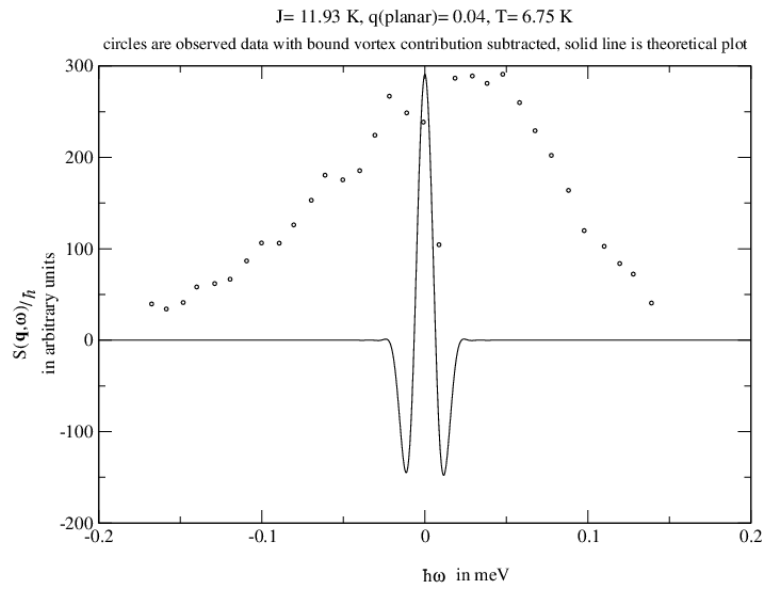


Figure 2.4: circles are observed (experimental) data, where only contributions from bound merons have been subtracted & solid line is the plot of properly convoluted out-of-plane dynamical structure function $S^{zz}(\mathbf{q}, \omega)$ (theoretical). $\xi = 22.25a$, $\bar{u} = 0.1352 \frac{a}{t_{nat}}$ [83].

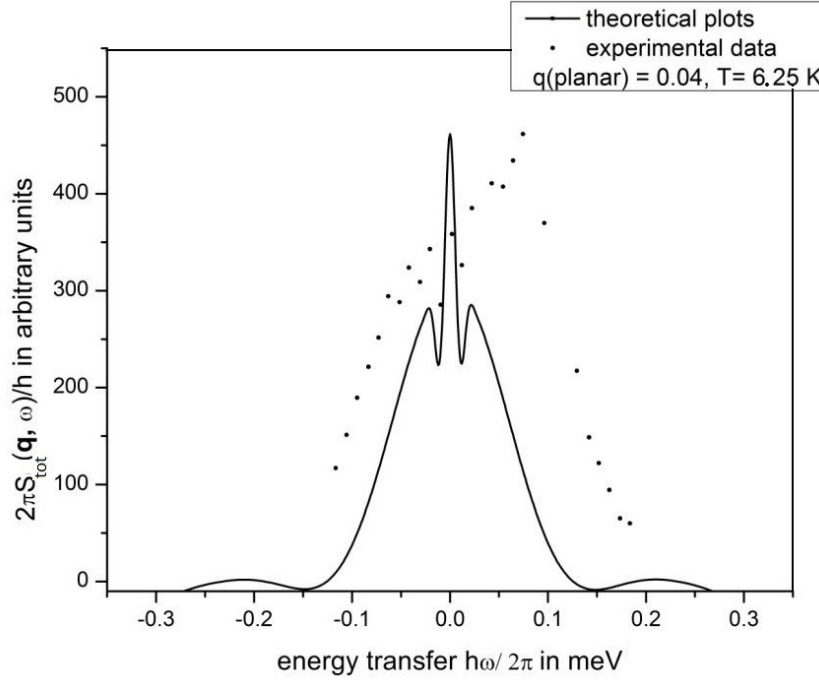


Figure 2.5: total dynamical structure function $S_{conv}^{total}(\mathbf{q}, \omega)$ at $T = 6.25$ K and $q = 0.04$ - solid line is for convoluted theoretical results and dots are filtered experimental data. $\xi = 58.09a$, $\bar{u} = 0.0614 \frac{a}{t_{nat}}$ [83].

The above calculations lead us to the theoretical estimate for the convoluted total dynamical structure function $S_{conv}^{total}(\mathbf{q}, \omega)$ given by (2.25). In Figures 2.5 and 2.6, $S_{conv}^{total}(\mathbf{q}, \omega)$ has been compared with the filtered experimental data obtained by subtracting the bound vortex contributions and fragile ‘spin wave like’ contributions (see Sec 2.2). In these plots the intensities of the experimental peaks and that of the central peaks of the $S_{conv}^{total}(\mathbf{q}, \omega)$ have been matched [83].

It is clear from Figure 2.5 that at 6.25 K the experimental peak occurs approximately at 0.08 meV, which is way outside the resolution width. At 6.75 K [see Figure 2.6] the peak of the experimental graph is not far from the central peak. It is reasonable to say that as the temperature is increased, we are getting better agreement of the $S_{conv}^{total}(\mathbf{q}, \omega)$ with the experimental observations. This agreement is regarding the position of the central peak [83]. Apart from the central peak there are two other peaks at finite frequency at both the temperatures. These are nothing but the reminiscent of the out-of-plane dynamical structure function contribution

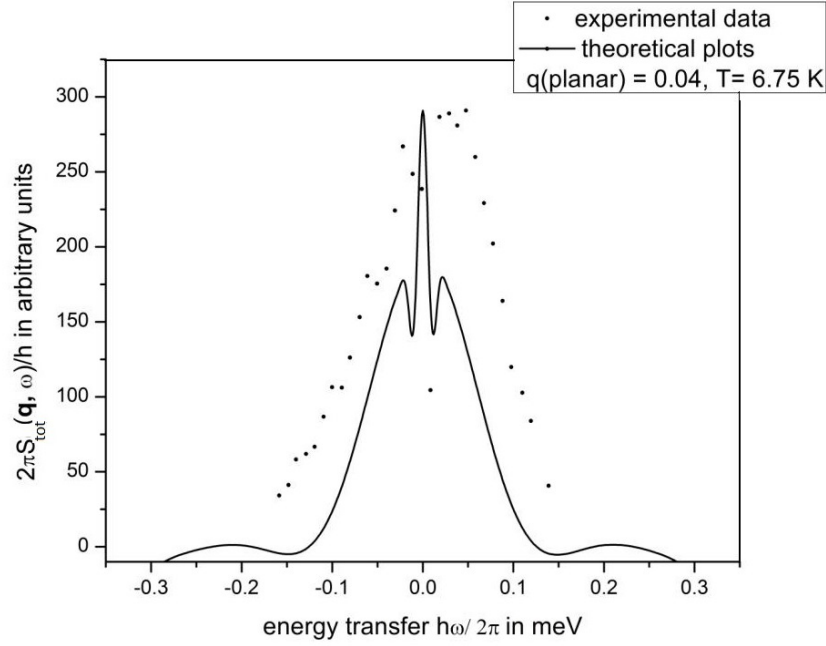


Figure 2.6: *total dynamical structure function $S_{conv}^{total}(\mathbf{q}, \omega)$ at $T = 6.75$ K and $q = 0.04$ - solid line is for convoluted theoretical results and dots are filtered experimental data. $\xi = 22.25a$, $\bar{u} = 0.1352 \frac{a}{t_{nat}}$ [83].*

as seen from Figures 2.3-2.6. These finite frequency peaks are well within the resolution width itself, and therefore do not have any individual significance as well.

The total DSF is still negative for $|\omega|$ just above 0.1 meV. Though it is true that the pure quantum mechanical DSF can never be negative, here in our case the negativity occurs as a result of the convolution of analytical expression of $S^{SC}(\mathbf{q}, \omega)$. Even for a conventional long range ordered system, the DSF corresponding to a classical pure spin wave comes out to be negative beyond a certain range of frequency when convoluted with any spectral window function (see Appendix D). Furthermore the above peculiarity persists even when quantum effects are incorporated through a detailed balance factor [83].

The inclusion of quantum mechanical detailed balance condition in the semi-classical like treatment for dynamics of mobile merons and anti-merons does not produce any appreciable asymmetry with respect to ‘ ω ’, as seen in the theoretical plots in our case of spin- $\frac{1}{2}$. The theoretical plots are largely symmetric around $\omega = 0$. A very small asymmetry in the theoretical

plots are being seen for higher values of ω while the experimental data are showing clearly the asymmetry [83].

It may be noted that in our analysis the bound vortex contributions have been approximately estimated only for out-of-plane dynamical structure function $S^{zz}(\mathbf{q}, \omega)$. This is because, in this case we are able to truncate the expression, as given in (2.15), to the regime $T < T_{BKT}$, by making $\bar{u} \rightarrow 0$. In (2.15), there exists no explicit dependence of $S^{zz}(\mathbf{q}, \omega)$ on the correlation length ξ . In case of in-plane correlation, as given in (2.9), we need to find ξ for $T < T_{BKT}$ due to its explicit appearance in that expression. Since ξ is not defined for $T < T_{BKT}$ we are not able to estimate the bound vortex contribution for in-plane dynamical structure function [83].

2.5 Summary

In this chapter, I have described in detail the successful analysis of the available INS data corresponding to spin 1/2 XXZ ferromagnetic material K_2CuF_4 . The limitations of a conventional semi-classical description of mobile topological excitations corresponding to a spin 1/2 ferromagnetic system have also been addressed quite elaborately. The conventional semi-classical formalism used here involves a model of ideal gas of mobile topological excitations. Let us summarize the results of our analysis. We find that the width of the convoluted in-plane dynamical structure function is much larger than that of the squared Lorentzian. Values of the in-plane dynamical structure function comes out to be negative beyond a finite range of energy transfer. The convoluted out-of-plane dynamical structure function becomes negative as well; however this happens within the resolution width about the central peak (peak at $\omega = 0$). The total convoluted dynamical structure function also becomes negative in the regime where the in-plane dynamical structure function had become negative. No appreciable asymmetry is created even after including the Windsor factor. We find that for both the temperatures the convoluted total dynamical structure function is symmetric around $\omega = 0$; whereas the experimental observation is not. The theoretical model of semi-classical treatment of ideal gas of unbound merons tends to agree with the experimental observations (corresponding to the spin 1/2 system considered here) better at higher temperatures, when we compare the experimental results corresponding to $T = 6.25$ K and $T = 6.75$ K. It is worthwhile to point out that same results hold for unbound anti-vortices also.

Based on the analysis carried out in the Appendix D, it can be inferred that for the dynamics of mobile topological excitations corresponding to ferromagnetic spin 1/2 XXZ model, the negative values of $S_{conv.}(\mathbf{q}, \omega)$ are occurring due to the following factors. Firstly, the choice of the resolution function is expected to affect the results and in our case this is chosen to be the Tukey function. However, it has been already mentioned that Tukey function is very commonly used in the field of spectral analysis [52,53]. The second factor turns out to be the choice of the value of resolution width $\Delta\omega$ and in this case it is made fixed by experimentally imposed one. Lastly and most importantly, the use of a semi-classical like treatment to extend the classical theory of dynamics of mobile merons (anti-merons) to a spin 1/2 (extreme quantum case) ferromagnetic system can easily lead to such unphysical results. To avoid the negativity in the $S_{conv.}(\mathbf{q}, \omega)$ a different resolution function may be chosen. Indeed, it has been shown that most of the resolution functions are more or less oscillatory in the Fourier space [52,53]. An extra smoothening factor can be used to dampen the oscillation of the resolution function. This extra factor happens to be a function of resolution width, and it makes the resolution function smoother if the resolution width is decreased [52,53]. However, in our case since the resolution width is fixed from the experiment, the oscillation of the resolution function can't be avoided by merely changing the resolution function. Another way to avoid the negativity is to assume, $S_{conv.}(\mathbf{q}, \omega) = 0$ outside the physically admissible range [87,89]. If this physically admissible range falls within the range of experimental interest then the assumption turns out to be inapplicable. In our case of spin 1/2 ferromagnet the physically admissible range is well within the range of ω over which the neutron scattering data has been taken in the experiment (as seen from Figures 2.5 and 2.6) and hence the occurrence of negative values of DSFs can't be avoided just by making $S_{conv.}(\mathbf{q}, \omega) = 0$. On the other hand, the range over which the semi-classical DSF remains positive, depends on the magnitude of spin occurring in the theoretical model under consideration and the resolution width [83]. On the basis of the analysis presented in Appendix D it is expected that even in the case of dynamics of mobile merons and anti-merons the physically admissible range would be larger for higher values of spin and smaller for lower values of spin. Hence, the negative values of $S_{conv.}(\mathbf{q}, \omega)$ occur because of the use of the semi-classical like treatment to extend the classical theory of dynamics of mobile merons and anti-vortices to a quasi two dimensional spin $\frac{1}{2}$ ferromagnet (K_2CuF_4). Therefore, a complete quantum mechanical formalism and treatment are indeed very crucial for the understanding of the spin dynamics induced by the topological excitations corresponding to low spin magnetic systems [83].

However, the agreement between the behaviour of DSF obtained from our theoretical calculations and that from the experiment, in terms of the peak position and the overall shape, is found to be fairly good at temperatures much larger than T_{KT} .

Calculation of the dynamical structure function in a completely quantum mechanical framework is highly non-trivial. Earlier attempts towards this goal could not explain the occurrence of the “central peak” in the DSF obtained in the INS experiment performed on several quasi-two-dimensional materials [4, 8, 90, 91]. Quite recently a theoretical framework had been developed based on the spin coherent state path integral formalism to describe the topological properties of static vortices and anti-vortices [76–79]. An extension of this framework to the case of mobile spin vortices/merons (and anti-vortices/anti-merons) is crucial for quantum mechanical calculations of the DSF and the integrated intensity as well. Insights from Quantum Monte Carlo calculations may be quite useful in this endeavour [92]. A possible scheme towards the understanding of the effects of the quantum fluctuations on BKT transition and the quantum mechanical calculation of DSFs has been explained in considerable details in chapter 5.

In the next chapter, a semi-classical formalism shall be applied to a spin 1/2 XXZ anti-ferromagnetic (AFM) material. The formalism shall be very similar in spirit, to the one described here. In the spin 1/2 AFM systems the quantum fluctuations are indeed very strong and therefore, application of such a semi-classical description to the corresponding experimental situation is expected to bring out the effects of quantum fluctuations even more strongly on the spin dynamics induced by topological excitations.

Chapter 3

Spin Dynamics In Quasi-two Dimensional Anti-ferromagnets: A Semi-classical Approach

3.1 Introduction

In low dimensional magnetic systems the topological excitations of soliton and vortex/meron type occur very naturally as they are thermodynamically feasible. Kosterlitz and Thouless, and Berezinskii independently introduced the concept of vortex and anti-vortex type topological spin excitations and the topological phase transition in the two dimensional classical XY model of ferromagnetic type [11–13]. Thermodynamics of this phase transition has been briefly explained in chapter 1. Subsequent analytical and numerical investigations have established the occurrence of such a topological phase transition in the XXZ models too [37–41]. In parallel to this, conjectures have also been made regarding the possible application of BKT scenario to 2s XXZ antiferromagnets [8, 40, 41] Experimental investigations along these lines have found a new impetus with the discovery of high T_c superconductivity in the doped cuprate materials. In the context of two-dimensional magnetism, the undoped (anti-ferromagnetic and non-superconducting) phases of the high T_c cuprate systems are excellent examples of layered spin systems which can be modelled by 2d XXZ Hamiltonian in an appropriate temperature regime. One member of this class of systems is La_2CuO_4 , on which extensive INS experiments have been performed [7, 8]. This is a truly spin-1/2 layered XY-anisotropic Heisenberg anti-ferromagnet with very small inter-layer

coupling. The intra-layer integrated intensity corresponding to the results of INS experiment performed on La_2CuO_4 , exhibits a central peak when plotted against the neutron energy transfer $\hbar\omega$ (or frequency ' ω '). The occurrence of such a “central peak” for quasi-two dimensional magnetic systems is now almost unanimously believed to be the signature for the dynamics of mobile topological excitations in a layer at least for ferromagnets. It is worthwhile to highlight here that the occurrence of the so-called “central peak” for La_2CuO_4 could not be reproduced by using the model put forward by Chakravarty- Halperin-Nelson (CHN) for the 2d quantum Heisenberg Anti-ferromagnets. The CHN model takes into account isotropic Heisenberg model with antiferromagnetic exchange coupling [8, 90]. However, our calculations with “meron gas phenomenology” has indeed produced the so-called “central peak” [37–41].

Furthermore, it has been shown that the results obtained from the combination of vortex gas phenomenology and numerical simulations lead to an anomaly in the case of layered anti-ferromagnetic systems having very low spin values ($S=1/2$) [80]. Strikingly enough, the value of T_{BKT} obtained from Renormalization group analysis and numerical simulations is four (4) times the value of T_{BKT} calculated from the classical expression obtained by Kosterlitz and Thouless [80]. In the previous chapter we have already established that for *quasi-two dimensional ferromagnetic systems having low spin values ($S= 1/2$)* the conventional semi-classical like formalism involving the ideal gas of unbound topological excitations corresponding to high temperature regime $T > T_{BKT}$, shows large inconsistency with the experimental situation and exhibits unphysical behaviour [83]. In this case the theoretically obtained DSFs turn out to be negative for a wide range of energy transfer! However the range, over which the theoretical DSFs remain positive, increases when the value of the spin is increased [83].

On the other hand, the short range 2d anti-ferromagnetic spin-spin correlation persists even in the superconducting phase of the underdoped cuprates. This has been verified via INS experiments [93]. Moreover, recent theoretical studies have pointed out that the spin fluctuations in the AFM quantum critical region of the layered Iron (Fe) based superconductors and in some heavy fermion compounds can be modelled by dissipative quantum XY model, and hence the statics and dynamics of topological excitations are the key factors for 2d spin-spin correlations [94, 95]. Therefore, investigation on the dynamics of the BKT vortices/merons may also substantially enhance the microscopic understanding of lightly doped anti-ferromagnetic cuprates and the above mentioned other systems as well [80, 94–96].

The above mentioned facts motivate us to investigate and test in detail the applicability of the semi-classical-like treatment mentioned above to the INS results corresponding to real anti-ferromagnetic systems with $S=1/2$ [84]. For this exercise La_2CuO_4 is selected as the reference system [7,8]. It is a quasi-2d spin $1/2$ AFM whose magnetic lattice structure is a square lattice with only nearest neighbour interaction and therefore, it becomes an ideal candidate for such an investigation.

In this chapter, I shall describe our semi-classical theory of spin dynamics induced by topological excitations corresponding to 2d XXZ anti-ferromagnetic systems. The theory is based on vortex-gas phenomenology explained in chapter 1. The formalism is very similar in spirit to the case of ferromagnetic systems described in Section 2.2 however, in this case topological excitations are built on the background of the Néel state, using the bipartite classical spin configuration corresponding to an XY- anisotropic Heisenberg anti-ferromagnet on a square lattice. The instrumental resolution has been incorporated via a suitably chosen spectral window function and the detailed balance condition has also been incorporated via the Windsor factor (see Section 2.2 for details) [84]. Subsequently, this formalism has been employed to analyse the available results from the INS experiment performed on La_2CuO_4 . Critical behaviour of this material remains similar to that of 2d XY model within a specific range of temperature, viz., $260 K < T < 360 K$. Numerical calculations for the integrated intensities have been presented in this chapter. The results for the integrated intensities for our spin $\frac{1}{2}$ model corresponding to different temperatures, show occurrence of vigorous unphysical oscillations [84]. The results for the calculation of moment of DSFs have also been presented to understand how far the vortex-gas phenomenology can capture the entire spin dynamics corresponding to La_2CuO_4 within the above mentioned temperature range.

Contents of the present chapter are organized as follows: Section 3.2 the semi-classical formalism of mobile topological excitations corresponding to 2d XXZ model is described. In Section 3.3, a brief description of the useful properties of the material La_2CuO_4 is provided. The integrated intensities for different temperatures are computed numerically in Section 3.4. In the same Section, the moment of the semi-classical convoluted DSFs are also calculated. We end this by summarising the outcome of our analysis in Section 3.5.

3.2 Spin dynamics in presence of topological excitations

The dynamics of mobile topological excitations in an anti-ferromagnetic system on a two-dimensional square lattice have been analysed both analytically and numerically [37–41]. The analytical studies have been performed by assuming a classical ideal gas of vortices/merons where the vortices/merons obey Maxwell’s velocity distribution. The model system is described the XY-anisotropic Heisenberg (XXZ) Hamiltonian, viz.,

$$\mathcal{H} = -J \sum_{\langle ij,pq \rangle} (S_{ij}^x S_{pq}^x + S_{ij}^y S_{pq}^y + \lambda S_{ij}^z S_{pq}^z), \quad (3.1)$$

where $\langle ij,pq \rangle$ label the nearest neighbour sites on a two-dimensional square lattice and $J(< 0)$ is the anti-ferromagnetic exchange coupling. Here λ is the anisotropy parameter whose pure XY and isotropic Heisenberg limit correspond to $\lambda = 0$ and 1 respectively [84].

The structures of the vortices/merons have been obtained by solving the classical equations of motion corresponding to the Hamiltonian given by (3.1). In deriving the classical equations of motion the spins have been considered to be classical objects (classical spin fields $S(\mathbf{r}, t)$) as a function of position coordinates and time, which are defined on the entire lattice. At even or odd lattice sites these spin fields become identical to the following bi-partite spin configurations,

$$\begin{aligned} S_{ij}^{even} &= +S[\sin(\Theta_{ij} + \theta_{ij}) \cos(\Phi_{ij} + \phi_{ij}), \sin(\Theta_{ij} + \theta_{ij}) \sin(\Phi_{ij} + \phi_{ij}), \cos(\Theta_{ij} + \theta_{ij})], \\ S_{ij}^{odd} &= -S[\sin(\Theta_{ij} - \theta_{ij}) \cos(\Phi_{ij} - \phi_{ij}), \sin(\Theta_{ij} - \theta_{ij}) \sin(\Phi_{ij} - \phi_{ij}), \cos(\Theta_{ij} - \theta_{ij})] \end{aligned} \quad (3.2)$$

where ‘*even*’ and ‘*odd*’ signifies the two different sub-lattices [34]. The static spin configuration corresponding to the merons are described by the capital angles $\Theta(\mathbf{r})$ (polar) and $\Phi(\mathbf{r})$ (azimuthal), and the time dependent small angles $\theta(\mathbf{r}, t)$ and $\phi(\mathbf{r}, t)$ describes the corresponding deviations from the static structure due to the motion of the merons and the spin dynamics above BKT transition temperature T_{BKT} [40, 41]. The expression for the vortex core radius is given by [40, 41]

$$r_v = \frac{a}{2} \sqrt{\frac{\lambda}{1-\lambda}}. \quad (3.3)$$

The methodology for calculation of the in-plane dynamical structure function (in-plane DSF) $S^{xx}(\mathbf{q}, \omega)$ is similar to that given in Section 2.2. Considering the velocity distribution obeyed by the merons to be of Maxwellian type the in-plane DSF is calculated to be,

$$S^{xx}(\mathbf{q}, \omega) = \frac{S(S+1)}{2\pi} \frac{\gamma^3 \xi^2}{(\omega^2 + \gamma^2 [1 + (\xi \mathbf{q}^*)^2])^2} \quad (3.4)$$

with $\gamma = \frac{\sqrt{\pi\bar{u}}}{2\xi}$, where $\mathbf{q}^* = (\mathbf{q}_0 - \mathbf{q})$; $\mathbf{q}_0 = (\pi/a, \pi/a)$ and in our case $S = \frac{1}{2}$. The above expression for the in-plane DSF is a squared Lorentzian exhibiting a central peak at $\omega = 0$ in ' ω '-space for a constant value of \mathbf{q} and exhibiting a central peak at the zone boundary of the first Brillouin Zone (BZ) in the ' q ' space for a constant value of ω [40, 41]. In the above expression \bar{u} is the root mean square (rms) velocity of the vortices and is given by,

$$\bar{u} = \sqrt{b\pi} \frac{JS(S+1)a^2}{\hbar} (\sqrt{n_v^f}) \tau^{-1/4}, \quad (3.5)$$

where $n_v^f \sim (2\xi)^{-2}$ is the density of free vortices at $T > T_{BKT}$ [37]. Here $\xi = \xi_0 e^{b/\sqrt{\tau}}$ is the intra-layer two-spin correlation length due to the presence of vortices, where ξ_0 is of the order of lattice spacing ' a ', $\tau = (\frac{T}{T_{BKT}} - 1)$ is the reduced temperature, and b is a dimensionless parameter whose numerical value is generally around 1.5 [65, 80]. The quantity $S^{xx}(\mathbf{q}, \omega)$ is sensitive to the in-plane structure of the vortices/merons [40, 41].

Following the steps similar to the case of ferromagnetic model (as explained in 2.2) it can be shown that the effective analytical expression for the out-of-plane dynamical structure function (out-of-plane DSF) $S^{zz}(\mathbf{q}, \omega)$ in the limit of very small ' q ' is given by [40, 41]

$$S^{zz}(\mathbf{q}, \omega) = \frac{n_v^f \bar{u}}{32(1+\lambda)^2 J^2 \sqrt{\pi} q^3} \exp[-(\frac{\omega}{\bar{u}q})^2]. \quad (3.6)$$

The above form of the out-of-plane dynamical structure function is a Gaussian, exhibiting again a central peak at $\omega = 0$, when plotted in the constant \mathbf{q} -scan. The function $S^{zz}(\mathbf{q}, \omega)$ is sensitive to the out-of-plane shape of the vortices/merons [40, 41].

In the case of layered systems, in a suitable regime in the parameter space comprising of temperature and wave vector where these systems behave effectively as two-dimensional systems, the integrated intensity corresponding to a typical inelastic neutron scattering experiment is given by

$$I(\omega) \approx \int \sum_{\alpha} S^{\alpha\alpha}(\mathbf{q}_{2D}, \omega) dq_x dq_y, \quad (3.7)$$

where the quantity $S^{\alpha\alpha}(\mathbf{q}_{2D}, \omega)$ represents the intra-layer in-plane spin dynamical structure function when $\alpha = x$ and y and the intra-layer out-of-plane spin dynamical structure function when $\alpha = z$ [21, 50, 51, 84].

The approach taken in this chapter is quite similar to that adopted in the previous chapter corresponding to the case of ferromagnetic systems [83]. In order to compare theoretical results

with experimental one the DSF, obtained from the model under consideration, is multiplied with the resolution function $R(t)$ (in time domain) or convoluted with $\tilde{R}(\omega - \omega')$ (in the frequency domain), as has been done in the case of ferromagnetic system (see Chapter 2) [84]. Hence, the components of the convoluted integrated intensity turn out to be,

$$I_{conv}^{\alpha\alpha}(\omega) = \int dq_x dq_y \int d\omega' \tilde{R}(\omega - \omega') S^{\alpha\alpha}(\mathbf{q}_{2D}, \omega'). \quad (3.8)$$

The resolution function has to be chosen in such a way that minimum ripples occur at the end points of the resolution width. The different parameters of the resolution function can be obtained from the resolution half width or the full width at the half maximum (FWHM) which are quoted in the experiments [84]. Since X and Y components of the spins are symmetric i.e., $S^{xx}(\mathbf{q}, \omega) = S^{yy}(\mathbf{q}, \omega)$ the total intensity comes out to be,

$$I(\omega) = 2I^{xx}(\omega) + I^{zz}(\omega). \quad (3.9)$$

Furthermore, keeping in mind the low spin situation the quantum mechanical detailed balance condition is incorporated in our formalism [54]. Then semi-classical estimate for $I(\omega)$, denoted by $I_{conv}^{SC}(\omega)$ is recovered by the relation,

$$I_{conv}^{SC}(\omega) = \frac{2}{1 + \exp(\frac{-\hbar\omega}{k_B T})} I_{conv}(\omega), \quad (3.10)$$

where the factor $\frac{2}{1 + \exp(\frac{-\hbar\omega}{k_B T})}$ is the detailed balance factor and is called the Windsor factor [87]. The superscript ‘SC’ stands for the term semi-classical [84].

It is worthwhile to mention that the above formulation based on dilute vortex/meron gas phenomenology hold for unbound anti-vortices/anti-merons too on the basis of the assumption that the vortices/merons and anti-vortices/anti-merons do not interact with each other [84].

3.3 Relevant information on La_2CuO_4

In this chapter, the formalism of Section 3.2 has been applied to the anti-ferromagnetic material La_2CuO_4 on which inelastic neutron scattering experiments (INS) involving polarized neutron beam have been performed [7, 8]. The behaviours of this material across the phase diagram as a function of temperature and doping are very interesting. In particular, the phase diagram of it is remarkably rich in terms of various competing phases and phase transitions. These include a tetragonal-orthorhombic structural transition, 3d AFM ordering, a crossover from

3d AFM phase to a phase exhibiting 2d magnetism, a low temperature 3d spin-glass phase and metal-insulator transition as well, and most importantly the superconducting transition (see Ref [7,8] and *references therein*). The undoped (non-superconducting) material is an XY-anisotropic quasi-two-dimensional spin 1/2 quantum Heisenberg anti-ferromagnet (AFM) where the Cu^{2+} ions corresponding to the CuO_2 planes order antiferromagnetically. The structure of this material is characterized by 2d square lattices corresponding to CuO_2 planes exhibiting an AFM interaction between the nearest-neighbours with very small AFM coupling between two different CuO_2 planes [7,8]. The spin Hamiltonian relevant to the above material is given by,

$$\mathcal{H} = \underbrace{\left(-J \sum_{\langle i,j \rangle} \mathbf{S}_i \cdot \mathbf{S}_j + J_A \sum_{\langle i,j \rangle} S_i^z S_j^z\right)}_{\text{intra-layer part}} - \underbrace{J' \sum_{\langle i,k \rangle} \mathbf{S}_i \cdot \mathbf{S}_k}_{\text{inter-layer part}} \quad (3.11)$$

where $\langle i,j \rangle$ represents the intra-layer nearest neighbour interaction and $\langle i,k \rangle$ represents the inter-layer nearest neighbour interaction. In the above Hamiltonian, J is the isotropic part and J_A is the anisotropic part of the intra-layer exchange coupling, and J' is the inter-layer exchange coupling. The temperature corresponding to conventional ordering i.e., the Néel temperature for the quasi-two dimensional system (La_2CuO_4) is given by $T_N = 240$ K. The intra-layer part of the above Hamiltonian (3.11) can be simplified by expressing $(J - J_A)$ as λJ to obtain the model Hamiltonian (3.1), where λ is the anisotropy parameter. The relevant physical parameters corresponding to La_2CuO_4 are given in the Table 3.1 [97].

Parameter	Magnitude
J (intra-layer)	~ 1345 K
J_A (intra-layer)	~ 0.269 K
J' (inter-layer)	~ 0.04 K
anisotropy parameter (λ)	0.9998
lattice parameter(a)	5.39 Å
Néel temperature (T_N)	240 K

Table 3.1: *Relevant parameters for La_2CuO_4 .*

Next we try to determine the temperature range over which the material La_2CuO_4 behaves effectively as a two-dimensional material. From the neutron scattering data for quasi-two-dimensional spin 1/2 XY-anisotropic ferromagnet K_2CuF_4 , it was found that in a temperature

regime $T_1 \leq T \leq T_2$, where the lower (T_1) and the upper (T_2) limits are defined by the following relations,

$$\begin{aligned}\xi(T_1) &= \sqrt{\frac{|J|}{|J'|}} \\ \xi(T_2) &= \sqrt{\frac{|J|}{|J_A|}}\end{aligned}\quad (3.12)$$

the system behaves as a 2D XY system [64,65]. Assuming that the above phenomenological argument holds for the layered anti-ferromagnetic systems as well, we can determine the above

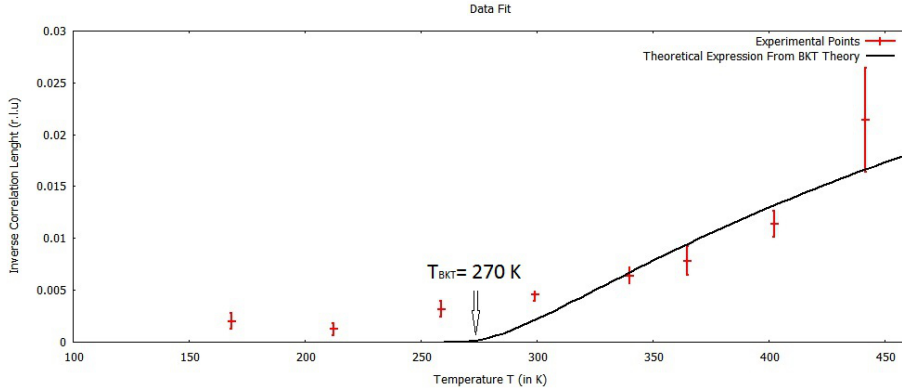


Figure 3.1: *Fitting of the experimentally obtained inverse correlation length with the corresponding theoretical expression (see (3.13)). Solid line corresponds to the theoretical expression. BKT transition temperature is $T_{BKT} = 270K$ [84].*

two temperature limits to be $T_1 \approx 260K$ and $T_2 \approx 360K$ for La_2CuO_4 . Within this temperature regime the Hamiltonian (3.11) can effectively be represented by the Hamiltonian (3.1). It is worthwhile to point out that since in the above temperature regime the system is effectively a two-dimensional one, long range anti-ferromagnetic ordering is absent in this regime [9]. Further, within the above mentioned temperature range the BKT inspired ideal vortex/meron- gas phenomenology is expected to be valid and we can therefore use the theoretical expression for the inverse correlation length (expressed in r.l.u),

$$\kappa(T) = \frac{1}{\pi} e^{-b/\sqrt{\tau}} \quad (3.13)$$

as predicted by Kosterlitz and Thouless, to fit the experimentally obtained inverse correlation length [12]. This gives the value of the BKT transition temperature as $T_{BKT} \approx 270K$ for

La_2CuO_4 (see Figure 3.1). In this work we shall make use of the above value of T_{BKT} to calculate the convoluted in-plane integrated intensity, $I_{conv}^{xx}(\omega)$ and the convoluted out-of-plane integrated intensity, $I_{conv}^{zz}(\omega)$ by making use of a series of equations starting from (3.4) to (3.8).

3.4 Calculations of the integrated intensities

In this section, I am going to present the calculation of the integrated intensities for the material La_2CuO_4 at different temperatures using the semi-classical formalism explained in Section 3.2 and compare the results with the corresponding experimental data [84]. Let us start by calculating the convoluted in-plane integrated intensity, $I_{conv}^{xx}(\omega)$. The expression for the $I_{conv}^{xx}(\omega)$ is given by (3.8) with $\alpha = x$, where the in-plane DSF, $S^{xx}(\mathbf{q}_{2D}, \omega)$ is given by (3.4). In the experimental investigations on La_2CuO_4 , to find the neutron intensity as a function of momentum transfer ' $\hbar\mathbf{q}$ ' the scans in the ' \mathbf{q} '-space have been performed about the zone boundary of the first Brillouin Zone within the range, $-0.1 \leq \mathbf{q}^* \leq 0.1$, expressed in r.l.u (see Figure 3.2) [7, 8]. In calculating $I_{conv}^{xx}(\omega)$ using (3.8) we have also made use of the above mentioned

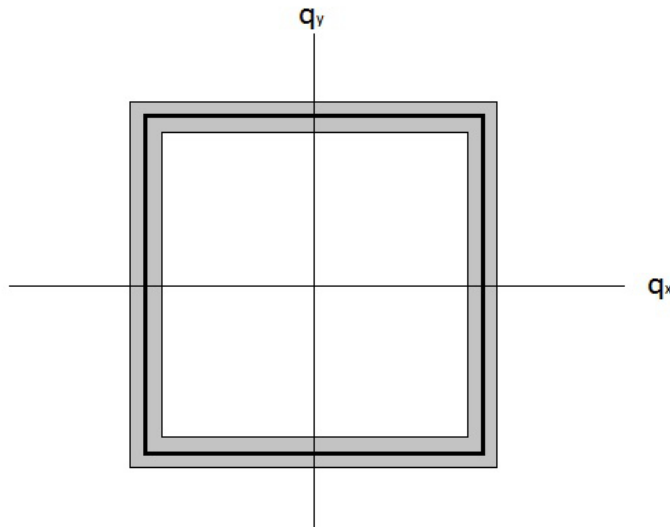


Figure 3.2: *Shaded part is the region of Brillouin zone over which the integration in the q -space is performed.*

regime of the Brillouin Zone. The resolution function has been chosen in the form of the Tukey window to convolute the in-plane DSF [84]. This is one of the most commonly used spectral smoothing functions in the field of spectral analysis [52, 53]. The experimental resolution width

is 1.4 meV at the full width at half maximum (FWHM), as specified in the experiment [7, 8]. We compute $I_{conv}^{xx}(\omega)$ for four different temperatures, viz., 290 K, 320 K, 350 K and 375 K. The

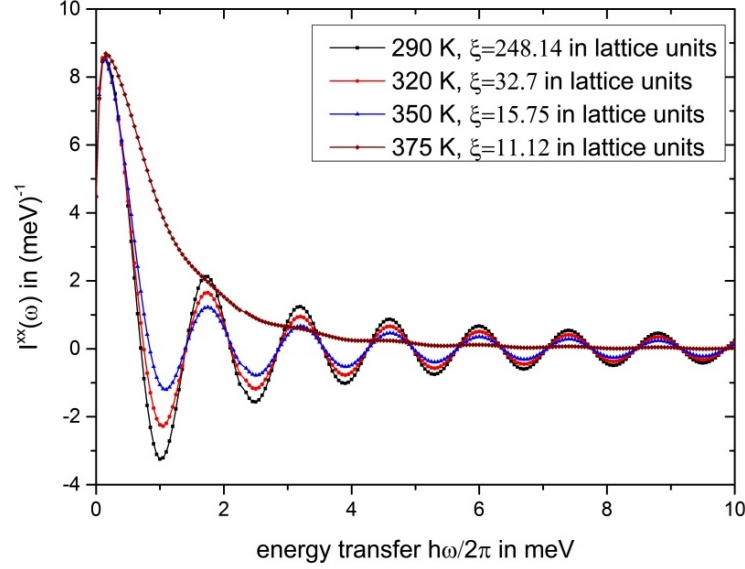


Figure 3.3: *The plot of convoluted (with Tukey window function) in-plane integrated intensity $I_{conv}^{xx}(\omega)|_{SC}$ at four different temperatures, viz., 290 K, 320 K, 350 K and 375 K. The rms velocities at these temperatures are $\bar{u} = 0.00365 \frac{a}{t_{nat}}$, $0.0836 \frac{a}{t_{nat}}$, $0.085 \frac{a}{t_{nat}}$, $0.2323 \frac{a}{t_{nat}}$ respectively [84].*

semi-classical convoluted in-plane integrated intensities denoted by, $I_{conv}^{xx}(\omega)|_{SC}$ are plotted as functions of energy transfer in Figure 3.3, where (3.10) have been used. The plots clearly exhibit that $I_{conv}^{xx}(\omega)|_{SC}$ oscillates vigorously after convoluting with the Tukey function, although the ‘central peak’ still persists [84]. This is quite contrary to what we experienced in the case of ferromagnet [83].

To avoid such oscillations we have tried performing the above calculations using a modified version of the Tukey function (see equations (C.4) and (C.5) in Appendix C). The integrated intensity (at 290 K) corresponding to this new window function is also plotted in Figure 3.4 along with the same corresponding to the use of Tukey function. From this figure it is clearly visible that the unwanted oscillations diminish considerably when we use the modified Tukey function [84]. More interestingly, Figure 3.5 indicates that at even higher temperature, viz., at around 375 K ($\approx 1.388T_{BKT}$) both Tukey function and modified Tukey function lead to

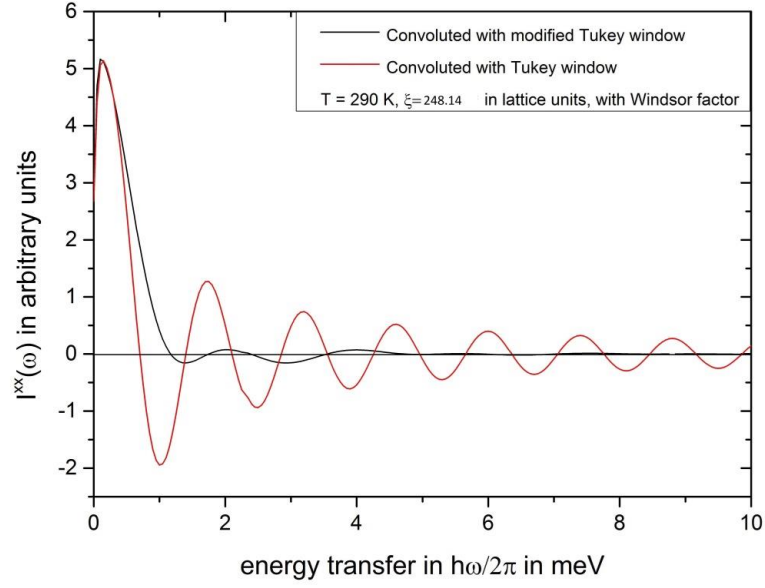


Figure 3.4: The plot of convoluted in-plane integrated intensity $I_{conv}^{xx}(\omega)|_{SC}$ at 290 K. The red solid line corresponds to the $I_{conv}^{xx}(\omega)|_{SC}$ obtained by using the Tukey window function (see (C.3)). The black solid line corresponds to the $I_{conv}^{xx}(\omega)|_{SC}$ obtained by using the modified Tukey window function (see (C.5)) [84].

very similar results. The oscillations are totally absent in the theoretical plot of $I_{conv}^{xx}(\omega)|_{SC}$ vs. energy transfers corresponding to both the resolution functions. It is worthwhile to mention that the corresponding temperature $T=375$ K ($> T_2$) falls just outside the range $T_1 \leq T \leq T_2$, within which the BKT phenomenology remains valid. However, the use of such a modified Tukey function may wipe out some of the genuine and intrinsic fluctuations present in the anti-ferromagnetic systems in two dimensions. Hence, we make use of the Tukey function only for our purpose [84].

We further notice a slight shift in the position of the central peak. This is due to the inclusion of quantum mechanical detailed balance condition [84]. The important point here is that the shift is well within the resolution width 1.4 meV at the FWHM, and hence the peak is truly a central peak situated at $\hbar\omega = 0$.

Exactly the same results hold for $I_{conv}^{yy}(\omega)|_{SC}$ which is obvious from the symmetry argument [84]. The normalization factors required for the quantitative comparison between the theoretical and the experimental results are estimated from the neutron count corresponding to

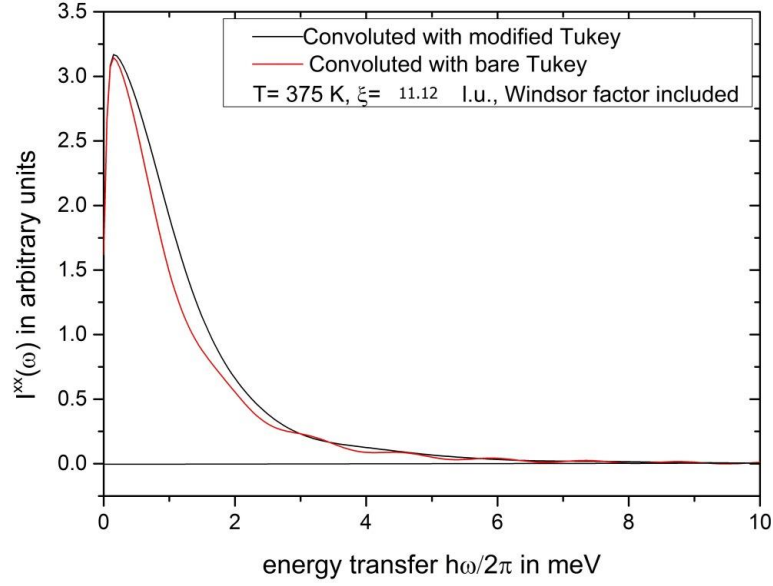


Figure 3.5: The plot of convoluted in-plane integrated intensity $I_{conv}^{xx}(\omega)|_{SC}$ at 375 K. The red solid line corresponds to the $I_{conv}^{xx}(\omega)|_{SC}$ obtained by using the Tukey window function (see (C.3)). The black solid line corresponds to the $I_{conv}^{xx}(\omega)|_{SC}$ obtained by using the modified Tukey window function (see (C.5)) [84].

the experimental results for La_2CuO_4 .

Out-of-plane integrated intensities, $I_{conv}^{zz}(\omega)|_{SC}$ are now evaluated for the same set of temperatures as have been considered earlier for the evaluation of $I_{conv}^{xx}(\omega)|_{SC}$ (see Figure 3.6). The expression for the $I_{conv}^{xx}(\omega)$ is given by (3.8) with $\alpha = z$, where the out-of-plane DSF, $S^{zz}(\mathbf{q}_2\mathbf{D}, \omega)$ is given by (3.6). In this case we find that the out-of-plane integrated intensity oscillates only at lower temperatures near $T = T_{BKT}$. It is worth recalling here that the magnitude of the out-of-plane integrated intensity is proportional to the density n_v^f and the rms velocity \bar{u} of the free vortices/merons. Since both density n_v^f and the rms velocity \bar{u} increases with increasing temperature the out-of-plane part of the spin-spin correlation (see eqns. (3.6) and (3.8)) acquire dominance (considerable magnitude) only at higher temperatures much above T_{BKT} [84].

Furthermore, the absolute magnitude of the integrated intensity $I_{conv}^{xx}(\omega)|_{SC}$ is higher (almost 10^7 times for the highest temperature considered here) than that of $I_{conv}^{zz}(\omega)|_{SC}$ at temperatures above T_{BKT} . This is so because, $I_{conv}^{zz}(\omega)|_{SC}$ is proportional to n_v^f and it increases with the increasing value of the rms velocity \bar{u} . The typical energy scales involved in the dynamics of

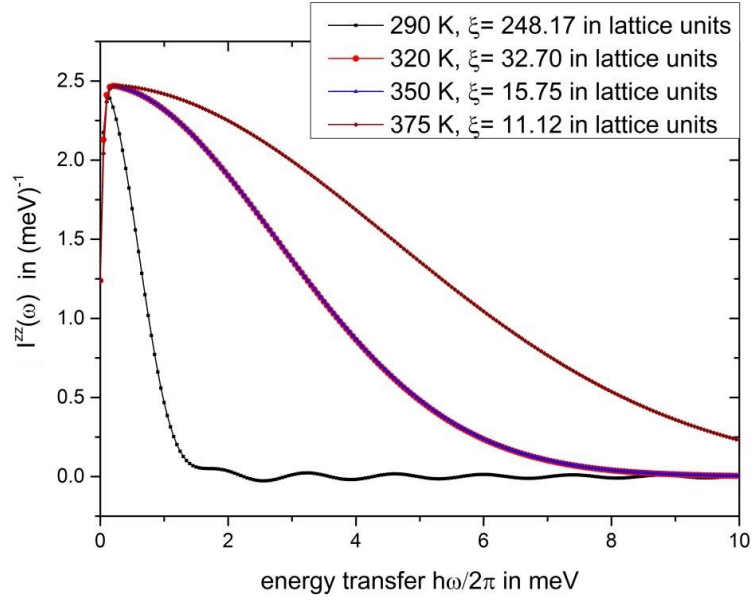


Figure 3.6: The plot of convoluted out-of-plane integrated intensity $I_{conv}^{zz}(\omega)|_{SC}$ at four different temperatures, viz., 290 K, 320 K, 350 K and 375 K. The rms velocities at these temperatures are $\bar{u} = 0.00365 \frac{a}{t_{nat}}$, $0.0836 \frac{a}{t_{nat}}$, $0.085 \frac{a}{t_{nat}}$, $0.2323 \frac{a}{t_{nat}}$ respectively. The order of magnitude of the $I_{conv}^{zz}(\omega)|_{SC}$ at the above mentioned four different temperatures are 10^{-13} , 10^{-10} , 10^{-8} and 10^{-7} respectively [84].

mobile vortices/merons corresponding to the anti-ferromagnetic system La_2CuO_4 are such that n_v^f is very small (compared to the case of ferromagnet where the free vortex number density turns out to be appreciable) [83, 84]. For the present case of La_2CuO_4 at $T = 350K$, the numerical value for the density of free vortices turns out to be $n_v^f = 1.36 \times 10^{-4} a^{-2}$ and the same for the rms velocity turns out to be $\bar{u} = 9163 m/sec = 0.085 \frac{a}{t_{nat}}$, where $t_{nat} = \frac{2\hbar}{\sqrt{3}J}$ ($\approx 5 \times 10^{-15}$ sec) is the natural time scale for the system [84]. In contrast, in the case of ferromagnetic system K_2CuF_4 the value of the density of free vortices is found to be $n_v^f = 1.009 \times 10^{-3} a^{-2}$ and that for the rms velocity is found to be $\bar{u} = 87.07 m/sec = 0.1352 \frac{a}{t_{nat}}$ at $T = 6.75K$, where $t_{nat} = 6.4 \times 10^{-13}$ sec is the natural time scale [83]. Interestingly enough, the unbound merons/vortices above T_{BKT} move much faster (with a rms velocity of 9163 m/sec at 350 K) than a typical Copper (Cu) atom whose rms velocity (generally considered to be the thermal velocity) is around 370.6 m/sec at 350 K [84].

The integrated intensities computed above correspond to the contributions only from the mobile vortices/merons. The experimental data whereas, contain contributions from both the mobile vortices/merons and fragile “spin wave like” modes. This spin wave like modes are damped and largely decaying above the Néel temperature. The extraction of the mobile vortex contribution from the experimental data is crucial for a more accurate comparison between the theoretical results and the experimental data and to do this one has to subtract the contributions from the above mentioned fragile “spin wave like” modes from the experimental data. It is worth recalling that in the case of ferromagnetic system, the fragile mode contributions have been subtracted by assuming the fragile mode contributions above T_c to be the same as the usual spin wave contributions below T_c . This assumption is however valid if and only if the temperature under consideration is in the near vicinity of the Curie temperature (T_c) of the system [83, 84].

In the present case corresponding to the anti-ferromagnetic system La_2CuO_4 , the situation is somewhat different from the ferromagnetic one in the sense that the temperatures dealt with are far above the Néel temperature T_N . Hence the above mentioned procedure, which was followed for the ferromagnetic systems to subtract the fragile mode contributions, is not valid in the present case [83, 84].

Moreover, at any finite temperature above T_{BKT} , it is to be kept in mind that not all vortices/merons are freely moving and that bound vortex-anti-vortex pair density remains finite. Hence, one has to estimate further the contribution from these bound vortex-anti-vortex pairs at different temperatures and subtract them from the experimental data. To estimate the bound vortex contribution we have tried to apply the same methodology that has been outlined and used earlier for the ferromagnetic system (See Section 2.2). However, unlike the case of ferromagnet in this case the methodology leads to an unphysical behaviour viz., the vanishing of the out-of-plane DSF (see eqn. (3.6)) in the limit $\bar{u} \rightarrow 0$. Hence the estimation of the bound vortex contribution has not been carried out here.

The above calculations for the components of integrated intensities enable us to estimate theoretically the total integrated intensity using (3.9). In Figures 3.7 and 3.8 the total intensity $I_{conv}(\omega)|_{SC}$ has been compared to the experimental data at two different temperatures, viz., 290K and 350K respectively. The contributions from the fragile “spin-wave-like” modes can not

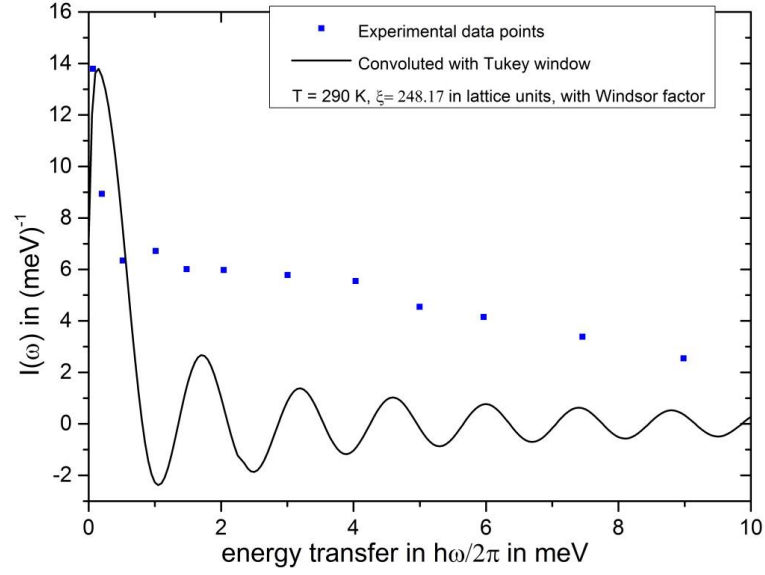


Figure 3.7: The plot of convoluted total integrated intensity $I_{conv}(\omega)|_{SC}$ at 290 K. The red solid line corresponds to the $I_{conv}(\omega)|_{SC}$ obtained theoretically by using the Tukey window function (see (C.3)). The dots are the experimental data [84].

be filtered out for the reasons stated earlier. It is clear from Figure 3.7 that the total intensity $I_{conv}(\omega)|_{SC}$ also oscillates vigorously at both the temperatures, when convoluted with the Tukey function. Moreover, the magnitude of the total intensity $I_{conv}(\omega)|_{SC}$, obtained theoretically at finite energy transfers, is very far from the corresponding values obtained in the experiment [84].

The inclusion of quantum mechanical detailed balance factor in our semi-classical like treatment has again caused a shift in the position of the central peak of the integrated total intensity at both the temperatures. However, this shift is well within the resolution width and therefore it is a genuine central peak at zero energy transfer. It is worthwhile to mention that all the above results based on dilute vortex/meron gas phenomenology hold for unbound anti-vortices/anti-merons too [84].

Let us further calculate the moment of the semi-classical dynamical structure function (DSF) $S_{SC}^{conv}(\mathbf{q}, \omega)$ (or simply the moment) using the following formula [21],

$$\int_{first\ B.Z.} \left(\frac{a}{2\pi}\right)^2 d^2\mathbf{q} \int_{-\infty}^{\infty} d\omega S_{conv}^{SC}(\mathbf{q}, \omega) = S(S+1),$$

$$\text{or } \int d\omega I_{conv}^{SC}(\omega) = S(S+1), \quad (3.14)$$

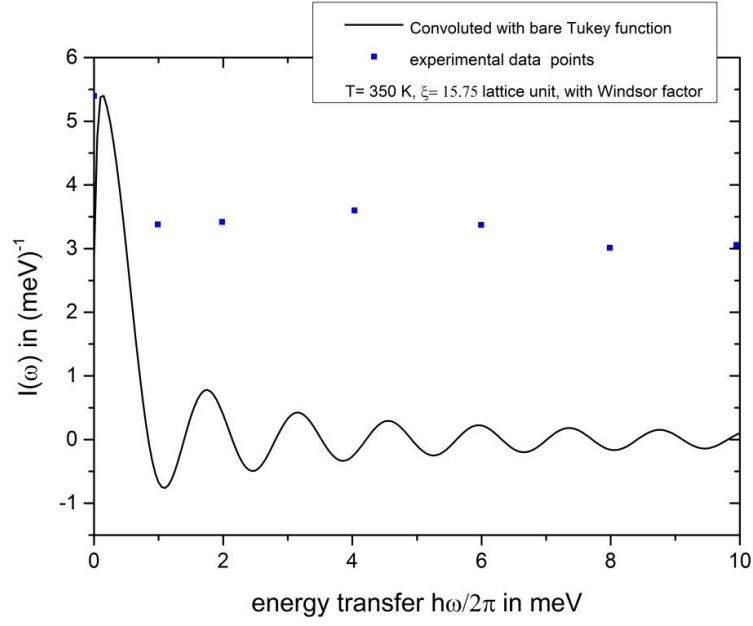


Figure 3.8: The plot of convoluted total integrated intensity $I_{conv}(\omega)|_{SC}$ at 350 K. The red solid line corresponds to the $I_{conv}(\omega)|_{SC}$ obtained theoretically by using the Tukey window function (see eqn. (C.3)). The dots are the experimental data [84].

where $I_{conv}^{SC}(\omega)$ is given by equation (3.10) and in obtaining the same, the integration over the wave vector space in equation (3.8) is performed over the first Brillouin zone (B.Z.) with contributions from both vortices and anti-vortices being summed; S is the value of the spin corresponding to the system under consideration and in our case it is $S = 1/2$. The above equation signifies that if the spin dynamics is entirely captured by the DSF corresponding to mobile vortices and anti-vortices, the value of the zeroth moment must be $S(S + 1)$.

T	$\frac{T}{T_{BKT}}$	moment in the unit of $S(S + 1)$ *
290 K	1.074	0.0400
320 K	1.185	0.2412
350 K	1.296	0.3583
375 K	1.388	0.3770

Table 3.2: *The zeroth moment of the semi-classical dynamical structure function corresponding to the dynamics of mobile vortices and anti-vortices*(* corresponding to the use of Tukey function) [84].

The values of the moment of the semi-classical convoluted DSF corresponding to the use of Tukey function at four different temperatures are tabulated in TABLE 3.2. At 290K i.e. around $1.074T_{BKT}$, the combined dynamics of mobile vortices and anti-vortices capture only about 4% of the entire spin dynamics of the system. However, at higher temperatures around $1.296T_{BKT}$, the combined dynamics of mobile vortices and anti-vortices capture more than 35% of the entire spin dynamics of the system. This happens because at lower temperatures near T_{BKT} , the number of freely mobile vortices and anti-vortices are not large enough to capture the whole spin dynamics and the presence of fragile or damped spin waves (or single magnons and multi-magnon like modes) makes important enough contribution to the spin dynamics [84]. At higher temperatures however, more topological excitations become free and drive a large portion of the spin dynamics of the system. At this point, it is worth mentioning that for quantum ferromagnetic systems on two dimensional square lattice it has been shown that the formation of topological excitations of vortex/ meron types from the fragile magnons and multi-magnon composites is quite plausible [85]. Moreover, some of the collective modes (i.e. magnon and multi-magnon modes) are expected to stay intact with their damped nature and thus can provide a significant contribution to the spin dynamics. In analogy with the three dimensional ferromagnetic systems where above the Curie temperature (T_c) the magnon-like collective excitations become fragile and damped, for pure two dimensional systems (where $T_c = 0$) the collective excitations become fragile at any finite temperature [57, 58, 85, 87, 98–100]. This process is expected to be operative in the anti-ferromagnetic systems too on pure two-dimensional lattices [84].

3.5 Summary

In this chapter, we have successfully addressed the role of quantum fluctuations in the spin dynamics induced by the topological excitations corresponding to low spin anti-ferromagnetic systems in low dimensions. The analysis in this chapter brings out both the strong and weak points of the conventional semi-classical theory for the dynamics induced by topological excitations. Let us first summarize the results of our calculations. We find vigorous oscillations in the convoluted in-plane integrated intensity when the Tukey window is used. These oscillations vanish only at higher temperatures which are outside the regime of validity of the BKT phenomenology. The use of a modified or refined Tukey function substantially removes the unwanted oscillations in the convoluted in-plane integrated intensity $I_{conv}^{xx}(\omega)|_{SC}$. Strikingly enough, at $T = 350$ K ($1.296 T_{BKT}$), we still find negative values of $I_{conv}^{xx}(\omega)|_{SC}$ even using the modified Tukey window function (see Figure 3.9). However, outside the temperature regime where the

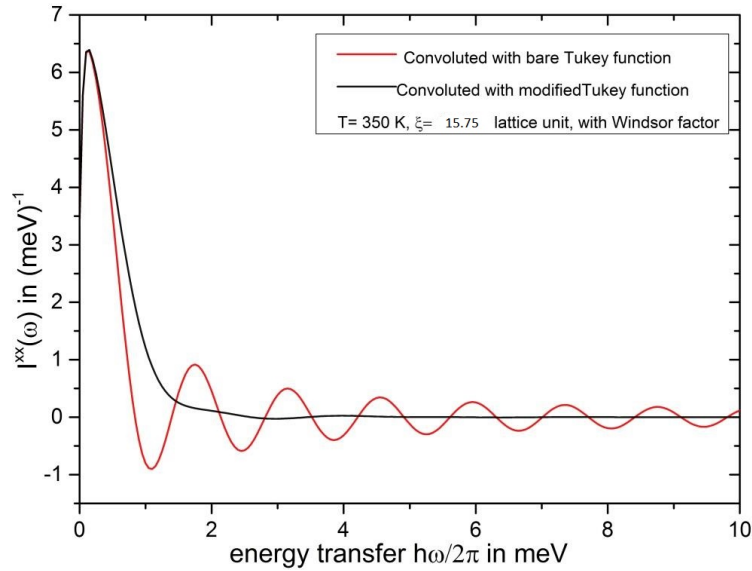


Figure 3.9: The plot of convoluted in-plane integrated intensity $I_{conv}^{xx}(\omega)|_{SC}$ at 350 K. The red solid line corresponds to the $I_{conv}^{xx}(\omega)|_{SC}$ obtained by using the Tukey window function (see (C.3)). The black solid line corresponds to the $I_{conv}^{xx}(\omega)|_{SC}$ obtained by using the modified Tukey window function (see (C.5)) [84].

BKT phenomenology is valid, computations with both the window functions give very similar results for $I_{conv}^{xx}(\omega)|_{SC}$. The possible explanation for these is that at higher temperatures the quantum effects are less prominent even for $S = \frac{1}{2}$ anti-ferromagnet. Therefore, the modified

Tukey window may actually be suppressing some genuine and inherent quantum fluctuation as well quite efficiently. The out-of-plane integrated intensities $I_{conv}^{zz}(\omega)|_{SC}$ (computed at different temperatures) are found to be sensitive to the choice of window function only at temperatures which are not very far from T_{BKT} (around $1.074 T_{BKT}$). Furthermore, it contributes negligibly to the total integrated intensity $I_{conv}(\omega)|_{SC}$ and hence the nature of the convoluted total integrated intensities at different temperatures turns out to be quite similar to that of the convoluted in-plane integrated intensities. However, the detailed quantitative comparison between the theoretical results and the experimental results corresponding to the total integrated intensities $I_{conv}(\omega)|_{SC}$ reveals that even though the conventional “semi-classical like” theory is able to predict the occurrence of the central peak, the magnitudes of the $I_{conv}(\omega)|_{SC}$ for finite values of energy transfer, obtained from theoretical analysis, differ by a huge factor from the corresponding experimental values. Moreover, apart from the spin dynamics induced by the mobile topological excitations, the fragile magnons and multi-magnon modes are quite likely to make important contribution towards this dynamics. Calculations of the moment of DSFs are indeed pointing towards this fact.

Let me further point out that the value of $\hbar\omega$ at which the onset of such unphysical behaviour occurs depends on the value of the spin (S). It has been shown in the case of ferromagnetic systems that the regime over which this unphysical behaviour persists, shrinks as the value of S increases [83]. Similar behaviour is expected to be operative in the anti-ferromagnetic systems also. It is also very important to emphasize the fact that in our calculational analysis the structure of the classical vortex/meron has been built in the background of the Néel state (see (3.2) of Section 3.2). Since the Néel state is not an exact ground state for the two-dimensional quantum anti-ferromagnetic spin systems, such a choice further adds to the reasons for the above mentioned unphysical behaviour.

Our investigations presented in this chapter and in chapter 2 establish the fact that a complete quantum treatment is essential to describe the detailed features of the dynamics of mobile topological excitations corresponding to the quasi-two-dimensional low-spin magnetic systems, by taking into consideration the interactions between the topological excitations and the conventional excitations (magnons) as well. The possible scheme for such a quantum formalism is quite similar to that has been sketched out in the case of ferromagnetic model in section 2.5. In chapter 5 this has been described in a considerable details. Furthermore, motivated by

the lack of understanding on the magnon-vortex interactions, in the second part of my thesis I shall describe our efforts in understanding the microscopic aspects of the topological excitations corresponding to 2d XXZ models.

Chapter 4

Microscopic description of quantum spin vortices and anti-vortices

4.1 Introduction

In magnetic systems in low dimensions, viz, one dimension (or rather quasi-one dimension) and two dimensions (or rather quasi-two dimensions), the topological excitations of solitons and vortices/merons types occur quite naturally, as they are thermodynamically feasible [12,13]. In particular, vortex/meron like topological excitations play a very important role in the physics of 2d magnetic systems. These excitations participate in bringing out the famous Berezinskii-Kosterlitz-Thouless (BKT) transition in the easy-plane magnetic systems. This phase transition is characterized by the binding to unbinding processes involving vortex, anti-vortex (or rather meron, anti-meron) excitations [12,13]. Above a transition temperature T_{BKT} the dynamics of freely moving topological excitations provides non-trivial contribution in the dynamical correlation function giving rise to the well-known “central peak in both two dimensional ferromagnetic and anti-ferromagnetic models [38–41]. In the inelastic neutron scattering (INS) experiment, the existence of such a central peak at $\omega = 0$ has been observed in the plot for the dynamical structure function $S(\mathbf{q}, \omega)$ versus neutron energy transfer $\hbar\omega$ in the constant “ \mathbf{q} ” scan in layered magnetic systems [4, 7, 8, 64, 65].

In chapters 2 and 3, I have already explained in details that the semi-classical phenomenological theories turn out quite inadequate in explaining the experimental results corresponding to low spin layered magnetic systems even after incorporation of suitable quantum corrections

in the calculations. In particular, in chapter 3 the calculations of the moment of the semi-classical dynamical structure function corresponding to the vortices and anti-vortices indicates that only the dynamics of mobile vortices and anti-vortices is not sufficient in capturing the full spin dynamics in the layered magnetic systems. This is expected to be true even for layered ferromagnetic systems. This is because the phenomenological description of ideal vortex gas assumes that the vortex/merons take the shapes of spin profiles independent of spin waves. Hence, a quantum description of the magnon-vortex interaction is of extreme necessity.

In last few years there has been a renewed research interest especially in the quasi-two dimensional magnetic systems motivated by the aims of building magnetic devices. These devices make use of mobile vortices [101–103]. In the magnetic thin films the interplay between the exchange interaction and the magnetic dipole - dipole interaction causes the formation of domain structures in absence of magnetic fields. Furthermore, each of these domains contains a magnetic vortex characterized by in-plane magnetization curling around the center. The component of magnetization perpendicular to the plane of the film serves as ‘Polarization’ of the vortex core [104]. Such a magnetic vortex has been proved to be a potential candidate for switching devices as well as for data storage where the ‘Polarization’ of the core can be manipulated in a controlled manner by applying external magnetic field [104]. Direct experimental evidences of such vortex states have been verified by Magnetic Force Microscopy (MFM) and also by the spin-polarized Scanning Tunnelling Microscopy (STM) [105, 106]. Although the vortices (in the sense of a domain structure) described above are fundamentally different from the vortices/merons arising in the BKT scenario the issue of the interaction between the magnons and vortices are quite generic. In this regard it has been found that the magnon modes which are present within the vortex core experience an effective magnetic field because of the vortex itself [107]. This effective magnetic field appears due to the topological property of the vortices. Therefore, magnons interact with the vortices/merons via the effective field mentioned above. The most important effect of such an interaction is the excitation of certain spin-wave modes due to vortex motion and subsequent modification of vortex motion due to these excited spin-wave modes [108]. However, all the above mentioned scenario of vortex-spin-wave interaction are described in the continuum description of the Hamiltonian (2.1) which is given in (2.3). Such a description comes with its own limitation of not being applicable to spin 1/2 systems where only two discrete states are available. In such a situation a microscopic understanding of the

composition or rather construction of these vortices and anti-vortices are extremely needful, of course taking into account the correct topological properties.

In this chapter, I describe our investigations on the possible composition of these topological excitations of true quantum nature in two-dimensional anisotropic quantum Heisenberg ferromagnetic model. It turns out that the interactions between the different multi-magnon modes play a very important role in the formation of the above excitations [85]. These multi-magnon interactions are generally neglected in the linear spin wave/one-magnon theory and even in the BKT theory. Magnon modes are low energy excitations and represent a quantized coherent precessional motion of all the spins around the direction of the spontaneous magnetization in the long range ordered phase. These modes however, become ill-defined in the short range ordered phase [57, 58]. In contrast, the quantum states representing topological spin excitations are found to be stable even in the short range ordered phase when the system size is very large, as I shall demonstrate in this chapter.

The present chapter is organized as follows. In Section 4.2, I shall explain our construction of the quantum state corresponding to charge 1 vortex (and charge 1 anti-vortex as well) in the strong anisotropy limit of the XXZ model. In section 4.3, I shall establish the connection between the quantized vortex states and the multi-magnon composite states. In section 4.4, I shall analyse the quantum mechanical stability of such vortex/anti-vortex states for both the cases of infinite dilute limit and the finite density limit. Finally in Section 4.6, I present the summary of the present chapter and discuss possible application of the results of our present investigation to the real magnetic systems.

4.2 Construction of quantum spin vortex and anti-vortex

The starting point of our construction is the XY anisotropic quantum Heisenberg (XXZ) Hamiltonian,

$$\mathcal{H} = -J \sum_{\langle ij, pq \rangle} (S_{ij}^x S_{pq}^x + S_{ij}^y S_{pq}^y + \lambda S_{ij}^z S_{pq}^z), \quad (4.1)$$

on a two-dimensional square lattice with nearest neighbour interaction, where $\lambda (0 \leq \lambda < 1)$ is the anisotropy parameter and for ferromagnetic systems $J > 0$, and the index ‘ ij ’ represents a lattice point on the $N \times N$ square lattice. Here S_{ij}^x, S_{ij}^y and S_{ij}^z are the x, y and z components

respectively of the spin operator on the ij -th lattice site. We shall concentrate on the $S = \frac{1}{2}$ ferromagnetic model in the very strongly XY- anisotropic limit ($\lambda \rightarrow 0$, i.e., λ is vanishingly small, but $\lambda \neq 0$). With this smallest 'S' value, the model is in-fact in the extreme quantum regime.

It is worthwhile to mention here that the classical counterpart of the above model admits of the well-known meron solution [37–40, 109, 110]. Numerical studies have led to the conclusion that there is a critical value of the anisotropy parameter, say λ_c , below which only the static flattened merons or ordinary vortices are stable and above that the normal merons are stable [109, 110].

The model Hamiltonian (4.1) is well known to possess a continuously degenerate ground state. The state (and eigen-state as well) with all spins aligned along the '+ve' or '-ve -z' direction can be achieved by applying a vanishingly small external magnetic field. Having said that, we start by taking a trial ground state with all the nearest neighbour spins being aligned in the -ve z direction, and the state is defined by $S_{ij}^-|0\rangle = 0$ for every i, j [85]. Explicit form for the ground state on the square lattice is given by,

$$\begin{aligned} |0\rangle &= |\downarrow\rangle_{11} \otimes |\downarrow\rangle_{12} \otimes |\downarrow\rangle_{13} \otimes \cdots \otimes |\downarrow\rangle_{ij} \otimes |\downarrow\rangle_{i+1j} \\ &\otimes |\downarrow\rangle_{i+1j+1} \otimes |\downarrow\rangle_{ij+1} \otimes \cdots \otimes |\downarrow\rangle_{NN} \end{aligned} \quad (4.2)$$

for an $N \times N$ square lattice, where S_{ij}^- is the spin lowering operator defined as $S_{ij}^- = S_{ij}^x - iS_{ij}^y$. The lattice has the structure of a torus for periodic boundary conditions [20, 21, 86, 111–113]. The ground state energy is denoted by,

$$E_0 = -\frac{\mathcal{N}}{2} \lambda J \hbar^2, \quad (4.3)$$

corresponding to the ground state $|0\rangle$, where $\mathcal{N} = N^2$.

It is important to recall that a quantum Heisenberg model (ferromagnetic or anti-ferromagnetic) on a three dimensional lattice exhibits long range ordering at finite temperature unlike its counterparts in one and two dimensions [9, 114, 115]. In this regard let us recall the Mermin-Wagner (MW-) theorem which states that at any non zero temperature a one dimensional or two dimensional isotropic Heisenberg model with sufficiently short range exchange interaction cannot exhibit any LRO, which implies $T_c = 0$ in ferromagnetic systems and $T_N = 0$ in anti-ferromagnetic systems [9]. It can be shown that the MW- theorem holds for 2d XY anisotropic Heisenberg

model as well [85]. In the three dimensional case the collective excitations, viz., magnons are well defined in the long ranged ordered phase and become fragile in the short ranged ordered phase above the transition temperature, Curie temperature (T_c) for ferromagnetic systems or Neel temperature (T_N) for anti-ferromagnetic systems [57, 58, 87]. Analogously, some fragile magnon-like excitations along with multi-magnon composites are expected to be present within a very small temperature regime above zero [57, 58, 87]. However, as a first approximation we consider, in our present analysis for the two dimensional ferromagnetic case, the magnon states and multi-magnon composite states to be stable in the vicinity of zero temperature. This makes our analytical calculations simpler [85]. Such magnon modes and their interactions are described briefly in the Appendix B. In the following we will make use of the various properties of these magnon states in our novel scheme for the construction of quantum spin vortices and anti-vortices in the flattened meron configuration [85].

We now start by defining a quantum spin vortex (anti-vortex) on a square lattice [63, 79]. A charge 1 vortex (anti-vortex) is defined on a square plaquette as a spin configuration in which the spin direction (horizontal and vertical spins as defined below) rotates through an angle $+2\pi(-2\pi)$ for a closed walk in an anti-clockwise (clockwise) direction around the plaquette. The vorticity of such a vortex is $+1(-1)$ (see Figure 4.1(a) and 4.1(b)). For our specific model, in the limit $\lambda \rightarrow 0$ (see equation 4.1) the in-plane components of spin operators constitute a vortex (anti-vortex) [85]. It is worthwhile to mention that this situation corresponding to $\lambda \rightarrow 0$ is very different from the case of $\lambda = 0$ corresponding to pure XY model. It is in this very limit that a vortex may be looked upon as a “flattened Meron” [79].

We first assign coordinates $(i, j)a; (i+1, j)a; (i+1, j+1)a$ and $(i, j+1)a$ to the four vertices of the vortex where “ a ” is the lattice parameter. The correct topological property of a vortex/anti-vortex is then incorporated by specifying the expectation values for the components of the spin operator \mathbf{S} at each vertex of the vortex/anti-vortex [85]. The relevant spin states at the vertices are constructed and explained below. For a vortex/anti-vortex having topological charge 1 (in the units of 2π) or simply 1-vortex/1-anti-vortex, the operator expectation values for the different components of spins \mathbf{S} at the vertices are given in the table below [85],

Let us first construct the quantum state representing a vortex having topological charge ‘1’. The arrows, representing the spin directions on the four vertices (see Figure. 4.1(a)), signify that the spin states at the four vertices are such that the expectation values for S^x, S^y and S^z

$\langle S_{ij}^x \rangle = \frac{1}{2}, \langle S_{ij}^y \rangle = 0, \langle S_{ij}^z \rangle = 0$	$\langle S_{i+1j}^x \rangle = 0, \langle S_{i+1j}^y \rangle = \pm \frac{1}{2}, \langle S_{i+1j}^z \rangle = 0,$ +sign for vortex and -sign for anti-vortex
$\langle S_{i+1j+1}^x \rangle = -\frac{1}{2}, \langle S_{i+1j+1}^y \rangle = 0, \langle S_{i+1j+1}^z \rangle = 0$	$\langle S_{ij+1}^x \rangle = 0, \langle S_{ij+1}^y \rangle = \pm \frac{1}{2}, \langle S_{ij+1}^z \rangle = 0,$ -sign for vortex and +sign for anti-vortex

Table 4.1: Topological property of the vortex / anti-vortex [85].

take the values as given in Table 4.1. The horizontal arrow $|\Rightarrow\rangle$ on the $(i, j)^{th}$ site represents a spin state which is the eigenstate of S_{ij}^x with eigenvalue $+\frac{1}{2}$ and the vertical arrow $|\uparrow\rangle$ on the $(i+1, j)^{th}$ site represents a spin state which is the eigenstate of S_{ij}^y with eigenvalue $+\frac{1}{2}$. Similarly, the spin state $|\Leftarrow\rangle$ at $(i+1, j+1)^{th}$ site and $|\Downarrow\rangle$ at $(i, j+1)^{th}$ site are the eigenstates of S^x and S^y respectively with the eigenvalue $-\frac{1}{2}$. The spin state corresponding to $|\Rightarrow\rangle$ can be written as a linear combination of the two eigen-states of S^z , viz. $|\uparrow\rangle$ and $|\Downarrow\rangle$. Then at the $(i, j)^{th}$ site, the spin state is given by $(a_{ij}|\uparrow\rangle + b_{ij}|\Downarrow\rangle)$. The value of a_{ij} and b_{ij} can be determined by using the expectation values for S_{ij}^x, S_{ij}^y and S_{ij}^z and the condition that the eigenvalue of S_{ij}^x is $+\frac{1}{2}$ in the state $(a_{ij}|\uparrow\rangle + b_{ij}|\Downarrow\rangle)$. Similarly, for the rest of the vertices corresponding to the vortex the spin states are taken to be of the form $(a|\uparrow\rangle + b|\Downarrow\rangle)$ [85].

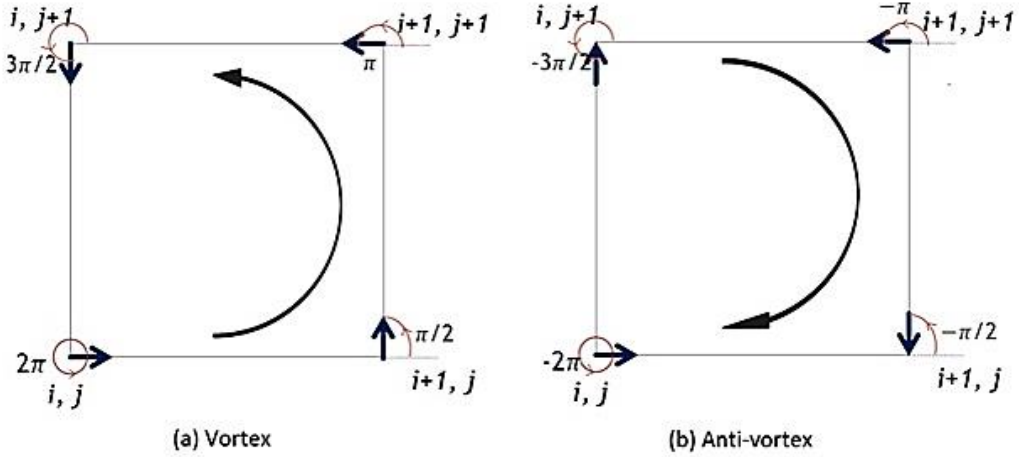


Figure 4.1: (a) quantum spin vortex of charge 1, (b) quantum spin anti-vortex of charge 1.

The coefficients 'a' and 'b' are determined from the expectation values for S^x, S^y and S^z and the eigenvalue conditions for the respective vertices as mentioned above [85]. The coefficients

‘ a ’ and ‘ b ’ for the four vertices turns out to be,

$$\begin{aligned}
a_{ij} &= b_{ij} = \frac{1}{\sqrt{2}}e^{i\theta_{ij}}; \\
a_{i+1j} &= \frac{1}{\sqrt{2}}e^{i\theta_{i+1j}}, b_{i+1j} = \frac{i}{\sqrt{2}}e^{i\theta_{i+1j}}; \\
a_{i+1j+1} &= b_{i+1j+1} = \frac{1}{\sqrt{2}}e^{i(\theta_{ij}+\pi)}; \\
a_{ij+1} &= \frac{1}{\sqrt{2}}e^{i(\theta_{i+1j}+\pi)}, b_{ij+1} = \frac{i}{\sqrt{2}}e^{i(\theta_{i+1j}+\pi)}.
\end{aligned} \tag{4.4}$$

Here θ_{ij} and θ_{i+1j} are arbitrary phase factors and for the diagonally opposite vertices, the coefficients have π phase difference. The coefficients given in (5) take care of the proper normalization of the spin states at each vertex. Therefore, the normalized charge-1 vortex state in the background of the original ground state can be defined on a plaquette $((ij); (i+1, j); (i+1, j+1); (i, j+1))$ as ,

$$\begin{aligned}
|1V\rangle &= |\downarrow\rangle_{11} \otimes |\downarrow\rangle_{12} \otimes |\downarrow\rangle_{13} \otimes \cdots \otimes (a_{ij}|\uparrow\rangle_{ij} + b_{ij}|\downarrow\rangle_{ij}) \otimes (a_{i+1,j}|\uparrow\rangle_{i+1,j} + b_{i+1,j}|\downarrow\rangle_{i+1,j}) \\
&\otimes (a_{i+1,j+1}|\uparrow\rangle_{i+1,j+1} + b_{i+1,j+1}|\downarrow\rangle_{i+1,j+1}) \otimes (a_{i,j+1}|\uparrow\rangle_{i,j+1} + b_{i,j+1}|\downarrow\rangle_{i,j+1}) \otimes \cdots \\
&\otimes |\downarrow\rangle_{NN}.
\end{aligned} \tag{4.5}$$

The vorticity operator is defined on the square plaquette as [63],

$$V_{op} = S_{ij}^x S_{i+1j}^y - S_{i+1j}^y S_{i+1j+1}^x + S_{i+1j+1}^x S_{ij+1}^y - S_{ij+1}^y S_{ij}^x. \tag{4.6}$$

When we operate the vorticity operator on the above 1-vortex state the eigenvalue comes out to be +1 as expected [85].

It may be remarked here that in our present formalism, we are implicitly assuming static vortex configuration [85]. This is conformity with the frozen vortex/anti-vortex scenario proposed below T_{BKT} [12, 13].

Similarly we can construct an anti-vortex with charge 1. For an anti-vortex coefficients at the four vertices come out to be,

$$\begin{aligned}
a_{ij} &= b_{ij} = \frac{1}{\sqrt{2}}e^{i\theta_{ij}}; \\
a_{i+1j} &= \frac{1}{\sqrt{2}}e^{i\theta_{i+1j}}, b_{i+1j} = -\frac{i}{\sqrt{2}}e^{i\theta_{i+1j}}; \\
a_{i+1j+1} &= b_{i+1j+1} = \frac{1}{\sqrt{2}}e^{i(\theta_{ij}+\pi)}; \\
a_{ij+1} &= \frac{1}{\sqrt{2}}e^{i(\theta_{i+1j}+\pi)}, b_{ij+1} = -\frac{i}{\sqrt{2}}e^{i(\theta_{i+1j}+\pi)}.
\end{aligned} \tag{4.7}$$

The explicit structure of the 1-anti-vortex state ($|1AV\rangle$) is same as the state $|1V\rangle$ of (4.5) with the coefficients ‘ a ’ and ‘ b ’ being different from that of the $|1V\rangle$. In this case, the eigenvalue of the vorticity operator defined in (4.6) comes out to be -1 , as expected [85].

4.3 Connection between the vortex and magnons

Considering the simplest situation corresponding to the presence of a single charge 1 vortex in the $N \times N$ square lattice, let us explore the connection between a vortex state and the magnon states. For each vertex of the vortex the spin state $|\uparrow\rangle_{ij}$ can be written as $S_{ij}^+|\downarrow\rangle_{ij}$, where $S_{ij}^+ = S_{ij}^x + iS_{ij}^y$ is the spin raising operator. The state $|1V\rangle$ in (4.5) can be rewritten as,

$$\begin{aligned}
|1V\rangle &= a_{ij}a_{i+1j}a_{i+1j+1}a_{ij+1}S_{ij}^+S_{i+1j}^+S_{i+1j+1}^+S_{ij+1}^+|0\rangle \\
&+ (b_{ij}a_{i+1j}a_{i+1j+1}a_{ij+1}S_{i+1j}^+S_{i+1j+1}^+S_{ij+1}^+|0\rangle \\
&+ \cdots + a_{ij}a_{i+1j}a_{i+1j+1}b_{ij+1}S_{ij}^+S_{i+1j}^+S_{i+1j+1}^+|0\rangle) \\
&+ (a_{ij}a_{i+1j}b_{i+1j+1}b_{ij+1}S_{ij}^+S_{i+1j}^+|0\rangle \\
&+ \cdots + a_{ij}b_{i+1j}b_{i+1j+1}a_{ij+1}S_{ij}^+S_{i+1j}^+|0\rangle) \\
&+ (a_{ij}b_{i+1j}b_{i+1j+1}b_{ij+1}S_{ij}^+|0\rangle + b_{ij}a_{i+1j}b_{i+1j+1}b_{ij+1}S_{i+1j}^+|0\rangle) \\
&+ b_{ij}b_{i+1j}a_{i+1j+1}b_{ij+1}S_{i+1j+1}^+|0\rangle + b_{ij}b_{i+1j}b_{i+1j+1}a_{ij+1}S_{ij+1}^+|0\rangle) \\
&+ b_{ij}b_{i+1j}b_{i+1j+1}b_{ij+1}|0\rangle, \tag{4.8}
\end{aligned}$$

where a and b 's are given by (4.4). The above equation (4.8) explicitly shows that the charge 1 quantum vortex state is a linear superposition of one 4-spin deviation state, four 3-spin deviation states, six 2-spin deviation states, four 1-spin deviation states and the ground state [85]. Using the definitions of magnon states, (see Appendix B) the charge 1 vortex state can now be expressed in terms of magnon states as,

$$\begin{aligned}
|1V\rangle &= A \sum_{\mathbf{k}_1, \mathbf{k}_2, \mathbf{k}_3, \mathbf{k}_4} f_{\mathbf{k}_1}^{i,j} f_{\mathbf{k}_2}^{i+1,j} f_{\mathbf{k}_3}^{i+1,j+1} f_{\mathbf{k}_4}^{i,j+1} |\mathbf{k}_1 \mathbf{k}_2 \mathbf{k}_3 \mathbf{k}_4\rangle \\
&+ \sum_{\mathbf{k}_1, \mathbf{k}_2, \mathbf{k}_3} (B_1 f_{\mathbf{k}_1}^{i,j} f_{\mathbf{k}_2}^{i+1,j} f_{\mathbf{k}_3}^{i+1,j+1} + B_2 f_{\mathbf{k}_1}^{i,j+1} f_{\mathbf{k}_2}^{i+1,j} f_{\mathbf{k}_3}^{i+1,j+1} \\
&+ B_3 f_{\mathbf{k}_1}^{i,j} f_{\mathbf{k}_2}^{i,j+1} f_{\mathbf{k}_3}^{i+1,j+1} + B_4 f_{\mathbf{k}_1}^{i,j} f_{\mathbf{k}_2}^{i,j+1} f_{\mathbf{k}_3}^{i+1,j}) |\mathbf{k}_1 \mathbf{k}_2 \mathbf{k}_3\rangle \\
&+ \sum_{\mathbf{k}_1, \mathbf{k}_2} (C_1 f_{\mathbf{k}_1}^{i,j} f_{\mathbf{k}_2}^{i+1,j} + C_2 f_{\mathbf{k}_1}^{i+1,j} f_{\mathbf{k}_2}^{i+1,j+1} + C_3 f_{\mathbf{k}_1}^{i+1,j+1} f_{\mathbf{k}_2}^{i,j+1} + C_4 f_{\mathbf{k}_1}^{i,j} f_{\mathbf{k}_2}^{i,j+1} \\
&+ C_5 f_{\mathbf{k}_1}^{i+1,j} f_{\mathbf{k}_2}^{i,j+1} + C_6 f_{\mathbf{k}_1}^{i,j} f_{\mathbf{k}_2}^{i+1,j+1}) |\mathbf{k}_1 \mathbf{k}_2\rangle \\
&+ \sum_{\mathbf{k}_1} (D_1 f_{\mathbf{k}_1}^{i,j} + D_2 f_{\mathbf{k}_1}^{i+1,j} + D_3 f_{\mathbf{k}_1}^{i+1,j+1} + D_4 f_{\mathbf{k}_1}^{i,j+1}) |\mathbf{k}_1\rangle + E|0\rangle. \tag{4.9}
\end{aligned}$$

The coefficients $A, B_1, B_2 \dots$ and E signify the weightage of the different spin deviation states in the composition of charge 1 vortex state and they are given by, $A = a_{ij} a_{i+1j} a_{i+1j+1} a_{ij+1}$, $B_1 = a_{ij} a_{i+1j} a_{i+1j+1} b_{ij+1}, \dots, E = b_{ij} b_{i+1j} b_{i+1j+1} b_{ij+1}$, where “ a ” and “ b ” are given in (4.4) [85].

In case of charge 1 anti-vortex the form of the state $|1AV\rangle$ will be same as the state $|1V\rangle$ except that the values for the coefficients $A = a_{ij} a_{i+1j} a_{i+1j+1} a_{ij+1}$, $B_1 = a_{ij} a_{i+1j} a_{i+1j+1} b_{ij+1}, \dots, E = b_{ij} b_{i+1j} b_{i+1j+1} b_{ij+1}$ are different from those for $|1V\rangle$. Their values are determined by the values of a and b , as given in (4.7) [85].

Thus equation (4.9) signifies the fact that the quantum state representing a 1-vortex (1- anti-vortex) is a combination of linear superpositions of 4-magnon composites, 3-magnon composites, 2-magnon composites, 1-magnon states and the ground state [85].

4.4 Quantum mechanical stability of the vortex/anti-vortex state

Operating the Hamiltonian \mathcal{H} (as given by (4.1)) on the 1- vortex state $|1V\rangle$ (see (4.8)), it can easily be shown that $|1V\rangle$ is not an exact eigenstate for the Hamiltonian \mathcal{H} . Therefore, the natural question arises that how stable the state $|1V\rangle$ is for a system, which is governed by the Hamiltonian \mathcal{H} . To investigate the quantum mechanical stability of the charge 1 vortex state $|1V\rangle$ we consider two special cases, viz., vortex (anti-vortex) in an infinitely dilute limit and also in the finite density limit. In the first case we shall consider the presence of only one charge 1 vortex in the $N \times N$ square lattice. This is the extreme dilute limit where the vortex density is vanishingly small. In the second one we shall consider a finite density of charge 1 vortices to be

present in the $N \times N$ square lattice. It is worthwhile to point out that in a realistic situation a macroscopic number of vortex anti-vortex pairs needs to be considered. However description of these in terms of multi-magnon composite states will be quite challenging and tough.

4.4.1 Single charge 1 vortex

Let us first consider a single 1-vortex in the $N \times N$ square lattice which is the “extreme dilute limit” of the vortex density. The quantum mechanical state $|1V\rangle$ describing such a situation is given by (4.8). Operating the Hamiltonian \mathcal{H} given by (4.1), on the state $|1V\rangle$ we get,

$$\mathcal{H}|1V\rangle = (E_0 + 2\lambda J\hbar^2)|1V\rangle + |\varphi_{resi}\rangle. \quad (4.10)$$

The right hand side of the above equation clearly shows the departure of the vortex state from being an eigenstate of \mathcal{H} where the state $|\varphi_{resi}\rangle$ (corresponding to (4.10)) is given by,

$$\begin{aligned} |\varphi_{resi}\rangle = & A \left[\sum_{\mathbf{k}_1, \mathbf{k}_2, \mathbf{k}_3, \mathbf{k}_4} f_{\mathbf{k}_1}^{i,j} f_{\mathbf{k}_2}^{i+1,j} f_{\mathbf{k}_3}^{i+1,j+1} f_{\mathbf{k}_4}^{i,j+1} \{2J\hbar^2(3\lambda - \gamma(\mathbf{k}_1) - \gamma(\mathbf{k}_2) - \gamma(\mathbf{k}_3) - \gamma(\mathbf{k}_4)) \right. \\ & \left. |\mathbf{k}_1 \mathbf{k}_2 \mathbf{k}_3 \mathbf{k}_4\rangle \right. \\ & \left. + \frac{1}{\mathcal{N}} \sum_{\mathbf{k}_1, \mathbf{k}_2, \mathbf{k}_3, \mathbf{k}_4} g_{4M}(\mathbf{k}_1, \mathbf{k}_2, \mathbf{k}_3, \mathbf{k}_4; \mathbf{k}_1, \mathbf{k}_2, \mathbf{k}_3, \mathbf{k}_4) |\mathbf{k}_1 \mathbf{k}_2 \mathbf{k}_3 \mathbf{k}_4\rangle \right] \\ & + \left[\sum_{\mathbf{k}_1, \mathbf{k}_2, \mathbf{k}_3} (B_1 f_{\mathbf{k}_1}^{i,j} f_{\mathbf{k}_2}^{i+1,j} f_{\mathbf{k}_3}^{i+1,j+1} + B_2 f_{\mathbf{k}_1}^{i,j+1} f_{\mathbf{k}_2}^{i+1,j} f_{\mathbf{k}_3}^{i+1,j+1} \right. \\ & \left. + B_3 f_{\mathbf{k}_1}^{i,j} f_{\mathbf{k}_2}^{i,j+1} f_{\mathbf{k}_3}^{i+1,j+1} + B_4 f_{\mathbf{k}_1}^{i,j} f_{\mathbf{k}_2}^{i,j+1} f_{\mathbf{k}_3}^{i+1,j}) \{2J\hbar^2(2\lambda - \gamma(\mathbf{k}_1) - \gamma(\mathbf{k}_2) \right. \\ & \left. - \gamma(\mathbf{k}_3)) |\mathbf{k}_1, \mathbf{k}_2, \mathbf{k}_3\rangle + \frac{1}{\mathcal{N}} \sum_{\mathbf{k}_1, \mathbf{k}_2, \mathbf{k}_3} g_{3M}(\mathbf{k}_1, \mathbf{k}_2, \mathbf{k}_3; \mathbf{k}_1, \mathbf{k}_2, \mathbf{k}_3) |\mathbf{k}_1 \mathbf{k}_2 \mathbf{k}_3\rangle \right] \\ & + \left[\sum_{\mathbf{k}_1, \mathbf{k}_2} (C_1 f_{\mathbf{k}_1}^{i,j} f_{\mathbf{k}_2}^{i+1,j} + C_2 f_{\mathbf{k}_2}^{i+1,j} f_{\mathbf{k}_1}^{i+1,j+1} \right. \\ & \left. + C_3 f_{\mathbf{k}_3}^{i+1,j+1} f_{\mathbf{k}_4}^{i,j+1} + C_4 f_{\mathbf{k}_1}^{i,j} f_{\mathbf{k}_4}^{i,j+1} + C_5 f_{\mathbf{k}_2}^{i+1,j} f_{\mathbf{k}_4}^{i,j+1} + C_6 f_{\mathbf{k}_1}^{i,j} f_{\mathbf{k}_3}^{i+1,j+1}) \{2J\hbar^2(\lambda - \gamma(\mathbf{k}_1) \right. \\ & \left. - \gamma(\mathbf{k}_2)) |\mathbf{k}_1 \mathbf{k}_2\rangle + \frac{1}{\mathcal{N}} \sum_{\mathbf{k}_1, \mathbf{k}_2} g_{2M}(\mathbf{k}_1, \mathbf{k}_2; \mathbf{k}_1, \mathbf{k}_2) |\mathbf{k}_1 \mathbf{k}_2\rangle \right] \\ & + \left[\sum_{\mathbf{k}_1} (D_1 f_{\mathbf{k}_1}^{i,j} + D_2 f_{\mathbf{k}_1}^{i+1,j} + D_3 f_{\mathbf{k}_1}^{i+1,j+1} + D_4 f_{\mathbf{k}_1}^{i,j+1}) [-\gamma(\mathbf{k}_1)] |\mathbf{k}_1\rangle \right] \\ & + (-E)2\lambda J\hbar^2|0\rangle. \end{aligned} \quad (4.11)$$

In the above equation (4.11) the first term on the right hand side corresponds to non-linear superposition of 4-magnon composites where the term $g_{4M}(k_1, \mathbf{k}_2, \mathbf{k}_3, \mathbf{k}_4; \mathbf{k}_1, \mathbf{k}_2, \mathbf{k}_3, \mathbf{k}_4)$, being in general a complex function, represents the interactions between the four magnon modes. Similarly, the second and third terms correspond to the nonlinear superposition of 3-magnon and

2-magnon composites respectively. The terms $g_{3M}(\mathbf{k}_1, \mathbf{k}_2, \mathbf{k}_3; \mathbf{k}_1, \mathbf{k}_2, \mathbf{k}_3)$ and $g_{2M}(\mathbf{k}_1, \mathbf{k}_2; \mathbf{k}_1, \mathbf{k}_2)$ represent the interactions between three magnon modes (identified by the subscript ‘3M’) and two magnon modes (identified by the subscript ‘2M’) respectively which are in general complex functions. The exact expression for $g_{2M}(\mathbf{k}_1, \mathbf{k}_2; \mathbf{k}_1, \mathbf{k}_2)$ has been given in Appendix B. The fourth term in (4.11) represents the contribution from the linear superposition of all the 1-magnon modes to the residual state $|\varphi_{resi}\rangle$ and the last term gives the ground state contribution [85]. The most important feature of the above equation (4.11) is that the residual state denoted by $|\varphi_{resi}\rangle$ is not a linear superposition of multi-magnon states unlike the state $|1V\rangle$ (eqn. (4.9)). To be more precise the state $|\varphi_{resi}\rangle$ contains terms which generate higher order inter-multi-magnonic correlations [85]. The expectation of the Hamiltonian in the state $|1V\rangle$ is evaluated from eqn. (4.8) and is given by,

$$\langle 1V | \mathcal{H} | 1V \rangle = (E_0 + 3\lambda J \hbar^2) = \mathcal{E}_0, \quad (4.12)$$

where $\mathcal{E}_0 \equiv (E_0 + 3\lambda J \hbar^2)$ and the quantity $3\lambda J \hbar^2$ signifies the energy required to excite one 1-vortex from the ground state, the ground state energy being E_0 as given in (4.3). The eqn. (4.10) can be rewritten as,

$$\mathcal{H} | 1V \rangle = \mathcal{E}_0 | 1V \rangle + (|\varphi_{resi}\rangle - \lambda J \hbar^2 | 1V \rangle) = \mathcal{E}_0 | 1V \rangle + |\psi_{resi}\rangle \quad (4.13)$$

where $|\psi_{resi}\rangle \equiv (|\varphi_{resi}\rangle - \lambda J \hbar^2 | 1V \rangle)$ is again not a linear superposition of multi-magnon states as explained above. Making use of eqns. (4.10) - (4.13), it is clear that $\langle 1V | \psi_{resi} \rangle = 0$ [85].

Now operating the Hamiltonian \mathcal{H} successively twice on $|1V\rangle$ the expectation value of \mathcal{H}^2 in the state $|1V\rangle$ turns out to be,

$$\langle 1V | \mathcal{H}^2 | 1V \rangle = (E_0 + 2\lambda J \hbar^2)^2 + (J \hbar^2)^2 (2 + \frac{3}{4} \lambda^2) \quad (4.14)$$

The quantum mechanical stability of the state $|1V\rangle$ is now verified by operating the time evolution operator $[\exp(-\frac{i}{\hbar} \mathcal{H} t)]$ on the state $|1V\rangle$. Since the state $|1V\rangle$ is not an eigenstate of \mathcal{H} let us take the expectation value of the time evolution operator in $|1V\rangle$, to study what fraction of the original one quantum vortex state is retained during the time evolution of the system [85]. Hence,

$$\langle 1V(0) | 1V(t) \rangle = \langle 1V | \exp(-\frac{i}{\hbar} \mathcal{H} t) | 1V \rangle = 1 - \frac{it}{\hbar} \langle 1V | \mathcal{H} | 1V \rangle + (\frac{i}{\hbar})^2 \frac{t^2}{2!} \langle 1V | \mathcal{H}^2 | 1V \rangle + \dots \quad (4.15)$$

where $|1V(0)\rangle$ is the initial state and $|1V(t)\rangle$ is the final state (i.e. the after time evolution for a duration of time t). On the right hand side of the above expression we retain terms up-to 2^{nd} order in time explicitly and then (4.15) becomes,

$$\langle 1V(0)|1V(t)\rangle = \left(1 - \frac{i}{\hbar}\mathcal{E}_0 t + \left(\frac{i}{\hbar}\right)^2 \frac{1}{2!}\mathcal{E}_0^2 t^2\right) - \frac{1}{\hbar^2}(J\hbar^2)^2 \left(1 + \frac{3}{8}\lambda^2\right)t^2 + O(t^3). \quad (4.16)$$

It is clear from (4.16) that the first three terms correspond to the series expansion of $[\exp(-\frac{i}{\hbar}\mathcal{E}_0 t)]$ up-to 2^{nd} order in time. The next one represents the deviation in the sense (of a damping) that in absence of this term, the expectation value of the time evolution operator describes a stationary state exhibiting phase oscillation with frequency $\omega_0 = \frac{\mathcal{E}_0}{\hbar}$ and therefore the state $|1V\rangle$ behaves like an approximate eigenstate of the Hamiltonian \mathcal{H} with energy \mathcal{E}_0 [85]. On the other hand the inverse time scale Γ_d corresponding to the damping term arising from inter-multi-magnonic correlations as explained above, is given by,

$$\Gamma_d = J\hbar\sqrt{\left(1 + \frac{3}{8}\lambda^2\right)}, \quad (4.17)$$

which essentially indicates the decay rate of the coherent phase oscillation. Hence up-to 2^{nd} order in time, the quantity of interest, viz. the ratio of the decay rate and the phase coherent oscillation frequency comes out to be,

$$\frac{\Gamma_d}{\omega_0} = \frac{1}{\left(\frac{\mathcal{N}}{2} - 3\right)}\sqrt{\left(\frac{1}{\lambda^2} + \frac{3}{8}\right)}. \quad (4.18)$$

In the above ratio the term under the squared root becomes approximately $1/\lambda$ for a very small but fixed value of the anisotropy parameter λ . Hence above equation (4.18) becomes,

$$\frac{\Gamma_d}{\omega_0} \approx \frac{1}{\left(\frac{\mathcal{N}}{2} - 3\right)\lambda} \quad (4.19)$$

The time duration of the evolution is assumed to be much shorter than the natural time scale $t_{nat} = \frac{2\hbar}{\sqrt{3}(J\hbar^2)}$ (for $S = 1/2$) for the system so that a truncation at 2^{nd} order in time can be considered safe, where the quantity $J\hbar^2$ has the dimension of energy [85]. At the first place, such an approximation physically means that the multi-magnon composites fuses to form such a vortex state of true quantum nature in a time scale which is much shorter than the natural time scale of the system. Furthermore, the ratio of the evolution time and t_{nat} is assumed to be much smaller than that of the time scale of decay and t_{nat} . It is clear from (4.19) that Γ_d becomes very small compared to ω_0 when the lattice size is very large and ensures the fulfillment of the above

conditions. In this case the deviation representing phase incoherence remains ineffective and the state $|1V\rangle$ remains a stable state for the Hamiltonian \mathcal{H} [85]. It is worthwhile to mention that in the confined phase below T_{BKT} (and above T_c) the form of the dynamical structure function for an ideal vortex gas is a pure delta function $\delta(\omega)$ [83]. However, just above $T_c(=0)$ taking into consideration the dynamics of all the magnon modes and the multi-magnon composites which are present in a fragile manner, the central peak of the dynamical structure function acquires a finite width. This width is expected to be of the order magnitude of the decay rate Γ_d [85].

For a fairly large system (4.19) can further be approximated to be, $\frac{\Gamma_d}{\omega_0} \approx \frac{2}{\mathcal{N}\lambda}$ which further implies that for the vortex state described in this chapter to be sufficiently stable the system size must exceed a certain threshold magnitude. Taking a typical value of $\lambda \approx 10^{-4}$ (since we are considering the extreme anisotropy limit, i.e., flattened meron configuration) we have from (4.19), the above threshold system size can be estimated to be of the order of 141×141 . Considering a typical value of 3\AA for the lattice spacing, the length scale of the system turns out to be of the order of 10^{-5} cm which falls into the mesoscopic length scale [85].

4.4.2 Finite density of charge 1 vortices

Let me now describe the calculations regarding the stability corresponding to the case of finite density of vortices. Since the Hamiltonian contains only the nearest neighbour interactions, the state $\mathcal{H}|1V\rangle$ will produce spin deviations only on the nearest neighbour sites of the vertices of the vortex. Thus to construct a finite density of charge 1 vortices in an infinite lattice, we employ the periodic boundary condition (PBC) for simplicity on a closed (torus) 4×4 cell, which is of minimum allowed size. By periodically repeating these cells we can fill up the entire $N \times N$ square lattice with a maximum of $n = \frac{N^2}{16}$ (where N is an integral multiple of 4) charge 1 vortices, without having interactions between them, as can be seen in Fig. 2. This is the other limit as opposed to the extreme dilute case studied in Section 4.4.1. The periodicity is therefore, given by the following equations involving spin operators (see Table 4.1 under Section 4.4.1),

$$\langle S_{i,j}^\alpha \rangle = \langle S_{i+4,j}^\alpha \rangle = \langle S_{i-4,j}^\alpha \rangle = \langle S_{i,j-4}^\alpha \rangle = \langle S_{i,j+4}^\alpha \rangle, \text{ where } \alpha = x, y, z \quad (4.20)$$

for all i and j on the lattice [85]. Under these conditions the magnon modes defined in each cell with the PBC will be repeated in the adjacent cell in a periodic manner. Therefore, the composite quantum state corresponding to ' n ' number of such 1-vortices can be written as [85],

$$|n1V\rangle = \cdots \otimes |C_{i-4,j}\rangle \otimes |C_{i,j-4}\rangle \otimes |C_{i,j}\rangle \otimes |C_{i+4,j}\rangle \otimes |C_{i,j+4}\rangle \otimes \cdots \quad (4.21)$$

where the quantum state corresponding to each cell is denoted as $|C_{i,j}\rangle$ which is of the same form as given in eqn. (9) with only exception being the fact that now the number of lattice points is 16 and only four lattice points correspond to the four vertices of the vortex (see Figure 2). Operating the Hamiltonian \mathcal{H} on the state $|n1V\rangle$ and making use of (4.13) and (4.21) we get,

$$\begin{aligned} \mathcal{H}|n1V\rangle &= n\tilde{\mathcal{E}}_0|n1V\rangle + (|\psi_{resi}^1\rangle \otimes |C_2\rangle \otimes |C_3\rangle \otimes \dots \otimes |C_n\rangle + |C_1\rangle \otimes |\psi_{resi}^2\rangle \otimes |C_3\rangle \otimes \dots \\ &+ \dots \otimes |C_n\rangle + \dots + |C_1\rangle \otimes |C_2\rangle \otimes |C_3\rangle \otimes \dots \otimes |\psi_{resi}^n\rangle), \end{aligned} \quad (4.22)$$

where $\tilde{\mathcal{E}}_0 = -5\lambda J\hbar^2$ and the residual state $|\psi_{resi}^i\rangle$ is the deviation of the vortex state from being an eigenstate of \mathcal{H} within the (i,j) -th cell [85].

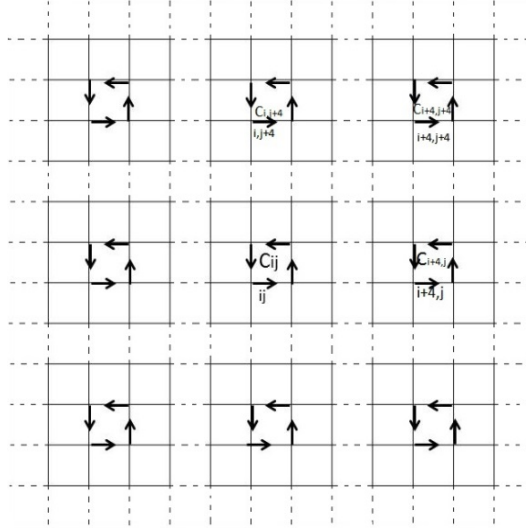


Figure 4.2: Finite number vortices of charge 1 in an $N \times N$ square lattice.

The expression for $\tilde{\mathcal{E}}_0$ corresponding to each (i,j) -th cell stands for \mathcal{E}_0 (see equation (4.20)) with $N = 4$. Also we make use of (4.21) with $N = 4$ in deducing eqn. (4.1). Furthermore, the notations $|C_r\rangle$ in place of $|C_{ij}\rangle$ and $|\psi_{resi}^r\rangle$ in place of $|\psi_{resi}^{ij}\rangle$ are used for convenience [85].

The expectation value of \mathcal{H} in the state $|n1V\rangle$ is given by,

$$\langle n1V|\mathcal{H}|n1V\rangle = n\tilde{\mathcal{E}}_0 \quad (4.23)$$

making use of the fact that for each cell $\langle C_r|\psi_{resi}^r\rangle = 0$. This residual state, defined within one cell, is again a non-linear superposition of multi-magnon states as explained in Section 4.4.1.

Proceeding along the same lines as in Section 4.4.1 we now have,

$$\langle n1V | \mathcal{H}^2 | n1V \rangle \approx n^2 \tilde{\mathcal{E}}^2 + n(J\hbar^2)^2 \left(2 + \frac{3}{4}\lambda^2\right) \quad (4.24)$$

To check the quantum mechanical stability of the state $|n1V\rangle$ under time evolution the same procedure as adopted in Section 4.4.1 is followed here too. Then the overlap between the initial state and the final state (i.e. the expectation value of the time evolution operator $[\exp(-\frac{i}{\hbar}\mathcal{H}t)]$ in the state $|n1V\rangle$) comes out to be,

$$\begin{aligned} \langle n1V(0) | n1V(t) \rangle &= \langle n1V | \exp(-\frac{i}{\hbar}\mathcal{H}t) | n1V \rangle = \left(1 - \frac{i}{\hbar}n\tilde{\mathcal{E}}_0 t + \left(\frac{i}{\hbar}\right)^2 \frac{1}{2!} n^2 \tilde{\mathcal{E}}_0^2 t^2\right) \\ &- \frac{1}{\hbar^2} n(J\hbar^2)^2 \left(1 + \frac{3}{8}\lambda^2\right) t^2 + O(t^3), \end{aligned} \quad (4.25)$$

where the exponential series has again been expanded up to 2^{nd} order in time and the justification for such an expansion remains the same as that of Section 4.4.1. The ratio of the decay rate $\Gamma_d^{(n)}$ corresponding to the deviation term (the superscript ‘ n ’ represents the fact that we are considering finite density of charge 1 vortices) and the frequency $\omega_0^{(n)}$ corresponding to the phase oscillation is given by,

$$\frac{\Gamma_d^{(n)}}{\omega_0^{(n)}} = \frac{4}{5} \sqrt{\frac{1}{N^2 \lambda^2} \left(1 + \frac{3}{8}\lambda^2\right)} \quad (4.26)$$

In order for the phase coherent mode to physically survive, it follows from the above equation that the necessary condition is $\Gamma_d^{(n)} < \omega_0^{(n)}$, which in turn implies,

$$N\lambda > \frac{4}{5}, \text{ for } N > N_c \quad (4.27)$$

Note that the term $\sqrt{1 + \frac{3}{8}\lambda^2}$ in (4.27) above is nearly equal to 1, since our starting model itself is strongly XY anisotropic i.e., λ is very small.

The above condition (4.27) signifies that there must be a critical system size $\mathcal{N}_c = N_c^2$ for a given value of λ for the stability of the ‘ n ’ 1-vortex state. As before we take $\lambda \approx 10^{-4}$ and in this case the threshold system size comes out to be of the order of 8000×8000 . Taking a typical value of 3\AA for the lattice spacing as before, the length scale of the system becomes of the order of 10^{-4} cm, which again is in the mesoscopic regime. Experimental studies of spin dynamics would be quite helpful in verifying our above prediction regarding threshold size [85].

4.5 Higher charged vortices

We now proceed to construct vortices with higher charges in the flattened meron configuration [116]. We start by constructing a 2-vortex using the elementary 1-vortex plaquettes. A 2-vortex (2-anti-vortex) is defined on a bigger plaquette consisting of four elementary vortex (anti-vortex) plaquettes, so that the spin directions (defined in Sec.3) rotates through an angle $+4\pi(4\pi)$ for a closed walk in an anti-clockwise (clockwise) direction around the boundary of the bigger plaquette. This is illustrated in the Figure 4.2. In this construction we follow the procedure introduced in Refs. [76–78], only difference being that, here we use Pauli spin basis instead of coherent basis.

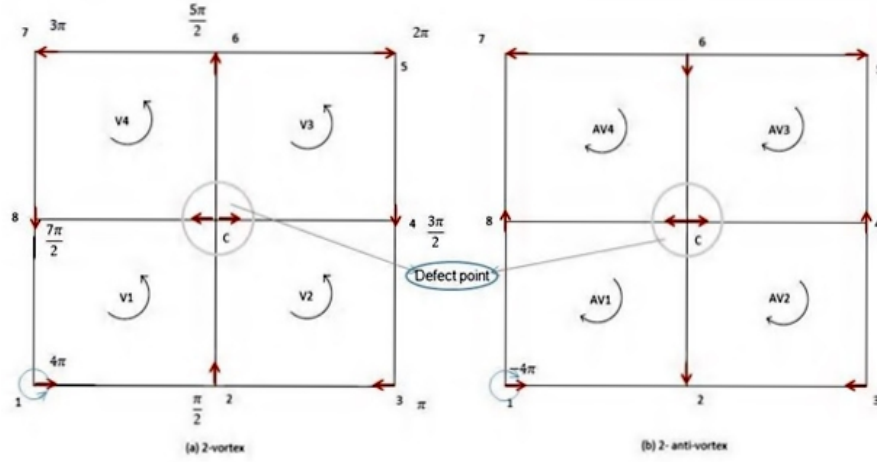


Figure 4.3: (a) quantum spin vortex of charge 2, (b) quantum spin anti-vortex of charge 2.

The 2-vortex constructed in this way, contains a central defect point [78, 79]. A consistent spin state can't be defined at this central point and the resultant expectation value for the spin component is vanishing at the central point C. In this way, the construction of any q -vortex state shall contain a defect point at the center whenever q is even. The ambiguity of the spin at the central point is similar to 'frustration' observed in several magnetic systems [117]. In the case of a 3-vortex state, a perfectly consistent spin label (horizontal or vertical), characterized by the expectation values of the components of the spin operators, can be assigned uniquely at each lattice site. In contrast to the vortices with even charge 2, we now have a bigger vortex plaquette with oppositely charged elementary 1-vortex (sub-vortex) situated at the central region. The 3-vortex (anti-vortex) constructed in this way consists of one elementary 1-anti-vortex (vortex) surrounded by eight elementary 1-vortex (anti-vortex) plaquettes. The spin direction (defined

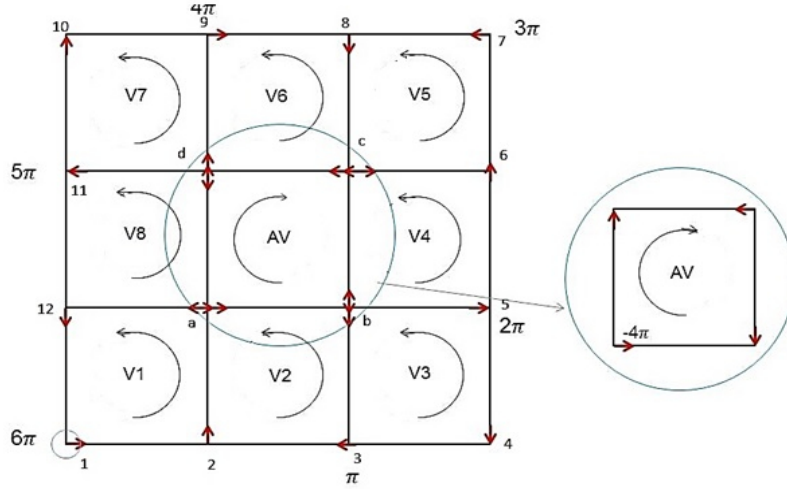


Figure 4.4: quantum spin vortex of charge 3.

in Sec. 3) rotates through an angle $+6$ for a closed walk in an anti-clock wise direction as shown in Figure 4.4. Physical realization (spin-profile) of a 3-vortex is determined by the expectation values of the components of the spin operator \mathbf{S} on all the 16 lattice sites. To each lattice point we assign a mixed quantum spin state of the form $(a_{ij}|\downarrow\rangle + b_{ij}|\uparrow\rangle)$, where the schemes for the determination of the coefficients have been explained in Section 4.4.1. A 3-vortex state, constructed in this way, takes the form:

$$\begin{aligned}
|3V\rangle &= |\downarrow\rangle \otimes |\downarrow\rangle \otimes \cdots \otimes (a_{i,j}S_{i,j}^+|\downarrow\rangle_{i,j} + b_{i,j}|\uparrow\rangle_{i,j}) \\
&\otimes (a_{i+1,j}S_{i+1,j}^+|\downarrow\rangle_{i+1,j} + b_{i+1,j}|\uparrow\rangle_{i+1,j}) \otimes (a_{i+1,j+1}S_{i+1,j+1}^+|\downarrow\rangle_{i+1,j+1} + b_{i+1,j+1}|\uparrow\rangle_{i+1,j+1}) \\
&\otimes (a_{i,j+1}S_{i,j+1}^+|\downarrow\rangle_{i,j+1} + b_{i,j+1}|\uparrow\rangle_{i,j+1}) \otimes (a_{i,j+2}S_{i,j+2}^+|\downarrow\rangle_{i,j+2} + b_{i,j+2}|\uparrow\rangle_{i,j+2}) \\
&\otimes \cdots \otimes (a_{i+2,j}S_{i+2,j}^+|\downarrow\rangle_{i+2,j} + b_{i+2,j}|\uparrow\rangle_{i+2,j}) \otimes \cdots \otimes (a_{i+3,j+3}S_{i+3,j+3}^+|\downarrow\rangle_{i+3,j+3} \\
&+ b_{i+3,j+3}|\uparrow\rangle_{i+3,j+3}) \otimes \cdots \otimes |\downarrow\rangle \otimes |\downarrow\rangle
\end{aligned} \tag{4.28}$$

Carrying out the analysis similar to that of Sections 4.4.1 and 4.4.2, we find that the state $|3V\rangle$ can be written as a linear combination of magnon states starting from 16-magnon composite, 15-magnon composite and so on, up-to 1-magnon state and the ground state. It can be generalized in a straight forward way via methods of induction to any vortex with odd-valued charge q and such a vortex state can be written as a linear combination of $(q+1)^2$ -magnon composite state, $[(q+1)^2 - 1]$ -magnon composite states and so on, up-to 1-magnon states and the ground

state. We now explain this construction of vortices with odd higher charge by gluing required number of elementary vortex or anti-vortex plaquettes [116]. We have to associate proper gluing rule along the common bond of the vortices or anti-vortices residing side by side. Since there is ambiguity of spin at the central point for vortices (anti-vortices) with even charges we start our analysis by constructing a 3-vortex. We first identify the lattice points corresponding to a 3- vortex as given in Figure 4.4, where the only constraint in performing such a gluing process is that, it should be consistent with the winding of the spin through an angle $3 \times (2\pi)$ in the anti-clockwise direction along the boundary. Our first step is to glue vortex V_2 with the vortex V_1 by assigning a gluing law along the common bond $2-a$, viz., $|2\rangle = (\frac{1}{2}|\uparrow\rangle_{V_1} + \frac{1}{2}|\uparrow\rangle_{V_2})$ and $|a\rangle = (\frac{1}{2}|\Rightarrow\rangle_{V_1} + \frac{1}{2}|\Rightarrow\rangle_{V_2})$, where $|2\rangle$ and $|a\rangle$ are spin states at their respective sites marked in Figure 4.3. Next the vortex V_3 is glued to the previously glued object V_1V_2 . In this case the gluing rule is, $|3\rangle = (\frac{1}{2}|\Leftarrow\rangle_{V_2} + \frac{1}{2}|\Leftarrow\rangle_{V_3})$ and $|b\rangle = (\frac{1}{2}|\Downarrow\rangle_{V_2} + \frac{1}{2}|\uparrow\rangle_{V_3})$, where $|3\rangle$ and $|b\rangle$ are spin states at their respective sites as marked in the Figure 4.4. The next step is to glue the vortex V_4 with the glued object V_1, V_2, V_3 , where the gluing rule at the respective lattice sites is, $|5\rangle = (\frac{1}{2}|\Rightarrow\rangle_{V_2} + \frac{1}{2}|\Rightarrow\rangle_{V_3})$ and $|b\rangle = (\frac{1}{2}|\Downarrow\rangle_{V_2} + \frac{1}{2}|\uparrow\rangle_{V_3}) + |\Downarrow\rangle_{V_4}$. In this manner one can keep on gluing V_5, V_6, V_7, V_8 , one after another, with the previous plaquette and finally V_8 with V_1 . As a result we get an anti-vortex at the central plaquette [116].

Let us now calculate the vortex excitation energies. The expectation value of the XY-anisotropic ferromagnetic Heisenberg Hamiltonian (given by (4.1)) in the 1-vortex state, defined in (4.8) is given by, $\langle 1V|\mathcal{H}|1V\rangle = E_0 + 3\lambda J\hbar^2$. Hence the 1- vortex excitation energy is $3\lambda J\hbar^2$. The 3- vortex excitation energy can be calculated from the expectation value $\langle 3V|\mathcal{H}|3V\rangle$, as $10\lambda J\hbar^2$ by using (4.1) and (4.28). The excitation energy of the 1- anti-vortex state comes out to be exactly the same as that of the 1-vortex, namely $3\lambda J\hbar^2$. Similar is the case for 3- anti-vortex, so to say the excitation energy is again $10\lambda J\hbar^2$. This signifies the fact that only a vorticity operator can identify the topological charge of the vortices [116].

In constructing a 3- vortex from the elementary vortex plaquettes, it has already been argued that for consistent construction of a 3- vortex eight 1- vortex plaquettes and one 1- anti-vortex plaquette are involved. The sum of the excitation energies of these nine elementary plaquettes is $27\lambda J\hbar^2$, while the 3-vortex excitation energy $10\lambda J\hbar^2$ is much lower than that. This lowering of the excitation energy can be associated with the physical effect of gluing. In the case of even charged vortices the spin at central point on the lattice site being ambiguous, calculation

of the excitation energies for any such vortices have not been performed here. The gluing scheme for constructing vortices with higher charges (odd) thus lowers the energy [116]. It should be emphasized that the fusing scheme referred above is not a physical process; rather it is a geometrical construction. In reality, the vortices and anti-vortices of charge ‘q’ and ‘-q’ respectively interact via logarithmic interaction which we have not taken into account in the gluing process [12, 13]. It is worthwhile to mention that, this process of fusion between two neighbouring elementary vortex plaquettes is consistent with the principle of superposition of quantum states. Again a quantum mechanical stability analysis similar to the one undertaken for charge 1 vortices/anti-vortices (see sections 4.4.1 & 4.4.2) can be carried out for higher charged vortices/anti-vortices as well. The results are expected to be qualitatively similar [116].

4.6 Summary and Discussion

In this chapter, I have described in detail the possible microscopic composition of topological excitations of vortex and anti-vortex type for a 2d ferromagnet. Our in depth analysis firmly establishes that the interaction between collective excitations originating from a strongly anisotropic quantum Heisenberg ferromagnet on two dimensional lattices, can lead to the formation of topological excitations of vortex or anti-vortex type (in a flattened meron configuration) which are localized objects. These collective excitations could be single magnon as well as multi-magnon composites. We find that in the situation of an infinitely dilute limit of vortex density, the corresponding 1-vortex state is quantum mechanically stable when the system size exceeds a threshold value, keeping the magnon modes well defined. Similar conclusion holds also for the case with finite density of vortices. The only difference in contrast to the dilute limit case is that, for finite density the threshold size is much larger. The above features are expected to be remained intact even quantitatively for anti-vortices as well. The method of construction of the quantum state representing a charge-1 vortex/anti-vortex has subsequently been extended to the higher charged vortices/ anti-vortices. We find that the quantum state representing any vortex/anti-vortex can be regarded as generated from the interactions between the various magnon modes and magnon-composites.

Let me now discuss the plausibility of the above mentioned picture in real a layered ferromagnetic system possessing easy-plane anisotropy (XY-anisotropy). For a layered system the inter-layer coupling i.e., the exchange interaction between the spins of two nearby layers make

T_c non-vanishing. With a very small inter-layer coupling, however, T_c still remains quite low above which the magnon like collective excitations become fragile. Assuming the above mentioned system to be in a temperature regime where it effectively becomes a two-dimensional (2d) one, the collective magnon modes considered here become fragile at any finite temperature. This is because in analogy with three-dimensional ferromagnets, the Curie temperature T_c corresponding to an XY-anisotropic ferromagnetic model identically vanishes on pure 2d lattices [5, 57, 58, 87, 98, 99]. On the other hand in the case of XY-anisotropic Heisenberg models on 2d spatial lattices, BKT transition temperature T_{BKT} is finite. Besides, in the paramagnetic phase above T_{BKT} , the vortices (and anti-vortices) move freely and contribute to the dynamical structure function. This provides one of the important mechanisms behind the occurrence of central peak in the dynamical structure function as discussed earlier [12, 13, 37–41]. According to our picture, the static vortices (anti-vortices) below T_{BKT} are themselves formed from the composite magnon modes which are expected to exist in this temperature regime in reality though, these modes may be in a highly fragile state [85]. Therefore, all the damped propagating composite multi-magnon and the single magnon modes superpose in a complicated manner to form the vortices as shown in this chapter and as a consequence the dynamics of mobile vortices gets very complicated in the regime $T > T_{BKT}$. Our investigation reveals that such a non-trivial combination of all the damped propagating modes gives rise to fairly stable localized vortex like topological excitation provided the system size exceeds a certain threshold magnitude. The temporal behavior of the dynamical spin-spin correlation is further expected to be governed by the various nonlinear processes entering through the higher order correlation functions, bearing the effects of the fragile multi-magnon composites as well [85].

The presence of damped propagating modes in the paramagnetic phase of 3d Heisenberg model is now a well-established fact [5, 57, 58, 87, 98, 99]. Temporal dependence of the spin-spin correlation function in this paramagnetic phase is governed by various higher order correlation functions with non-trivial temperature and \mathbf{q} (wave vector) dependence, and is diffusive in nature with an oscillatory component present sometimes. Such a diffusive nature is manifested through the occurrence of the central peak in DSF (in the constant \mathbf{q} scan) [5, 57, 58, 87, 98, 99]. However, this central peak is fundamentally different from the “central peak” that I had talked about in relation to the mobile BKT vortices. The central peak originating from the diffusive modes corresponding to 2d XY-anisotropic Heisenberg model can indeed provide a substantial

contribution to the “central peak” (in BKT scenario) both below and above T_{BKT} owing to the fact that apart from forming vortices, some modes are expected to stay intact with their original damped nature.

It is worthwhile to point out that although the results of our investigations presented in this chapter pertain to strongly- XY anisotropic case, the material systems of interest to experimentalists mostly belong to weakly- XY anisotropic category. In these experimental systems the topological excitations are of truly meronic/ anti-meronic type rather than “flattened meron/ anti-meron” configurations which have been considered in this chapter.

Chapter 5

Summary and Outlook

In chapters 2 and 3, I have described our semi-phenomenological investigations of the spin dynamics corresponding to layered quantum spin systems of both ferromagnetic (FM) and antiferromagnetic (AFM) type in the presence of topological excitations of vortex/meron type occurring in the BKT scenario . Only the spin $\frac{1}{2}$ models corresponding to both FM and AFM type have been considered within the context of semi-classical vortex/meron gas phenomenology. Although the application of such BKT inspired semi-classical treatment can reproduce the central peaks, both the models show occurrence of negative values of DSFs (and hence integrated intensities) when convoluted with a realistic spectral window function, even if a detailed balance correction is incorporated via the “Windsor factor” (see Appendix A). This is quite unphysical because the DSF must always be positive definite. (*It is worthwhile to point out that Windsor’s prescription for the detailed balance correction works quite well in the case of 3d spin systems, which is unlike the present case corresponding to 2d systems [58].*) However, the theoretical model of semi-classical treatment of ideal gas of unbound merons tends to agree better (in terms of overall shape of DSFs) with the corresponding experimental results, when the classical limit is approached either by increasing the value of spin or by increasing the temperature even for 2d systems. I have further explained in chapters 2 and 3, that the occurrences of such negative values of DSFs have its root in the assumptions that the spins are classical objects (even if the systems under consideration are spin 1/2) and topological vortices/merons are point like objects obeying Maxwell’s speed distribution law. Therefore, a complete quantum mechanical formalism and treatment are indeed very crucial for the understanding the quantum effects on the BKT scenario and the corresponding spin dynamics of the quasi-2d/2d systems.

The possibility of BKT transition in quantum XXZ model has been a long standing unsolved problem in statistical physics. Since the quantum XXZ model falls under the XY universality class it is expected to undergo a BKT transition as well. In this regard the quantum XY model has been investigated by using Quantum Monte Carlo (QMC) method on finite lattice [75, 118]. It has been found that the critical exponents are independent of the value of the spin S . Furthermore, the critical behaviours have been found to be exactly same as those of classical XY model. This is quite unusual owing to the fact that in quantum XY model the z-component of spin, S^z remains present as required by the $SU(2)$ commutation relation, $[S_i^\alpha, S_j^\beta] = \delta_{ij} \epsilon^{\alpha\beta\gamma} S_j^\gamma$. Therefore, this extra dimension in the spin space, which is naturally occurring in the quantum case should modify the critical behaviour. Detailed investigations on the quantum XXZ model on 2d lattices are expected to shed some light on this. However, this model has been investigated within the “*pure quantum self consistent harmonic approximation* (PQSCHA)” which is in principle a semi-classical approach and the thermodynamic quantities are found to obey nothing but a renormalized classical BKT behaviour [119].

A systematic analysis of quantum XXZ model on 2d lattices has been performed in recent years. The formalism is based on the application of path integral technique in the spin-coherent state basis to obtain an effective action corresponding to the above mentioned model [76–79]. This formalism is purely a quantum mechanical one and have figured out the existence of a topological term in the effective action. Such a topological term has indeed provided a strong possibility for the existence of topological excitations in the model. This formalism can in principle be used to address the issue of the quantum -BKT picture. To do so, the calculation of the static spin-spin correlation function using this formalism needs to be performed along with the estimations, within this formalism itself, of other thermodynamic quantities such as specific heat, helicity modulus, etc. In particular, effects of the existence of a topological term in the quantum effective action on the thermodynamic quantities are expected to be quite interesting. Such a calculational approach is expected to bring out the quantum effects on T_{BKT} as well as on the temperature dependence of the correlation length $\xi(T)$. Then the above mentioned procedure can be suitably extended to calculate the DSF. The beauty of the coherent-state path integral technique is that it is naturally within the imaginary time formalism and therefore, can be used quite easily to determine finite temperature properties of the above mentioned model. However, to calculate the DSF one need to incorporate the real temporal dynamics in

the formalism. At this juncture, inputs from the QMC methods look promising. In QMC, the accessible counterpart of the DSF is the imaginary time spin-spin correlation. Recently, the DSFs have been calculated by using a method which is very aptly expressed by the following equation,

$$\tilde{S}^{\alpha\alpha}(\mathbf{q}, \tau) = \int_0^\infty \kappa(\tau, \omega) S^{\alpha\alpha}(\mathbf{q}, \omega), \quad (5.1)$$

where $\tilde{S}^{\alpha\alpha}(\mathbf{q}, \tau)$ is the imaginary time spin-spin correlation, $\kappa(\tau, \omega)$ is a suitable Kernel [92]. The imaginary time τ has in general the dimension of inverse of temperature $\beta = \frac{1}{k_B T}$, where T is the real thermodynamic temperature corresponding to the system under consideration. Therefore, use of such a Kernel $\kappa(\tau, \omega)$ can in principle provide a possible way for the calculation DSFs at finite temperatures.

In chapter 4, I have further described in detail the possible microscopic composition of topological vortices/anti-vortices occurring in the BKT scenario corresponding to a ferromagnetic XXZ model exhibiting a strong XY-like anisotropy on 2d square lattice. Collective excitations originating from the strongly XY-anisotropic Heisenberg ferromagnet can very well generate topological excitations. However, such topological excitations are metastable in nature owing to the fact that the quantum state representing a vortex is not an exact eigen-state of the ferromagnetic XXZ Hamiltonian (4.1) and therefore due the time evolution under the operation of this Hamiltonian, the quantum vortex state decomposes into the constituent magnons and multi-magnon composite states. This happens unless the system size exceeds a threshold value which depends on the degree of the anisotropy. The above mentioned picture is quite plausible in view of the fact that in a very small temperature regime above the ferromagnetic Curie temperature T_c ($=0$ in 2d), magnons and multi-magnon composite state can coexist with single magnons being fragile and damped.

Apart from the investigations on the quantum BKT scenario and quantum mechanical calculations of the DSFs, the work presented in this thesis can provide motivations for further research towards the following direction:

- In this thesis, I have described in considerable details the semi-classical BKT inspired phenomenology and the limitations of its applicability in the low spin layered magnetic systems. However, this phenomenological theory can well be applied to high spin magnetic

systems. In this regard it is worthwhile to mention that the spin dynamics in a Mn^{2+} based spin $\frac{5}{2}$ Honeycomb lattice anti-ferromagnetic material $MnPS_3$ has been investigated via INS experiment [120]. The critical properties of this material have been reported to be well described by 2D XXZ Hamiltonian (anisotropy parameter being equal to 0.998) only in the low $\mathbf{q}^*(= [(\frac{\pi}{a}, \frac{\pi}{a}) - \mathbf{q}])$ regime. Looking at the Honeycomb lattice structure the semi-classical phenomenological theory (which, at present, is applicable only for square lattice) has to be extended to incorporate lattice structures other than square one.

- Since the real magnetic materials exhibit finite inter-layer coupling, the above phenomenology should also be extended to incorporate the effects of the same. Such a phenomenology is expected to bring out the effects of inter-layer coupling on different thermodynamic quantities. So far, the phenomenological approach was taking into account only 2d square lattice structure. It has been already mentioned in chapter 1 that the anomalous jump in specific heat (c_v) near T_{BKT} is a very unique signature of BKT transition. To the best of my knowledge such an anomaly in c_v has not been found so far in experiments performed (in absence of external magnetic field) on layered magnetic systems. A possible reason for this is that the presence of interlayer coupling, however small, in real materials screens such a typical behaviour of c_v , as has been mentioned in chapter 1. It is worthwhile to mention that, only very recently such a specific heat anomaly has been reported in a chemically constructed magnetic multilayer $C_{36}H_{48}Cu_2F_6N_8O_{12}S_2$ (also called TK91) [123]. However, this is under the application of external magnetic field and therefore corresponds to a field-induced BKT scenario, unlike the case of a spontaneous (in absence of external magnetic field) BKT scenario considered in this thesis.
- Our findings regarding the possible microscopic composition of a topological quantum vortex in terms of conventional magnon and multi-magnon composite states can be extended to investigate the effects of magnon-magnon interaction and magnon-vortex interaction on the DSFs especially on the properties (such as width) of the “central peak”.

Appendices

Appendix A

Windsor factor

In Sections 2.2 and 3.2, analytical expressions for the dynamical structure function (DSF) have been obtained by assuming the vortices/merons to constitute a classical ideal gas above T_{BKT} . Convolted DSFs are also calculated in the same classical assumption. Convolted DSFs obtained in this manner are symmetric in energy transfer, $\hbar\omega$ which are in conflict with the experiments. Therefore, a DSF appropriate for comparison with experiment must include a detailed balance factor ensuring that neutron energy-loss scattering ($\hbar\omega > 0$) is correctly weighted with respect to neutron energy-gain scattering ($\hbar\omega < 0$). One thus needs a prescription by which the quantum corrected semi-classical DSFs can be recovered from the DSFs obtained under the classical assumptions. In the following, I am going to describe such a prescription first proposed by Windsor [87]. The central idea of the prescription is to identify the real space classical spin-spin correlation function with the real part of the semi-classical one. Thus,

$$S_{cl}(\mathbf{q}, \omega) = \frac{V}{(2\pi)^4} \int d^3r \int dt e^{i(\mathbf{q}\cdot\mathbf{r} - \omega t)} \frac{1}{2} (\langle \mathbf{S}(\mathbf{0}, 0) \cdot \mathbf{S}(\mathbf{r}, t) \rangle + \text{complex conjugate}), \quad (\text{A.1})$$

where V is the volume of the system under consideration. Since the experimentally measured $S(\mathbf{q}, \omega)$ must always be real, the above equation may be rewritten as,

$$S_{cl}(\mathbf{q}, \omega) = \frac{1}{2} (S(\mathbf{q}, \omega) + S(-\mathbf{q}, -\omega)), \quad (\text{A.2})$$

and for a centro-symmetric system,

$$S_{cl}(\mathbf{q}, \omega) = \frac{1}{2} (S(\mathbf{q}, \omega) + S(\mathbf{q}, -\omega)). \quad (\text{A.3})$$

Once the detailed balance condition corresponding to equation 1.10 is incorporated in the above equation it gives,

$$S(\mathbf{q}, \omega) = \frac{2S_{cl}(\mathbf{q}, \omega)}{1 + \exp(-\hbar\omega/k_B T)}, \quad (\text{A.4})$$

where the factor $\frac{2}{1+\exp(-\hbar\omega/k_B T)}$ is called the *Windsor factor*. This produces semi-classical (detailed balance corrected) DSF from the classical one.

Appendix B

Magnons and Magnon-Magnon interaction

Quanta of the spin waves are called magnons. Spin waves are collective low energy excitations in the long range ordered phase of magnetic materials which can be adequately modelled by Heisenberg exchange Hamiltonian. According to Mermin-Wagner theorem it is only the 3d isotropic Heisenberg model and Ising anisotropic model possess stable magnons at any finite temperatures [111, 114, 115, 121]. In this thesis, we are considering only the two-dimensional systems in a very small temperature regime above zero temperature and the entire soup of magnon-like fragile modes and the composite magnon modes are expected to be found [57, 58, 100]. In this appendix magnon states and the interactions between the magnon modes will be reviewed briefly to develop notations for our convenience.

B.1 One Magnon States

Spin waves are the low energy excitations in the long range ordered phase of magnetic systems [111, 114, 115, 121]. When a spin-deviation is introduced on a particular site of the lattice it does not remain localized on that site. It rather propagates through the lattice due to the exchange interaction between the nearest neighbor spins and thereby constitutes the “spin wave” [111, 114, 115, 121]. The basic unit of the quantized spin waves is the magnons. The normalized quantum state of one spin-deviation is defined as,

$$|ij\rangle = \frac{1}{\sqrt{2S\hbar}} S_{ij}^+ |0\rangle. \quad (\text{B.1})$$

There are $\mathcal{N}(= N^2)$ such orthogonal and normalized states containing one spin deviation each corresponding to all choices of the lattice points. For spin 1/2 systems, assuming the translational invariance and the periodic boundary condition the one magnon state is defined as,

$$|\mathbf{k}\rangle = \sum_{i,j} \frac{e^{i\mathbf{k}\cdot\mathbf{R}_{ij}}}{\sqrt{\mathcal{N}}} S_{ij}^+ |0\rangle = \sum_{i,j} (f_{\mathbf{k}}^{i,j})^* S_{ij}^+ |0\rangle \quad (\text{B.2})$$

where \mathbf{k} is the Bloch wave vector restricted in the first Brillouin zone, describing the propagation of the magnon, \mathbf{R}_{ij} is the position vector of ij^{th} lattice site on the square lattice and $f_{\mathbf{k}}^{ij} = \frac{e^{-i\mathbf{k}\cdot\mathbf{R}_{ij}}}{\sqrt{\mathcal{N}}}$. The one magnon states defined above are normalized to unity, i.e., $\langle \mathbf{k} | \mathbf{k}' \rangle = \delta_{\mathbf{k}\mathbf{k}'}$ and $|\mathbf{k}\rangle$ forms a complete set of orthonormal states [112, 113, 121]. The $|\mathbf{k}\rangle$ States are the exact eigen-states of the Hamiltonian \mathcal{H} corresponding to (4.1) with the eigenvalue $E_0 + \hbar\omega(\mathbf{k})$

The one magnon excitation energy $\hbar\omega(\mathbf{k})$, above the ground state, is given by,

$$\hbar\omega(\mathbf{k}) = 2\hbar^2 Jz(\lambda - \gamma_{\mathbf{k}}), \quad (\text{B.3})$$

where ‘ z ’ is the number of nearest neighbours, $\gamma_{\mathbf{k}} = \frac{1}{z} \sum_{\delta} e^{i\mathbf{k}\cdot\delta}$ and δ is a vector connecting a typical site to its nearest neighbours. For square lattice considered in this thesis $z = 2$. The one spin deviation states can be obtained from (B.2) by the inverse transformation. In the long range ordered phase below the transition temperature (T_C or T_N), as the number of magnon increases with the increasing temperature they are more prone to interact with each other and therefore, the composite magnon modes are very natural to occur [20, 21, 85, 111, 114, 115, 121]. This happens when the spatial lattice is three-dimensional [85]. In the following, we shall restate the well-known definitions of composite magnon states [112, 113, 121].

B.2 Two magnon states

The two-magnon states can be defined, in a similar manner as the one magnon state (see (B.2)) as follows,

$$|\mathbf{k}, \mathbf{k}'\rangle = \sum_{i,j;p,q} \frac{e^{i(\mathbf{k}\cdot\mathbf{R}_{ij} + \mathbf{k}'\cdot\mathbf{R}_{pq})}}{(\sqrt{\mathcal{N}})^2} S_{ij}^+ S_{pq}^+ |0\rangle = \sum_{i,j;p,q} (f_{\mathbf{k}}^{i,j})^* (f_{\mathbf{k}'}^{p,q})^* S_{ij}^+ S_{pq}^+ |0\rangle \quad (\text{B.4})$$

The 2-spin-deviation states $|ij, pq\rangle$ are related to $|\mathbf{k}, \mathbf{k}'\rangle$ in the following way,

$$S_{ij}^+ S_{pq}^+ |0\rangle = \sum_{\mathbf{k}, \mathbf{k}'} f_{\mathbf{k}}^{i,j} f_{\mathbf{k}'}^{p,q} |\mathbf{k}, \mathbf{k}'\rangle. \quad (\text{B.5})$$

These two-magnon states are approximately orthonormal with an error of no more than $O(\frac{1}{N})$ which can be seen from the form of the scalar product, viz., $\langle \mathbf{k}, \mathbf{k}' | \lambda, \lambda' \rangle = \hbar^4 \delta_{\lambda+\lambda', \mathbf{k}+\mathbf{k}'} (\delta_{\lambda, \mathbf{k}} + \delta_{\lambda', \mathbf{k}' - \frac{2}{\mathcal{N}}})$. The very choice of the form of the two-magnon state (B.4) leads to what are called Dyson's "kinematical" and "dynamical" interactions [112, 113].

B.3 Higher magnon states

Using the analogous scheme the 3-magnon composite states are defined as,

$$|\mathbf{k}_1, \mathbf{k}_2, \mathbf{k}_3\rangle = \sum_{i,j;p,q;r,s} (f_{\mathbf{k}_1}^{i,j})(f_{\mathbf{k}_2}^{p,q})(f_{\mathbf{k}_3}^{r,s}) S_{ij}^+ S_{pq}^+ S_{rs}^+ |0\rangle \quad (\text{B.6})$$

The 3-spin-deviations state, $S_{ij}^+ S_{pq}^+ S_{rs}^+ |0\rangle$ is defined as the inverse transformation of the 3-magnon which is similar to the definition of the two spin-deviations in (B.5) [85, 122]. The quantum state of 4-magnon composites can be defined analogously as,

$$|\mathbf{k}_1, \mathbf{k}_2, \mathbf{k}_3, \mathbf{k}_4\rangle = \sum_{i,j;p,q;r,s;l,m} (f_{\mathbf{k}_1}^{i,j})(f_{\mathbf{k}_2}^{p,q})(f_{\mathbf{k}_3}^{r,s})(f_{\mathbf{k}_4}^{l,m}) S_{ij}^+ S_{pq}^+ S_{rs}^+ S_{lm}^+ |0\rangle \quad (\text{B.7})$$

and 4-spin-deviations state $S_{ij}^+ S_{pq}^+ S_{rs}^+ S_{lm}^+ |0\rangle$ is defined as the inverse transformation of the 4-magnon composite states [85]. The simultaneous spin deviations on the direct lattice are governed by the nearest neighbor interaction between the spins.

The set of two-magnon states defined in (B.4) has the scalar product $\langle \mathbf{k}, \mathbf{k}' | \lambda, \lambda' \rangle = \hbar^4 \delta_{\lambda+\lambda', \mathbf{k}+\mathbf{k}'} (\delta_{\lambda, \mathbf{k}} + \delta_{\lambda', \mathbf{k}' - \frac{2}{\mathcal{N}}})$ and therefore two distinct state vectors are not orthogonal in general. These two-magnon states are approximately orthonormal with an error of no more than $O(\frac{1}{N})$ [20, 112, 113]. The effect of the Hamiltonian \mathcal{H} operating on $|\mathbf{k}\mathbf{k}'\rangle$ is given by,

$$\begin{aligned} \mathcal{H}|\mathbf{k}, \mathbf{k}'\rangle &= [E_0 + \hbar\omega(\mathbf{k}) + \hbar\omega(\mathbf{k}')]| \mathbf{k}, \mathbf{k}' \rangle + 2\lambda J \hbar^2 \sum_{i,j;\delta} f_{\mathbf{k}+\mathbf{k}'}^{ij} (1 - \lambda e^{i\mathbf{k}' \cdot \delta}) |ij, ij + \delta\rangle \\ &= [E_0 + \hbar\omega(\mathbf{k}) + \hbar\omega(\mathbf{k}')]| \mathbf{k}, \mathbf{k}' \rangle + \frac{2J\hbar^2}{\mathcal{N}} \sum_{\tilde{\mathbf{k}}, \tilde{\mathbf{k}}'; \delta} \delta_{\mathbf{k}+\mathbf{k}', \tilde{\mathbf{k}}+\tilde{\mathbf{k}}'} e^{-i\tilde{\mathbf{k}}' \cdot \delta} (1 - \lambda e^{i\mathbf{k}' \cdot \delta}) | \tilde{\mathbf{k}}, \tilde{\mathbf{k}}' \rangle, \end{aligned} \quad (\text{B.8})$$

where $f_{\mathbf{k}}^{ij} = \frac{e^{-i\mathbf{k} \cdot R_{ij}}}{N}$ as in (B.2) [85]. The above equation can be rewritten in a convenient form,

$$\mathcal{H}|\mathbf{k}, \mathbf{k}'\rangle = [E_0 + \hbar\omega(\mathbf{k}) + \hbar\omega(\mathbf{k}')]| \mathbf{k}\mathbf{k}' \rangle + \frac{1}{\mathcal{N}} \left[\sum_{\tilde{\mathbf{k}}, \tilde{\mathbf{k}}'} g_{2M}(\mathbf{k}, \mathbf{k}'; \tilde{\mathbf{k}}, \tilde{\mathbf{k}}') | \tilde{\mathbf{k}}, \tilde{\mathbf{k}}' \rangle \right], \quad (\text{B.9})$$

where $g_{2M} = 2J\hbar^2 \sum_{\delta} \delta_{\mathbf{k}+\mathbf{k}', \tilde{\mathbf{k}}+\tilde{\mathbf{k}}'} e^{-i\tilde{\mathbf{k}}'\cdot\delta} (1 - \lambda e^{i\mathbf{k}'\cdot\delta})$ and δ is a vector connecting a typical lattice site to its nearest neighbours [85]. The last term in the equation (B.9) represents the deviation of the 2-magnon state $|\mathbf{k}, \mathbf{k}'\rangle$ from being an eigenstate of the Hamiltonian \mathcal{H} . The 2-magnon energy $E_{2M}(\mathbf{k}, \mathbf{k}')$ is defined as $E_{2M}(\mathbf{k}, \mathbf{k}') = \frac{\langle \mathbf{k}, \mathbf{k}' | \mathcal{H} | \tilde{\mathbf{k}}, \tilde{\mathbf{k}}' \rangle}{\langle \mathbf{k}, \mathbf{k}' | \mathbf{k}, \mathbf{k}' \rangle}$ and is given by,

$$E_{2M}(\mathbf{k}, \mathbf{k}') = E_0 + \hbar\omega(\mathbf{k}) + \hbar\omega(\mathbf{k}') + \frac{1}{\mathcal{N}} \delta E_{2M}(\mathbf{k}, \mathbf{k}'), \quad (\text{B.10})$$

within an error of $O(\frac{1}{\mathcal{N}})$ [20, 85, 112, 113]. Here the quantity $\delta E_{2M}(\mathbf{k}, \mathbf{k}')$ is given by,

$$\delta E_{2M}(\mathbf{k}, \mathbf{k}') = 2J\hbar^2 \sum_{\tilde{\mathbf{k}}, \tilde{\mathbf{k}}'; \delta} \delta_{\mathbf{k}+\mathbf{k}', \tilde{\mathbf{k}}+\tilde{\mathbf{k}}'} e^{-i\tilde{\mathbf{k}}'\cdot\delta} (1 - \lambda e^{i\mathbf{k}'\cdot\delta}) \frac{\langle \mathbf{k}, \mathbf{k}' | \tilde{\mathbf{k}}, \tilde{\mathbf{k}}' \rangle}{\langle \mathbf{k}, \mathbf{k}' | \mathbf{k}, \mathbf{k}' \rangle} \quad (\text{B.11})$$

The very choice of the form of the two-magnon state (B.4) leads to what are called Dyson's "kinematical" and "dynamical" interactions [20, 112, 113]. The term $\delta E_{2M}(\mathbf{k}, \mathbf{k}')$ is in general a complex quantity whose real part represents the interaction energy between two 1-magnons. The imaginary part is related to the inverse scattering lifetime of a given 1-magnon $|\mathbf{k}\rangle$ in the presence of a finite, but low, density of other excitations [20, 112, 113]. Calculation of the complex binary interaction term $\delta E_{2M}(\mathbf{k}, \mathbf{k}')$ is not necessary for our present purpose [85]. A straightforward generalization of (B.9) for the 3-magnon states is given by,

$$\begin{aligned} \mathcal{H} |\mathbf{k}_1, \mathbf{k}_2, \mathbf{k}_3\rangle &= [E_0 + \hbar\omega(\mathbf{k}_1) + \hbar\omega(\mathbf{k}_2) + \hbar\omega(\mathbf{k}_3)] |\mathbf{k}_1, \mathbf{k}_2, \mathbf{k}_3\rangle \\ &+ \frac{1}{\mathcal{N}} \left[\sum_{\tilde{\mathbf{k}}_1, \tilde{\mathbf{k}}_2, \tilde{\mathbf{k}}_3} g_{3M}(\mathbf{k}_1, \mathbf{k}_2, \mathbf{k}_3; \tilde{\mathbf{k}}_1, \tilde{\mathbf{k}}_2, \tilde{\mathbf{k}}_3) |\tilde{\mathbf{k}}_1, \tilde{\mathbf{k}}_2, \tilde{\mathbf{k}}_3\rangle \right] \end{aligned} \quad (\text{B.12})$$

Energy corresponding to the 3-magnon states is given by,

$$E_{3M}(\mathbf{k}_1, \mathbf{k}_2, \mathbf{k}_3) = E_0 + \hbar\omega(\mathbf{k}_1) + \hbar\omega(\mathbf{k}_2) + \hbar\omega(\mathbf{k}_3) + \frac{1}{\mathcal{N}} \delta E_{3M}(\mathbf{k}_1, \mathbf{k}_2, \mathbf{k}_3), \quad (\text{B.13})$$

within an error of $O(\frac{1}{\mathcal{N}})$. The term $\delta E_{3M}(\mathbf{k}_1, \mathbf{k}_2, \mathbf{k}_3)$ is in general complex and represents three-magnon interactions corresponding to three simultaneous spin deviations on the direct lattice [85]. The effect of the Hamiltonian H operating on the 4-magnon states (given by (B.7)) is,

$$\begin{aligned} \mathcal{H} |\mathbf{k}_1, \mathbf{k}_2, \mathbf{k}_3, \mathbf{k}_4\rangle &= [E_0 + \hbar\omega(\mathbf{k}_1) + \hbar\omega(\mathbf{k}_2) + \hbar\omega(\mathbf{k}_3) + \hbar\omega(\mathbf{k}_4)] |\mathbf{k}_1, \mathbf{k}_2, \mathbf{k}_3, \mathbf{k}_4\rangle \\ &+ \frac{1}{\mathcal{N}} \left[\sum_{\tilde{\mathbf{k}}_1, \tilde{\mathbf{k}}_2, \tilde{\mathbf{k}}_3, \tilde{\mathbf{k}}_4} g_{4M}(\mathbf{k}_1, \mathbf{k}_2, \mathbf{k}_3, \mathbf{k}_4; \tilde{\mathbf{k}}_1, \tilde{\mathbf{k}}_2, \tilde{\mathbf{k}}_3, \tilde{\mathbf{k}}_4) |\tilde{\mathbf{k}}_1, \tilde{\mathbf{k}}_2, \tilde{\mathbf{k}}_3, \tilde{\mathbf{k}}_4\rangle \right] \end{aligned} \quad (\text{B.14})$$

Similarly, the energy corresponding to the 4-magnon states are given, within an error of $O(\frac{1}{\mathcal{N}})$ as,

$$E_{4M}(\mathbf{k}_1, \mathbf{k}_2, \mathbf{k}_3, \mathbf{k}_4) = E_0 + \hbar\omega(\mathbf{k}_1) + \hbar\omega(\mathbf{k}_2) + \hbar\omega(\mathbf{k}_3) + \hbar\omega(\mathbf{k}_4) + \frac{1}{\mathcal{N}} \delta E_{4M}(\mathbf{k}_1, \mathbf{k}_2, \mathbf{k}_3, \mathbf{k}_4) \quad (\text{B.15})$$

Here the quantity $\delta E_{4M}(\mathbf{k}_1, \mathbf{k}_2, \mathbf{k}_3, \mathbf{k}_4)$ represents 4-magnon interactions corresponding to four simultaneous spin deviations on the direct lattice. [85]

Appendix C

The Tukey and the modified Tukey function

The most general form for the Tukey function is given by,

$$R(t) = \begin{cases} \frac{1}{2}[1 + \cos(\frac{\pi}{1-\alpha} \frac{2t}{t_m} + \frac{\pi}{1-\alpha} - \pi)], & \text{for } \frac{-t_m}{2} \leq t < \frac{-t_m}{2}\alpha \\ 1, & \text{for } \frac{-t_m}{2}\alpha \leq t \leq \frac{t_m}{2}\alpha \\ \frac{1}{2}[1 + \cos(\frac{\pi}{1-\alpha} \frac{2t}{t_m} - \frac{\pi}{1-\alpha} + \pi)], & \text{for } \frac{t_m}{2}\alpha < t \leq \frac{t_m}{2} \\ 0, & \text{otherwise,} \end{cases} \quad (\text{C.1})$$

where α is called the tapering parameter [52, 53].

The Tukey function we have used in this thesis is corresponding to $\alpha = 0$. In this case the above general expression takes the form,

$$R(t) = \begin{cases} \frac{1}{2}[1 + \cos(\frac{2\pi t}{t_m})], & \text{for } |t| \leq \frac{t_m}{2} \\ 0, & \text{otherwise,} \end{cases} \quad (\text{C.2})$$

which is corresponding to zero tapering. The Fourier transform of the above Tukey function (corresponding to zero tapering) is given by,

$$\tilde{R}(\omega) = \frac{1}{4\pi} \sin(\frac{\omega t_m}{2}) (\frac{2}{\omega} - \frac{1}{\omega + \frac{2\pi}{t_m}} - \frac{1}{\omega - \frac{2\pi}{t_m}}). \quad (\text{C.3})$$

The full width at half maximum (FWHM) for the above function is given by $\Delta_{FWHM}^{(T)} = \frac{4\pi}{t_m}$, expressed in the units of energy, where the superscript T signifies the Tukey function [58]. To

find the value of t_m the above expression for $\Delta_{FWHM}^{(T)}$ is equated to the value of the resolution width which is generally specified in the experiment.

The modified Tukey (MT) function we have used in our analysis is corresponding to 50% tapering, i.e. $\alpha = 0.5$, and is given by,

$$\mathcal{R}(t) = \begin{cases} \frac{1}{2}[1 - \cos(\frac{4\pi t}{t_m})], & \text{for } \frac{-t_m}{2} \leq t \leq \frac{-t_m}{4} \\ 1, & \text{for } \frac{-t_m}{4} \leq t \leq \frac{t_m}{4} \\ \frac{1}{2}[1 - \cos(\frac{4\pi t}{t_m})], & \text{for } \frac{t_m}{4} \leq t \leq \frac{t_m}{2} \\ 0, & \text{otherwise.} \end{cases} \quad (\text{C.4})$$

Fourier transform of the above modified Tukey function is given by,

$$\tilde{\mathcal{R}}(\omega) = \frac{1}{4\pi} [\sin(\frac{\omega t_m}{2}) + \sin(\frac{\omega t_m}{4})] (\frac{2}{\omega} - \frac{1}{\omega + \frac{4\pi}{t_m}} - \frac{1}{\omega - \frac{4\pi}{t_m}}). \quad (\text{C.5})$$

The full width at half maximum corresponding to the above function $\mathcal{R}(\omega)$ can be found out to be $\Delta_{FWHM}^{(MT)} \approx \frac{3.2\pi}{t_m}$, expressed in the units of energy. In this case, to find the value of t_m we have to equate $\Delta_{FWHM}^{(MT)}$ to the value of the resolution width specified in the experiment.

Appendix D

Dependence Of The Physical Range On The Magnitude Of The Value Of Spin

For classical spin wave at very low temperature corresponding to a classical Heisenberg ferromagnet, the dynamical structure function has the following form:-

$$\begin{aligned} S(\mathbf{q}, \omega) &= \delta(\omega^2 - \omega_q^2) \\ &= \frac{1}{2\omega_q} [\delta(\omega - \omega_q) + \delta(\omega + \omega_q)], \end{aligned} \quad (\text{D.1})$$

where, $\omega_q = \hbar^{-1} J \sqrt{S(S+1)} z(1 - \gamma_q)$ for a cubic lattice [83]. Here ‘ z ’ is the number of nearest neighbours and $\gamma_q = \frac{1}{z} \sum_r \cos(\mathbf{q} \cdot \mathbf{r})$.

Convolved dynamical structure function, $S_{conv}(\mathbf{q}, \omega)$ has been defined in (2.17), where $\tilde{R}(\omega - \omega')$ is the Fourier transform of a suitably chosen spectral function. So far Tukey function has been used and the same is used in this case also. The Fourier transform of Tukey function is given by (C.3). Using (2.17), (2.27) and (D.1) we find the convolved dynamical structure function corresponding to spin wave, $S_{conv}^{SW}(\mathbf{q}, \omega)$ to be,

$$S_{conv}^{SW}(\mathbf{q}, \omega) = \frac{1}{2\omega_q} [R(\omega - \omega_q) + R(\omega + \omega_q)]. \quad (\text{D.2})$$

Analysing (D.2) we find that there exists a range

$$|\omega| \leq \left(\omega_q + \frac{4\pi}{t_m}\right) \quad (\text{D.3})$$

within which $S_{conv}^{SW}(\mathbf{q}, \omega)$ remains positive and outside, it becomes negative. This remains true even if we choose any other resolution function [83]. This is basically due to the fact that when Fourier transform is performed on spectral functions (defined in time domain), the resulting functions in (\mathbf{q}, ω) space mostly turn out to be oscillatory [53].

One way to avoid these negative values of $S_{conv}(\mathbf{q}, \omega)$ would be to assume $S_{conv}(\mathbf{q}, \omega) = 0$ outside $|\omega| \leq (\omega_q + \frac{4\pi}{t_m})$ [83,89]. This prescription however, can't be taken into consideration when comparing theoretical predictions with experimental results, if the energy range of experimental interest contains the above mentioned range of ω . Another way to avoid the negative values of $S_{conv}(\mathbf{q}, \omega)$ is to decrease the value of t_m [see (D.3)], where t_m is related to the experimental resolution width ($\Delta\omega$) by the relation,

$$t_m \simeq \frac{\hbar}{2\Delta\omega}, \quad (\text{D.4})$$

$\Delta\omega$ being in energy units. Decrease in t_m means increase in the value of $\Delta\omega$ which signifies a poor experimental resolution width. However, in comparing the theoretical predictions with the experimental results, t_m is determined by the relation (D.4), where the value of $\Delta\omega$ remains fixed because it is generally mentioned in the experiment [83].

Another interesting feature of (D.3) is the fact that the region of ω where $S_{conv}(\mathbf{q}, \omega)$ remains positive, depends on the spin value S via the relation,

$$|\omega| \leq (\hbar^{-1} J \sqrt{S(S+1)} z [1 - \gamma_q] + \frac{4\pi}{t_m}). \quad (\text{D.5})$$

This shows that when t_m is fixed from the experimental resolution width, S remains as the free parameter to determine the range of ω as mentioned in (D.3). Increase in S will increase the range of ω where $S_{conv}(\mathbf{q}, \omega)$ remains positive [83]. Hence for a system with high spin value ' S ', the range of positive $S_{conv}(\mathbf{q}, \omega)$ may actually be at par with the energy range of experimental interest, unlike the case of spin $\frac{1}{2}$.

It can be shown from (D.2) that the range of ω , given by (D.3), will not change even if a detailed balance factor (in this case Windsor factor) is introduced to incorporate the quantum effects.

Bibliography

- [1] E. Ising, Z. Phys. “*Beitrag zur theorie des ferromagnetismus,*” **31**, 253258 (1925); S. G. Brush, “*History of the Lenz-Ising model,*” Rev. Mod. Phys **39**, 883 (1967)
- [2] H. Bethe, “*On the theory of metals I. Eigenvalues and eigenfunctions of the linear atom chain,*” Z. Phys. **71**, 205(1931).
- [3] L. Onsager, “*Crystal Statistics: I. A Two-Dimensional Model with an Order-Disorder Transition,*” Phys. Rev. **65**, 117 (1944).
- [4] L. J. De Jongh, Ed., “*Magnetic properties of layered transition metal compounds,*” Kluwer Academic Publishers (1990).
- [5] T. Chatterji, “*Magnetic Neutron Scattering,*” in T. Chatterji (Eds), Neutron Scattering from Magnetic Materials, Elsevier B. V. (2006).
- [6] J. G. Bednorz and A. K. Müller, “*Possible high T_c superconductivity in the Ba-La-Cu-O system,*” Z. Phys. B **64** (2), 189193 (1986).
- [7] Y. Endoh, et.al., “*Static and dynamic spin correlations in pure and doped La_2CuO_4 ,*” Phys. Rev. B **37**, 7443 (1988).
- [8] K. Yamada, et.al., “*Spin dynamics in the two-dimensional quantum antiferromagnet La_2CuO_4 ,*” Phys. Rev B **40**, 4557-4565, (1989).
- [9] N. D. Mermin and H. Wagner, “*Absence of Ferromagnetism or Antiferromagnetism in One- or Two-Dimensional Isotropic Heisenberg Models,*” Phys. Rev. Letts. **17**, 1133 (1966); erratum: Phys. Rev. Letts. **17**, 1307 (1966).
- [10] S. Coleman, “*There are no Goldstone bosons in two dimensions,*” Commun. Math. Phys. **31**, 259 (1973).

- [11] J. V. José, Ed., “*40 Years of Berezinskii-Kosterlitz-Thouless Theory*,” World Scientific (2013), Chap. 1.
- [12] J. M. Kosterlitz and D. J. Thouless, “*Ordering, metastability and phase transitions in two-dimensional systems*,” J. Phys. C **6** 1181(1973).
- [13] V. L. Berezinskii, “*Destruction of Long-range Order in One-dimensional and Two-dimensional Systems having a Continuous Symmetry Group I. Classical Systems*,” Sov. Phys. JETP **32**, 493(1970); “*Destruction of Long-range Order in One-dimensional and Two-dimensional Systems having a Continuous Symmetry Group II. Quantum Systems*,” Sov. Phys. JETP **34**, 610(1972).
- [14] C. K. Majumdar and D. K. Ghosh, “*On NextNearestNeighbor Interaction in Linear Chain. I*,” J. Math. Phys., **10**, 1388 (1969).
- [15] E. Fradkin, “*Field Theories of Condensed Matter Physics*,” Second Edition, Cambridge University Press (2013).
- [16] A. Sandvik, arXiv:1101.3281v1 [cond-mat.str-el] 17 Jan 2011.
- [17] I. U. Heilmann, G. Shirane, Y. Endoh, R.J. Birgeneau, S.L. Holt, “*Neutron study of the line-shape and field dependence of magnetic excitations in $\text{CuCl}_2 \cdot 2\text{N}(\text{C}_5\text{D}_5)$* ,” Phys. Rev. B **18**, 3530 (1978).
- [18] M. Hase, I. Terasaki, K. Uchinokura, “*Observation of the spin-Peierls transition in linear Cu^{2+} (*spin-1/2*) chains in an inorganic compound CuGeO_3* ,” Phys. Rev. Lett. **70**, 3651 (1993).
- [19] H.-J. Mikeska and M. Steiner, “*Solitary excitations in one-dimensional magnets*,” Adv. Phys. **40**, 191 (1991).
- [20] D. C. Mattis, “*Theory of Magnetism Made Simple*,” Chapter 5 (World Scientific, Singapore, 2006).
- [21] S. W. Lovesey, “*Theory of Neutron Scattering from Condensed Matter*,” Vol. 2, Chapter 9 (Oxford University Press, New York, 1984).

- [22] C. K. Majumdar, “Antiferromagnets” in “*Exactly Solvable Models in Condensed Matter and Relativistic Field Theory*,” Ed. by B. S. Shastry, S. S. Jha, and V. Singh, Springer-Verlag Berlin (1985), Pages 142- 157.
- [23] J. Villain, “*Propagative spin relaxation in the Ising-like antiferromagnetic linear chain*,” Physica B+C **79**, 1 (1975).
- [24] E. Lieb, T. D. Schultz, and D. C. Mattis, “*Two soluble models of an antiferromagnetic chain*,” Ann. Phys. (NY) **16**, 407 (1961).
- [25] B. M. McCoy, “*Spin correlation functions of the XY model*,” Phys. Rev. **173**, 531 (1968).
- [26] J. des Cloizeaux and J. J. Pearson, “*Spin-wave spectrum of the antiferromagnetic linear chain*,” Phys. Rev **128**, 2131 (1962).
- [27] L. D. Fadeev and L. A. Takhtajan, “*What is the spin of a spin wave?*,” Phys. Lett **85A**, 375 (1981).
- [28] F. D. M. Haldane, “*Spontaneous dimerization in the $S=1/2$ Heisenberg antiferromagnetic chain with competing interactions*,” Phys. Rev. B **25**, 4925 (1982).
- [29] K. Okamoto and K. Nomura, “*Fluid-dimer critical point in $S = 1/2$ antiferromagnetic Heisenberg chain with next nearest neighbor interactions*,” Phys. Lett. **A169**, 169 (1992).
- [30] M. Hase, I. Terasaki, and K. Uchinokura, “*Observation of the spin-Peierls transition in linear Cu^{2+} ($spin-1/2$) chains in an inorganic compound $CuGeO_3$* ,” Phys. Rev. Lett. **70**, 3651 (1993).
- [31] K. Uchinokura, “*Spin-Peierls transition in $CuGeO_3$ and impurity-induced ordered phases in low-dimensional spin-gap systems*,” J. Phys.: Condens. Matter **14** R195R237 (2002).
- [32] F. D. M. Haldane, “*Continuum dynamics of the 1-D Heisenberg anti-ferromagnet: Identification with the $O(3)$ non-linear sigma model*,” Phys. Lett. **A93**, 464 (1983); “*Nonlinear Field Theory of Large-Spin Heisenberg Antiferromagnets: Semiclassically Quantized Solitons of the One-Dimensional Easy-Axis Néel State*,” Phys. Rev. Lett. **50**, 1153 (1983).
- [33] M. Hagiwara, K. Katsumata, Ian Affleck, B. I. Halperin, and J. P. Renard, “*Observation of $S=1/2$ degrees of freedom in an $S=1$ linear-chain Heisenberg antiferromagnet*,” Phys. Rev. Lett. **65**, 3181 (1990).

- [34] H. J. Mikeska and A. K. Kolezhuk, “*One-Dimensional Magnetism*,” Lect. Notes Phys **645**, 1-83 (2004).
- [35] C. Lacroix, P. Mendels, and F. Mila, “*Introduction to frustrated magnetism: Materials, Experiments, Theory*,” Springer (2010).
- [36] L. D. Landau and E. M. Lifshitz, “*Statistical Physics- Part 1*,” 3rd Ed., Pergamon Press Ltd, New York, USA (1980), p 482.
- [37] D. L. Huber, “*Critical slowing down in the transverse autocorrelation function of a two dimensional planar magnet*,” Phys. Lett. **68A**, 125 (1978); “*Dynamics of spin vortices in two-dimensional planar magnets*,” Phys. Rev. B. **26**, 3758(1982).
- [38] F. G Mertens, A. R. Bishop, G. M. Wysin and C. Kawabata, “*Vortex signatures in dynamic structure factors for two-dimensional easy-plane ferromagnets*,” Phys. Rev. Lett, **59**, 117(1987); “*Dynamical correlations from mobile vortices in two-dimensional easy-plane ferromagnets*,” Phys. Rev. B. **39**, 591(1989).
- [39] M. E. Gouvêa, G. M. Wysin, A. R. Bishop, F. G. Mertens, “*Vortices in the classical two-dimensional anisotropic Heisenberg model*,” Phys. Rev. B, **39**, 11840(1989).
- [40] A. R. Völkel, G. M. Wysin, A. R. Bishop and F. G. Mertens, “*Dynamic correlations in the classical two-dimensional antiferromagnetic Heisenberg model with easy-plane symmetry*,” Phys. Rev. B. **44**, 10066(1991).
- [41] G. M. Wysin and A. R. Bishop, “*Dynamic correlations in a classical two-dimensional Heisenberg antiferromagnet*,” Phys. Rev. B., **42**, 810 (1990).
- [42] P. W. Anderson, S. John, G. Baskaran, B. Doucot and S. D. Liang, Princeton University Preprint, 1988.
- [43] K. G. Wilson and J. B. Kogut, “*The Renormalization Group and The ϵ Expansion*,” Phys. Rep. **12C**, 75 (1974); J. Zinn-Justin, “*Quantum Field Theory and Critical Phenomena*,” Oxford University Press (2002), Chapters 24, 29 and 37.
- [44] P. C. Hohenberg and B. I. Halperin, “*Theory of dynamic critical phenomena*,” Rev. Mod. Phys. **49**, 435 (1977); J. Cardy, “*Scaling and Renormalization in Statistical Physics*,” Cambridge University Press (1996), Page 199.

- [45] H. E. Stanley, “*Introduction to Phase Transition and Critical Phenomena*,” Clarendon Press, Oxford (1971).
- [46] N. Goldenfeld, “*Lectures on Phase Transitions and the Renormalization Group*,” Perseus Books, NY, USA (30 June 1992)
- [47] P. M. Chaikin and T. C. Lubensky, “*Principles of Condensed Matter Physics*,” Cambridge University Press India Pvt. Ltd, New Delhi, India (1998).
- [48] J. M. Kosterlitz, “*Critical properties of 2-dimensional XY model*,” J. Phys **C7**, 1046 (1974).
- [49] J. Als-Nielsen, “*Neutron scattering and spatial correlations near the critical point*,” in “*Phase transition and critical phenomena*,” Vol. 5a, Ed. by C. Domb and M. S. Green, Academic Press, London, 1976.
- [50] G. Shirane, S. M. Shapiro, and J. M. Tranquada, “*Neutron Scattering with a Triple-Axis Spectrometer, Basic Techniques*,” (Cambridge University Press) 2004, Chaps. : 1, 4.
- [51] R. Currat, “*THREE-AXIS INELASTIC NEUTRON SCATTERING*,” Chap 12, in “*NEUTRON AND X-RAY SPECTROSCOPY*,” Ed. by F. Hippert, et.al., Springer, Netherlands (2006); Page 400.
- [52] G. M. Jenkins and D. G. Watts, *Spectral Analysis and Its Applications*, (Holden-Day), 1968, Chap:6.
- [53] F. J. Harris, “*On the use of windows for harmonic analysis with the discrete Fourier transform*,” Proceedings of The IEEE, **66**, 51(1978).
- [54] R. C. Tolman, “*The Principles of Statistical Mechanics*,” (Dover Publication), 1976, Chap. XII .
- [55] J. E. Mooij, “*The Vortex State*,” Ed. by N. Bontemps, Y. Bruynseraede, and G. Deutscher, Kluwer, Dordrecht (1994).
- [56] R. Fazio and G. Schön, “*Charges and Vortices in Josephson Junction Arrays*”, in “*40 Years of Berezinskii-Kosterlitz-Thouless Theory*,” edited by J. V. José, World Scientific (2013).
- [57] P. Böni and G. Shirane, “*Paramagnetic neutron scattering from the Heisenberg ferromagnet EuO*,” Phys. Rev. B **33**, 3012 (1986).

- [58] R. Chaudhury and B. S. Shastry, “*Spin dynamics of EuO in the paramagnetic phase,*” Phys. Rev. B. **37**, 5216(1988); “*Spin dynamics of EuS in the paramagnetic phase,*” Phys. Rev. B **40**, 5036 (1989).
- [59] L. P. Regnault and J. Rossat-Mignod, “*Phase Transitions in Quasi-Two Dimensional Planar Magnets,*” in “*Magnetic properties of layered transition metal compounds,*” , Ed. by L. J. deJongh, Kluwer Academic Publishers (1990).
- [60] L. P. Regnault, et.al., in “*Magnetic Excitations and Fluctuations,*” Ed. by, S. W. Lovesey, et.al., Springer Series in Solid State Sciences **54**, 1984, page 201.
- [61] D. R. Nelson and J. M. Kosterlitz, “*Universal Jump in the Superfluid Density of Two-Dimensional Superfluids,*” Phys. Rev. Lett **39**, 1201 (1977).
- [62] V. L. Pokrovsky and G. V. Uimin, “*Magnetic properties of two-dimensional and layered systems,*” Phys. Lett **45A**, 467 (1973).
- [63] D. D. Betts, in “*Phase Transitions and Critical Phenomena,*” Ed. by C. Domb and M. S. Green, Vol. 3, Academic Press (1974).
- [64] K. Hirakawa, H. Yoshizawa, K. Ubukoshi, “*Neutron Scattering Study of the Phase Transition in Two-Dimensional Planar Ferromagnet K_2CuF_4 ,*” J. Phys. Soc. Jpn., **51**, 2151 (1982).
- [65] K. Hirakawa, et.al., J. Phys. Soc. Jpn. Part-2, “*Neutron Scattering Study of Spin Dynamics at the Magnetic Phase Transition in Two-Dimensional Planar Ferromagnet K_2CuF_4 ,*” **52**, 4220 (1983).
- [66] M. Hemmida, et.al., “*Vortex dynamics and frustration in two-dimensional triangular chromium lattices,*” Phys. Rev B **80**, 054406 (2009).
- [67] M. Heinrich, H.-A. Krug von Nidda, A. Loidl, N. Rogado, and R. J. Cava, “*Potential Signature of a Kosterlitz-Thouless Transition in $BaNi_2V_2O_8$,*” Phys. Rev. Lett **91**, 137601-1 (2003).
- [68] T. Förster, et.al., “*Spin fluctuations with two-dimensional XY behavior in a frustrated $S = 1/2$ square-lattice ferromagnet,*” Phys. Rev B **87**, 180401(R) (2013), and references therein.

- [69] B. A. Ivanov et al., “*Magnon modes and magnon-vortex scattering in two dimensional easy-plane ferromagnets,*” Phys. Rev. B **58**, 8464 (1998).
- [70] G. M. Wysin and A. R. Vökel, “*Normal modes of vortices in easy-plane ferromagnets,*” Phys. Rev. B **52**, 7412 (1995).
- [71] B. V. Costa, M. E. Gouvea and A. S. T. Pires, “*Vortex-magnon interaction in the 2d XY ferromagnetic model,*” Phys. Lett. **A165**, 179 (1992).
- [72] B. V. Costa and A. B. Lima, “*Dynamical behavior of vortices in thin film magnetic systems,*” J. Magn. Magn. Mater. **324**, 1999 (2012).
- [73] D. D. Betts, F. C. Salevsky and J. Rogiers, “*Vortices in the two-dimensional $s = 1/2$ XY model,*” J. Phys. A: Math. Gen. **14**, 531 (1981).
- [74] E. Loh Jr., D. J. Scalapino and P. M. Grant, “*Monte Carlo studies of the quantum XY model in two dimensions,*” Phys. Rev. B: Rapid. Commun. **31**, 4712 (1985).
- [75] K. Harada and N. Kawashima, “*Kosterlitz-Thouless transition of quantum XY model in two dimensions,*” J. Phys. Soc. Jpn. **67**, 2768 (1998).
- [76] R. Chaudhury and S. K. Paul, “*Possible existence of topological excitations in quantum spin models in low dimensions,*” Phys. Rev. B **60**, 6234(1999).
- [77] R. Chaudhury and S. K. Paul, “*Effective theory for a quantum spin system in low dimensions -beyond the long wavelength limit,*” Mod. Phys. Lett. B, **16**, 251-259(2002).
- [78] R. Chaudhury and S. K. Paul, “*Physical realization of topological excitations in quantum Heisenberg ferromagnet on lattice,*” Eur. Phys. J. B **76**, 391-398(2010).
- [79] R. Chaudhury and S. K. Paul, “*Topological Excitations in Quantum Spin Systems,*” Adv. Condens. Matter Phys. 2013, 783420 (2013).
- [80] R. Chaudhury, “*High temperature superconductivity-current status, our theoretical and experimental work,*” Indian J.Phys **66A**, 159 (1992).
- [81] J. V. José, L. P. Kadanoff, Scott Kirkpatrick and D. R. Nelson, “*Renormalization, vortices, and symmetry-breaking perturbations in the two-dimensional planar model,*” Phys. Rev. B **16**, 1217 (1977).

- [82] G. M. Wysin and A. R. Völkel, “Normal modes of vertices in easy-plane ferromagnets,” Phys. Rev. B **52**, 7412 (1995).
- [83] S. Sarkar, S. K. Paul and R. Chaudhury, “Theoretical analysis of neutron scattering results for quasi-two dimensional ferromagnets,” Eur. Phys. J. B, **85**, 380 (2012).
- [84] S. Sarkar, R. Chaudhury and S. K. Paul, “Semi-phenomenological analysis of neutron scattering results for quasi-two dimensional quantum anti-ferromagnet,” arXiv:1410.5921v3 [cond-mat.str-el] (2015).
- [85] S. Sarkar, R. Chaudhury and S. K. Paul, “The connection between vortex-like topological excitations and conventional excitations in quantum ferromagnetic spin systems on two-dimensional lattice and their stability,” Int. J. Mod. Phys. B **29**, 1550209 (2015) [22 pages].
- [86] S. Hikami and T. Tsuneto, “Phase Transition of Quasi-Two Dimensional Planar Syatems,” Prog. Theor. Phys **63**, 387 (1980).
- [87] C. G Windsor and J. Locke-Wheaton, “Computer simulation of the dynamics of one-dimensional Heisenberg magnets,” J. Phys. C**9**, 2749 (1976); M. T. Evans and C. G. Windsor, “Spin correlations in $RbMnF_3$ at $1.17T_N$,” J. Phys. C **6**, 495 (1973).
- [88] K. Hirakawa and H. Ikeda, “Neutron Scattering Experiments on Two-Dimensional Heisenberg and Ising Magnets,” in “Magnetic properties of layered transition metal compounds,” , Ed. by. L. J. deJongh, Kluwer Academic Publishers (1990); Page 238.
- [89] M. Takahashi, “Spin-Wave Mode of Classical Heisenberg Model at High Temperature,” J. Phys. Soc. Jpn **52**, 3592 (1983).
- [90] S. Chakravarty, B. I. Halperin, and D. R. Nelson, *Low-temperature behavior of two-dimensional quantum antiferromagnets,*” Phys. Rev. Lett **60**, 1057 (1988).
- [91] D. P. Arovas and A. Auerbach, *Functional integral theories of low dimensional quantum Heisenberg models,*” Phys. Rev. B, **38**, 316-332, (1988).
- [92] E. Vitali, M. Rossi, L. Reatto, and D. E. Galli, “Ab initio low-energy dynamics of superfluid and solid 4He ,” Phys. Rev. B **82**, 174510 (2010); O. F. Syljuasen, “Using average spectrum method to extract dynamics from quantum Monte Carlo simulations,” Phys. Rev. B **78**, 174429 (2008).

- [93] M. A. Kastner, R. J. Birgeneau, G. Shirane, and Y. Endoh, “*Magnetic, transport, and optical properties of monolayer copper oxides*,” *Rev. Mod. Phys.*, **70**, No. 3, (1998).
- [94] C. M. Varma, “*Quantum criticality in quasi-two-dimensional itinerant antiferromagnets*,” *Phys. Rev. Lett* **115**, 186405 (2015).
- [95] C. M. Varma, Lijun Zhu, and Almut Schröder, “*Quantum critical response function in quasi-two-dimensional itinerant antiferromagnets*,” *Phys. Rev. B* **92**, 155150 (2015).
- [96] Y. H. Chen, F. Wilczek, E. Witten and B. I. Helperin, “*On Anyon superconductivity*,” *Int. J. Mod. Phys. B*, **3**, 1001 (1989).
- [97] T. Thio, T. R. Thurston, N. W. Preyer, P. J. Picone, M. A. Kastner, H. P. Jenssen, D. R. Gabbe, C. Y. Chen, R. J. Birgeneau, and A. Aharony, “*Antisymmetric exchange and its influence on the magnetic structure and conductivity of La_2CuO_4* ,” *Phys. Rev. B* **38**, 905 (1988).
- [98] R. Chaudhury, F. Demmel and T. Chatterji, “*Dynamical Response of Single Bi-layer Spin Model : A Theoretical Analysis*,” arXiv:1104.4197v1.
- [99] R. Chaudhury, “*Spin dynamics of layered triangular antiferromagnets with uniaxial anisotropy*,” *J. Magn. Magn. Mater.* **307**, 99 (2006).
- [100] T. Chatterji, F. Demmel and R. Chaudhury, “*Spin dynamics of the quasi-2D ferromagnetic bilayer manganite $La_{1.2}Sr_{1.8}Mn_2O_7$* ,” *Physica B* **385-386**, 428 (2006).
- [101] L. Berger, Y. Labaye, M. Tamine, and J. M. D. Coey, “*Ferromagnetic nanoparticles with strong surface anisotropy: Spin structures and magnetization processes*,” *Phys. Rev. B* **77**, 104431, (2008).
- [102] A. Wachowiak, J. Wiebe, M. Bode, O. Pietzsch, M. Morgenstern and R. Wiesendanger, “*Direct Observation of Internal Spin Structure of Magnetic Vortex Cores*,” *Science*, **298**, 577 (2002).
- [103] R. P. Cowburn, D. K. Koltsov, A. O. Adeyeye, M. E. Welland, and D. M. Tricker, “*Single-Domain Circular Nanomagnets*,” *Phys. Rev. Lett*, **83**, 1042, (1999).
- [104] B. Van Waeyenberge, et.al., “*Magnetic vortex core reversal by excitation with short bursts of an alternating field*,” *Nature*, **444**, 461 (2006).

- [105] H. Hauser, J. Hochreiter, G. Stangl, R. Chabicovsky, M. Janiba and K. Riedling,, J. Magn. Mater., “*Anisotropic magnetoresistance effect field sensors,*” **215**, 788 (2000).
- [106] J. McCord and J. Westwood, “,” IEEE Trans. Magn., “*Domain Optimization of Sputtered Permalloy Shields for Recording Heads,*” **37**, 1755, (2001).
- [107] D. D. Sheka, et.al., “*Amplitudes for magnon scattering by vortices in two-dimensional weakly easy-plane ferromagnets,*” Phys. Rev. B **69**, 054429 (2004).
- [108] A. S. Kovalev, F. G. Mertens, and H. J. Schnitzer, “*Cycloidal vortex motion in easy-plane ferromagnets due to interaction with spin waves,*” Eur. Phys. J. B **33**, 133-145 (2003).
- [109] J. E. R. Costa and B. V. Costa, “*Static and dynamic simulation in the classical two-dimensional anisotropic Heisenberg model,*” Phys. Rev. B **54**, 994 (1996).
- [110] J. E. R. Costa, B. V. Costa and D.P. Landau, “*Monte Carlo and spin dynamics study of the anisotropic Heisenberg model in two dimensions,*” J. Appl. Phys. **81**, 5746(1997).
- [111] K. Yoshida, “*Theory of Magnetism,*” Springer-Verlag (1996), Chap. 8, Pages 107- 124.
- [112] R. G. Boyd and J. Callaway, “*Spin-Wave Spin-Wave Scattering in a Heisenberg Ferromagnet,*” Phys. Rev. **138**, A1621 (1965).
- [113] F. J. Dyson, “*General theory of spin-wave interactions,*” Phys. Rev. **102**, 1217 (1956).
- [114] C. Kittel, “*Introduction to Solid State Physics,*” Seventh Edition, John Wiley & Sons (Asia) Pte. Ltd. (1995), Chap. 15, Pages 443- 468.
- [115] E. L. Nagaev, “*Physics of Magnetic Semiconductors,*” Mir Publishers, Moscow (1983), Chap. 2, Pages 60- 95.
- [116] S. Sarkar, R. Chaudhury and S. K. Paul, Under Preparation (2016).
- [117] P. Fazekas and P. W. Anderson, “*On the ground state properties of the anisotropic triangular antiferromagnet,*” Phil. Mag., **30**, 423 (1974).
- [118] H.-Q. Ding and M. S. Makivic, “*Kosterlitz-Thouless transition in the two-dimensional quantum XY model,*” Phys. Rev. B **42**, 6827(R) (1990).

- [119] Alessandro Cuccoli, Valerio Tognetti, Paola Verrucchi, and Ruggero Vaia, “*Quantum effects on the Berezinskii-Kosterlitz-Thouless transition in the ferromagnetic two-dimensional XXZ model,*” *Phys. Rev. B* **51**, 12840 (1995).
- [120] A. R. Wildes, H. M. Rønnow, B. Roessli, M. J. Harris and, K. W. Godfrey, “*Static and dynamic properties of the quasi-two-dimensional antiferromagnet $MnPS_3$,*” *Phys. Rev. B* **74**, 094422 (2006).
- [121] E. Rastelli, “*Statistical Mechanics of Magnetic Excitations: From Spin Waves to Stripes and Checkerboards,*” World Scientific (2013), Chap. 1, Pages 12- 31.
- [122] S. K. Mukhopadhyay and C. K. Majumdar, “*Solutions of the three magnon bound state equation II,*” *J. Math. Phys.*, **17**, 478 (1976); C. K. Majumdar and I. Bose, “*Solutions of the three-magnon bound state equation. III. The physical eigenstate,*” *J. Math. Phys.*, **19**, 2187 (1978); D. C. Mattis and S. Rudin, “*Three-Body Bound States on a Lattice,*” *Phys. Rev. Letts*, **52**, 755 (1984).
- [123] U. Tutsch, et al. “*Evidence of a field-induced Berezinskii KosterlitzThouless scenario in a two-dimensional spindimer system,*” *Nat. Commun.* **5**:5169 doi: 10.1038/ncomms6169 (2014).

REPRINTS

Theoretical analysis of neutron scattering results for quasi-two dimensional ferromagnets

S. Sarkar^a, S.K. Paul, and R. Chaudhury

S N Bose National Centre for Basic Sciences, Block- JD, Sector- III, Salt Lake, 700098 Kolkata, India

Received 6 March 2012 / Received in final form 9 July 2012

Published online 22 November 2012 – © EDP Sciences, Società Italiana di Fisica, Springer-Verlag 2012

Abstract. A theoretical study has been carried out to analyse the available results from the inelastic neutron scattering experiment performed on a quasi-two dimensional spin- $\frac{1}{2}$ ferromagnetic material K_2CuF_4 . Our formalism is based on a conventional semi-classical like treatment involving a model of an ideal gas of vortices/anti-vortices corresponding to an anisotropic XY Heisenberg ferromagnet on a square lattice. The results for dynamical structure functions for our model corresponding to spin- $\frac{1}{2}$, show occurrence of negative values in a large range of energy transfer even encompassing the experimental range, when convoluted with a realistic spectral window function. This result indicates failure of the conventional theoretical framework to be applicable to the experimental situation corresponding to low spin systems. A full quantum formalism seems essential for treating such systems.

1 Introduction

Low dimensional and in particular two dimensional magnetism has attracted a great deal of interest in the past three decades [1–12]. In particular, in one dimension the existence of both solitonic and spin wave excitations were thoroughly studied through inelastic neutron scattering experiments as well as theoretical analysis for $CsNiF_3$ [13–15]. Similar studies were carried out searching for topological excitations in various quasi-one dimensional systems which are almost ideal realization of nearest neighbour Heisenberg antiferromagnetic chain [16–18].

In many of the above systems the experiments showed a central peak (peak corresponding to $\omega = 0$) in the dynamical structure function when plotted in constant “ q ” scan. This motivated the experimentalists further to investigate two dimensional and quasi-two dimensional magnetic materials. With the availability of improved quasi two-dimensional ferromagnetic and anti-ferromagnetic materials investigations along this line has become today's one of the primary interests both theoretically and experimentally. These include layered systems such as K_2CuF_4 , Rb_2CrCl_4 , magnetically intercalated graphites such as $CoCl_2$, layered ruthenates, layered manganites and high T_c cuprates [1–15, 19–26]. Moreover large amount of information on the spin dynamics, extracted from inelastic neutron scattering are available. Advances in numerical and computational techniques have also contributed to the understanding of both spin wave and topological excitations [27–35].

On two dimensional magnetic systems the concept of topological order was introduced by Kosterlitz and Thouless [36] and independently by Berezinskii [37,38]. Their ideas backed by analytical and numerical calculations led to the proposal for the existence of topological vortices and anti-vortices in a typical ferromagnetic XY model on a two dimensional lattice. According to these ideas vortices and anti-vortices are frozen as bound pairs below certain transition temperature called T_{KT} or T_{BKT} and, above this temperature, they become mobile and nearly free [36–38].

In this work we initiate a theoretical investigation regarding the applicability of a semi-classical like treatment of the dynamics of topological excitations to the inelastic neutron scattering results for real systems [19,20,27–30,39]. In recent years inelastic neutron scattering experiments are being done mostly on layered ruthenates like $Ca_{2-x}Sr_xRuO_4$, layered anti-ferromagnet like $CuGeO_3$, layered manganites and some layered cuprates [1–12,24,25,40]. The layered anti-ferromagnet, $CuGeO_3$ being spin-Peierls compound, is proposed to exhibit a Berezinskii-Kosterlitz-Thouless transition in the vicinity of spin-Peierls transition temperature. The two dimensional spin half XY model was investigated and the validity of Berezinskii-Kosterlitz-Thouless transition was confirmed [41]. The existence of Berezinskii-Kosterlitz-Thouless transition was proposed long ago in K_2CuF_4 ($S = \frac{1}{2}$ layered ferromagnet) [19,20]. According to our knowledge, layered ferromagnets with spin- $\frac{1}{2}$ are the least studied systems, from both theoretical and experimental points of view, till date.

An extensive experimental study of spin-dynamics in a layered ferromagnet has been carried out by Hirakawa

^a e-mail: sbhjt72@gmail.com

et al. [19,20] using a neutron scattering probe on K_2CuF_4 . Their results exhibit a central peak (at $\omega = 0$) in the plot of “neutron count vs. frequency” at a fixed value of the wave-vector q . Subsequent developments of approximate analytical theories and Monte Carlo molecular dynamics (MCMD) analysis have suggested that the existence of central peaks is partly due to scattering of neutrons from moving vortices and anti-vortices [29–31].

Here we aim to examine how far the picture of ideal gas of vortices and anti-vortices could be extended to the quantum spin models. For this purpose, we choose K_2CuF_4 as the reference system. This is a spin- $\frac{1}{2}$ quasi-two-dimensional ferromagnetic material, on which extensive neutron scattering studies have been done.

The plan of the paper is as follows. In Section 2, we briefly describe the classical theory of mobile vortices and anti-vortices. In the same section we explain our mathematical formulations in detail. In Section 3 we discuss our calculations and results. In Section 4 we present the conclusions and the future plan.

2 Mathematical formulation

The dynamics of mobile vortices in a ferromagnetic system have already been treated both analytically and numerically by Huber [27,28] and Mertens et al. [29,30]. In this work we apply their classical formalism to study the phase transition in K_2CuF_4 . We calculate the spin-spin correlations taking the experimental situations into account. For our purpose we present a brief description of the analytical treatment developed in references [29,30]. The starting Hamiltonian is

$$\mathcal{H} = -J \sum_{\langle ij \rangle} (S_i^x S_j^x + S_i^y S_j^y + \lambda S_i^z S_j^z), \quad (1)$$

where i, j label the nearest neighbour sites on a two dimensional square lattice, J is the coupling constant and the classical spin vector is $\mathbf{S}_i \equiv (S_i^x, S_i^y, S_i^z)$. This is an anisotropic Heisenberg Hamiltonian which, for $J > 0$, represents a ferromagnetic system. The quantity λ is the anisotropy parameter whose XY and isotropic Heisenberg limit correspond to $\lambda = 0$ and 1, respectively. The general time dependent spin configuration in spherical polar coordinate system is given by

$$\begin{aligned} S_x &= S \cos \phi(\mathbf{r}, t) \sin \theta(\mathbf{r}, t), \\ S_y &= S \sin \phi(\mathbf{r}, t) \sin \theta(\mathbf{r}, t), \\ S_z &= S \cos \theta(\mathbf{r}, t), \end{aligned} \quad (2)$$

with $\mathbf{r} = (x, y)$. Following the formulation of Hikami and Tsuneto, the solutions are given by [39], $\phi = \pm \arctan(\frac{y}{x})$ and

$$\begin{aligned} \theta &= \frac{\pi}{2} (1 \pm e^{-r/r_v}) & \text{for } r \gg r_v, \\ &= 0 \text{ or } \pi & \text{for } r \rightarrow 0, \end{aligned} \quad (3)$$

for single vortex centred at $\mathbf{r} = (0, 0)$, where (3) describes the asymptotic behaviour of θ . Here vortex core radius is

given by $r_v = \frac{a}{\sqrt{2(1-\lambda)}}$ [31]. This type of spin configuration defines a ‘meronic’ type of the spin vortex.

The definition of the spin-spin correlation function is given by

$$\begin{aligned} S(\mathbf{r}, t) &= \langle \mathbf{S}(\mathbf{r}, t) \cdot \mathbf{S}(\mathbf{0}, 0) \rangle \\ &= \langle S^x(\mathbf{r}, t) S^x(\mathbf{0}, 0) \rangle + \langle S^y(\mathbf{r}, t) S^y(\mathbf{0}, 0) \rangle \\ &\quad + \langle S^z(\mathbf{r}, t) S^z(\mathbf{0}, 0) \rangle, \end{aligned} \quad (4)$$

where $\langle \dots \rangle$ represents the thermal average. In the case of classical ideal gas of vortices, the thermal average has to be done by taking Maxwellian velocity distribution function. Here $S^{xx}(\mathbf{r}, t) = \langle S_x(\mathbf{r}, t) S_x(\mathbf{0}, 0) \rangle$ and $S^{yy}(\mathbf{r}, t) = \langle S_y(\mathbf{r}, t) S_y(\mathbf{0}, 0) \rangle$ are in-plane correlations and $S^{zz}(\mathbf{r}, t) = \langle S_z(\mathbf{r}, t) S_z(\mathbf{0}, 0) \rangle$ is the out-of-plane correlation.

The effective analytical expression for the in-plane correlation can be taken as

$$S^{xx}(\mathbf{r}, t) = \frac{S^2}{2} \exp \left\{ \left[\frac{r^2}{\xi^2} + \gamma^2 t^2 \right]^{1/2} \right\}, \quad (5)$$

with $\gamma = \frac{\sqrt{\pi \bar{u}}}{2\xi}$, where \bar{u} is the root mean square velocity [29,30]. Here $\xi = \xi_0 e^{b/\sqrt{\tau}}$ is the vortex-vortex correlation length. The root-mean squared velocity of the vortices was first calculated by Huber as

$$\bar{u} = \sqrt{b\pi} \frac{JS(S+1)a^2}{\hbar} \sqrt{n_v^f \tau^{-1/4}}, \quad (6)$$

where n_v^f is the density of free vortices at $T > T_{KT}$ [39]. The Fourier transform of $S^{xx}(\mathbf{r}, t)$ in (5) gives rise to the in-plane dynamical structure function given by

$$S^{xx}(\mathbf{q}, \omega) = \frac{S^2}{2\pi^2} \frac{\gamma^3 \xi^2}{[\omega^2 + \gamma^2(1 + \xi^2 q^2)]^2}. \quad (7)$$

This is a squared Lorentzian, peaked at $\omega = 0$, with q dependent width,

$$\Gamma = \frac{1}{2} \left\{ \pi(\sqrt{2} - 1) \right\}^{1/2} \left(\frac{\bar{u}}{\xi} \sqrt{1 + \xi^2 q^2} \right). \quad (8)$$

Exactly same results hold for $S^{yy}(\mathbf{q}, \omega)$ also.

From the definition of $S^{zz}(\mathbf{r}, t)$, it can be shown that the out-of-plane correlation is given by [29,30]

$$\begin{aligned} S^{zz}(\mathbf{r}, t) &= n_v^f S^2 \int \int d^2R d^2u P(\mathbf{u}) \\ &\quad \times \cos \theta(\mathbf{r} - \mathbf{R} - \mathbf{u}t) \cos \theta(\mathbf{R}), \end{aligned} \quad (9)$$

where $P(\mathbf{u})$ is the Maxwell velocity distribution for a single vortex. Performing first the spatial Fourier transform and then the temporal Fourier transform, it can be shown that the out-of-plane dynamical structure function has the form

$$S^{zz}(\mathbf{q}, \omega) = \frac{S^2}{4\pi^{5/2}} n_v^f \frac{|f(q)|^2}{\bar{u}q} \exp \left(-\frac{\omega^2}{\bar{u}^2 q^2} \right). \quad (10)$$

Here $|f(q)|$ is the velocity independent vortex form factor and it has the form $f(\mathbf{q}) = \int d^2\mathbf{r} \cos\theta(\mathbf{r})e^{-i\mathbf{q}\cdot\mathbf{r}}$. The form of $S^{zz}(\mathbf{q}, \omega)$ as in equation (10) exhibits a central peak at $\omega = 0$. The width of the central peak is $\Gamma_z = \bar{u}q$, i.e., linear in q .

In a typical inelastic neutron scattering experiment the count rate is related to the dynamical structure function [42,43] as

$$I(\mathbf{q}, \omega) \propto S(\mathbf{q}, \omega). \quad (11)$$

At finite temperature there always exist creation and annihilation of excitations. A detailed balance condition is always needed to relate the intensities of up scattering ($\hbar\omega < 0$) and down scattering ($\hbar\omega > 0$). True quantum mechanical $S(\mathbf{q}, \omega)$, denoted by $S_{DB}(\mathbf{q}, \omega)$ is recovered by the relation

$$S_{DB}(\mathbf{q}, \omega) = \frac{2}{1 + \exp(\frac{\hbar\omega}{k_B T})} S(\mathbf{q}, \omega), \quad (12)$$

where the factor $\frac{2}{1 + \exp(\frac{\hbar\omega}{k_B T})}$ is called the Windsor factor [33–35]. This $S_{DB}(\mathbf{q}, \omega)$ incorporates the detailed balance condition, as required by the thermal equilibrium. Another important factor, which has to be taken into account, is the instrumental resolution function $R(t)$ or $R(\omega - \omega')$. This essentially incorporates the different independent instrumental properties that affect the incident and scattered beam of neutrons [42,43]. In order to compare theory with experiment one has to convolute the theoretical expression, obtained from a model under consideration, by the resolution function [44]. Thus we consider the convoluted dynamical structure function $S_{conv.}(\mathbf{q}, \omega)$ given by

$$\begin{aligned} S_{conv.}(\mathbf{q}, \omega) &= \int dt \int d^2r R(t) S(\mathbf{r}, t) e^{i(\mathbf{q}\cdot\mathbf{r} - \omega t)} \\ &= \int R(\mathbf{q}, \omega - \omega') S(\mathbf{q}, \omega') d\omega'. \end{aligned} \quad (13)$$

The resolution function has to be chosen so as to give minimum ripples at the end points of the resolution width. For this purpose a suitable window function such as the Tukey window function may be chosen:

$$\begin{aligned} R(t) &= \frac{1}{2} [1 + \cos(2\pi t/t_m)] \quad \text{for } |t| \leq t_m/2 \\ &= 0 \quad \text{otherwise.} \end{aligned} \quad (14)$$

The parameter t_m , occurring in the window function, can be set from the resolution half width obtained from experimental data.

2.1 In-plane dynamical structure function

In our formulation for the in-plane dynamical structure function we take into account the Tukey window function, as mentioned above (see Eq. (14)). Using equa-

tions (5), (13) and (14) we compute the Fourier transform of in-plane spin-spin correlation

$$\begin{aligned} S_{conv.}^{xx}(\mathbf{q}, \omega) &= \frac{1}{(2\pi)^{3/2}} \int d^2r \int_{-\frac{t_m}{2}}^{\frac{t_m}{2}} dt S^{xx}(\mathbf{r}, t) R(t) \\ &\quad \times e^{i(\mathbf{q}\cdot\mathbf{r} - \omega t)}. \end{aligned} \quad (15)$$

Now,

$$\int d^2r e^{i\mathbf{q}\cdot\mathbf{r}} = \int_0^\infty r dr \int_0^{2\pi} d\theta e^{iqr \cos\theta} = \int_0^\infty r dr J_0(qr),$$

where $J_0(qr)$ is the Bessel function of order zero. The spatial integration is performed from zero to a certain radius R_0 . A final expression for the convoluted in-plane dynamical structure function takes the form

$$\begin{aligned} S_{conv.}^{xx}(\mathbf{q}, \omega) &= \frac{1}{(2\pi)^{1/2}} \int_0^{R_0} dr \int_{-\frac{t_m}{2}}^{\frac{t_m}{2}} dt S^{xx}(\mathbf{r}, t) \\ &\quad \times r J_0(qr) R(t) \cos(\omega t). \end{aligned} \quad (16)$$

Since, $S^{xx}(\mathbf{r}, t)$ and $R(t)$ are both even function in t , only $\cos(\omega t)$ contributes to the temporal part of the integration. From symmetry Y component of the in-plane dynamical structure function $S_{conv.}^{yy}(\mathbf{q}, \omega)$ is the same as X component of the in-plane dynamical structure function $S_{conv.}^{xx}(\mathbf{q}, \omega)$. Let us note that in the above analysis the formulation holds only for $T > T_{KT}$. For $T < T_{KT}$ the vortex-vortex correlation length ξ is not defined and hence the formalism cannot be extrapolated below T_{KT} .

2.2 Out-of-plane dynamical structure function

The out-of-plane dynamical structure function is given by

$$S_{conv.}^{zz}(\mathbf{q}, \omega) = \int R(\omega - \omega') S^{zz}(\mathbf{q}, \omega') d\omega', \quad (17)$$

where $R(\omega - \omega')$ is the Fourier transform of $R(t)$. The reason for taking (17) as the expression for convoluted out-of-plane dynamical structure function is that, unlike (5), an analytical expression for $S^{zz}(\mathbf{r}, t)$ cannot be evaluated from (9). So one has to start from (10).

The integral in (17) has been computed numerically. The $S_{conv.}^{zz}(\mathbf{q}, \omega)$ defined here corresponds only to the mobile vortices; whereas the experimental data contain the contributions from bound vortices and fragile ‘spin wave like’ modes. These fragile ‘spin wave like’ modes are the largely decaying spin wave modes above the ferromagnetic-paramagnetic transition temperature (Curie temperature). In order to compare with the experimental observations, one has to extract the mobile vortex contribution from the experimental data. This can be done by subtracting the fragile mode contribution and the frozen vortex contribution from the experimental data. The fragile mode contribution has been subtracted by taking the fragile mode contribution above transition temperature to be same as the spin wave contribution just

below the transition temperature. This is valid as long as we are considering the temperature, which is not far below or above from the transition temperature. To find the approximate analytical expression for $S^{zz}(\mathbf{q}, \omega)$ due to bound vortex contribution, the limiting value of \bar{u} is taken as $\bar{u} \rightarrow 0$ in (10). Then from (10) it is easy to find an expression for $S_{bound}^{zz}(\mathbf{q}, \omega)$ namely:

$$S_{bound}^{zz}(\mathbf{q}, \omega) = \frac{S^2}{4\pi^2} n_v^b |f(q)|^2 \delta(\omega), \quad (18)$$

where n_v^b is the bound vortex density. Since, the system has no net topological charge we can assume that there are equal number of vortices and anti-vortices present in the system and we can take $n_v^f + n_v^b = \frac{1}{2}$ assuming square lattice structure. This is correct as long as the temperature is just below T_{KT} where all the vortices are frozen but once the temperature crosses T_{KT} some of the bound vortices become mobile and the bound vortex density can be approximated as

$$n_v^b \approx \left(\frac{1}{2} - n_v^f \right), \quad (19)$$

where, n_v^b is in the units of inverse of plaquette size (a^2). Since, $n_v^f \sim \xi_0^{-2} \exp(-2b/\sqrt{\tau})$ [29,30], n_v^b given by (19) is temperature dependent. Here ξ_0 is of the order of lattice parameter (a). Using (18) and (19) the bound vortex contribution has to be subtracted carefully from the experimentally observed count.

We would like to point out that we could not apply this procedure to extract out bound vortex contributions in the case of in-plane dynamical structure function (see Sect. 3).

2.3 Total dynamical structure function (spin-spin correlation)

The general expression for the total dynamical structure function is

$$S(\mathbf{q}, \omega) = \frac{1}{(2\pi)^{3/2}} \int d^2r \int dt S(\mathbf{r}, t) R(t) e^{i(\mathbf{q}\cdot\mathbf{r} - \omega t)}, \quad (20)$$

where the total spin-spin correlation $S(\mathbf{r}, t)$ is defined by (4). So, the total dynamical structure function is $S(\mathbf{q}, \omega) = S^{xx}(\mathbf{q}, \omega) + S^{yy}(\mathbf{q}, \omega) + S^{zz}(\mathbf{q}, \omega)$. Since, X and Y components of the spins are symmetric, we have $S^{xx}(\mathbf{q}, \omega) = S^{yy}(\mathbf{q}, \omega)$ and the total dynamical structure function takes the form

$$S(\mathbf{q}, \omega) = 2S^{xx}(\mathbf{q}, \omega) + S^{zz}(\mathbf{q}, \omega). \quad (21)$$

Here, we would consider (21) only for mobile vortices.

It is an important fact that the formalism explained above incorporates the Windsor factor and the presence of \hbar in the quantum expression of magnetic moment corresponding to the spins constituting the vortex [27,28]. Therefore the formalism looks like a semi-classical one. Henceforth we will call our combined theoretical approach ‘semi-classical like’.

Table 1. Relevant parameters for K_2CuF_4 [19,20].

Parameter	Magnitude
exchange coupling (J)	11.93 K
lattice parameter (a)	4.123 Å
‘ b ’	1.5
‘ T_{KT} ’	5.5 K

3 Calculations and results

We apply the formalism of Section 2 on a real material K_2CuF_4 for which neutron scattering experiments have been performed [19,20]. It is a quasi-two-dimensional spin- $\frac{1}{2}$ ferromagnet, where the interaction is mainly Heisenberg type with only 1% X-Y like anisotropy. The transition is close to KT type with slight modification due to Heisenberg type interaction. The magnetic lattice structure for K_2CuF_4 is approximately a body centred tetragonal lattice, i.e. a lattice composed of stacking of 2D square lattices [19,20]. The physical parameters are given in Table 1, which have been used throughout the calculation.

We start with the investigation of the in-plane correlation (in-plane dynamical structure function) $S^{xx}(\mathbf{q}, \omega)$. The radius R_0 in (16) is $(\sqrt{100^2 + 100^2})a$ for a 100×100 lattice, as used in the MCMD analysis by Mertens et al. [29,30], where a is the lattice parameter. We set the value of t_m according to the experimental resolution width (0.01 meV) [19,20]. We compute $S_{conv}^{xx}(\mathbf{q}, \omega)$ numerically, for two different temperatures, 6.25 K and 6.75 K, for $q(\text{planar}) = 0.04$ reciprocal lattice units (in the units of $\frac{\pi}{a}$), experimentally $\hbar q$ being the momentum transfer. There are two threshold values of q [19,20], namely $q_1 = 0.06$ and $q_2 = 0.01$, where for $q > q_1$ the system behaves like 2D Heisenberg system and for $q < q_2$ the system behaves as 3D XY system. For $q_2 < q < q_1$ the system behaves as 2D XY system. We have varied the energy transfer $\hbar\omega$ from -0.3 meV to $+0.3$ meV, which includes the range -0.2 meV to $+0.2$ meV as taken in experiment [19,20]. The convoluted in-plane dynamical structure function is plotted in Figures 1 and 2, where $t_{nat} = \frac{\hbar}{\mathcal{J}S(S+1)}$ is the natural time unit for the system/material (in our case K_2CuF_4). These figures indicate that after convoluting with the Tukey window function, the in-plane dynamical structure function no longer remains squared Lorentzian, though in both the cases central peaks persist. The width of the $S_{conv}^{xx}(\mathbf{q}, \omega)$ curve is much larger than that of the squared Lorentzian.

We notice that the convoluted in-plane dynamical structure function $S_{conv}^{xx}(\mathbf{q}, \omega)$ has become negative just above 0.1 meV. The occurrence of negative values of the dynamical structure function has been dealt with in detail in Section 4 and in Appendix.

Again comparing Figures 1 and 2 we find that the width of the squared Lorentzian increases with the increase of temperature whereas that of the $S_{conv}^{xx}(\mathbf{q}, \omega)$ does not undergo any change. Later, we will present a comparison of the convoluted total dynamical structure function with the experimental one (see Figs. 5 and 6).

We now evaluate the out-of-plane dynamical structure function $S_{conv}^{zz}(\mathbf{q}, \omega)$ for two different temperatures, 6.25 K

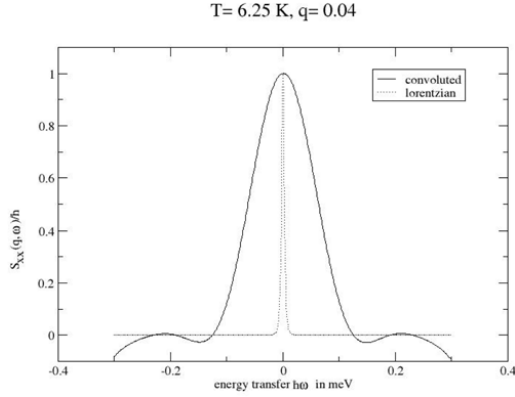


Fig. 1. Comparison between the convoluted in-plane dynamical structure function $S_{conv}^{xx}(\mathbf{q}, \omega)$ (Eq. (16)) and unconvoluted in-plane dynamical structure function $S^{xx}(\mathbf{q}, \omega)$ (Eq. (7)) at $T = 6.25$ K and $q = 0.04$. Solid line is for convoluted theoretical expression and dotted line is for unconvoluted theoretical expression (squared Lorentzian). $\xi = 58.09a$, $\bar{u} = 0.0614 \frac{a}{t_{nat}}$, and width $\Gamma_{xx} = 0.0012$ meV for squared Lorentzian at $T = 6.25$ K.

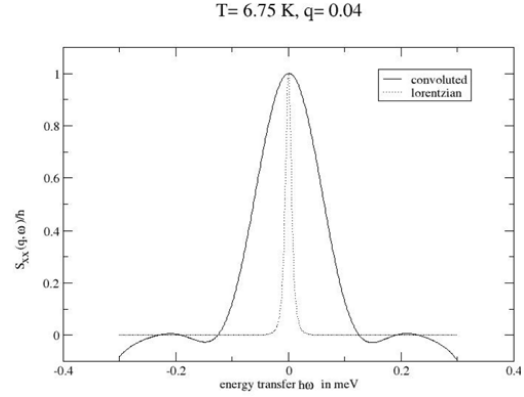


Fig. 2. Comparison between the convoluted in-plane dynamical structure function $S_{conv}^{xx}(\mathbf{q}, \omega)$ (Eq. (16)) and unconvoluted in-plane dynamical structure function $S^{xx}(\mathbf{q}, \omega)$ (Eq. (7)) at $T = 6.75$ K and $q = 0.04$. Solid line is for convoluted theoretical expression and dotted line is for unconvoluted theoretical expression (squared Lorentzian). $\xi = 22.25a$, $\bar{u} = 0.1352 \frac{a}{t_{nat}}$, and width $\Gamma_{xx} = 0.0035$ meV for squared Lorentzian at $T = 6.25$ K.

and 6.75 K, for $q(\text{planar}) = 0.04$ r.l.u, using (17). The expression for $R(\omega - \omega')$ is

$$R(\omega - \omega') = \frac{1}{4\pi} \sin \left[\frac{(\omega - \omega')t_m}{2} \right] \times \left[\frac{2}{\omega - \omega'} - \frac{1}{\omega - \omega' + 2\pi/t_m} - \frac{1}{\omega - \omega' - 2\pi/t_m} \right]. \quad (22)$$

We use the same value of t_m as used for $S_{conv}^{xx}(\mathbf{q}, \omega)$. Here also the reasons for the choice of temperatures and $q(\text{planar})$ are same as that for the in-plane dynamical structure function. In Figures 3 and 4 we have plotted the out-of-plane correlation, $S_{conv}^{zz}(\mathbf{q}, \omega)$. We have varied the ω' from $-\frac{\pi}{t_m}$ to $\frac{\pi}{t_m}$ in (17), where t_m is estimated from the resolution width as before.

In this case the bound vortex contribution has been subtracted carefully, using (18) and (19), from the observed count at 6.25 K to obtain the effective mobile vortex contribution. The methodology for extracting the mobile vortex contributions from the experimental data has been explained in Section 2.2. As long as the counts at 6.75 K are concerned, the fragile 'spin wave like' modes are highly decaying so that it cannot be assumed to be the same as the true spin wave modes observed at 5 K. So, only bound vortex contribution has been subtracted at 6.75 K. The normalization factors, required for the quantitative comparison between the theoretical and the experimental results, have been estimated from the neutron count extracted from the experiment on K_2CuF_4 [19,20].

We find that the out-of-plane dynamical structure function is also negative within the resolution width (see Figs. 3 and 4). Moreover experimental peak is outside the resolution width, while the peak corresponding to the $S_{conv}^{zz}(\mathbf{q}, \omega)$ is at $\omega = 0$.

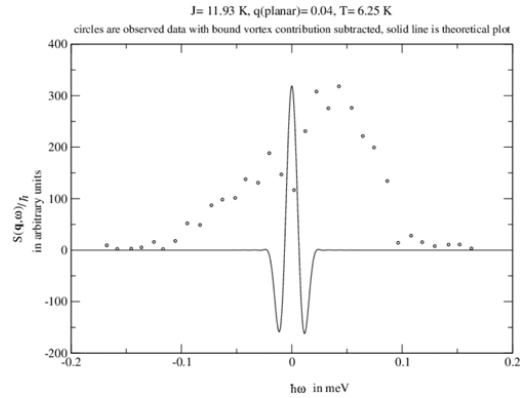


Fig. 3. Circles are observed (experimental) data, where contributions from the fragile modes as well as the bound vortex contributions have been subtracted and solid line is the plot of properly convoluted out-of-plane dynamical structure function $S^{zz}(\mathbf{q}, \omega)$ (theoretical). $\xi = 58.09a$ and $\bar{u} = 0.0614 \frac{a}{t_{nat}}$.

The above calculations lead us to the theoretical estimate for the convoluted total dynamical structure function $S_{conv}^{total}(\mathbf{q}, \omega)$ given by (21). In Figures 5 and 6, $S_{conv}^{total}(\mathbf{q}, \omega)$ has been compared with the filtered experimental data obtained by subtracting the bound vortex contributions and fragile 'spin wave like' contributions (see Sects. 2.1 and 2.2). In these plots the intensities of the experimental peak and those of the central peak of the $S_{conv}^{total}(\mathbf{q}, \omega)$ have been matched.

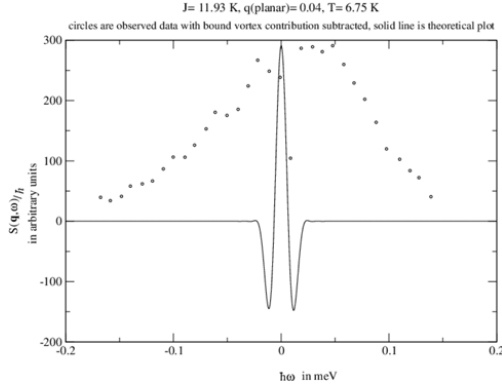


Fig. 4. Circles are observed (experimental) data, where only contributions from bound vortices have been subtracted and solid line is the plot of properly convoluted out-of-plane dynamical structure function $S^{zz}(\mathbf{q}, \omega)$ (theoretical). $\xi = 22.25a$ and $\bar{u} = 0.1352 \frac{a}{t_{nat}}$.

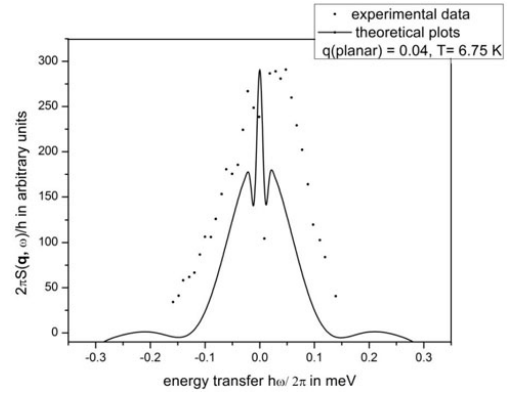


Fig. 6. Total dynamical structure function $S_{conv}^{total}(\mathbf{q}, \omega)$ at $T = 6.75$ K and $q = 0.04$; solid line is for convoluted theoretical results and dots are filtered experimental data. $\xi = 22.25a$ and $\bar{u} = 0.1352 \frac{a}{t_{nat}}$.

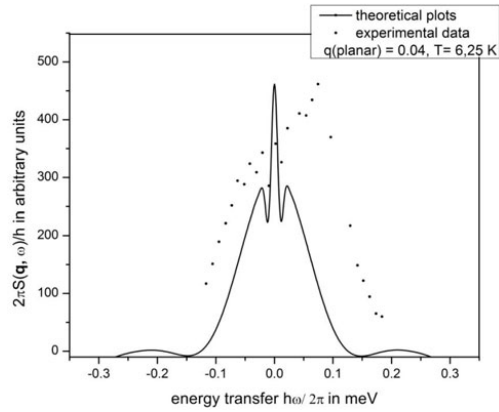


Fig. 5. Total dynamical structure function $S_{conv}^{total}(\mathbf{q}, \omega)$ at $T = 6.25$ K and $q = 0.04$; solid line is for convoluted theoretical results and dots are filtered experimental data. $\xi = 58.09a$ and $\bar{u} = 0.0614 \frac{a}{t_{nat}}$.

It is clear from Figure 5 that at 6.25 K the experimental peak occurs approximately at 0.08 meV, which is way outside the resolution width. At 6.75 K (see Fig. 6) the peak of the experimental graph is not far from the central peak. It is reasonable to say that as the temperature is increased, we are getting better agreement of the $S_{conv}^{total}(\mathbf{q}, \omega)$ with the experimental observations. This agreement is regarding the position of the central peak. Apart from the central peak there are two other peaks at finite frequency at both the temperatures. These are nothing but the reminiscent of the out-of-plane dynamical structure function contribution as seen from Figures 3–6. This signifies that the in-plane correlation is largely dominating over the out-of-plane correlation.

The total spin-spin correlation is still negative just above 0.1 meV. Though it is true that the dynamical structure function cannot be negative, here in our case the negativity occurs as a result of the convolution of analytical expression of $S(\mathbf{q}, \omega)$. Even for a conventional long range ordered system, the dynamical structure function corresponding to a classical pure spin wave comes out to be negative beyond a certain range of frequency when convoluted with any spectral window function. Furthermore the above peculiarity persists even when quantum effects are incorporated through a detailed balance factor (see Appendix).

The inclusion of quantum mechanical detailed balance factor in the semi-classical like treatment for dynamics of mobile vortices and anti-vortices, is not even causing any appreciable asymmetry, as seen in the theoretical plots in our case of spin- $\frac{1}{2}$. The theoretical plots are largely symmetric around $\omega = 0$. A very small asymmetry in the theoretical plots are being seen for higher values of ω while the experimental data are showing clearly the asymmetry.

It may be noted that in our analysis the bound vortex contributions have been approximately estimated only for out-of-plane dynamical structure function $S^{zz}(\mathbf{q}, \omega)$. This is because, in this case, we are able to truncate the expression, as given in (10), to the regime $T < T_{KT}$, by making $\bar{u} \rightarrow 0$. In (10), there exists no explicit dependence of $S^{zz}(\mathbf{q}, \omega)$ on the correlation length ξ . In case of in-plane correlation, as given in (5), we need to find ξ for $T < T_{KT}$ due to its explicit appearance in that expression. Since ξ is not defined for $T < T_{KT}$ we are not able to estimate the bound vortex contribution for in-plane dynamical structure function.

In summary, we find that the width of the convoluted in-plane dynamical structure function is much larger than that of the squared Lorentzian. Values of the in-plane dynamical structure function comes out to be negative beyond a finite range of energy transfer. The convoluted

out-of-plane dynamical structure function becomes negative as well. However this happens within the resolution width about the central peak (peak at $\omega = 0$). The total convoluted dynamical structure function also becomes negative in the regime where the in-plane dynamical structure function had become negative. No appreciable asymmetry is created even after including the Windsor factor. We find that for both the temperatures the convoluted total dynamical structure function is symmetric around $\omega = 0$, whereas the experimental observation is not. The theoretical model of semi-classical treatment of ideal gas of unbound vortices tends to agree with the experimental observations better at higher temperatures (for spin- $\frac{1}{2}$ system), when we consider the experimental results at $T = 6.25$ K and $T = 6.75$ K (Figs. 5 and 6). It is worthwhile to point out that same results hold for unbound anti-vortices also.

4 Conclusions and discussions

The laws of quantum mechanics which govern all real systems, ensure the dynamical structure functions to be always positive definite [42,43]. We find in our analysis however, that the semi-classical treatment based on ideal gas of vortices (anti-vortices) for a low spin system leads to the occurrence of negative values of dynamical structure function, over a large range of energy transfer, when convoluted with any standard resolution function.

Based on the analysis carried out in the Appendix we can infer that for the dynamics of mobile vortices and anti-vortices, the negative values of $S_{conv.}(\mathbf{q}, \omega)$ are occurring due to the following factors:

- (i) the choice of the resolution function, which in our case is the Tukey function;
- (ii) the choice of the value of resolution width $\Delta\omega$, which in this case is made fixed by experimentally imposed resolution width;
- (iii) use of a semi-classical like treatment to extend the classical theory of dynamics of mobile vortices (anti-vortices) to a quasi two dimensional spin- $\frac{1}{2}$ ferromagnet which is quantum mechanical.

To avoid the negativity in the $S_{conv.}(\mathbf{q}, \omega)$ we have chosen a different resolution function. Indeed, it has been shown that most of the resolution functions are more or less oscillatory in the Fourier space [44,45]. An extra smoothing factor can be used to dampen the oscillation of the resolution function. This extra factor is eventually related to the resolution width and it makes the resolution function smoother if the resolution width is decreased [44]. However, in our case the resolution width is fixed from the experiment and consequently the oscillation of the resolution function cannot be avoided by merely changing the resolution function.

It has been found that there is a range of ω over which $S_{conv.}(\mathbf{q}, \omega)$ remains positive. We can call it as the physically admissible range. This range is related to the magnitude of the spin occurring in the theoretical model under consideration and to the resolution width. On the

basis of the analysis (presented in the Appendix) it is expected that even in the case of dynamics of mobile vortices and anti-vortices the physically admissible range would be larger for higher spin value and smaller for lower spin values.

Another way to avoid the negativity is to assume, $S_{conv.}(\mathbf{q}, \omega) = 0$ outside the physically admissible range [44]. If this physically admissible range is within the range of experimental interest then the assumption is not applicable. In our case of spin-half ferromagnet the physically admissible range is well within the range of ω over which the neutron scattering data has been taken in the experiment (as seen from Figs. 5 and 6).

Hence, the negative values of $S_{conv.}(\mathbf{q}, \omega)$ can only be due to the use of the semi-classical like treatment to extend the classical theory of dynamics of mobile vortices and anti-vortices to a quasi two dimensional spin- $\frac{1}{2}$ ferromagnet (K_2CuF_4).

Moreover, the convoluted out-of-plane dynamical structure function, computed from our semi-classical like treatment, becomes negative within the experimentally imposed resolution width itself. Thus the central peak occurring in this case may not possess a well defined width.

The agreement between the behaviour of dynamical structure functions obtained from our theoretical calculations and the one from the experiment, in terms of the peak position and the overall shape, is found to be fairly good at temperatures much larger than T_{KT} .

Although the vortices (and anti-vortices) are extended objects the Maxwell-Boltzmann distribution can still be used for the motion of the centre of mass of these objects.

Our investigation presented in this paper brings out the fact that a complete quantum mechanical treatment is essential for describing the detailed features of the dynamics of unbound spin vortices and anti-vortices corresponding to low spin magnetism systems. As a first step towards this, a theoretical framework for describing static quantum spin vortices and anti-vortices and their topological properties has been developed [46–53]. An extension of this formalism to the case of mobile spin vortices and anti-vortices is crucial for the quantum mechanical calculation of dynamical structure function. This would go a long way towards an explanation for the experimental results observed for the genuine quantum spin systems like K_2CuF_4 .

One of the authors (SS) acknowledges the financial support through Junior Research Fellowship (09/575 (0089)/2010 EMR-1) provided by Council of Scientific & Industrial Research (CSIR). The authors would like to express their appreciation for the valuable suggestions and criticism of the referee in preparing the revised manuscript.

Appendix: $S_{conv}(\mathbf{q}, \omega)$ corresponding to classical spin-wave

For classical spin wave at very low temperature corresponding to a classical Heisenberg ferromagnet, the

dynamical structure function has the form:

$$\begin{aligned} S(\mathbf{q}, \omega) &= \delta(\omega^2 - \omega_q^2) \\ &= \frac{1}{2\omega_q} [\delta(\omega - \omega_q) + \delta(\omega + \omega_q)]. \end{aligned} \quad (\text{A.1})$$

Where, $\omega_q = \hbar^{-1} J \sqrt{S(S+1)} z(1 - \gamma_q)$ for a cubic lattice. Here z is the number of nearest neighbours and $\gamma_q = \frac{1}{z} \sum_r \cos(\mathbf{q} \cdot \mathbf{r})$.

Convolved dynamical structure function, $S_{conv}(\mathbf{q}, \omega)$ has been defined in (13), where $R(\omega - \omega')$ is the Fourier transform of a suitably chosen spectral function. So far the Tukey function has been used and the same is also used in this case. The Fourier transform of Tukey function is given by (22). Using (13), (22) and (A.1) we find the convoluted dynamical structure function corresponding to spin wave, $S_{conv}^{SW}(\mathbf{q}, \omega)$ to be

$$S_{conv}^{SW}(\mathbf{q}, \omega) = \frac{1}{2\omega_q} [R(\omega - \omega_q) + R(\omega + \omega_q)]. \quad (\text{A.2})$$

Analyzing (A.2) we find that there exists a range

$$|\omega| \leq \left(\omega_q + \frac{4\pi}{t_m} \right) \quad (\text{A.3})$$

within which $S_{conv}^{SW}(\mathbf{q}, \omega)$ remains positive, and outside it becomes negative. This remains true even if we choose any other resolution function. This is basically due to the fact that when Fourier transform is performed on spectral functions (defined in time domain), the resulting functions in (\mathbf{q}, ω) space mostly turn out to be oscillatory [45].

One way to avoid these negative values of $S_{conv}(\mathbf{q}, \omega)$ would be to assume $S_{conv}(\mathbf{q}, \omega) = 0$ outside $|\omega| \leq (\omega_q + \frac{4\pi}{t_m})$ [44]. This prescription however, cannot be taken into consideration when comparing theoretical predictions with experimental results, if the energy range of experimental interest contains the above mentioned range of ω . Another way to avoid the negative values of $S_{conv}(\mathbf{q}, \omega)$ is to decrease the value of t_m (see (A.3)), where t_m is related to the experimental resolution width ($\Delta\omega$) by the relation

$$t_m \simeq \frac{\hbar}{2\Delta\omega}, \quad (\text{A.4})$$

$\Delta\omega$ being in energy units. Decrease in t_m means increase in the value of $\Delta\omega$ which signifies a poor experimental resolution width. In comparing the theoretical predictions with the experimental results, t_m is determined by the relation (A.4), where $\Delta\omega$ is fixed from the experiment.

Another interesting feature of (A.3) is the fact that the region of ω where $S_{conv}(\mathbf{q}, \omega)$ remains positive depends on the spin value S via the relation

$$|\omega| \leq \left(\hbar^{-1} J \sqrt{S(S+1)} z [1 - \gamma_q] + \frac{4\pi}{t_m} \right). \quad (\text{A.5})$$

This shows that when t_m is fixed from the experimental resolution width, S remains as the free parameter to determine the range of ω as mentioned in (A.3). Increase in S will increase the range of ω where $S_{conv}(\mathbf{q}, \omega)$ remains

positive. Hence for a system with high spin value S , the range of positive $S_{conv}(\mathbf{q}, \omega)$ may actually be at par with the energy range of experimental interest, unlike the case of spin $\frac{1}{2}$.

It can be shown from (A.2) that the range of ω , given by (A.3), will not change even if a detailed balance factor (in this case Windsor factor) is introduced to incorporate the quantum effects.

References

1. A.A. Katanin, V. Yu Irkhin, *Physcis-Uspekh* **50**, 613 (2007)
2. J. Prokop, W.X. Tang, Y. Zhang, I. Tudosa, T.R.F. Peixoto, Kh. Zakeri, J. Kirschner, *Phys. Rev. Lett.* **102**, 177206 (2009)
3. M. Cwik, M. Benomar, T. Finger, Y. Sidis, D. Senff, M. Reuther, T. Lorenz, M. Braden, *Phys. Rev. Lett.* **102**, 057201 (2009)
4. F. Demmel, T. Chatterji, *Phys. Rev. B* **76**, 212402 (2007)
5. T. Chatterji, S. Ghosh, A. Singh, L.P. Regnault, M. Rheinstädter, *Phys. Rev. B* **76**, 144406 (2007)
6. F. Weber, S. Rosenkranz, J.-P. Castellan, R. Osborn, H. Zheng, J.F. Mitchell, Y. Chen, Songxue Chi, J.W. Lynn, D. Reznik, *Phys. Rev. Lett.* **107**, 207202 (2011)
7. S.M. Yusuf, A.K. Bera, *Phys. Rev. B* **84**, 064407 (2011)
8. H. Ulbrich, F. Krüger, A.A. Nugroho, D. Lamago, Y. Sidis, M. Braden, *Phys. Rev. B* **84**, 094453 (2011)
9. H.J. Lewtas, A.T. Boothroyd, M. Rotter, D. Prabhakaran, *Phys. Rev. B* **82**, 184420 (2010)
10. L. Braicovich et al., *Phys. Rev. B* **81**, 174533 (2010)
11. R. Chaudhury, in ULT 2011, 2011 (KAIST, Daejeon, South Korea)
12. Yong-il Shin, in ULT 2011, 2011 (KAIST, Daejeon, South Korea)
13. J.K. Kjemsand, M. Steiner, *Phys. Rev. Lett.* **41**, 1137 (1978)
14. I.U. Heilmann, J.K. Kjems, Y. Endoh, G.F. Reiter, G. Shirane, R.J. Birgeneau, *Phys. Rev. B* **24**, 3939 (1981)
15. G. Reiter, *Phys. Rev. Lett.* **46**, 202 (1981)
16. H. Bethe, *Z. Physik* **71**, 205 (1931)
17. Y. Endoh, G. Shirane, R.J. Birgeneau, P.M. Richards, S.L. Holt, *Phys. Rev. Lett.* **32**, 170 (1974)
18. F.D.M. Haldane, *Phys. Rev. Lett.* **50**, 1153 (1983)
19. K. Hirakawa, H. Yoshizawa, K. Ubukoshi, *J. Phys. Soc. Jpn* **51**, 2151 (1982)
20. K. Hirakawa, Y. Yoshizawa, J.D. Axe, G. Shirane, *J. Phys. Soc. Jpn Part. 2* **52**, 4220 (1983)
21. M.T. Hutchings, J. Als-Nielsen, P.A. Lindgard, P.J. Walker, *J. Phys. C: Solid State Phys.* **14**, 5327 (1981)
22. M.T. Hutchings, P. Day, E. Janke, R. Pynn, *J. Magn. Mater* **54-57**, 673 (1986)
23. D.G. Wiesler, M. Suzuki, H. Zobel, S.M. Shapiro, R.M. Nicklow, *Physica B* **136**, 22 (1986)
24. P. Steffens, O. Friedt, Y. Sidis, P. Link, J. Kulda, K. Schmalzl, S. Nakatsuji, M. Braden, *Phys. Rev. B* **83**, 054429 (2011)
25. L. Capogna et al., *Phys. Rev. B* **67**, 012504 (2003)
26. K. Yamada et al., *Phys. Rev. B* **40**, 4557 (1989)
27. D.L. Huber, *Phys. Lett. A* **68**, 125 (1978)
28. D.L. Huber, *Phys. Rev. B* **26**, 3758 (1982)

29. F.G. Mertens, A.R. Bishop, G.M. Wysin, C. Kawabata, Phys. Rev. Lett. **59**, 117 (1987)
30. F.G. Mertens, A.R. Bishop, G.M. Wysin, C. Kawabata, Phys. Rev. B **39**, 591 (1989)
31. M.E. Gouva, G.M. Wysin, A.R. Bishop, F.G. Mertens, Phys. Rev. B **39**, 11840 (1989)
32. A.R. Volkell, G.M. Wysin, A.R. Bishop, F.G. Mertens, Phys. Rev. B **44**, 10066 (1991)
33. M.T. Evans, C.G. Windsor, J. Phys. C **6**, 495 (1973)
34. C.G. Windsor, J. Locke-Wheaton, J. Phys. C **9**, 2749 (1973)
35. R. Chaudhury, B.S. Shastry, Phys. Rev. B **37**, 5216 (1988)
36. J.M. Kosterlitz, D.J. Thouless, J. Phys. C **6**, 1181 (1973)
37. V.L. Berezinskii, Sov. Phys. JETP **32**, 493 (1970)
38. V.L. Berezinskii, Sov. Phys. JETP **34**, 610 (1972)
39. S. Hikami, T. Tsuneto, Prog. Theor. Phys. **63**, 387 (1980)
40. J.E. Lorenzo et al., Europhys. Lett. **45**, 45 (1999)
41. K. Harada, N. Kawashima, J. Phys. Soc. Jpn **67**, 2768 (1998)
42. S.W. Lovesey, *Theory of Neutron Scattering from Condensed Matter* (Clarendon Press, Oxford 1984)
43. F. Hippert, E. Geissler, Jean. L. Hodeau, E.-L. Berna, J.-R. Regnard, *Neutron and X-Ray Spectroscopy* (Grenoble Sciences, Springer, 2006)
44. M. Takahashi, J. Phys. Soc. Jpn **52**, 3592 (1983)
45. F.J. Harris, Proc. IEEE **66**, 51 (1978)
46. E. Fradkin, M. Stone, Phys. Rev. B **38**, 7215 (1988)
47. E. Fradkin, *Field Theories of Condensed Matter Systems* (Addison-Wesley Pub. Co., CA, 1991)
48. F.D.M. Halden, Phys. Rev. Lett. **61**, 1029 (1988)
49. E. Loh Jr., D.J. Scalapino, P.M. Grant, Phys. Rev. B **31**, 4712 (1985)
50. D.D. Betts, F.C. Salevsky, J. Rogiers, J. Phys. A **14**, 531 (1981)
51. R. Chaudhury, S.K. Paul, Phys. Rev. B **60**, 6234 (1999)
52. R. Chaudhury, S.K. Paul, Mod. Phys. Lett. B **16**, 251 (2002)
53. R. Chaudhury, S.K. Paul, Eur. Phys. J. B **76**, 391 (2010)

The connection between vortex-like topological excitations and conventional excitations in quantum ferromagnetic spin systems on two-dimensional lattice and their stability

Subhajit Sarkar*, Ranjan Chaudhury† and Samir K. Paul‡

*S. N. Bose National Centre for Basic Sciences,
Block-JD, Sector-III, Salt Lake, Kolkata 700098, India*

* *subhajit@bose.res.in*

† *ranjan@bose.res.in*

‡ *smr@bose.res.in*

Received 30 July 2015

Accepted 28 August 2015

Published 3 November 2015

In this paper, we present a scheme for the construction of quantum states of vortex-like topological excitations corresponding to spin-1/2 strongly XY-anisotropic nearest neighbor Heisenberg ferromagnet on two-dimensional lattice. The procedure involving Pauli spin basis states is carried out corresponding to both infinite dilute limit and finite density limit of vortex/anti-vortex. It is found that the corresponding quantum mechanical states representing charge 1 quantum vortices/anti-vortices can be expressed as linear combinations of single magnon states, composite multi-magnon states and the ground state. Detailed calculations show that these states are quantum mechanically stable states of the Hamiltonian only when the system size exceeds certain threshold value. Our analysis indicates that the interactions between different magnon modes can very well generate these topological excitations. Possible applications of our calculations to real magnetic systems are also discussed. Magnetic measurements probing spin dynamics may be undertaken to verify the existence of the threshold size for the stability of vortices.

Keywords: Anisotropic quantum Heisenberg spin systems; topological excitations; collective excitations; Berezinskii–Kosterlitz–Thouless scenario.

PACS numbers: 75.10.-b, 75.10.Jm, 75.30.Ds, 75.40.-s

1. Introduction

In magnetic systems in low dimensions, viz, one dimension (or rather quasi-one dimension) and two dimensions (or rather quasi-two dimensions), the occurrences of topological excitations of solitons and vortices/merons, respectively are natural as they are thermodynamically feasible.^{1–11} In these systems, vortices/merons play

*Corresponding author.

a crucial role in bringing out a nonconventional phase transition in the two spatial dimensions.¹²

In the last few years, there has been a renewed research interest especially in the quasi-two dimensional magnetic systems motivated by the aims of building magnetic devices. These devices make use of mobile vortices.^{13–15} In the magnetic thin films, the interplay between the exchange interaction and the magnetic dipole–dipole interaction causes the formation of domain structures in absence of magnetic fields. Furthermore, each of these domains contain a magnetic vortex characterized by curling in-plane magnetization located at the center. The component of magnetization perpendicular to the plane of the film serves as “Polarization” of the vortex core.¹⁶ Such a magnetic vortex has been proved to be a potential candidate for switching devices as well as for data storage where the “Polarization” of the core can be manipulated in a controlled manner.¹⁶ Direct experimental evidences of such vortex states have been verified by magnetic force microscopy (MFM) and also by the spin-polarized scanning tunneling microscopy (STM).^{17,18}

The concept of topological phase transition driven by binding to unbinding processes involving vortex, anti-vortex-like topological excitations in two-dimensional ferromagnetic systems was introduced by Kosterlitz and Thouless and independently by Berezinskii.^{19,20} Their ideas backed up by analytical and numerical studies led to the signature of the above transition (BKT) in the dynamical correlation function, in two-dimensional Heisenberg ferromagnetic models of both XY-type and XY-anisotropic type.^{21–26} Attempts were also made later to extend the proposal of BKT to case of XY-anisotropic anti-ferromagnetic two-dimensional systems.^{24,27,28} The phase transition described above occurs at a temperature T_{BKT} characterized by degree of anisotropy. Above this, the dynamics of freely moving vortices and anti-vortices (or merons and anti-merons) provides nontrivial contribution in the dynamical correlation function as mentioned above, giving rise to the well-known “central peak”. In the inelastic neutron scattering (INS) experiment, the existence of such a central peak at $\omega = 0$ has been observed in the plot for the dynamical structure function $S(\mathbf{q}, \omega)$ versus neutron energy transfer $\hbar\omega$ in the constant “ \mathbf{q} ” scan.^{8,9} The materials on which such experiments have been performed include different layered ferromagnetic and anti-ferromagnetic materials such as K_2CuF_4 , La_2CuO_4 , CuGeO_3 , $\text{BaNi}_2\text{V}_2\text{O}_8$, $\text{BaNi}_2(\text{PO}_4)_2$ and stage-2 CoCl_2 graphite intercalation compound.^{8–11,29–34} The existence of BKT transition in these materials has been proposed on the basis of investigations performed on these materials using both INS and the electron spin resonance (ESR) techniques.

Some attempts have been made in the past to describe the dynamics of mobile vortices or merons corresponding to XY or XY-anisotropic Heisenberg model assuming that these topological excitations constitute a classical ideal gas.^{21–24} Approximate analytical theories and Monte Carlo molecular dynamics (MCMD) simulations have suggested that the existence of the central peak in the dynamical structure function is partly due to the scattering of neutrons from the above mobile topological excitations.^{21–24} However, the semi-classical ideal vortex gas

phenomenology turns out to be quite inadequate even for ferromagnets, in explaining the experimental results corresponding to systems having low spin values, even after incorporation of suitable quantum corrections in the calculations.³⁵ Although the occurrence of central peak is ensured, the theoretical dynamical structure function turns out to be negative for a considerable range of ω , when the appropriate experimental conditions are taken into account in the calculations! This very peculiar feature clearly signals total failure of the semi-classical treatment based on ideal gas phenomenology corresponding to low spin systems. Therefore, a full-fledged quantum mechanical description and treatment of such topological spin excitations become very crucial.³⁵ Besides, none of these semi-classical approaches so far have incorporated any spin wave–vortices/merons interaction and rather assumes that the vortex/merons take the shapes of spin profiles independent of spin waves.

The question of existence of the topological excitations, namely, vortices and merons in two-dimensional quantum ferromagnetic spin systems have been explored both numerically and analytically.^{36–40} It has been determined numerically that in this case, the vortex–anti-vortex pair density is nonzero even at $T = 0$.³⁶ In a pure quantum mechanical treatment, it has been found that almost all the vortices and anti-vortices are bound in pairs on square lattice and the number of isolated free vortices per site vanishes for $T < T_{\text{BKT}}$.³⁶ Monte Carlo simulations have also been performed on quantum XY model on two-dimensional lattices. The validity of the BKT transition for this model has been confirmed.^{37,38} A full-fledged quantum treatment has also been performed based on the application of path integral techniques using the coherent state basis, for XY-anisotropic Heisenberg ferromagnet on a square lattice.^{39,40} The partition function for the above quantum spin model has been expressed in terms of an effective action containing a topological part (Wess–Zumino term) which contains a genuine topological term as a charge measuring object for the vortices/merons (anti-vortices/anti-merons) alongside a nontopological term. It has been shown that in the very large anisotropy limit (corresponding to $\lambda \rightarrow 0$) the topological term can characterize the topological excitations viz, vortices and anti-vortices.^{39,40} In this formalism, the topological term arises from the path integral formulation of the quantum partition function in contrast to the situation where the vorticity operator has been introduced heuristically.³⁶

Incidentally, a rather different approach has been put forward to explain the origin of the central peak in the dynamical structure function $S(\mathbf{q}, \omega)$ corresponding to XY-anisotropic classical Heisenberg ferromagnetic model in two spatial dimensions. In this theory, the occurrence of the peak has been attributed to the fluctuations of the density of the topological excitations due to local diffusion and creation-annihilation of merons and anti-merons.⁴¹

The behavior of the collective modes like spin waves in the presence of a single vortex/meron corresponding to two-dimensional easy plane classical Heisenberg ferromagnet have been investigated using approximate analytical treatment in the continuum limit and numerical diagonalization techniques. It is found that the

renormalized spin wave modes show a strong localization of their amplitudes near the vortex core.^{42–44}

In this paper, we describe our investigations on the possible composition of these topological excitations of true quantum nature in low-dimensional anisotropic quantum Heisenberg ferromagnetic model. It turns out that the interactions between the different multi-magnon modes play a very important role in the formation of the above excitations. These multi-magnon interactions are generally neglected in the linear spin wave/one-magnon theory and even in the BKT theory. Theoretical attempts were made afterward to study the interplay between classical spin waves and vortices (merons) in the regime $T < T_{\text{BKT}}$.²⁵ These treatments lead to a renormalization of the exchange coupling without any explicit spin wave–vortex coupling.²⁶ Magnon modes are low energy excitations and represent a quantized coherent precessional motion of all the spins around the direction of the spontaneous magnetization in the long range ordered phase. These modes however, become ill-defined in the short range ordered phase.^{45–48} In contrast, the quantum states representing topological spin excitations are found to be stable even in the short range ordered phase when the system size is very large, as we will demonstrate in this paper.

The paper is organized as follows. In Sec. 2, we explain our mathematical formulation by constructing the quantum state corresponding to 1-vortex (and 1-anti-vortex as well) in the strong anisotropy limit of the XXZ model and establish the connection between the quantized vortex states and the magnon states; in Sec. 3, we analyze the quantum mechanical stability of such vortex/anti-vortex states for both the cases of infinite dilute limit and the finite density limit; finally in Sec. 4, we present the conclusions and discussions and also highlight the possible application of the results of our present investigation to the real magnetic systems.

2. Mathematical Formulations

Most of the material systems showing the so-called “central peak” (described in the introduction), are governed by the XY-anisotropic quantum Heisenberg (XXZ) Hamiltonian

$$\mathcal{H} = -J \sum_{\langle ij,pq \rangle} (S_{ij}^x S_{pq}^x + S_{ij}^y S_{pq}^y + \lambda S_{ij}^z S_{pq}^z), \quad (1)$$

on a two-dimensional square lattice with nearest neighbor interaction, where $\lambda(0 \leq \lambda < 1)$ is the anisotropy parameter and for ferromagnetic systems $J > 0$. Here, S_{ij}^x , S_{ij}^y and S_{ij}^z are the x , y and z components, respectively of the spin operator on the ij th lattice site. We shall concentrate on the $S = 1/2$ ferromagnetic model in the very strongly XY-anisotropic limit ($\lambda \rightarrow 0$, i.e., λ is vanishingly small, but $\lambda \neq 0$). With this smallest “ S ” value, the model is in fact in the extreme quantum regime.

It is worthwhile to mention here that the classical counterpart of the above model admits of the well-known meron solution.^{21–24,49,50} In classical case, spins are considered to be classical vectors of magnitude “ S ” in spherical polar coordinate.

The static meron solution corresponding to the classical version of model (1) is given by

$$\begin{aligned} \phi(x, y) = \pm \arctan \frac{y}{x}, \quad \theta(x, y) = \frac{\pi}{2} (1 \pm e^{-\frac{r}{r_v}}) \quad \text{for } r \gg r_v, \\ = 0 \quad \text{or} \quad \pi \quad \text{for } r \rightarrow 0, \end{aligned} \quad (2)$$

for single meron centered at $\mathbf{r} = (0, 0)$, where $\phi(x, y)$ is the azimuthal angle and $\theta(x, y)$ is the polar one and r_v is the meron core radius.^{21-24,51} Equation (2) describes the asymptotic behavior $\theta(x, y)$. Numerical studies have led to the conclusion that there is a critical value of the anisotropy parameter, say λ_c , below which only the static flattened merons or ordinary vortices are stable and above that the normal merons are stable.^{49,50}

Let us now come back to the properties of the quantum ferromagnetic XY-anisotropic Heisenberg model (ferromagnetic XXZ model) at very low temperature. First of all, this model is well known to possess its ground state (and eigenstate as well) having spins all aligned along the “+ve” or “-ve” z -direction. The normalized ground state $|0\rangle$ for the Hamiltonian in the case of ferromagnetic model as in Eq. (1) is chosen along the negative z -axis and is defined as $S_{ij}^-|0\rangle = 0$ for every i, j . Explicit form for the ground state on the square lattice is given by

$$\begin{aligned} |0\rangle = |\downarrow\rangle_{11} \otimes |\downarrow\rangle_{12} \otimes |\downarrow\rangle_{13} \otimes \cdots \otimes |\downarrow\rangle_{ij} \otimes |\downarrow\rangle_{i+1,j} \otimes |\downarrow\rangle_{i+1,j+1} \\ \otimes |\downarrow\rangle_{i,j+1} \otimes \cdots \otimes |\downarrow\rangle_{NN}, \end{aligned} \quad (3)$$

for an $N \times N$ square lattice, where S_{ij}^- is the spin lowering operator defined as $S_{ij}^- = S_{ij}^x - iS_{ij}^y$. The lattice has the structure of a torus for periodic boundary conditions.⁵¹⁻⁵⁶ The ground state energy is denoted by

$$\varepsilon_0 = -\frac{N}{2} \lambda J \hbar^2, \quad (4)$$

corresponding to the ground state $|0\rangle$, where $\mathcal{N} = N^2$.

It is important to recall that a quantum Heisenberg model (ferromagnetic or anti-ferromagnetic) on a three-dimensional lattice exhibits long range ordering at finite temperature unlike its counterparts in one and two dimensions.^{a,57-59} In the three-dimensional case, the collective excitations, viz, magnons are well defined in the long ranged ordered phase and become fragile in the short ranged ordered phase above the transition temperature, Curie temperature (T_c) for ferromagnetic systems or Néel temperature (T_N) for anti-ferromagnetic systems.⁴⁵⁻⁴⁸ In analogy with the above three-dimensional case, it is expected that in two dimensions, we can still find

^aAccording to Mermin–Wagner (MW) theorem [see Refs. 57–59], at any nonzero temperature, a one- or two-dimensional isotropic spin “ S ” Heisenberg model with finite range exchange interaction cannot exhibit any long range ferromagnetic order (implying $T_c = 0$) or antiferromagnetic order (implying $T_N = 0$). It can be shown that even for XY-anisotropic Heisenberg ferromagnet/anti-ferromagnet on two-dimensional lattice, the deviation from the spontaneous magnetization has infrared logarithmic divergence. This implies that the MW theorem holds for two-dimensional XY-anisotropic Heisenberg ferromagnet/anti-ferromagnet as well.

some fragile magnon-like excitations along with multi-magnon composites within a very small temperature regime above zero.^{45–48}

However, as a first approximation, in our present analysis for the two-dimensional ferromagnetic case, we assume the magnon states and multi-magnon composite states to be stable in the vicinity of zero temperature. This makes our analytical calculations simpler. Such magnon modes and their interactions are described briefly in Appendix A. In the next section, we will make use of the various properties of these magnon states in our novel scheme for the construction of quantum spin vortices and anti-vortices in the flattened meron configuration.

2.1. Construction of a quantum spin vortex and anti-vortex

We now start by defining a quantum spin vortex (anti-vortex) on a square lattice.^{36,39,40} A charge 1 vortex (anti-vortex) is defined on a square plaquette as a spin configuration in which the spin direction (horizontal and vertical spins as defined below) rotates through an angle $+2\pi$ (-2π) for a closed walk in an anti-clockwise (clockwise) direction around the plaquette. The vorticity of such a vortex is $+1$ (-1) [see Figs. 1(a) and 1(b)]. For our specific model with $\lambda \rightarrow 0$ [see Eq. (1)] the in-plane components of spin operators constitute a vortex (anti-vortex). It is worthwhile to mention that this situation corresponding to $\lambda \rightarrow 0$ is very different from the case of $\lambda = 0$ corresponding to pure XY model. It is in this very limit that a vortex may be looked upon as a “flattened meron.”^{39,40,60}

We first assign coordinates $(i, j)a$; $(i + 1, j)a$; $(i + 1, j + 1)a$ and $(i, j + 1)a$ to the four vertices of the vortex where “ a ” is the lattice parameter. Then, the physical realization (spin profile) of the vortex/anti-vortex is determined by the expectation values for the components of the spin operator S on the vertices of the vortex/anti-vortex. The relevant spin states at the vertices are constructed and explained below. For a vortex/anti-vortex having topological charge 1 (in the units of 2π) or simply 1-vortex/1-anti-vortex, the operator expectation values for the different components of spins (\mathbf{S}) at the vertices are given in Table 1.

Let us first construct the quantum state representing a vortex having topological charge “1”. The arrows, representing the spin directions on the four vertices [see Fig. 1(a)], signify that the spin states at the four vertices are such that the expectation values for S^x , S^y and S^z take the values as given in Table 1. The horizontal arrow $|\Rightarrow\rangle$ on the (i, j) th site represents a spin state which is the eigenstate of S_{ij}^x

Table 1. Expectation values for the components of the spin operator at four vertices of the vortex.

$\langle S_{ij}^x \rangle = \frac{1}{2}, \langle S_{ij}^y \rangle = 0, \langle S_{ij}^z \rangle = 0.$	$\langle S_{i+1,j}^x \rangle = 0, \langle S_{i+1,j}^y \rangle = \pm \frac{1}{2}, \langle S_{i+1,j}^z \rangle = 0,$ +sign for vortex and –sign for anti-vortex.
$\langle S_{i+1,j+1}^x \rangle = -\frac{1}{2}, \langle S_{i+1,j+1}^y \rangle = 0, \langle S_{i+1,j+1}^z \rangle = 0.$	$\langle S_{i,j+1}^x \rangle = 0, \langle S_{i,j+1}^y \rangle = \pm \frac{1}{2}, \langle S_{i,j+1}^z \rangle = 0,$ –sign for vortex and +sign for anti-vortex.

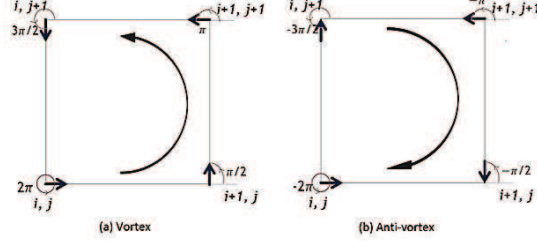


Fig. 1. (a) Quantum spin vortex of charge 1, (b) quantum spin anti-vortex of charge 1.

with eigenvalue $+(1/2)$ and the vertical arrow $|\uparrow\rangle$ on the $(i+1, j)$ th site represents a spin state which is the eigenstate of S_{ij}^y with eigenvalue $+(1/2)$. Similarly, the spin state $|\Leftarrow\rangle$ at $(i+1, j+1)$ th site and $|\Downarrow\rangle$ at $(i, j+1)$ th site are the eigenstates of S^x and S^y , respectively with the eigenvalue $-(1/2)$. The spin state corresponding to $|\Rightarrow\rangle$ can be written as a linear combination of the two eigenstates of S^z , viz $|\uparrow\rangle$ and $|\downarrow\rangle$. Then, at the (i, j) 'th site, the spin state is given by $(a_{ij}|\uparrow\rangle + b_{ij}|\downarrow\rangle)$. The value of a_{ij} and b_{ij} can be determined by using the expectation values for S_{ij}^x , S_{ij}^y and S_{ij}^z and the condition that the eigenvalue of S_{ij}^x is $+(1/2)$ in the state $(a_{ij}|\uparrow\rangle + b_{ij}|\downarrow\rangle)$. Similarly, for the rest of the vertices corresponding to the vortex, the spin states are taken to be of the form $(a|\uparrow\rangle + b|\downarrow\rangle)$.

The coefficients “ a ” and “ b ” are determined from the expectation values for S^x , S^y and S^z and the eigenvalue conditions for the respective vertices as mentioned above. The coefficients “ a ” and “ b ” for the four vertices turns out to be

$$\begin{aligned} a_{ij} &= b_{ij} = \frac{1}{\sqrt{2}} e^{i\theta_{ij}}; & a_{i+1,j} &= \frac{1}{\sqrt{2}} e^{i\theta_{i+1,j}}, & b_{i+1,j} &= \frac{i}{\sqrt{2}} e^{i\theta_{i+1,j}}, \\ a_{i+1,j+1} &= b_{i+1,j+1} = \frac{1}{\sqrt{2}} e^{i(\theta_{ij}+\pi)}; & a_{i,j+1} &= \frac{1}{\sqrt{2}} e^{i(\theta_{i+1,j}+\pi)}, & b_{i,j+1} &= \frac{i}{\sqrt{2}} e^{i(\theta_{i+1,j}+\pi)}. \end{aligned} \quad (5)$$

Here, θ_{ij} and $\theta_{i+1,j}$ are arbitrary phase factors and for the diagonally opposite vertices, the coefficients have π phase difference. The coefficients given in (5) take care of the proper normalization of the spin states at each vertex. Therefore, the normalized charge 1 vortex state in the background of the original ground state can be defined on a plaquette $((i, j); (i+1, j); (i+1, j+1); (i, j+1))$ as^b

$$\begin{aligned} |1V\rangle &= |\downarrow\rangle_{11} \otimes |\downarrow\rangle_{12} \otimes |\downarrow\rangle_{13} \otimes \cdots \otimes (a_{ij}|\uparrow\rangle_{ij} + b_{ij}|\downarrow\rangle_{ij}) \otimes (a_{i+1,j}|\uparrow\rangle_{i+1,j} \\ &\quad + b_{i+1,j}|\downarrow\rangle_{i+1,j}) \otimes (a_{i+1,j+1}|\uparrow\rangle_{i+1,j+1} + b_{i+1,j+1}|\downarrow\rangle_{i+1,j+1}) \\ &\quad \otimes (a_{i,j+1}|\uparrow\rangle_{i,j+1} + b_{i,j+1}|\downarrow\rangle_{i,j+1}) \otimes \cdots \otimes |\downarrow\rangle_{NN}. \end{aligned} \quad (6)$$

^bIt may be remarked here that in our present formalism, we are implicitly assuming a static vortex configuration. This is in conformity with the frozen vortex/anti-vortex scenario proposed below T_{BKT} .^{19,20}

The vorticity operator is defined on the square plaquette as³⁶

$$V_{op} = S_{ij}^x S_{i+1,j}^y - S_{i+1,j}^y S_{i+1,j+1}^x + S_{i+1,j+1}^x S_{i,j+1}^y - S_{i,j+1}^y S_{ij}^x. \quad (7)$$

When we operate the vorticity operator on the above 1-vortex state, the eigenvalue comes out to be +1 as expected.

Similarly we can construct an anti-vortex with charge 1. For an anti-vortex, coefficients at the four vertices come out to be

$$\begin{aligned} a_{ij} = b_{ij} &= \frac{1}{\sqrt{2}} e^{i\theta_{ij}}; \quad a_{i+1,j} = \frac{1}{\sqrt{2}} e^{i\theta_{i+1,j}}, \quad b_{i+1,j} = -\frac{i}{\sqrt{2}} e^{i\theta_{i+1,j}}, \\ a_{i+1,j+1} = b_{i+1,j+1} &= \frac{1}{\sqrt{2}} e^{i(\theta_{ij}+\pi)}; \quad a_{i,j+1} = \frac{1}{\sqrt{2}} e^{i(\theta_{i+1,j}+\pi)}, \quad b_{i,j+1} = -\frac{i}{\sqrt{2}} e^{i(\theta_{i+1,j}+\pi)}. \end{aligned} \quad (8)$$

The explicit structure of the 1-anti-vortex state ($|1AV\rangle$) is same as the state $|1V\rangle$ of (6) with the coefficients “ a ” and “ b ” being different from that of the $|1V\rangle$. In this case, the eigenvalue of the vorticity operator defined in (7) comes out to be -1 , as expected.

2.2. Connection between quantum vortex and magnons

Let us consider the simplest situation where there is a single vortex on a $N \times N$ square lattice. To explore the connection between a vortex state and the magnon states, we rewrite the one vortex state in a suitable way. For each vertex of the vortex the spin state, $|\uparrow\rangle_{ij}$ can be written as $S_{ij}^+ |\downarrow\rangle_{ij}$, where $S_{ij}^+ = S_{ij}^x + iS_{ij}^y$ is the spin raising operator. The state $|1V\rangle$ in Eq. (6) can be rewritten as

$$\begin{aligned} |1V\rangle &= a_{ij} a_{i+1,j} a_{i+1,j+1} a_{i,j+1} S_{ij}^+ S_{i+1,j}^+ S_{i+1,j+1}^+ S_{i,j+1}^+ |0\rangle \\ &+ (b_{ij} a_{i+1,j} a_{i+1,j+1} a_{i,j+1} S_{i+1,j}^+ S_{i+1,j+1}^+ S_{i,j+1}^+ |0\rangle \\ &+ \cdots + a_{ij} a_{i+1,j} a_{i+1,j+1} b_{i,j+1} S_{ij}^+ S_{i+1,j}^+ S_{i+1,j+1}^+ |0\rangle) \\ &+ (a_{ij} a_{i+1,j} b_{i+1,j+1} b_{i,j+1} S_{ij}^+ S_{i+1,j}^+ |0\rangle \\ &+ \cdots + a_{ij} b_{i+1,j} b_{i+1,j+1} a_{i,j+1} S_{ij}^+ S_{i,j+1}^+ |0\rangle) \\ &+ (a_{ij} b_{i+1,j} b_{i+1,j+1} b_{i,j+1} S_{ij}^+ |0\rangle) + b_{ij} a_{i+1,j} b_{i+1,j+1} b_{i,j+1} S_{i+1,j}^+ |0\rangle \\ &+ b_{ij} b_{i+1,j} a_{i+1,j+1} b_{i,j+1} S_{i+1,j+1}^+ |0\rangle + b_{ij} b_{i+1,j} b_{i+1,j+1} a_{i,j+1} S_{i,j+1}^+ |0\rangle) \\ &+ b_{ij} b_{i+1,j} b_{i+1,j+1} b_{i,j+1} |0\rangle, \end{aligned} \quad (9)$$

where a and b 's are given by Eq. (5). Equation (9) explicitly shows that the charge 1 quantum vortex state is a linear superposition of one four-spin deviation state, four three-spin deviation states, six two-spin deviation states, four one-spin deviation states and the ground state. Using the definitions of magnon states, (see Appendix A) the charge 1 vortex state can now be expressed in terms of magnon

states as

$$\begin{aligned}
 |1V\rangle = & A \sum_{\mathbf{k}_1, \mathbf{k}_2, \mathbf{k}_3, \mathbf{k}_4} f_{\mathbf{k}_1}^{i,j} f_{\mathbf{k}_2}^{i+1,j} f_{\mathbf{k}_3}^{i+1,j+1} f_{\mathbf{k}_4}^{i,j+1} |\mathbf{k}_1 \mathbf{k}_2 \mathbf{k}_3 \mathbf{k}_4\rangle \\
 & + \sum_{\mathbf{k}_1, \mathbf{k}_2, \mathbf{k}_3} (B_1 f_{\mathbf{k}_1}^{i,j} f_{\mathbf{k}_2}^{i+1,j} f_{\mathbf{k}_3}^{i+1,j+1} + B_2 f_{\mathbf{k}_1}^{i,j+1} f_{\mathbf{k}_2}^{i+1,j} f_{\mathbf{k}_3}^{i+1,j+1} \\
 & + B_3 f_{\mathbf{k}_1}^{i,j} f_{\mathbf{k}_2}^{i,j+1} f_{\mathbf{k}_3}^{i+1,j+1} + B_4 f_{\mathbf{k}_1}^{i,j} f_{\mathbf{k}_2}^{i,j+1} f_{\mathbf{k}_3}^{i+1,j}) |\mathbf{k}_1 \mathbf{k}_2 \mathbf{k}_3\rangle \\
 & + \sum_{\mathbf{k}_1, \mathbf{k}_2} (C_1 f_{\mathbf{k}_1}^{i,j} f_{\mathbf{k}_2}^{i+1,j} + C_2 f_{\mathbf{k}_2}^{i+1,j} f_{\mathbf{k}_3}^{i+1,j+1} + C_3 f_{\mathbf{k}_3}^{i+1,j+1} f_{\mathbf{k}_4}^{i,j+1} + C_4 f_{\mathbf{k}_1}^{i,j} f_{\mathbf{k}_4}^{i,j+1} \\
 & + C_5 f_{\mathbf{k}_2}^{i+1,j} f_{\mathbf{k}_4}^{i,j+1} + C_6 f_{\mathbf{k}_1}^{i,j} f_{\mathbf{k}_3}^{i+1,j+1}) |\mathbf{k}_1 \mathbf{k}_2\rangle \\
 & + \sum_{\mathbf{k}_1} (D_1 f_{\mathbf{k}_1}^{i,j} + D_2 f_{\mathbf{k}_1}^{i+1,j} + D_3 f_{\mathbf{k}_1}^{i+1,j+1} + D_4 f_{\mathbf{k}_1}^{i,j+1}) |\mathbf{k}_1\rangle + E |0\rangle. \quad (10)
 \end{aligned}$$

The coefficients A , B_1 , B_2, \dots and E signify the weightage of the different spin deviation states in the composition of charge 1 vortex state and they are given by, $A = a_{ij} a_{i+1,j} a_{i+1,j+1} a_{i,j+1}$, $B_1 = a_{ij} a_{i+1,j} a_{i+1,j+1} b_{i,j+1}, \dots$, $E = b_{ij} b_{i+1,j} b_{i+1,j+1} b_{i,j+1}$, where “ a ” and “ b ” are given in Eq. (5).

In case of charge 1 anti-vortex, the form of the state $|1AV\rangle$ will be same as the state $|1V\rangle$ except that the values for the coefficients $A = a_{ij} a_{i+1,j} a_{i+1,j+1} a_{i,j+1}$, $B_1 = a_{ij} a_{i+1,j} a_{i+1,j+1} b_{i,j+1}, \dots$, $E = b_{ij} b_{i+1,j} b_{i+1,j+1} b_{i,j+1}$ are different from those for $|1V\rangle$. Their values are determined by the values of a and b , as given in Eq. (8).

Thus, Eq. (10) signifies the fact that the quantum state representing a 1-vortex (1-anti-vortex) is a combination of linear superpositions of four-magnon composites, three-magnon composites, two-magnon composites, one-magnon states and the ground state.

3. Calculations and Results Regarding Stability of the Vortex State

In a realistic situation, a macroscopic number of vortex–anti-vortex pairs needs to be considered. However, description of these in terms of multi-magnon composite states will be quite challenging and tough. Therefore, as a first step we handle here two special cases, viz, vortex (anti-vortex) in an infinitely dilute limit and also in the finite density limit, as explained below.

Let us now investigate the quantum mechanical stability of the charge 1 vortex state $|1V\rangle$. Operating the Hamiltonian \mathcal{H} [as given by Eq. (1)] on the 1-vortex state $|1V\rangle$ [see Eq. (9)], it can easily be shown that $|1V\rangle$ is not an exact eigenstate for the Hamiltonian \mathcal{H} [see Eq. (11)]. Therefore, the natural question arises that how stable the state $|1V\rangle$ is for a system, which is governed by the Hamiltonian \mathcal{H} .

For the stability analysis, two cases shall be treated separately. In the first one, we shall consider the presence of only one charge 1 vortex in the $N \times N$ square lattice. This is the extreme dilute limit where the vortex density is vanishingly

small. In the second case, we shall consider a finite density of charge 1 vortices to be present in the $N \times N$ square lattice.

3.1. Single charge 1 vortex

Let us first consider a single 1-vortex in a $N \times N$ square lattice which is the “extreme dilute limit” of the vortex density. The quantum mechanical state $|1V\rangle$ describing such a situation is given by Eq. (9). Operating the Hamiltonian \mathcal{H} given by Eq. (1), on the state $|1V\rangle$ we get

$$\mathcal{H}|1V\rangle = (\varepsilon_0 + 2\lambda J\hbar^2)|1V\rangle + |\phi_{\text{resi}}\rangle, \quad (11)$$

(see Appendix B). The right-hand side of the above equation clearly shows departure of the vortex state from being an eigenstate of \mathcal{H} .

Let us note that the residual state denoted by $|\phi_{\text{resi}}\rangle$ is not a linear superposition of multi-magnon states [Appendix B, Eq. (B.1)] unlike the state $|1V\rangle$ [Eq. (10)]. In fact $|\phi_{\text{resi}}\rangle$ [see Appendix B, Eq. (B.2)] contains terms which generate higher order inter-multi-magnonic correlations.

The expectation of the Hamiltonian in the state $|1V\rangle$ is evaluated from Eq. (9) and is given by

$$\langle 1V|\mathcal{H}|1V\rangle = (\varepsilon_0 + 3\lambda J\hbar^2) = E_0, \quad (12)$$

where $E_0 \equiv (\varepsilon_0 + 3\lambda J\hbar^2)$ and the quantity $3\lambda J\hbar^2$ signifies the energy required to excite one 1-vortex from the ground state, the ground state energy being ε_0 as given in (4). Equation (11) can be rewritten as

$$\mathcal{H}|1V\rangle = E_0|1V\rangle + (|\phi_{\text{resi}}\rangle - \lambda J\hbar^2|1V\rangle) = E_0|1V\rangle + |\psi_{\text{resi}}\rangle, \quad (13)$$

where $|\psi_{\text{resi}}\rangle \equiv (|\phi_{\text{resi}}\rangle - \lambda J\hbar^2|1V\rangle)$ is again not a linear superposition of multi-magnon states as explained above. Making use of Eqs. (11)–(13), it is clear that $\langle 1V|\psi_{\text{resi}}\rangle = 0$.

Now, operating the Hamiltonian \mathcal{H} successively twice on $|1V\rangle$ the expectation value of \mathcal{H}^2 in the state $|1V\rangle$ turns out to be

$$\langle 1V|\mathcal{H}^2|1V\rangle = (\varepsilon_0 + 2\lambda J\hbar^2)^2 + (J\hbar^2)^2 \left(2 + \frac{3}{4}\lambda^2\right). \quad (14)$$

The quantum mechanical stability of the state $|1V\rangle$ is now verified by operating the time evolution operator $[\exp(-i/\hbar)\mathcal{H}t]$ on the state $|1V\rangle$. Since the state $|1V\rangle$ is not an eigenstate of \mathcal{H} , let us take the expectation value of the time evolution operator in $|1V\rangle$ to study what fraction of the original one quantum vortex state is retained during the time evolution of the system. Hence

$$\begin{aligned} \langle 1V(0)|1V(t)\rangle &= \left\langle 1V \left| \exp\left(-\frac{i}{\hbar}\mathcal{H}t\right) \right| 1V \right\rangle \\ &= 1 - \frac{it}{\hbar}\langle 1V|\mathcal{H}|1V\rangle + \left(\frac{i}{\hbar}\right)^2 \frac{t^2}{2!}\langle 1V|\mathcal{H}^2|1V\rangle + \dots, \end{aligned} \quad (15)$$

where $|1V(0)\rangle$ is the initial state and $|1V(t)\rangle$ is the final state (i.e., the state after time evolution for a duration of time t). On the right-hand side of the above expression, we retain terms up to second-order in time explicitly and then Eq. (15) becomes

$$\langle 1V(0)|1V(t)\rangle = \left(1 - \frac{i}{\hbar}E_0t + \left(\frac{i}{\hbar}\right)^2 \frac{1}{2!}E_0^2t^2 \right) - \frac{1}{\hbar^2}(J\hbar^2)^2 \left(1 + \frac{3}{8}\lambda^2 \right) t^2 + O(t^3). \quad (16)$$

It is clear from Eq. (16) that the first three terms correspond to the series expansion of $[\exp(-i/\hbar)E_0t]$ up to second-order in time. The next one represents the deviation in the sense (of a damping) that in absence of this term, the expectation value of the time evolution operator describes a stationary state exhibiting phase oscillation with frequency $\omega_0 = (E_0/\hbar)$ and therefore, the state $|1V\rangle$ behaves like an approximate eigenstate of the Hamiltonian \mathcal{H} with energy E_0 . On the other hand, the inverse time scale Γ_d corresponding to the damping term arising from inter-multi-magnonic correlations as explained above, is given by

$$\Gamma_d = J\hbar\sqrt{\left(1 + \frac{3}{8}\lambda^2\right)}, \quad (17)$$

which essentially indicates the decay rate of the coherent phase oscillation. Hence up to second-order in time, the quantity of interest, viz the ratio of the decay rate and the phase coherent oscillation frequency comes out to be

$$\frac{\Gamma_d}{\omega_0} = \frac{1}{\left(\frac{N}{2} - 3\right)} \sqrt{\left(\frac{1}{\lambda^2} + \frac{3}{8}\right)}. \quad (18)$$

In the above ratio, the term under the squared root becomes approximately $1/\lambda$ for a very small but fixed value of the anisotropy parameter λ . Hence, Eq. (18) becomes

$$\frac{\Gamma_d}{\omega_0} \approx \frac{1}{\left(\frac{N}{2} - 3\right)\lambda}. \quad (19)$$

The time duration of the evolution is assumed to be much shorter than the natural time scale $t_{\text{nat}} = 2\hbar/(\sqrt{3}(J\hbar^2))$ (for $S = 1/2$) for the system so that a truncation at second-order in time can be considered safe, where the quantity $J\hbar^2$ has the dimension of energy. At the first place, such an approximation physically means that the multi-magnon composites fuses to form such a vortex state of true quantum nature in a time scale which is much shorter than the natural time scale of the system. Furthermore, the ratio of the evolution time and t_{nat} is assumed to be much smaller than that of the time scale of decay and t_{nat} . It is clear from Eq. (19) that Γ_d becomes very small compared to ω_0 when the lattice size is very large and ensures the fulfillment of the above conditions. In this case, the deviation

representing phase incoherence remains ineffective and the state $|1V\rangle$ remains a stable state for the Hamiltonian \mathcal{H} . It is worthwhile to mention that in the confined phase below T_{BKT} (and above T_c) the form of the dynamical structure function for an ideal vortex gas is a pure delta function $\delta(\omega)$.³⁵ However, just above $T_c (= 0)$ taking into consideration the dynamics of all the magnon modes and the multi-magnon composites which are present in a fragile manner, the central peak of the dynamical structure function acquires a finite width. This width is expected to be of the order of magnitude of the decay rate Γ_d .

Let us now estimate the threshold size of the system beyond which the 1-vortex state remains stable. Taking a typical value of $\lambda \approx 10^{-4}$ (since we are considering extreme anisotropy limit, i.e., flattened meron configuration) we have from Eq. (19), $(\Gamma_d/\omega_0) \approx (2/N^2\lambda)$. This leads to the above threshold system size to be of the order of 141×141 . Considering a typical value of 3\AA for the lattice spacing, the length scale of the system is of the order of 10^{-5} cm which falls into the mesoscopic length scale.

3.2. Finite density of charge 1 vortices

Since the Hamiltonian contains only the nearest neighbor interactions, the state $\mathcal{H}|1V\rangle$ will produce spin deviations only on the nearest neighbor sites of the vertices of the vortex. Thus to construct a finite density of charge 1 vortices in an infinite lattice, we employ the periodic boundary condition (PBC) for simplicity on a closed (torus) 4×4 cell, which is of minimum allowed size. By periodically repeating these cells, we can fill up the entire $N \times N$ square lattice with a maximum of $n = (N^2/16)$ (where N is an integral multiple of 4) charge 1 vortices, without having interactions between them, as can be seen in Fig. 2. This is the other limit as opposed to the extreme dilute case studied in Sec. 3.1. The periodicity is therefore, given by the following equations involving spin operators (see Table 1 under Sec. 3.1):

$$\langle S_{i,j}^\alpha \rangle = \langle S_{i+4,j}^\alpha \rangle = \langle S_{i-4,j}^\alpha \rangle = \langle S_{i,j-4}^\alpha \rangle = \langle S_{i,j+4}^\alpha \rangle, \quad \text{where } \alpha = x, y, z, \quad (20)$$

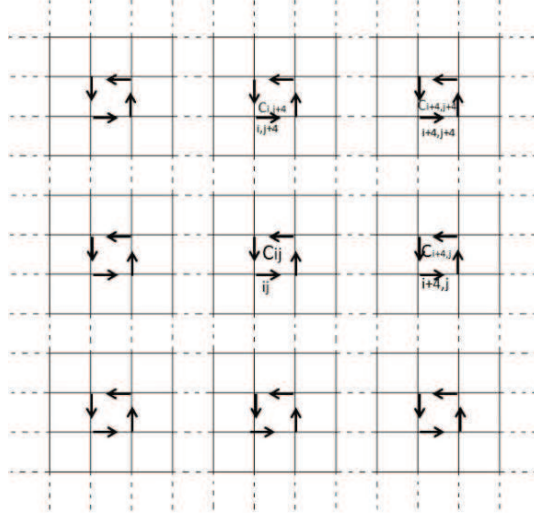
for all i and j on the lattice, where $\alpha \equiv x, y, z$.

Under these conditions the magnon modes defined in each cell with the PBC will be repeated in the adjacent cell in a periodic manner. Therefore, the composite quantum state corresponding to “ n ” number of such 1-vortices can be written as,

$$|n1V\rangle = \cdots \otimes |C_{i-4,j}\rangle \otimes |C_{i,j-4}\rangle \otimes |C_{i,j}\rangle \otimes |C_{i+4,j}\rangle \otimes |C_{i,j+4}\rangle \otimes \cdots \quad (21)$$

where the quantum state corresponding to each cell is denoted as $|C_{i,j}\rangle$ which is of the same form as given in Eq. (9) with only exception being the fact that now the number of lattice points is 16 and only four lattice points correspond to the four vertices of the vortex (see Fig. 2). Operating the Hamiltonian \mathcal{H} on the state $|n1V\rangle$ and making use of Eqs. (13) and (21) we get,

$$\begin{aligned} \mathcal{H}|n1V\rangle = & n\tilde{E}_0|n1V\rangle + \{|\psi_{\text{resi}}^1\rangle \otimes |C_2\rangle \otimes |C_3\rangle \otimes \cdots \otimes |C_n\rangle + |C_1\rangle \otimes |\psi_{\text{resi}}^2\rangle \otimes |C_3\rangle \\ & \otimes \cdots \otimes |C_n\rangle + \cdots + |C_1\rangle \otimes |C_2\rangle \otimes |C_3\rangle \otimes \cdots \otimes |\psi_{\text{resi}}^n\rangle\}, \quad (22) \end{aligned}$$


 Fig. 2. Finite number vortices of charge 1 in an $N \times N$ lattice.

where $\tilde{E}_0 = -5\lambda J\hbar^2$ and the residual state $|\psi_{\text{rest}}^i\rangle$ is the deviation of the vortex state from being an eigen-state of \mathcal{H} within the (i, j) th cell.

The expression for \tilde{E}_0 corresponding to each (i, j) th cell stands for E_0 [see Eq. (20)] with $N = 4$. Also, we make use of Eq. (21) with $N = 4$ in deducing Eq. (22). Further we have used the notation $|C_r\rangle$ in place of $|C_{ij}\rangle$ and $|\psi_{\text{resi}}^r\rangle$ in place of $|\psi_{\text{resi}}^{ij}\rangle$ for convenience.

The expectation value of \mathcal{H} in the state $|n1V\rangle$ is given by

$$\langle n1V|\mathcal{H}|n1V\rangle = n\tilde{E}_0, \quad (23)$$

making use of the fact that for each cell $\langle C_r|\psi_{\text{resi}}^r\rangle = 0$. This residual state, defined within one cell, is again a nonlinear superposition of multi-magnon states as explained in Sec. 3.1. Proceeding along the same lines as in Sec. 3.1, we now have

$$\langle n1V|\mathcal{H}^2|n1V\rangle \approx n^2\tilde{E}_0^2 + n(J\hbar^2)^2 \left(2 + \frac{3}{4}\lambda^2\right). \quad (24)$$

To check the quantum mechanical stability of the state $|n1V\rangle$ under time evolution, we follow the same procedure as adopted in Sec. 3.1. Then, the overlap between the initial state and the final state (i.e., the expectation value of the time evolution operator $[\exp(-i/\hbar)\mathcal{H}t]$ in the state $|n1V\rangle$) comes out to be

$$\begin{aligned} \langle n1V(0)|n1V(t)\rangle &= \langle n1V \left| \exp\left(-\frac{i}{\hbar}\mathcal{H}t\right) \right| n1V\rangle = \left(1 - \frac{i}{\hbar}nE_0t + \left(\frac{i}{\hbar}\right)^2 \frac{1}{2!}n^2E_0^2t^2\right) \\ &\quad - \frac{1}{\hbar^2}n(J\hbar^2)^2 \left(1 + \frac{3}{8}\lambda^2\right) t^2 + O(t^3), \end{aligned} \quad (25)$$

where the exponential series has again been expanded up to second-order in time and the justification for such an expansion remains the same as that of Sec. 3.1. The ratio of the decay rate $\Gamma_d^{(n)}$ corresponding to the deviation term (the superscript n represents the fact that we are considering finite density of charge 1 vortices) and the frequency $\omega_0^{(n)}$ corresponding to the phase oscillation is given by

$$\frac{\Gamma_d^{(n)}}{\omega_0^{(n)}} = \frac{4}{5} \sqrt{\frac{1}{N^2 \lambda^2} \left(1 + \frac{3}{8} \lambda^2\right)}. \quad (26)$$

In order for the phase coherent mode to physically survive, it follows from the above equation that the necessary condition is:

$$\Gamma_d^{(n)} < \omega_0^{(n)},$$

which in turn implies

$$N\lambda > \frac{4}{5}, \quad \text{for } N > N_c. \quad (27)$$

Note that the term $\sqrt{(1 + (3/8)\lambda^2)}$ in Eq. (26) is nearly equal to 1, since our starting model itself is strongly XY-anisotropic i.e., λ is very small.

The condition in Eq. (27) signifies that there must be a critical system size $N_c = N_c^2$ for a given value of λ for the stability of the n 1-vortex state. As before, we take $\lambda \approx 10^{-4}$ and in this case, the threshold system size comes out to be of the order of 8000×8000 . Taking a typical value of 3\AA for the lattice spacing as before, the length scale of the system becomes of the order of 10^{-4} cm, which again is in the mesoscopic regime.

Experimental studies of spin dynamics would be quite helpful in verifying our prediction regarding threshold size.

4. Conclusions and Discussions

Our analysis firmly establishes that the interaction between collective excitations originating from a strongly anisotropic quantum Heisenberg ferromagnet on two-dimensional lattices, can lead to the formation of topological excitations of vortex or anti-vortex type (in a flattened meron configuration) which are localized objects. These collective excitations could be single magnon as well as multi-magnon composites.

We find that in the situation of an infinitely dilute limit of vortex density, the corresponding 1-vortex state is quantum mechanically stable when the system size exceeds a threshold value, keeping the magnon modes well defined. Similar conclusion holds also for the case with finite density of vortices. The only difference in contrast to the dilute limit case is that, for finite density the threshold size is much larger. It is expected that the above features would remain intact even quantitatively for anti-vortices as well.

Regarding the collective modes referred above, it may be remarked that these modes become fragile at any finite temperature. This is because the ferromagnetic

Curie temperature T_c identically vanishes on pure two-dimensional lattices. Therefore, magnon-like collective excitations become fragile at any finite temperature, in analogy with three-dimensional ferromagnets.^{45–48,61–63} For layered systems, the interlayer coupling i.e., the exchange interaction between the spins of two nearby layers make T_c nonvanishing. With a very small interlayer coupling, however, T_c still remains quite low and above this transition temperature, the collective excitations again become fragile.^{45–48,61–63}

It is now a well-established fact that in the paramagnetic phase of the Heisenberg model on three-dimensional spatial lattices, the damped propagating modes exist.^{45–48} The temporal dependence of the spin–spin correlation function in this paramagnetic phase is diffusive in nature with an oscillatory component present sometimes. This is manifested through the occurrence of the central peak for dynamical structure function (in the constant \mathbf{q} scan).^{45–48} It should be emphasized that this central peak is fundamentally different from the central peak that we had talked about in relation to the mobile BKT vortices. The primary reason for the truly diffusive or damped propagating behavior of the dynamical structure function is due to the temporal evolution of the spin–spin correlation function, which is governed by various higher order correlation functions with nontrivial temperature and \mathbf{q} (wave vector) dependence.^{45–48}

As we stated before, in the case of XY-anisotropic Heisenberg models on two-dimensional spatial lattices, the Curie temperature $T_c = 0$; whereas the BKT transition temperature (T_{BKT}) is finite. Besides, in the paramagnetic phase above T_{BKT} , the vortices (and anti-vortices) move freely and contribute to the dynamical structure function. This provides one of the important mechanisms behind the occurrence of central peak in the dynamical structure function.^{19–24} According to our picture, the static vortices (anti-vortices) below T_{BKT} are formed from the composite magnon modes which are expected to exist in this temperature regime in a highly fragile manner. Since all the damped propagating composite multi-magnons and the single magnon modes superpose in a complicated manner to form the vortices as shown in this paper, the dynamics of mobile vortices gets very complicated in the regime $T > T_{\text{BKT}}$. Our investigation reveals that such a nontrivial combination of all the damped propagating modes gives rise to localized vortex-like topological excitations. The temporal behavior of the dynamical spin–spin correlation is further expected to be governed by the various nonlinear processes entering through the higher order correlation functions, bearing the effects of the fragile multi-magnon composites as well.

Apart from forming vortices, some modes are expected to stay intact with their original damped nature. Their dynamics is again either diffusive or damped propagating and can provide a substantial contribution to the central peak both below and above T_{BKT} .

Of course, detailed investigations are needed to look into how the diffusive dynamics of the highly damped and fragile multi-magnon composites and the single magnons contribute to the dynamical structure function corresponding to the two-

dimensional XY-anisotropic Heisenberg spin systems in the temperature regime below and above T_{BKT} .

It is however worthwhile to mention that although our investigations pertain to strongly XY-anisotropic case, the material systems of interest to experimentalists mostly belong to weakly XY-anisotropic category.^{8–11} In these experimental systems, the topological excitations are of truly meronic/anti-meronic type rather than “flattened meron/anti-meron” configurations we have dealt with in our calculations.

Last but not least, the method of construction of the quantum state representing a charge 1 vortex/anti-vortex has subsequently been extended to the higher charged vortices/anti-vortices. We find that the quantum state representing any vortex/anti-vortex can be regarded as generated from the interactions between the various magnon modes and magnon composites.⁶⁴

Acknowledgment

One of the authors (SS) acknowledges the financial support through Senior Research Fellowship (09/575 (0089)/2010 EMR–1) provided by Council of Scientific and Industrial Research (CSIR), Govt. of India.

Appendix A

In this paper, we are considering only the two-dimensional systems and in a very small temperature regime above zero temperature and the entire soup of magnon-like fragile modes and the composite magnon modes are expected to be found.^{45–48} In this appendix, magnon states and the interactions between the magnon modes will be reviewed briefly to develop notations for our convenience.

A.1. One-magnon states

When a spin deviation is introduced on a particular site of the lattice it does not remain localized on that site. It rather propagates through the lattice due to the exchange interaction between the nearest neighbor spins and thereby constitutes the “spin wave”.^{52–56,65} The basic unit of the quantized spin waves is the magnons. The normalized quantum state of one spin deviation is defined as

$$|ij\rangle = \frac{1}{\sqrt{2S\hbar}} S_{ij}^+ |0\rangle. \quad (\text{A.1})$$

There are $\mathcal{N}(= N^2)$ such orthogonal and normalized states containing one spin deviation each corresponding to all choices of the lattice points. For spin 1/2 systems, assuming the translational invariance and the periodic boundary condition, the one-magnon state is defined as

$$|\mathbf{k}\rangle = \sum_{i,j} \frac{e^{ik \cdot R_{ij}}}{\sqrt{\mathcal{N}}} S_{ij}^+ |0\rangle = \sum_{i,j} (J_k^{i,j})^* S_{ij}^+ |0\rangle, \quad (\text{A.2})$$

where \mathbf{k} is the Bloch wave vector restricted in the first Brillouin zone, describing the propagation of the magnon, \mathbf{R}_{ij} is the position vector of ij th lattice site on the square lattice and $f_{\mathbf{k}}^{ij} = (e^{-i\mathbf{k}\cdot\mathbf{R}_{ij}}/\sqrt{\mathcal{N}})$. The one-magnon states defined above are normalized to unity, i.e., $\langle \mathbf{k}|\mathbf{k}' \rangle = \delta_{\mathbf{k}\mathbf{k}'}$ and $|\mathbf{k}\rangle$ forms a complete set of orthonormal states. The $|\mathbf{k}\rangle$ states are the exact eigenstates of the Hamiltonian \mathcal{H} corresponding to Eq. (1) with the eigenvalue $\varepsilon_0 + \hbar\omega(\mathbf{k})$.

The one-magnon excitation energy $\hbar\omega(\mathbf{k})$, above the ground state, is given by

$$\omega(\mathbf{k}) = 2\hbar J(\lambda - \gamma_{\mathbf{k}}), \quad (\text{A.3})$$

where $\gamma_{\mathbf{k}} = (1/4) \sum_{\delta} e^{i\mathbf{k}\cdot\delta}$ and δ is a vector connecting a typical site to its nearest neighbors. The one spin deviation states can be obtained from Eq. (A.2) by the inverse transformation.^{52-56,65}

In the long range ordered phase below the transition temperature (T_c or T_N), as the number of magnon increases with the increasing temperature they are more prone to interact with each other and therefore, the composite magnon modes are very natural to occur.^{54,55} This happens when the spatial lattice is three-dimensional. In the following, we shall restate the well-known definitions of composite magnon states.^{52-56,65}

A.2. Two-magnon states

The two-magnon states can be defined in a similar manner as the one-magnon state [see Eq. (A.2)] as follows:

$$|\mathbf{k}, \mathbf{k}'\rangle = \sum_{i,j;p,q} \frac{e^{i(\mathbf{k}\cdot\mathbf{R}_{ij} + \mathbf{k}'\cdot\mathbf{R}_{pq})}}{(\sqrt{\mathcal{N}})^2} S_{ij}^+ S_{pq}^+ |0\rangle = \sum_{i,j;p,q} (f_{\mathbf{k}}^{i,j})^* (f_{\mathbf{k}'}^{p,q})^* S_{ij}^+ S_{pq}^+ |0\rangle. \quad (\text{A.4})$$

The two spin deviation states $|ij, pq\rangle$ are related to $|\mathbf{k}, \mathbf{k}'\rangle$ in the following way:

$$S_{ij}^+ S_{pq}^+ |0\rangle = \sum_{\mathbf{k}, \mathbf{k}'} f_{\mathbf{k}}^{i,j} f_{\mathbf{k}'}^{p,q} |\mathbf{k}, \mathbf{k}'\rangle. \quad (\text{A.5})$$

These two-magnon states are approximately orthonormal with an error of no more than $O(1/N)$ which can be seen from the form of the scalar product, viz, $\langle \mathbf{k}, \mathbf{k}' | \lambda, \lambda' \rangle = \hbar^4 \delta_{\lambda+\lambda', \mathbf{k}+\mathbf{k}'} (\delta_{\lambda, \mathbf{k}} + \delta_{\lambda', \mathbf{k}'} - (2/\mathcal{N}))$. The very choice of the form of the two-magnon state [Eq. (A.4)] leads to what are called Dyson's "kinematical" and "dynamical" interactions.^{52-56,65}

A.3. Higher magnon states

Using the analogous scheme, the three-magnon composite states are defined as

$$|\mathbf{k}_1, \mathbf{k}_2, \mathbf{k}_3\rangle = \sum_{i,j;p,q;r,s} (f_{\mathbf{k}_1}^{i,j})^* (f_{\mathbf{k}_2}^{p,q})^* (f_{\mathbf{k}_3}^{r,s})^* S_{ij}^+ S_{pq}^+ S_{rs}^+ |0\rangle. \quad (\text{A.6})$$

The three-spin deviations state, $S_{ij}^+ S_{pq}^+ S_{rs}^+ |0\rangle$ is defined as the inverse transformation of the three-magnon which is similar to the definition of the two spin deviations in Eq. (A.5).⁶⁶⁻⁶⁸

The quantum state of four-magnon composites can be defined analogously as

$$|\mathbf{k}_1, \mathbf{k}_2, \mathbf{k}_3, \mathbf{k}_4\rangle = \sum_{\substack{i,j;p,q \\ r,s;l,m}} (f_{\mathbf{k}_1}^{i,j})^* (f_{\mathbf{k}_2}^{p,q})^* (f_{\mathbf{k}_3}^{r,s})^* (f_{\mathbf{k}_4}^{l,m})^* S_{ij}^+ S_{pq}^+ S_{rs}^+ S_{lm}^+ |0\rangle \quad (\text{A.7})$$

and four-spin deviations state $S_{ij}^+ S_{pq}^+ S_{rs}^+ S_{lm}^+ |0\rangle$ is defined as the inverse transformation of the four-magnon composite states. The simultaneous spin deviations on the direct lattice are governed by the nearest neighbor interaction between the spins.

The set of two-magnon states defined in (A.4) has the scalar product $\langle \mathbf{k}, \mathbf{k}' | \boldsymbol{\lambda}, \boldsymbol{\lambda}' \rangle = \hbar^4 \delta_{\boldsymbol{\lambda} + \boldsymbol{\lambda}', \mathbf{k} + \mathbf{k}'} (\delta_{\boldsymbol{\lambda}, \mathbf{k}} + \delta'_{\boldsymbol{\lambda}, \mathbf{k}'} - (2/N))$ and therefore, two distinct state vectors are not orthogonal in general. These two-magnon states are approximately orthonormal with an error of no more than $O(1/N)$.^{54,55,65} The effect of the Hamiltonian \mathcal{H} operating on $|\mathbf{k}, \mathbf{k}'\rangle$ is given by

$$\begin{aligned} \mathcal{H}|\mathbf{k}, \mathbf{k}'\rangle &= [\varepsilon_0 + \hbar\omega(\mathbf{k}) + \hbar\omega(\mathbf{k}')]| \mathbf{k}, \mathbf{k}'\rangle + 2\lambda J \hbar^2 \sum_{i,j;\boldsymbol{\delta}} f_{\mathbf{k}+\mathbf{k}'}^{ij} (1 - \lambda e^{i\mathbf{k}' \cdot \boldsymbol{\delta}}) [ij, ij + \boldsymbol{\delta}] \\ &= [\varepsilon_0 + \hbar\omega(\mathbf{k}) + \hbar\omega(\mathbf{k}')]| \mathbf{k}, \mathbf{k}'\rangle \\ &\quad + \frac{2J\hbar^2}{\mathcal{N}} \sum_{\tilde{\mathbf{k}}, \tilde{\mathbf{k}}'; \boldsymbol{\delta}} \delta_{\mathbf{k}+\mathbf{k}', \tilde{\mathbf{k}}+\tilde{\mathbf{k}}'} e^{i\mathbf{k}' \cdot \boldsymbol{\delta}} (1 - \lambda e^{i\mathbf{k}' \cdot \boldsymbol{\delta}}) |\tilde{\mathbf{k}}, \tilde{\mathbf{k}}'\rangle, \end{aligned} \quad (\text{A.8})$$

where $f_{\mathbf{k}}^{ij} = (e^{-i\mathbf{k} \cdot \mathbf{R}_{ij}} / \mathcal{N})$ as in (A.2). The above equation can be rewritten in a convenient form

$$\mathcal{H}|\mathbf{k}, \mathbf{k}'\rangle = [\varepsilon_0 + \hbar\omega(\mathbf{k}) + \hbar\omega(\mathbf{k}')]| \mathbf{k}, \mathbf{k}'\rangle + \frac{1}{\mathcal{N}} \left[\sum_{\tilde{\mathbf{k}}, \tilde{\mathbf{k}}'} g_{2M}(\mathbf{k}, \mathbf{k}'; \tilde{\mathbf{k}}, \tilde{\mathbf{k}}') |\tilde{\mathbf{k}}, \tilde{\mathbf{k}}'\rangle \right], \quad (\text{A.9})$$

where $g_{2M} = 2J\hbar^2 \sum_{\boldsymbol{\delta}} \delta_{\mathbf{k}+\mathbf{k}', \tilde{\mathbf{k}}+\tilde{\mathbf{k}}'} e^{-i\tilde{\mathbf{k}}' \cdot \boldsymbol{\delta}} (1 - \lambda e^{i\mathbf{k}' \cdot \boldsymbol{\delta}})$ and $\boldsymbol{\delta}$ is a vector connecting a typical lattice site to its nearest neighbors. The last term in Eq. (A.9) represents the deviation of the two-magnon state $|\mathbf{k}, \mathbf{k}'\rangle$ from being an eigenstate of the Hamiltonian \mathcal{H} . The two-magnon energy $\varepsilon_{2M}(\mathbf{k}, \mathbf{k}')$ is defined as $\varepsilon_{2M}(\mathbf{k}, \mathbf{k}') = \langle \mathbf{k}, \mathbf{k}' | \mathcal{H} | \tilde{\mathbf{k}}, \tilde{\mathbf{k}}' \rangle / \langle \mathbf{k}, \mathbf{k}' | \mathbf{k}, \mathbf{k}' \rangle$ and is given by

$$\varepsilon_{2M}(\mathbf{k}, \mathbf{k}') = \varepsilon_0 + \hbar\omega(\mathbf{k}) + \hbar\omega(\mathbf{k}') + \frac{1}{\mathcal{N}} \delta \varepsilon_{2M}(\mathbf{k}, \mathbf{k}'), \quad (\text{A.10})$$

within an error of $O(1/N)$,^{54,55,64} where the quantity $\delta \varepsilon_{2M}(\mathbf{k}, \mathbf{k}')$ is given by

$$\delta \varepsilon_{2M}(\mathbf{k}, \mathbf{k}') = 2J\hbar^2 \sum_{\tilde{\mathbf{k}}, \tilde{\mathbf{k}}'; \boldsymbol{\delta}} \delta_{\mathbf{k}+\mathbf{k}', \tilde{\mathbf{k}}+\tilde{\mathbf{k}}'} e^{-i\tilde{\mathbf{k}}' \cdot \boldsymbol{\delta}} (1 - \lambda e^{i\mathbf{k}' \cdot \boldsymbol{\delta}}) \frac{\langle \mathbf{k}, \mathbf{k}' | \tilde{\mathbf{k}}, \tilde{\mathbf{k}}' \rangle}{\langle \mathbf{k}, \mathbf{k}' | \mathbf{k}, \mathbf{k}' \rangle}. \quad (\text{A.11})$$

The very choice of the form of the two-magnon state [Eq. (A.4)] leads to what are called Dyson's "kinematical" and "dynamical" interactions.⁵²⁻⁵⁵ The term $\delta \varepsilon_{2M}(\mathbf{k}, \mathbf{k}')$ is in general a complex quantity whose real part represents the interaction energy between two one-magnons. The imaginary part is related to the inverse scattering lifetime of a given one-magnon (\mathbf{k}) in the presence of a finite, but low,

density of other excitations.^{54,55,65} Calculation of the complex binary interaction term $\delta\varepsilon_{2M}(\mathbf{k}, \mathbf{k}')$ is not necessary for our present purpose.

A straightforward generalization of (A.9) for the three-magnon states is given by

$$\begin{aligned} \mathcal{H}|\mathbf{k}_1, \mathbf{k}_2, \mathbf{k}_3\rangle &= [\varepsilon_0 + \hbar\omega(\mathbf{k}_1) + \hbar\omega(\mathbf{k}_2) + \hbar\omega(\mathbf{k}_3)]|\mathbf{k}_1, \mathbf{k}_2, \mathbf{k}_3\rangle \\ &+ \frac{1}{\mathcal{N}} \left[\sum_{\tilde{\mathbf{k}}_1, \tilde{\mathbf{k}}_2, \tilde{\mathbf{k}}_3} g_{3M}(\mathbf{k}_1, \mathbf{k}_2, \mathbf{k}_3; \tilde{\mathbf{k}}_1, \tilde{\mathbf{k}}_2, \tilde{\mathbf{k}}_3) |\tilde{\mathbf{k}}_1, \tilde{\mathbf{k}}_2, \tilde{\mathbf{k}}_3\rangle \right]. \end{aligned} \quad (\text{A.12})$$

Energy corresponding to the three-magnon states is given by

$$\varepsilon_{3M}(\mathbf{k}_1, \mathbf{k}_2, \mathbf{k}_3) = \varepsilon_0 + \hbar\omega(\mathbf{k}_1) + \hbar\omega(\mathbf{k}_2) + \hbar\omega(\mathbf{k}_3) + \frac{1}{\mathcal{N}} \delta\varepsilon_{3M}(\mathbf{k}_1, \mathbf{k}_2, \mathbf{k}_3), \quad (\text{A.13})$$

within an error of $O(1/\mathcal{N})$. The term $\delta\varepsilon_{3M}(\mathbf{k}_1, \mathbf{k}_2, \mathbf{k}_3)$ is in general complex and represents three-magnon interactions corresponding to three simultaneous spin deviations on the direct lattice.

The effect of the Hamiltonian \mathcal{H} operating on the four-magnon states [given by (A.7)] is

$$\begin{aligned} \mathcal{H}|\mathbf{k}_1, \mathbf{k}_2, \mathbf{k}_3, \mathbf{k}_4\rangle &= [\varepsilon_0 + \hbar\omega(\mathbf{k}_1) + \hbar\omega(\mathbf{k}_2) + \hbar\omega(\mathbf{k}_3) + \hbar\omega(\mathbf{k}_4)]|\mathbf{k}_1, \mathbf{k}_2, \mathbf{k}_3, \mathbf{k}_4\rangle \\ &+ \frac{1}{\mathcal{N}} \left[\sum_{\tilde{\mathbf{k}}_1, \tilde{\mathbf{k}}_2, \tilde{\mathbf{k}}_3, \tilde{\mathbf{k}}_4} g_{4M}(\mathbf{k}_1, \mathbf{k}_2, \mathbf{k}_3, \mathbf{k}_4; \tilde{\mathbf{k}}_1, \tilde{\mathbf{k}}_2, \tilde{\mathbf{k}}_3, \tilde{\mathbf{k}}_4) |\tilde{\mathbf{k}}_1, \tilde{\mathbf{k}}_2, \tilde{\mathbf{k}}_3, \tilde{\mathbf{k}}_4\rangle \right]. \end{aligned} \quad (\text{A.14})$$

Similarly, the energy corresponding to the four-magnon states are given within an error of $O(1/\mathcal{N})$ as

$$\begin{aligned} \varepsilon_{4M}(\mathbf{k}_1, \mathbf{k}_2, \mathbf{k}_3, \mathbf{k}_4) &= \varepsilon_0 + \hbar\omega(\mathbf{k}_1) + \hbar\omega(\mathbf{k}_2) + \hbar\omega(\mathbf{k}_3) + \hbar\omega(\mathbf{k}_4) + \frac{1}{\mathcal{N}} \delta\varepsilon_{4M}(\mathbf{k}_1, \mathbf{k}_2, \mathbf{k}_3, \mathbf{k}_4). \end{aligned} \quad (\text{A.15})$$

Here, the quantity $\delta\varepsilon_{4M}(\mathbf{k}_1, \mathbf{k}_2, \mathbf{k}_3, \mathbf{k}_4)$ represents four-magnon interactions corresponding to four simultaneous spin deviations on the direct lattice.

Appendix B

Operating the Hamiltonian \mathcal{H} [Eq. (1)] on the quantum state corresponding to charge 1 vortex [as given in Eq. (9)] and using Eqs. (4), (A.3), (A.9), (A.12) and (A.14) we find

$$\mathcal{H}|1V\rangle = (\varepsilon_0 + 2\lambda J\hbar^2)|1V\rangle + |\phi_{\text{resi}}\rangle, \quad (\text{B.1})$$

where the state $|\phi_{\text{resi}}\rangle$ [corresponding to Eqs. (11) as well as (B.1)] is given by

$$\begin{aligned}
 |\phi_{\text{resi}}\rangle = & A \left[\sum_{\mathbf{k}_1, \mathbf{k}_2, \mathbf{k}_3, \mathbf{k}_4} f_{\mathbf{k}_1}^{i,j} f_{\mathbf{k}_2}^{i+1,j} f_{\mathbf{k}_3}^{i+1,j+1} f_{\mathbf{k}_4}^{i,j+1} \right. \\
 & \times \left\{ 2J\hbar^2(3\lambda - \gamma(\mathbf{k}_1) - \gamma(\mathbf{k}_2) - \gamma(\mathbf{k}_3) - \gamma(\mathbf{k}_4))|\mathbf{k}_1, \mathbf{k}_2, \mathbf{k}_3, \mathbf{k}_4\rangle \right. \\
 & \left. \left. + \frac{1}{\mathcal{N}} \sum_{\tilde{\mathbf{k}}_1, \tilde{\mathbf{k}}_2, \tilde{\mathbf{k}}_3, \tilde{\mathbf{k}}_4} g_{4M}(\mathbf{k}_1, \mathbf{k}_2, \mathbf{k}_3, \mathbf{k}_4; \tilde{\mathbf{k}}_1, \tilde{\mathbf{k}}_2, \tilde{\mathbf{k}}_3, \tilde{\mathbf{k}}_4)|\tilde{\mathbf{k}}_1, \tilde{\mathbf{k}}_2, \tilde{\mathbf{k}}_3, \tilde{\mathbf{k}}_4\rangle \right\} \right] \\
 & + \left[\sum_{\mathbf{k}_1, \mathbf{k}_2, \mathbf{k}_3} (B_1 f_{\mathbf{k}_1}^{i,j} f_{\mathbf{k}_2}^{i+1,j} f_{\mathbf{k}_3}^{i+1,j+1} + B_2 f_{\mathbf{k}_1}^{i,j+1} f_{\mathbf{k}_2}^{i+1,j} f_{\mathbf{k}_3}^{i+1,j+1} \right. \\
 & \left. + B_3 f_{\mathbf{k}_1}^{i,j} f_{\mathbf{k}_2}^{i,j+1} f_{\mathbf{k}_3}^{i+1,j+1} + B_4 f_{\mathbf{k}_1}^{i,j} f_{\mathbf{k}_2}^{i,j+1} f_{\mathbf{k}_3}^{i+1,j}) \right. \\
 & \times \left\{ 2J\hbar^2(2\lambda - \gamma(\mathbf{k}_1) - \gamma(\mathbf{k}_2) - \gamma(\mathbf{k}_3))|\mathbf{k}_1, \mathbf{k}_2, \mathbf{k}_3\rangle \right. \\
 & \left. \left. + \frac{1}{\mathcal{N}} \sum_{\tilde{\mathbf{k}}_1, \tilde{\mathbf{k}}_2, \tilde{\mathbf{k}}_3} g_{3M}(\mathbf{k}_1, \mathbf{k}_2, \mathbf{k}_3; \tilde{\mathbf{k}}_1, \tilde{\mathbf{k}}_2, \tilde{\mathbf{k}}_3)|\tilde{\mathbf{k}}_1, \tilde{\mathbf{k}}_2, \tilde{\mathbf{k}}_3\rangle \right\} \right] \\
 & + \left[\sum_{\mathbf{k}_1, \mathbf{k}_2} (C_1 f_{\mathbf{k}_1}^{i,j} f_{\mathbf{k}_2}^{i+1,j} + C_2 f_{\mathbf{k}_2}^{i,j+1} f_{\mathbf{k}_3}^{i+1,j+1} + C_3 f_{\mathbf{k}_3}^{i+1,j+1} f_{\mathbf{k}_4}^{i,j+1} \right. \\
 & \left. + C_4 f_{\mathbf{k}_1}^{i,j} f_{\mathbf{k}_4}^{i,1+j} + C_5 f_{\mathbf{k}_2}^{i+1,j} f_{\mathbf{k}_4}^{i,j+1} + C_6 f_{\mathbf{k}_1}^{i,j} f_{\mathbf{k}_3}^{i+1,j+1}) \right. \\
 & \times \left\{ 2J\hbar^2(\lambda - \gamma(\mathbf{k}_1) - \gamma(\mathbf{k}_2))|\mathbf{k}_1, \mathbf{k}_2\rangle \right. \\
 & \left. \left. + \frac{1}{\mathcal{N}} \sum_{\tilde{\mathbf{k}}_1, \tilde{\mathbf{k}}_2} g_{2M}(\mathbf{k}_1, \mathbf{k}_2; \tilde{\mathbf{k}}_1, \tilde{\mathbf{k}}_2)|\tilde{\mathbf{k}}_1, \tilde{\mathbf{k}}_2\rangle \right\} \right] \\
 & + \left[\sum_{\mathbf{k}_1} (D_1 f_{\mathbf{k}_1}^{i,j} + D_2 f_{\mathbf{k}_1}^{i+1,j} + D_3 f_{\mathbf{k}_1}^{i+1,j+1} + D_4 f_{\mathbf{k}_1}^{i,j+1})[-\gamma(\mathbf{k}_1)]|\mathbf{k}_1\rangle \right] \\
 & + (-E)2\lambda J\hbar^2|0\rangle. \tag{B.2}
 \end{aligned}$$

The significance of the above residual state $|\phi_{\text{resi}}\rangle$ has been explained in Sec. 2.1. In Eq. (B.1), the first term on the right-hand side corresponds to nonlinear superposition of four-magnon composites where the term $g_{4M}(\mathbf{k}_1, \mathbf{k}_2, \mathbf{k}_3, \mathbf{k}_4; \tilde{\mathbf{k}}_1, \tilde{\mathbf{k}}_2, \tilde{\mathbf{k}}_3, \tilde{\mathbf{k}}_4)$, being in general a complex function, represents the interactions between the four-

magnon modes. Similarly, the second and third terms correspond to the nonlinear superposition of three-magnon and two-magnon composites, respectively. The terms $g_{3M}(\mathbf{k}_1, \mathbf{k}_2, \mathbf{k}_3; \tilde{\mathbf{k}}_1, \tilde{\mathbf{k}}_2, \tilde{\mathbf{k}}_3)$ and $g_{2M}(\mathbf{k}_1, \mathbf{k}_2; \tilde{\mathbf{k}}_1, \tilde{\mathbf{k}}_2)$ represent the interactions between three-magnon modes (identified by the subscript “3M”) and two-magnon modes (identified by the subscript “2M”), respectively which are in general complex functions. The exact expression for $g_{2M}(\mathbf{k}_1, \mathbf{k}_2; \tilde{\mathbf{k}}_1, \tilde{\mathbf{k}}_2)$ has been given in Appendix A [see Eq. (A.9)]. The fourth term in the Eq. (B.1) represents the contribution from the linear superposition of all the one-magnon modes to the residual state $|\phi_{\text{resi}}\rangle$ and the last term gives the ground state contribution. Hence, altogether the residual states $|\phi_{\text{resi}}\rangle$ and $|\psi_{\text{resi}}\rangle \equiv |\phi_{\text{resi}}\rangle - \lambda J \hbar^2 |1V\rangle$ [see Eq. (13)] are arising from the inter-multi-magnonic correlations as stated in Sec. 2.1. The quantum state $|\psi_{\text{resi}}^i\rangle$ corresponding to Eq. (22) is obtained by replacing \mathcal{N} by 16 in the above equation and then using the relation $|\psi_{\text{resi}}^i\rangle \equiv |\phi_{\text{resi}}^i\rangle - \lambda J \hbar^2 |C_i\rangle$ (see Sec. 2.2).

References

1. J. K. Kjemsand and M. Steiner, *Phys. Rev. Lett.* **41**, 1137 (1978).
2. I. U. Heilmann *et al.*, *Phys. Rev. B* **24**, 3939 (1981).
3. G. Reiter, *Phys. Rev. Lett.* **46**, 202 (1981).
4. H. Bethe, *Z. Phys.* **71**, 205 (1931).
5. Y. Endoh *et al.*, *Phys. Rev. Lett.* **32**, 170 (1974).
6. F. D. M. Haldane, *Phys. Rev. Lett.* **50**, 1153 (1983).
7. A. A. Katanin and V. Y. Irkhin, *Phys.-Usp.* **50**, 613 (2007).
8. K. Hirakawa, H. Yoshizawa and K. Ubukoshi, *J. Phys. Soc. Jpn.* **51**, 2151 (1982).
9. K. Hirakawa *et al.*, *J. Phys. Soc. Jpn, Part. 2* **52**, 4220 (1983).
10. Y. Endoh *et al.*, *Phys. Rev. B* **37**, 7443 (1988).
11. K. Yamada *et al.*, *Phys. Rev. B* **40**, 4557 (1989).
12. J. V. Jose (ed.), *40 Years of Berezinskii-Kosterlitz-Thouless Theory*, Chapter 1 (World Scientific, Singapore, 2013).
13. L. Berger *et al.*, *Phys. Rev. B* **77**, 104431, (2008).
14. A. Wachowiak *et al.*, *Science* **298**, 577 (2002).
15. R. P. Cowburn *et al.*, *Phys. Rev. Lett.* **83**, 1042 (1999).
16. B. Van Waeyenberge *et al.*, *Nature* **444**, 461 (2006).
17. H. Hauser *et al.*, *J. Magn. Magn. Mater.* **215**, 788 (2000).
18. J. McCord and J. Westwood, *IEEE Trans. Magn.* **37**, 1755 (2005).
19. J. M. Kosterlitz and D. J. Thouless, *J. Phys. C* **6**, 1181 (1973).
20. V. L. Berezinskii, *Sov. Phys. J. Exp. Theor. Phys.* **32**, 493 (1970); *Sov. Phys. J. Exp. Theor. Phys.* **34**, 610 (1972).
21. D. L. Huber, *Phys. Lett. A* **68**, 125 (1978); *Phys. Rev. B* **26**, 3758 (1982).
22. F. G. Mertens *et al.*, *Phys. Rev. Lett.* **59**, 117 (1987); *Phys. Rev. B* **39**, 591 (1989).
23. M. E. Gouvêa *et al.*, *Phys. Rev. B* **39**, 11840 (1989).
24. A. R. Völkel *et al.*, *Phys. Rev. B* **44**, 10066 (1991).
25. A. Luther and D. J. Scalapino, *Phys. Rev. B* **16**, 1153 (1977).
26. J. V. José *et al.*, *Phys. Rev. B* **16**, 1217 (1977).
27. P. W. Anderson *et al.*, Fermions and topology in the two dimensional quantum anti-ferromagnet, Princeton University Preprint, 1988.
28. A. R. Pereira and A. S. T. Pires, *Phys. Rev. B* **51**, 996 (1995).
29. P. Steffens *et al.*, *Phys. Rev. B* **83**, 054429 (2011).

30. L. Capogna *et al.*, *Phys. Rev. B* **67**, 012504 (2003).
31. J. E. Lorenzo *et al.*, *Europhys. Lett.* **45**, 45 (1999).
32. M. Heinrich *et al.*, *Phys. Rev. Lett.* **91**, 137601 (2003).
33. P. Gaveau, *J. Appl. Phys.* **69**, 6228 (1991).
34. D. G. Wiesler *et al.*, *Physica B* **136**, 22 (1986).
35. S. Sarkar, S. K. Paul and R. Chaudhury, *Eur. Phys. J. B* **85**, 380 (2012).
36. D. D. Betts, F. C. Salevsky and J. Rogiers, *J. Phys. A: Math. Gen.* **14**, 531 (1981).
37. E. Loh Jr., D. J. Scalapino and P. M. Grant, *Phys. Rev. B: Rapid. Commun.* **31**, 4712 (1985).
38. K. Harada and N. Kawashima, *J. Phys. Soc. Jpn.* **67**, 2768 (1998).
39. R. Chaudhury and S. K. Paul, *Eur. Phys. J. B* **76**, 391 (2010).
40. R. Chaudhury and S. K. Paul, *Adv. Condens. Matter Phys.* **2013**, 783420 (2013).
41. B. V. Costa and A. B. Lima, *J. Magn. Magn. Mater.* **324**, 1999 (2012).
42. B. A. Ivanov *et al.*, *Phys. Rev. B* **58**, 8464 (1998).
43. G. M. Wysin and A. R. Vökel, *Phys. Rev. B* **52**, 7412 (1995).
44. B. V. Costa, M. E. Gouvea and A. S. T. Pires, *Phys. Lett. A* **165**, 179 (1992).
45. R. Chaudhury and B. S. Shastry, *Phys. Rev. B* **37**, 5216 (1988).
46. P. Böni and G. Shirane, *Phys. Rev. B* **33**, 3012 (1986).
47. M. T. Evans and C. G. Windsor, *J. Phys. C* **6**, 495 (1973).
48. H. A. Mook, *Phys. Rev. Lett.* **46**, 508 (1981).
49. J. E. R. Costa and B. V. Costa, *Phys. Rev. B* **54**, 994 (1996).
50. J. E. R. Costa, B. V. Costa and D. P. Landau, *J. Appl. Phys.* **81**, 5746 (1997).
51. S. Hikami and T. Tsuneto, *Prog. Theor. Phys.* **63**, 387 (1980).
52. R. G. Boyd and J. Callaway, *Phys. Rev.* **138**, A1621 (1965).
53. F. J. Dyson, *Phys. Rev.* **102**, 1217 (1956).
54. D. C. Mattis, *Theory of Magnetism Made Simple*, Chapter 5 (World Scientific, Singapore, 2006), p. 176.
55. S. W. Lovesey, *Theory of Neutron Scattering from Condensed Matter*, Vol. 2, Chapter 9 (Oxford University Press, New York, 1984), p. 57.
56. K. Yoshida, *Theory of Magnetism*, Chapter 8 (Springer-Verlag, Berlin, 1996), p. 107.
57. C. Kittel, *Introduction to Solid State Physics*, 7th edn., Chapter 15 (John Wiley & Sons (Asia) Pte. Ltd., Singapore, 1995), p. 443.
58. E. L. Nagaev, *Physics of Magnetic Semiconductors*, Chapter 2 (Mir Publishers, Moscow, 1983), p. 60.
59. N. D. Mermin and H. Wagner, *Phys. Rev. Lett.* **17**, 1133 (1966); Erratum *Phys. Rev. Lett.* **17**, 1307 (1966).
60. R. Chaudhury and S. K. Paul, *Phys. Rev. B* **60**, 6234 (1999).
61. R. Chaudhury, F. Demmel and T. Chatterji, arXiv:1104.4197v1.
62. R. Chaudhury, *J. Magn. Magn. Mater.* **307**, 99 (2006).
63. T. Chatterji, F. Demmel and R. Chaudhury, *Physica B* **385–386**, 428 (2006).
64. S. Sarkar, R. Chaudhury and S. K. Paul, under preparation (2015).
65. E. Rastelli, *Statistical Mechanics of Magnetic Excitations: From Spin Waves to Stripes and Checkerboards*, Chapter 1 (World Scientific, Singapore, 2013), p. 12.
66. S. K. Mukhopadhyay and C. K. Majumdar, *J. Math. Phys.* **17**, 478 (1976).
67. C. K. Majumdar and I. Bose, *J. Math. Phys.* **19**, 2187 (1978).
68. D. C. Mattis and S. Rudin, *Phys. Rev. Lett.* **52**, 755 (1984).

Erratum:

**The connection between vortex-like topological excitations and
conventional excitations in quantum ferromagnetic
spin systems on two-dimensional lattice and their stability**

[Int. J. Mod. Phys. B, Vol. 29, 1550209 (2015) (22 pages)]

Subhajit Sarkar*, Ranjan Chaudhury† and Samir K. Paul‡

*S. N. Bose National Centre for Basic Sciences,
Block-JD, Sector-III, Salt Lake, Kolkata 700098, India*

* *subhajit@bose.res.in*

† *ranjan@bose.res.in*

‡ *smr@bose.res.in*

Published 24 November 2015

In page 5 equation (4) viz., $\varepsilon_0 = -(N/2)\lambda J\hbar^2$ should be read as $\varepsilon_0 = -(\mathcal{N}/2)\lambda J\hbar^2$.
In page 11 in the equations (18) and (19) the symbol N should be read as \mathcal{N} .

Semi-phenomenological analysis of neutron scattering results for quasi-two dimensional quantum anti-ferromagnet

Subhajit Sarkar,^{1,*} Ranjan Chaudhury,^{1,†} and Samir K. Paul^{1,‡}

¹*S. N. Bose National Centre For Basic Sciences,
Block - JD, Sector - III, Salt Lake, Kolkata - 700098, India*
(Dated: June 15, 2016)

The available results from the inelastic neutron scattering experiment performed on the quasi-two dimensional spin $\frac{1}{2}$ anti-ferromagnetic material La_2CuO_4 have been analysed theoretically. The formalism of ours is based on a semi-classical like treatment involving a model of an ideal gas of mobile vortices and anti-vortices built on the background of the Néel state, using the bipartite classical spin configuration corresponding to an XY- anisotropic Heisenberg anti-ferromagnet on a square lattice. The results for the integrated intensities for our spin $\frac{1}{2}$ model corresponding to different temperatures, show occurrence of vigorous unphysical oscillations, when convoluted with a realistic spectral window function. These results indicate failure of the conventional semi-classical theoretical model of ideal vortex/anti-vortex gas arising in the Berezinskii-Kosterlitz-Thouless theory for the low spin magnetic systems. A full fledged quantum mechanical formalism and calculations seem crucial for the understanding of topological excitations in such low spin systems. Furthermore, a severe disagreement is found to occur at finite values of energy transfer between the integrated intensities obtained theoretically from the conventional formalism and those obtained experimentally. This further suggests strongly that the full quantum treatment should also incorporate the interaction between the fragile-magnons and the topological excitations. This is quite plausible in view of the recent work establishing such a process in XXZ quantum ferromagnet on 2D lattice. The high spin XXZ quasi-two dimensional antiferromagnet like $MnPS_3$ however follows the conventional theory quite well.

Keywords: Spin dynamics, Topological spin excitations, Berezinskii-Kosterlitz-Thouless transition, Spin 1/2 easy plane Anti-ferromagnet.

Highlights:

- Inadequacies in the conventional meron gas phenomenology in explaining the spin dynamics corresponding to layered low-spin anti-ferromagnets.
- Requirement of a full fledged quantum mechanical formalism for the understanding of spin dynamics induced by both topological and conventional excitations.
- Necessity of a proper understanding of the interaction between the conventional and topological excitations at the quantum level.

I. INTRODUCTION

Spin dynamics in low dimensional magnetic systems have generated a significant research interest during the last three decades[1–31]. Different types of one and quasi-one dimensional as well as two and quasi-two dimensional systems have been studied both experimentally and theoretically to probe and understand the spin dynamics arising from the conventional spin wave excitations and their mutual interactions, as well as from vortex/meron and soliton like topological excitations [15–17, 19, 20, 27]. In many of these systems the topological excitations of soliton and vortex/meron type occur naturally as they are thermodynamically feasible.

Motivated by the distinct possibilities of applications towards building of magnetic devices, the quasi-two dimensional systems have attracted a renewed research

interest in recent times. Magnetic vortices present in these systems, have proved to be potential candidates for switching devices [32–35]. Direct experimental evidences of such vortices have been verified by both the Magnetic Force Microscopy (MFM) and the spin-polarized Scanning Tunnelling Microscopy (STM) [36, 37].

The spin dynamics in many of the above magnetic systems has been investigated experimentally using the Inelastic Neutron Scattering (INS) and the Nuclear Magnetic Resonance (NMR) techniques. These include quasi-one dimensional systems such as $CsNiF_3$, layered systems such as K_2CuF_4 , Rb_2CrCl_4 , $LiCrO_2$, magnetically intercalated graphites, layered ruthenates, layered manganites and the high- T_C cuprates [16–18, 20–29, 31]. In the INS experiments performed on several of above materials, the existence of a prominent “central peak” (at $\hbar\omega = 0$) has been confirmed in the plot for the dynamical structure function $S(\mathbf{q}, \omega)$ vs. neutron energy transfer ‘ $\hbar\omega$ ’ in the constant ‘ \mathbf{q} ’ scan [21, 22]. These findings further serve as the motivation behind the huge variety of experiments performed on the layered magnetic systems. Moreover, the advancement of numerical and computa-

* subhajit@bose.res.in

† ranjan@bose.res.in

‡ smr@bose.res.in

tional techniques also contributed to the understanding of the possible role of both the spin waves and the topological excitations in emergence of the central peak.

Kosterlitz and Thouless, and Berezinskii independently introduced the concept of vortex and anti-vortex like topological spin excitations in the two dimensional classical magnetic (spin) systems [38–40]. According to their ideas, there exists a non-conventional topological phase transition (known as Berezinskii-Kosterlitz-Thouless or BKT transition) characterized by the crossover between binding to unbinding phases of vortex-anti-vortex pairs at a transition temperature T_{BKT} . Below this temperature all the vortices and anti-vortices are in a bound state and above this temperature some of them start moving freely. Further analytical and numerical studies and suitable extension of these approaches led to the proposal for the existence of topological vortices and anti-vortices in pure XY model and merons and anti-merons in XY-anisotropic Heisenberg model, for both ferromagnetic and anti-ferromagnetic types, on two-dimensional lattices [41–46]. Furthermore, approximate analytical calculations and Monte Carlo-Molecular Dynamics (MCMD) simulations have strongly suggested that the freely moving topological excitations in the regime $T > T_{BKT}$, contribute non-trivially to the spin-spin correlation and give rise to the “central peak”, as mentioned above [41–44]. The occurrence of such a “central peak” in quasi-two dimensional magnetic systems is now unanimously believed to be the signature for the dynamics of mobile topological excitations in a layer.

In spite of a lot of studies on the anisotropic Heisenberg model on two dimensional lattices the contributions of vortices/anti-vortices to the dynamics of the model, especially the detailed quantitative features of the DSFs are still not completely understood.

In the context of two-dimensional magnetism, the undoped (anti-ferromagnetic and non-superconducting) phases of the high T_c cuprate systems are believed to be excellent examples of two dimensional XY anisotropic Heisenberg Hamiltonian in an appropriate temperature regime. One member of this class of systems is La_2CuO_4 , on which extensive INS experiments have been performed [30, 31]. This is a truly spin-1/2 layered anti-ferromagnet. The intra-layer integrated intensity corresponding to the results of INS experiment performed on La_2CuO_4 , exhibits a central peak when plotted against the neutron energy transfer $\hbar\omega$ (or frequency ‘ ω ’).

It has been shown that the results of vortex gas phenomenology and numerical simulations lead to an anomaly in the case of layered anti-ferromagnetic systems having very low spin values ($S=1/2$) [47]. Strikingly enough, the value of T_{BKT} obtained from Renormalization group analysis and numerical simulations is four (4) times the value of T_{BKT} calculated from the classical expression obtained by Kosterlitz and Thouless [47]. Furthermore, in our previous work we have already established that for quasi-two dimensional ferromagnetic systems having low spin values ($S=1/2$) the conventional

semi-classical like treatment involving the ideal gas of unbound vortices/merons and anti-vortices/anti-merons corresponding to high temperature regime $T > T_{BKT}$, shows large inconsistency with the experimental situation and exhibits unphysical behaviour [48]. In this case the theoretical dynamical structure function (DSF) turns out to be negative for a wide range of energy transfers! However the range, over which the theoretical DSF remains positive, increases when the value of the spin is increased [48]. These facts motivate us to investigate and test in detail the applicability of the semi-classical-like treatment mentioned above to the INS results corresponding to real anti-ferromagnetic systems with $S=1/2$. For this exercise we select La_2CuO_4 as the reference system [30, 31].

It is worthwhile to mention that the BKT transition can also be identified at the transition temperature T_{BKT} where the spin-stiffness jumps discontinuously from a universal value below T_{BKT} to zero above T_{BKT} [49]. Moreover, in anti-ferromagnetic model possessing Ising like anisotropy (in the z-direction) on two dimensional lattices, with external field being applied in the z-direction, such a discontinuous jump has been observed [50]. However, the discontinuous jump in this case may have its origin different from the vortex-anti-vortex unbinding mechanism since it is well known that the BKT transition in magnetic systems can only occur when the anisotropy is XY like [41–44].

The plan of the paper is as follows:- in section II we describe the formulation of our semi-classical like treatment; in section III we discuss our calculations and results and finally in section IV the conclusions and discussions of our present investigation are presented.

II. MATHEMATICAL FORMULATION

The dynamics of mobile topological excitations in an anti-ferromagnetic system on a two-dimensional square lattice have been analysed both analytically and numerically [41–45]. The analytical studies have been performed by assuming a classical ideal gas of vortices/merons where the vortices/merons obey Maxwell’s velocity distribution. The model system is described the XY-anisotropic Heisenberg (XXZ) Hamiltonian, viz.,

$$\mathcal{H} = -J \sum_{\langle ij,pq \rangle} (S_{ij}^x S_{pq}^x + S_{ij}^y S_{pq}^y + \lambda S_{ij}^z S_{pq}^z), \quad (1)$$

where $\langle ij,pq \rangle$ label the nearest neighbour sites on a two-dimensional square lattice and $J(< 0)$ is the anti-ferromagnetic exchange coupling. Here λ is the anisotropy parameter whose pure XY and isotropic Heisenberg limit correspond to $\lambda = 0$ and 1 respectively.

The structures of the vortices/merons have been obtained by solving the classical equations of motion corresponding to the Hamiltonian given by eqn. (1). In deriving the classical equations of motion the spins have been considered to be classical objects (classical spin fields)

$S(\mathbf{r}, t)$ as a function of position coordinates and time, which are defined on the entire lattice. At even or odd

lattice sites these spin fields become identical to the following bi-partite spin configurations:

$$\begin{aligned} S_{ij}^{even} &= +S[\sin(\Theta_{ij} + \theta_{ij}) \cos(\Phi_{ij} + \phi_{ij}), \sin(\Theta_{ij} + \theta_{ij}) \sin(\Phi_{ij} + \phi_{ij}), \cos(\Theta_{ij} + \theta_{ij})], \\ S_{ij}^{odd} &= -S[\sin(\Theta_{ij} - \theta_{ij}) \cos(\Phi_{ij} - \phi_{ij}), \sin(\Theta_{ij} - \theta_{ij}) \sin(\Phi_{ij} - \phi_{ij}), \cos(\Theta_{ij} - \theta_{ij})], \end{aligned} \quad (2)$$

where ‘even’ and ‘odd’ signifies the two different sublattices [51]. The static spin configuration corresponding to the merons are described by the capital angles $\Theta(\mathbf{r})$ (polar) and $\Phi(\mathbf{r})$ (azimuthal), and the time dependent small angles $\theta(\mathbf{r}, t)$ and $\phi(\mathbf{r}, t)$ describes the corresponding deviations from the static structure due to the motion of the merons and the spin dynamics above BKT transition temperature [44, 45]. The expression of the vortex core radius is given by [44, 45]

$$r_v = \frac{a}{2} \sqrt{\frac{\lambda}{1-\lambda}}. \quad (3)$$

From the above considerations the in-plane dynamical structure function (in-plane DSF) $S^{xx}(\mathbf{q}, \omega)$ is given by,

$$S^{xx}(\mathbf{q}, \omega) = \frac{S(S+1)}{2\pi} \frac{\gamma^3 \xi^2}{(\omega^2 + \gamma^2 [1 + (\xi \mathbf{q}^*)^2])^2}, \quad (4)$$

with $\gamma = \frac{\sqrt{\pi \bar{u}}}{2\xi}$, where $\mathbf{q}^* = (\mathbf{q}_0 - \mathbf{q})$; $\mathbf{q}_0 = (\pi/a, \pi/a)$ and in our case $S = \frac{1}{2}$. The above expression for the in-plane dynamical structure function is a squared Lorentzian exhibiting a central peak at $\omega = 0$ in ‘ ω ’-space for constant \mathbf{q} -scan and exhibiting a central peak at the zone boundary of the first Brillouin Zone (BZ) in the ‘ q ’ space for constant ω -scan [44, 45]. In the above expression \bar{u} is the root mean square (rms) velocity of the vortices and is given by,

$$\bar{u} = \sqrt{b\pi} \frac{JS(S+1)a^2}{\hbar} (\sqrt{n_v^f}) \tau^{-1/4}, \quad (5)$$

where $n_v^f \sim (2\xi)^{-2}$ is the density of free vortices at $T > T_{BKT}$ [41]. Here $\xi = \xi_0 e^{b/\sqrt{\tau}}$ is the intra-layer two-spin correlation length due to the presence of vortices, where ξ_0 is of the order of lattice spacing ‘ a ’; $\tau = (\frac{T}{T_{BKT}} - 1)$ is the reduced temperature and b is a dimensionless parameter whose numerical value is generally around 1.5 [22, 47]. The quantity $S^{xx}(\mathbf{q}, \omega)$ is sensitive to the in-plane structure of the vortices/merons [44, 45].

Again the effective analytical expression for the out-of-plane dynamical structure function (out-of-plane DSF) $S^{zz}(\mathbf{q}, \omega)$ in the limit of very small ‘ q ’ is given by [44, 45]

$$S^{zz}(\mathbf{q}, \omega) = \frac{n_v^f \bar{u}}{32(1+\lambda)^2 J^2 \sqrt{\pi} q^3} \exp[-(\frac{\omega}{\bar{u}q})^2]. \quad (6)$$

The above form of the out-of-plane dynamical structure function is a Gaussian, exhibiting again a central peak

at $\omega = 0$, when plotted in the constant \mathbf{q} -scan. The function $S^{zz}(\mathbf{q}, \omega)$ is sensitive to the out-of-plane shape of the vortices/merons [44, 45].

In the case of layered systems, in a suitable regime in the parameter space comprising of temperature and wave vector where these systems behave effectively as two-dimensional systems, the integrated intensity corresponding to a typical inelastic neutron scattering experiment is given by

$$I(\omega) = \int \sum_{\alpha} S^{\alpha\alpha}(\mathbf{q}_{2D}, \omega) dq_x dq_y, \quad (7)$$

where the quantity $S^{\alpha\alpha}(\mathbf{q}_{2D}, \omega)$ represents the intra-layer in-plane spin dynamical structure function when $\alpha = x$ and y and the intra-layer out-of-plane spin dynamical structure function when $\alpha = z$ [15, 52, 53].

The approach in our present work is quite similar to that adopted earlier in the case of ferromagnetic systems [48]. In order to compare theory with experiment the dynamical structure function, obtained from the model under consideration, is multiplied with the resolution function $R(t)$ (in time domain) or convoluted with $\tilde{R}(\omega - \omega')$ (in the frequency domain), as has been done in the case of ferromagnetic system [48, 52, 54]. Hence, the components of the convoluted integrated intensity comes out to be,

$$I_{conv}^{\alpha\alpha}(\omega) = \int dq_x dq_y \int d\omega' \tilde{R}(\omega - \omega') S^{\alpha\alpha}(\mathbf{q}_{2D}, \omega'). \quad (8)$$

The resolution function has to be chosen in such a way that minimum ripples occur at the end points of the resolution width. The different parameters of the resolution function can be obtained from the resolution half width or the full width at the half maximum (FWHM) which are quoted in the experiments. Since X and Y components of the spins are symmetric i.e., $S^{xx}(\mathbf{q}, \omega) = S^{yy}(\mathbf{q}, \omega)$ the total intensity comes out to be,

$$I(\omega) = 2I^{xx}(\omega) + I^{zz}(\omega). \quad (9)$$

Furthermore, keeping in mind the low spin situation the quantum mechanical detailed balance condition is incorporated in our formalism [55]. Then semi-classical estimate for $I(\omega)$, denoted by $I_{SC}(\omega)$ is recovered by the relation,

$$I^{SC}(\omega) = \frac{2}{1 + \exp(\frac{-\hbar\omega}{k_B T})} I(\omega), \quad (10)$$

where the factor $\frac{2}{1+\exp(\frac{-\hbar\omega}{k_B T})}$ is the detailed balance factor and is called the Windsor factor [56, 57]. The superscript ‘SC’ stands for the term semi-classical.

As has been pointed out in the case of ferromagnetic systems, this approach of ours is truly ‘semi-classical-like’ in the sense that the expression for the rms vortex velocity ‘ \bar{u} ’, as given in eqn. (4), contains ‘ \hbar ’ and in addition the quantum mechanical detailed balance condition has been incorporated through the Windsor factor[48].

It is worthwhile to mention that the above formulation based on dilute vortex/meron gas phenomenology hold for unbound anti-vortices/anti-merons too on the basis of the assumption that the vortices/merons and anti-vortices/anti-merons do not interact with each other.

III. CALCULATIONS AND RESULTS

In this work the formalism of Section II is applied to an anti-ferromagnetic material La_2CuO_4 on which inelastic neutron scattering experiments (INS) involving polarized neutron beam have been performed [30, 31]. The material is an XY-anisotropic quasi-two-dimensional spin 1/2 quantum Heisenberg anti-ferromagnet. The magnetic lattice structure of it is composed of stacking of two-dimensional square lattices [30, 31]. The spin Hamiltonian relevant to the above material is given by,

$$\mathcal{H} = \underbrace{(-J \sum_{\langle i,j \rangle} \mathbf{S}_i \cdot \mathbf{S}_j + J_A \sum_{\langle i,j \rangle} S_i^z S_j^z)}_{\text{intra-layer part}} - \underbrace{J' \sum_{\langle i,k \rangle} \mathbf{S}_i \cdot \mathbf{S}_k}_{\text{inter-layer part}} \quad (11)$$

where $\langle i, j \rangle$ represents the intra-layer nearest neighbour interaction and $\langle i, k \rangle$ represents the inter-layer nearest neighbour interaction. In the above Hamiltonian, J is the isotropic part and J_A is anisotropic part of the intra-layer exchange coupling and, J' is the inter-layer exchange coupling. The ordering temperature i.e., the Néel temperature for the quasi-two dimensional system (La_2CuO_4) is given by $T_N = 240$ K. The intra-layer part of the above Hamiltonian (11) can be simplified, by expressing $(J - J_A)$ as λJ , to obtain the model Hamiltonian (1), where λ is the anisotropy parameter. The relevant physical parameters corresponding to La_2CuO_4 are given in the TABLE I [58].

Parameter	Magnitude
J (intra-layer)	~ 1345 K
J_A (intra-layer)	~ 0.269 K
J' (inter-layer)	~ 0.04 K
anisotropy parameter (λ)	0.9998
lattice parameter(a)	5.39 Å
Néel temperature (T_N)	240 K

TABLE I. Relevant parameters for La_2CuO_4

Next we try to determine the temperature range over which the material La_2CuO_4 behaves effectively as a two-dimensional material. From the neutron scattering data for quasi-two-dimensional spin 1/2 XY-anisotropic ferromagnet K_2CuF_4 , it was found that in a temperature regime $T_1 \leq T \leq T_2$, where the lower (T_1) and the upper (T_2) limits are defined by the following relations,

$$\xi(T_1) = \sqrt{\frac{|J|}{|J'|}} \quad (12)$$

$$\xi(T_2) = \sqrt{\frac{|J|}{|J_A|}}$$

the system behaves as a 2D XY-like anisotropic system [21, 22]. Assuming that the above phenomenological argument holds for the layered anti-ferromagnetic systems

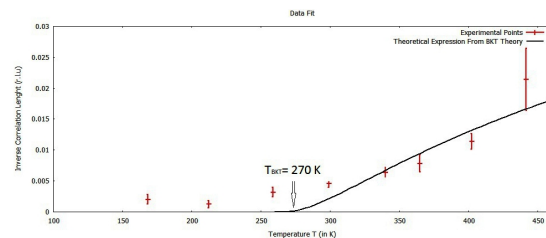


FIG. 1. Fitting of the experimentally obtained inverse correlation length with the corresponding theoretical expression (see eqn. (13)). Solid line corresponds to the theoretical expression. BKT transition temperature is $T_{BKT} = 270$ K.

as well, we determine the above two temperature limits as $T_1 \approx 260$ K and $T_2 \approx 360$ K for La_2CuO_4 . Within this temperature regime the Hamiltonian (11) can effectively be represented by the Hamiltonian (1). It is worthwhile to point out that since in the above temperature regime the system is effectively a two-dimensional one, long range anti-ferromagnetic ordering is absent in this regime [59]. Further, within the above mentioned temperature range the BKT inspired ideal vortex/meron-gas phenomenology is valid and we can therefore use the theoretical expression for the inverse correlation length (expressed in r.l.u.),

$$\kappa(T) = \frac{1}{\pi} e^{-b/\sqrt{T}} \quad (13)$$

as predicted by Kosterlitz and Thouless, to fit the experimentally obtained inverse correlation length [38]. This gives the value of the BKT transition temperature as $T_{BKT} \approx 270$ K for La_2CuO_4 (see FIG. 1). In this work we shall make use of the above value of T_{BKT} to calculate the convoluted in-plane integrated intensity, $I_{conv}^{xx}(\omega)$ and the convoluted out-of-plane integrated intensity $I_{conv}^{zz}(\omega)$, by making use of eqns. (4) to (6), and then eqns. (7) and (8).

We now study the convoluted in-plane integrated intensities $I_{conv}^{xx}(\omega)$ at different temperatures. The expression for the $I_{conv}^{xx}(\omega)$ is given by eqn. (8) with $\alpha = x$, where the in-plane DSF, $S^{xx}(\mathbf{q}_2\mathbf{D}, \omega)$ is given by eqn. (4). In the experimental investigations on La_2CuO_4 , to find the neutron intensity as a function of momentum transfer ' $\hbar\mathbf{q}$ ' the scans in the ' \mathbf{q} '-space have been performed about the zone boundary of the first BZ within the range, $-0.1 \leq \mathbf{q}^* \leq 0.1$, expressed in r.l.u [30, 31]. In calculating $I_{conv}^{xx}(\omega)$ using eqn. (13) we have also made use of the above mentioned regime only. The resolution function has been chosen in the form of the Tukey window to convolute the in-plane DSF. This is one of the most commonly used spectral smoothing functions in the field of spectral analysis [60, 61]. The experimental resolution width is 1.4 meV at the full width at half maximum (FWHM) as specified in the experiment [30, 31]. We compute $I_{conv}^{xx}(\omega)$ for four different temperatures, viz., 290 K, 320 K, 350 K and 375 K. The

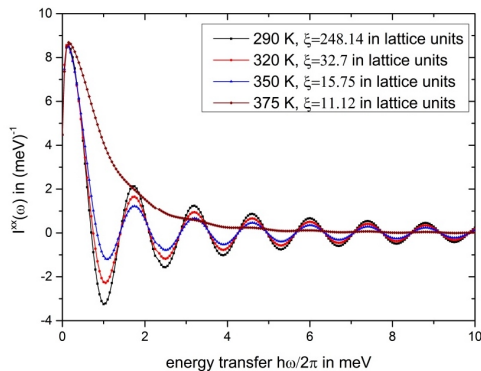


FIG. 2. The plot of convoluted (with Tukey window function) in-plane integrated intensity $I_{conv}^{xx}(\omega)|_{SC}$ at four different temperatures, viz., 290 K, 320 K, 350 K and 375 K. The rms velocities at these temperatures are $\bar{u} = 0.00365 \frac{a}{t_{nat}}$, $0.0836 \frac{a}{t_{nat}}$, $0.085 \frac{a}{t_{nat}}$, $0.2323 \frac{a}{t_{nat}}$ respectively.

semi-classical convoluted in-plane integrated intensities denoted by, $I_{conv}^{xx}(\omega)|_{SC}$ are plotted as functions of energy transfers in FIG. 2, where eqns. (9) and (10) have been used. The figures clearly exhibit that $I_{conv}^{xx}(\omega)|_{SC}$ oscillates vigorously after convoluting with the Tukey function, although the 'central peak' still persists. This is quite contrary to what we experienced in the case of ferromagnet [48].

To avoid such oscillations we later tried performing the above calculations using a modified version of the Tukey function (see eqns. (A4) and (A5) in the Appendix). The integrated intensity (at 290 K) corresponding to this new window function is also plotted in FIG 3 along with the same corresponding to the use of Tukey function. From this figure it is clearly visible that the

unwanted oscillations diminish considerably when we use the modified Tukey function. More interestingly, FIG. 4

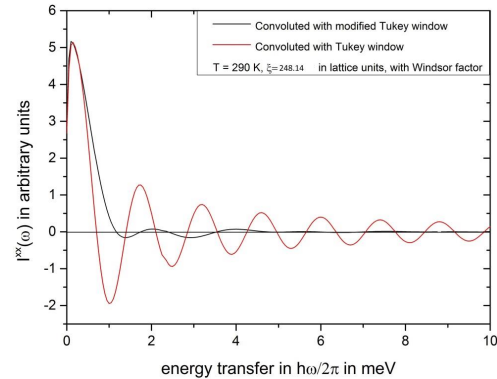


FIG. 3. The plot of convoluted in-plane integrated intensity $I_{conv}^{xx}(\omega)|_{SC}$ at 290 K. The red solid line corresponds to the $I_{conv}^{xx}(\omega)|_{SC}$ obtained by using the Tukey window function (see (A4)). The black solid line corresponds to the $I_{conv}^{xx}(\omega)|_{SC}$ obtained by using the modified Tukey window function (see (A5)).

indicates that at even higher temperature, viz., at around 375 K ($\approx 1.388 T_{BKT}$) both the Tukey function and the modified Tukey function lead to very similar results. The oscillations are totally absent in the theoretical plot of $I_{conv}^{xx}(\omega)|_{SC}$ vs. energy transfers corresponding to both the resolution functions. It is worthwhile to mention that the corresponding temperature $T=375$ K ($> T_2$) falls just outside the range $T_1 \leq T \leq T_2$ within which the BKT phenomenology remains valid. However, the use of such a modified Tukey function may wipe out some of the genuine and intrinsic fluctuations present in the anti-ferromagnetic systems in two dimensions. Hence, we make use of the Tukey function only for our purpose because it is very frequently used in the field of spectral analysis.

We further notice a slight shift in the position of the central peak. This is due to the inclusion of detailed balance condition. The important point here is that the shift is well within the resolution width 1.4 meV at the FWHM, and hence the peak is truly a central peak situated at $\hbar\omega = 0$.

Exactly the same results hold for $I_{conv}^{yy}(\omega)|_{SC}$ which is obvious from the symmetry argument. The normalization factor required for the quantitative comparison between the theoretical and the experimental results is estimated from the neutron count corresponding to the experimental results for La_2CuO_4 .

We now evaluate the out-of-plane integrated intensity $I_{conv}^{zz}(\omega)|_{SC}$ for the same set of temperatures as have been considered earlier for the evaluation of $I_{conv}^{xx}(\omega)|_{SC}$ (see FIG 5). The expression for the $I_{conv}^{xx}(\omega)$ is given

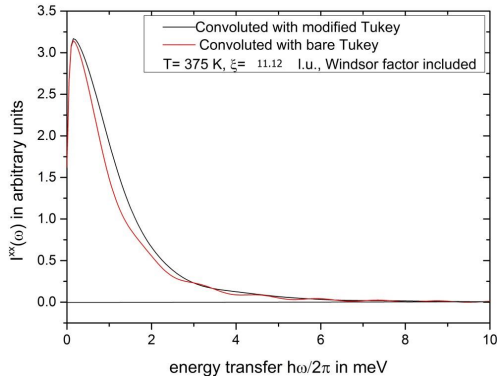


FIG. 4. The plot of convoluted in-plane integrated intensity $I_{conv}^{xx}(\omega)|_{SC}$ at 375 K. The red solid line corresponds to the $I_{conv}^{xx}(\omega)|_{SC}$ obtained by using the Tukey window function (see (A4)). The black solid line corresponds to the $I_{conv}^{xx}(\omega)|_{SC}$ obtained by using the modified Tukey window function (see (A5)).

by, eqn. (8) with $\alpha = z$, where the out-of-plane DSF, $S^{zz}(\mathbf{qD}, \omega)$ is given by eqn. (6). In this case we find

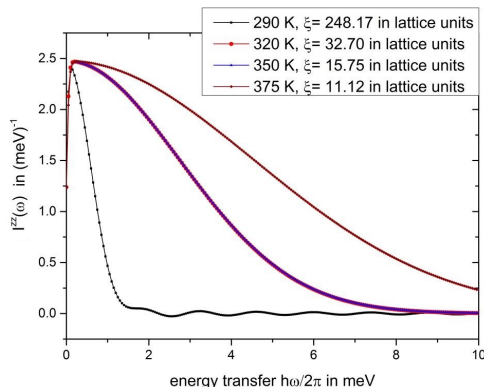


FIG. 5. The plot of convoluted out-of-plane integrated intensity $I_{conv}^{zz}(\omega)|_{SC}$ at four different temperatures, viz., 290 K, 320 K, 350 K and 375 K. The rms velocities at these temperatures are $\bar{u} = 0.00365 \frac{a}{t_{nat}}$, $0.0836 \frac{a}{t_{nat}}$, $0.085 \frac{a}{t_{nat}}$, $0.2323 \frac{a}{t_{nat}}$ respectively. The order of magnitude of the $I_{conv}^{zz}(\omega)|_{SC}$ at the above mentioned four different temperatures are 10^{-13} , 10^{-10} , 10^{-8} and 10^{-7} respectively.

that the out-of-plane integrated intensity oscillates only at lower temperatures near $T = T_{BKT}$. It is worth recalling here that the magnitude of the out-of-plane integrated intensity is proportional to the density n_v^f and the rms velocity \bar{u} of the free vortices/merons. Since

both density n_v^f and the rms velocity \bar{u} increases with increasing temperature the out-of-plane part of the spin-spin correlation (see eqns. (6) and (8)) acquire dominance (considerable magnitude) only at higher temperatures much above T_{BKT} .

Furthermore, the absolute magnitude of the integrated intensity $I_{conv}^{xx}(\omega)|_{SC}$ is higher (almost 10^7 times for the highest temperature considered here) than that of $I_{conv}^{zz}(\omega)|_{SC}$ at temperatures above T_{BKT} . This is so because, $I_{conv}^{zz}(\omega)|_{SC}$ is proportional to n_v^f and it increases with the increasing value of the rms velocity \bar{u} . The typical energy scales involved in the dynamics of mobile vortices/merons corresponding to the anti-ferromagnetic system La_2CuO_4 are such that n_v^f is very small (compared to the case of ferromagnet where the free vortex number density turns out to be appreciable [48]). For the present case of La_2CuO_4 at $T = 350K$, the numerical value for the density of free vortices comes out to be $n_v^f = 1.36 \times 10^{-4} a^{-2}$ and the same for the rms velocity comes out to be $\bar{u} = 9163 m/sec = 0.085 \frac{a}{t_{nat}}$, where $t_{nat} = \frac{2\hbar}{\sqrt{3}J}$ ($\approx 5 \times 10^{-15}$ sec) is the natural time scale for the system. In contrast, in the case of ferromagnetic system K_2CuF_4 the value of the density of free vortices was found to be $n_v^f = 1.009 \times 10^{-3} a^{-2}$ and that for the rms velocity was found to be $\bar{u} = 87.07 m/sec = 0.1352 \frac{a}{t_{nat}}$ at $T = 6.75K$, where $t_{nat} = 6.4 \times 10^{-13}$ sec is the natural time scale [48].

Interestingly enough, the unbound merons/vortices above T_{BKT} move much faster (with a rms velocity of $9163 m/sec$ at 350 K) than a typical Copper (Cu) atom whose rms velocity (generally considered to be the thermal velocity) is around $370.6 m/sec$ at 350 K.

The integrated intensities computed above correspond to the contributions only from the mobile vortices/merons. The experimental data whereas, contain contributions from both the mobile vortices/merons and fragile “spin wave like” modes. This spin wave like modes are damped and largely decaying above the Néel temperature. The extraction of the mobile vortex contribution from the experimental data is crucial for a more accurate comparison between the theoretical results and the experimental data and to do this one has to subtract the contributions from the above mentioned fragile “spin wave like” modes from the experimental data. It is worth recalling that in the case of ferromagnetic system, the fragile mode contributions have been subtracted by assuming the fragile mode contributions above T_c to be the same as the usual spin wave contributions below T_c . This assumption is however valid if and only if the temperature under consideration is in the near vicinity of the Curie temperature (T_c) of the system [48].

In the present case corresponding to the anti-ferromagnetic system La_2CuO_4 , the situation is somewhat different from the case of ferromagnetic systems in the sense that the temperatures dealt with are far above the Néel temperature T_N . Hence the above mentioned procedure, which was followed for the ferromagnetic sys-

tems to subtract the fragile mode contributions, is not valid.

Moreover at any finite temperature above T_{BKT} , it is to be kept in mind that not all vortices/merons are freely moving and that bound vortex-anti-vortex pair density remains finite. Hence, one has to estimate further the contribution from these bound vortex-anti-vortex pairs at different temperatures and subtract them from the experimental data. To estimate the bound vortex contribution we have tried to apply the same methodology that has been outlined and used earlier for the ferromagnetic system [48]. However, unlike the case of ferromagnet in this case the methodology leads to an unphysical behaviour viz., the vanishing of the out-of-plane DSF (see eqn. (6)) in the limit $\bar{u} \rightarrow 0$. Hence the estimation of the bound vortex contribution has not been carried out here.

The above calculations for the components of integrated intensities enable us to estimate theoretically the total integrated intensity using (9). In FIGs. 6 and

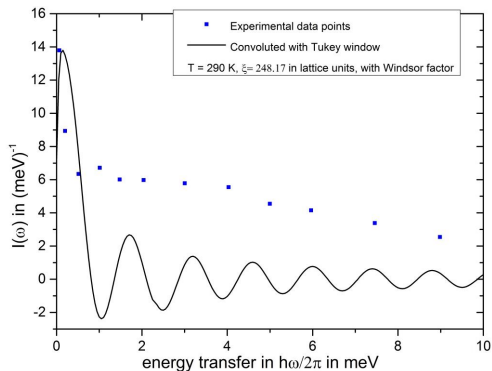


FIG. 6. The plot of convoluted total integrated intensity $I_{conv}(\omega)|_{SC}$ at 290 K. The red solid line corresponds to the $I_{conv}(\omega)|_{SC}$ obtained theoretically by using the Tukey window function (see (A4)). The dots are the experimental data.

7 the total intensity $I_{conv}(\omega)|_{SC}$ has been compared to the experimental data at two different temperatures, viz., 290K and 350K respectively. The contributions from the fragile “spin-wave-like” modes can not be filtered out for the reasons stated earlier. It is clear from FIG. 6 that the total intensity $I_{conv}(\omega)|_{SC}$ also oscillates vigorously at both the temperatures, when convoluted with the Tukey function. Besides, the theoretical results show negative values for $I_{conv}(\omega)|_{SC}$ with both the resolution functions! Moreover, the magnitude of the total intensity $I_{conv}(\omega)|_{SC}$, obtained theoretically at finite energy transfers, is very far from the corresponding values obtained in the experiment.

The inclusion of quantum mechanical detailed balance factor in our semi-classical like treatment has again caused a shift in the position of the central peak of the in-

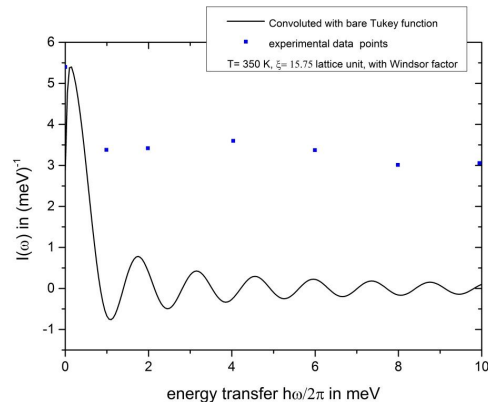


FIG. 7. The plot of convoluted total integrated intensity $I_{conv}(\omega)|_{SC}$ at 350 K. The red solid line corresponds to the $I_{conv}(\omega)|_{SC}$ obtained theoretically by using the Tukey window function (see eqn. (A4)). The dots are the experimental data.

tegrated total intensity at both the temperatures. However, this shift is well within the resolution width and therefore it is a genuine central peak at zero energy transfer.

It is worthwhile to mention that all the above results based on dilute vortex/meron gas phenomenology hold for unbound anti-vortices/anti-merons too.

Let us further calculate the zeroth moment of the semi-classical dynamical structure function (DSF) $S_{SC}^{conv}(\mathbf{q}, \omega)$ (or simply the moment) using the following formula [15],

$$\int_{\text{first B.Z.}} \left(\frac{a}{2\pi}\right)^2 d^2\mathbf{q} \int_{-\infty}^{\infty} d\omega S_{conv}^{SC}(\mathbf{q}, \omega) = S(S+1),$$

$$\text{or } \int d\omega I_{conv}^{SC}(\omega) = S(S+1), \quad (14)$$

where $I_{conv}^{SC}(\omega)$ is given by equation (10) and in obtaining the same the integration over the wave vector space in equation (8) is performed over the first Brillouin zone (B.Z.) with contributions from both vortices and anti-vortices being summed; S is the value of the spin corresponding to the system under consideration and in our case it is $S = 1/2$. The above equation signifies that if the spin dynamics is entirely captured by the DSF, the value of the zeroth moment must be $S(S+1)$.

T	$\frac{T}{T_{BKT}}$	moment in the unit of $S(S+1)$ *
290 K	1.074	0.0400
320 K	1.185	0.2412
350 K	1.296	0.3583
375 K	1.388	0.3770

TABLE II. *The zeroth moment of the semi-classical dynamical structure function corresponding to the dynamics of mobile vortices and anti-vortices* (* corresponding to the use of Tukey function.)

The values of the moment of the semi-classical convoluted DSF corresponding to the use of Tukey function at four different temperatures are tabulated in TABLE II. At 290K i.e. around $1.074T_{BKT}$, the combined dynamics of mobile vortices and anti-vortices capture only about 4% of the entire spin dynamics of the system. However, at higher temperatures around $1.296T_{BKT}$, the combined dynamics of mobile vortices and anti-vortices capture more than 35% of the entire spin dynamics of the system. This happens because at lower temperatures near T_{BKT} , the number of freely mobile vortices and anti-vortices are not large enough to capture the whole spin dynamics and the presence of fragile or damped spin waves (or single magnons and multi-magnon like modes) makes important enough contribution to the spin dynamics. At higher temperatures however, more topological excitations become free and drive a large portion of the spin dynamics of the system. At this point, it is worth mentioning that for quantum ferromagnetic systems on two dimensional square lattice it has been shown that the formation of topological excitations of vortex/meron types from the fragile magnons and multi-magnon composites is quite plausible [62]. Moreover, some of the collective modes (i.e. magnon and multi-magnon modes) are expected to stay intact with their damped nature and thus can provide a significant contribution to the spin dynamics. In analogy with the three dimensional systems where above the Curie temperature (T_c) the magnon-like collective excitations become fragile and damped, for pure two dimensional systems (where $T_c = 0$) the collective excitations become fragile at any finite temperature [56, 62–67]. This process is expected to be operative too in the anti-ferromagnetic systems on pure two-dimensional lattices.

To summarize, we find vigorous oscillations in the convoluted in-plane integrated intensity when the Tukey window is used. These oscillations vanish only at higher temperatures which are outside the regime of validity of the BKT phenomenology. The use of a modified or refined Tukey function substantially removes the unwanted oscillations in the convoluted in-plane integrated intensity $I_{conv}^{xx}(\omega)|_{SC}$. Strikingly enough, at $T = 350$ K ($1.296 T_{BKT}$), we still find negative values of $I_{conv}^{xx}(\omega)|_{SC}$ even using the modified Tukey window function. However, outside the temperature regime where the BKT phenomenology is valid, computations with both the window functions give very similar results for $I_{conv}^{xx}(\omega)|_{SC}$. The

possible explanation for this is that at higher temperatures the quantum effects are less prominent even for $S = \frac{1}{2}$ anti-ferromagnet. Therefore, the modified Tukey window may actually be suppressing quantum fluctuation as well quite efficiently. The out-of-plane integrated intensities $I_{conv}^{zz}(\omega)|_{SC}$ (computed at different temperatures) are found to be sensitive to the choice of window function only at temperatures which are not very far from T_{BKT} (around $1.074 T_{BKT}$). Furthermore, it contributes negligibly to the total integrated intensity $I_{conv}(\omega)|_{SC}$ and hence the nature of the convoluted total integrated intensities at different temperatures turns out to be quite similar to that of the convoluted in-plane integrated intensities. However, the detailed quantitative comparison between the theoretical results and the experimental results corresponding to the total integrated intensities $I_{conv}(\omega)|_{SC}$ reveals that even though our “semi-classical like” theory is able to predict the occurrence of the central peak, the magnitudes of the $I_{conv}(\omega)|_{SC}$ for finite values of energy transfer, obtained from theoretical analysis, differ by a huge factor from the corresponding experimental values. Moreover, apart from the spin dynamics induced by the mobile topological excitations, the fragile magnons and multi-magnon modes are quite likely to make important contribution towards this dynamics.

IV. CONCLUSIONS AND DISCUSSIONS

It is a well known fundamental fact that the spin-dynamical structure function (DSF) and hence the integrated intensity corresponding to all real magnetic systems must be positive definite [15, 52, 53]. Our detailed calculations and analysis however, brings out an important fact that for quasi-two dimensional low-spin anti-ferromagnetic systems, the semi-classical treatment of ideal gas of mobile vortices/merons (anti-vortices/anti-merons) leads to negative values of total integrated intensities even in the low energy regime, when convoluted with commonly used resolution functions. Similar results were obtained for $S = 1/2$ layered ferromagnets [48]. Such a behaviour is purely unphysical. These facts highlight the inapplicability of the semi-classical vortex/meron gas phenomenology to the quasi-two dimensional (or rather layered) low-spin anti-ferromagnetic systems very strongly and necessitates the demand for a full quantum treatment of the problem. Let us further point out that the value of $\hbar\omega$ at which the onset of such unphysical behaviour occurs depends on the value of the spin (S). It has been shown in the case of ferromagnetic systems that the regime over which this unphysical behaviour persists, shrinks as the value of S increases [48]. Similar behaviour is expected in the anti-ferromagnetic systems also. This may be verified from the studies on the compounds based on Gd and Mn.

To the best of our knowledge there are no materials based on Gd^{3+} (spin $\frac{7}{2}$) which can be modelled

by 2D XXZ Hamiltonian (XY anisotropic Heisenberg Hamiltonian). However, some high spin magnetic systems such as Rb_2MnF_4 , Cs_2MnCl_4 , both being spin $\frac{5}{2}$ compound, turn out to be a layered Heisenberg AFM with Ising like anisotropy [68]. In this case the BKT scenario does not hold. On the other hand applicability of the Berezinskii-Kosterlitz-Thouless scenario on triangular chromium-lattice AFM with $S = 3/2$ has been investigated only via electron spin resonance (ESR) technique [69]. In this regard it is worthwhile to mention that the spin dynamics in a Mn^{2+} based spin $\frac{5}{2}$ Honeycomb lattice anti-ferromagnetic material $MnP\bar{S}_3$ has been investigated via INS experiment [70]. The critical properties of this material have been reported to be well described by 2D XXZ Hamiltonian (anisotropy parameter being equal to 0.998) only in the low \mathbf{q}^* regime. We have performed an initial study towards the calculation of DSF for $MnP\bar{S}_3$ using our model and this reveals that the semi-classical BKT phenomenology is producing a much better agreement with the experimental data corresponding to this material at 85 K [71]. The agreement is only in terms of peak position and the range of energy transfer over which we get acceptable (positive) values of DSF. This range encompasses a considerable portion of the range of experimental interest. Regardless of this, the possibility of meron dynamics in this material can not be adequately described with the available INS data. To be very specific, the available INS data is at 85 K whereas, the critical dynamics is completely confined within the plane (and therefore, corresponding to a perfect 2D system) only above 105 K [70]. Furthermore, in this material $T_N > T_{BKT}$ and therefore, above T_{BKT} and below T_N well defined magnon modes persist which is in contrast to the case corresponding to La_2CuO_4 .

Presently it seems that there is a scarcity of INS data in search for the spin dynamics induced by topological excitations corresponding to XY anisotropic (easy plane anisotropic, i.e., XXZ type) layered Heisenberg anti-ferromagnetic materials having higher values of spin. More INS experiments on this type of materials (in a suitable temperature range) would be quite interesting in view of the fact that it would serve as a good testing ground for the applicability of such a conventional semi-classical theory of spin dynamics induced by topological excitations.

It is also very important to emphasize the fact that in our calculational analysis the structure of the classical vortex/meron has been built in the background of the Néel state (see (2) of section II). Since the Néel state is not an exact ground state for the two-dimensional quantum anti-ferromagnetic spin systems, such a choice further adds to the reasons for the above mentioned unphysical behaviour.

Keeping aside the occurrences of unphysical negative values of the integrated intensities obtained from the conventional semi-classical-like theory, the results agree with those from the experiment quite well in terms of the existence of the central peak. However, this peak is

a genuine one only in the sense that it occurs well within the experimental resolution width.

Moreover, quantitative disagreement, at the finite values of energy transfer, between the magnitudes of the theoretically calculated integrated intensities and those obtained experimentally strongly indicates that formation of the topological excitations from fragile collective modes and interactions between them can play a very crucial role in the spin dynamics. The values of the moment at different temperatures further strongly suggest the same. Therefore, the interplay between the fragile single magnons or multi-magnon composites and the topological excitation is very crucial for the proper understanding of the dynamics induced by free movement of the latter in the quasi-two-dimensional low-spin anti-ferromagnetic systems. This further takes care of the fragile magnon contributions to the total integrated intensities as well which has not been filtered out from the experimental data (for the reasons stated earlier in the section III). In addition, the severe inadequacy of the semi-classical treatment in the case of quantum anti-ferromagnet may also contribute to such quantitative disagreement for the integrated intensities.

Our investigations presented in this communication establish the fact that a complete quantum treatment is essential to describe the detailed features of the dynamics of mobile topological excitations corresponding to the quasi-two-dimensional low-spin anti-ferromagnetic systems, by taking into consideration the vortex/meron-fragile magnon interactions as well. This further brings out the possibility of a characterization of different layered materials into two classes, viz., conventional BKT-like and quantum corrected BKT-like. Moreover, since the Néel state is not an exact ground state for the two-dimensional quantum spin systems, the construction of the quantum vortices/merons in the complete quantum treatment has to be supplemented with proper choice of the ground state too. However, calculation of the dynamical structure function in a completely quantum mechanical framework is highly non-trivial. Earlier attempts towards this goal could not explain the occurrence of the “central peak” in the DSF obtained in the INS experiment performed on several quasi-two-dimensional materials [31, 72–74]. Quite recently a theoretical framework had been developed based on the spin coherent state path integral formalism to describe the topological properties of static vortices and anti-vortices [75–80]. An extension of this framework to the case of mobile spin vortices/merons (and anti-vortices/anti-merons) is crucial for quantum mechanical calculations of the DSF and the integrated intensity as well. Insights from Quantum Monte Carlo calculations may be quite useful in this endeavour [81]. This would be taken up in future. More importantly the short range 2D anti-ferromagnetic spin-spin correlation persists even in the superconducting phase of the underdoped cuprates. This has been investigated and verified via INS experiments [82]. Moreover it has been shown very recently that the

spin fluctuations in the AFM quantum critical region of the Fe based superconductors and some heavy fermion compounds can be modelled by dissipative quantum XY model and hence, the static and dynamics of topological excitations are the key factors for 2D spin-spin correlations [84, 85]. Therefore, this investigation of the dynamics of the BKT vortices/merons may also contribute substantially to the microscopic understanding of lightly doped anti-ferromagnetic cuprates and the above mentioned other systems as well [47, 83–85].

Acknowledgements:

One of the authors (SS) acknowledges the financial support through Senior Research Fellowship (09/575 (0089)/2010 EMR–1) provided by Council of Scientific and Industrial Research (CSIR), Govt. of India.

Author contribution statement:

All authors have contributed equally to this communication.

Appendix A: The Tukey and the modified Tukey function

The most general form for the Tukey function is given by,

$$R(t) = \begin{cases} \frac{1}{2}[1 + \cos(\frac{\pi}{1-\alpha}\frac{2t}{t_m} + \frac{\pi}{1-\alpha} - \pi)], & \text{for } \frac{-t_m}{2} \leq t < \frac{-t_m}{2}\alpha \\ 1, & \text{for } \frac{-t_m}{2}\alpha \leq t \leq \frac{t_m}{2} \\ \frac{1}{2}[1 + \cos(\frac{\pi}{1-\alpha}\frac{2t}{t_m} - \frac{\pi}{1-\alpha} + \pi)], & \text{for } \frac{t_m}{2}\alpha < t \leq \frac{t_m}{2} \\ 0, & \text{otherwise,} \end{cases} \quad (\text{A1})$$

where α is called the tapering parameter [60, 61].

The Tukey function we have used in this communication is corresponding to $\alpha = 0$. In this case the above general expression takes the form, The Tukey function is given by,

$$R(t) = \begin{cases} \frac{1}{2}[1 + \cos(\frac{2\pi t}{t_m})], & \text{for } |t| \leq \frac{t_m}{2} \\ 0, & \text{otherwise,} \end{cases} \quad (\text{A2})$$

which is corresponding to zero tapering [60, 61]. The Fourier transform of the above Tukey function (corresponding to zero tapering) is given by,

$$\tilde{R}(\omega) = \frac{1}{4\pi} \sin(\frac{\omega t_m}{2}) (\frac{2}{\omega} - \frac{1}{\omega + \frac{2\pi}{t_m}} - \frac{1}{\omega - \frac{2\pi}{t_m}}). \quad (\text{A3})$$

The full width at half maximum (FWHM) for the above function is given by $\Delta_{FWHM}^{(T)} = \frac{4\pi}{t_m}$, expressed in the units of energy, where the superscript T signifies the

Tukey function [63]. To find the value of t_m the above expression for $\Delta_{FWHM}^{(T)}$ is equated to the value of the resolution width, 1.4 meV at FWHM, specified in the experimental observations corresponding to La_2CuO_4 .

The modified Tukey (MT) function we have used in our analysis is corresponding to 50% tapering and it is given by [60, 61],

$$\mathcal{R}(t) = \begin{cases} \frac{1}{2}[1 - \cos(\frac{4\pi t}{t_m})], & \text{for } \frac{-t_m}{2} \leq t \leq \frac{-t_m}{4} \\ 1, & \text{for } \frac{-t_m}{4} \leq t \leq \frac{t_m}{4} \\ \frac{1}{2}[1 - \cos(\frac{4\pi t}{t_m})], & \text{for } \frac{t_m}{4} \leq t \leq \frac{t_m}{2} \\ 0, & \text{otherwise.} \end{cases} \quad (\text{A4})$$

Fourier transform of the above modified Tukey function is given by,

$$\tilde{\mathcal{R}}(\omega) = \frac{1}{4\pi} [\sin(\frac{\omega t_m}{2}) + \sin(\frac{\omega t_m}{4})] (\frac{2}{\omega} - \frac{1}{\omega + \frac{4\pi}{t_m}} - \frac{1}{\omega - \frac{4\pi}{t_m}}). \quad (\text{A5})$$

The full width at half maximum corresponding to the above function $\tilde{\mathcal{R}}(\omega)$ can be found out to be $\Delta_{FWHM}^{(MT)} \approx$

$\frac{3.2\pi}{t_m}$, expressed in the units of energy. In this case, to find the value of t_m we have equated $\Delta_{FWHM}^{(MT)}$ to the value of the resolution width specified in the experiment.

-
- [1] H. Bethe, Z. Physik **71**, 205(1931).
 [2] Y. Endoh, et.al., Phys. Rev. Lett., **32**, 170(1974).
 [3] A. A. Katanin, V. Yu Irkhin, Physcis– Uspekhi, **50**(6), 613– 635(2007) and references therein.
 [4] J. Prokop et. al., Phys. Rev. Lett **102** 177206(2009).
 [5] M. Cwik et. al., Phys. Rev. Lett **102** 057201(2009).
 [6] F. Demmel and T. Chatterji, Phys. Rev. B **76** 212402(2007).
 [7] T. Chatterji et. al., Phys. Rev. B **76** 144406(2007).
 [8] F. Weber et. al., Phys. Rev. Lett **107** 207202(2011).
 [9] S. M. Yusuf et. al., Phys. Rev. B **84** 064407(2011).
 [10] H. Ulbrich et. al., Phys. Rev. B **84** 094453(2011).
 [11] H. J. Lewtas et. al., Phys. Rev. B **82** 184420(2010).
 [12] L. Braicovich et. al., Phys. Rev. B **81** 174533(2010).
 [13] Ranjan Chaudhury, *Spin dynamics of quantum spin models in layered systems– signature of Kosterlitz– Thouless scenario?* – presented at ULT 2011 (August 19– 22, 2011), held at KAIST, Daejeon, South Korea.
 [14] Yong– il Shin, *Creation of 2D Skyrmions in spin– 1 polar Bose– Einstein Condensates* – presented at ULT 2011 (August 19– 22, 2011), held at KAIST, Daejeon, South Korea.
 [15] S. W. Lovesey, *Theory of Neutron Scattering from Condensed Matter*(Oxford– Clarendon Press) 1986, Vol. 2, Chap: 8, 9.
 [16] I. U. Heilmann, et.al., Phys. Rev. B., **24**, 3939(1981).
 [17] J. K. Kjems and M. Steiner, Phys. Rev. Lett., **41**, 1137(1978).
 [18] M. Steiner, K. Kakurai, W. Knop, R. Pynn, J.K. Kjems, Solid State Comm., **41**, Pages 329-332 (1982).
 [19] L.V. Yakushevich, Journal of Biological Physics **24**, 131–139 (1999).
 [20] G. Reiter, Phys. Rev. Lett., **46**, 202(1981).
 [21] K. Hirakawa, H. Yoshizawa, K. Ubukoshi, J. Phys. Soc. Jpn., **51**, 2151(1982).
 [22] K. Hirakawa, et.al., J. Phys. Soc. Jpn. Part-2, **52**, 4220(1983).
 [23] M. T. Hutchings, J. Als-Nielsen, P. A. Lindgard and P. J. Walker, J. Phys. C: Solid State Phys., **14**, 5327–5345(1981).
 [24] M. T. Hutchings, P. Day, E. Janke and R. Pynn, J. Magn. Mater. **54-57**, 673(1986).
 [25] L. K. Alexander, N. Büttgen, R. Nath, A. V. Mahajan, and A. Loidl, Phys. Rev. B **76**, 064429 (2007).
 [26] D. G. Wiesler, et.al., Physica **136B**, 22-24(1986).
 [27] P. Steffens et.al., Phys. Rev. B., **83**, 054429(2011).
 [28] L. Capogna et. al.; Phys. Rev. B., **67**, 012504(2003).
 [29] G. Castilla, S. Chakravarty, and V. J. Emery, Phys. Rev. Lett. **75**, 1823 (1995).
 [30] Y. Endoh, et.al. Phys. Rev. B **37**, 7443 (1988).
 [31] K. Yamada et.al., Phys. Rev. B., **40**, 4557(1989).
 [32] L. Berger, Y. Labaye, M. Tamine, and J. M. D. Coey, Phys. Rev. B., **77**, 104431, (2008).
 [33] A. Wachowiak, J. Wiebe, M. Bode, O. Pietzsch, M. Morgenstern and R. Wiesendanger, Science, **298**, 577 (2002).
 [34] R. P. Cowburn, D. K. Koltsov, A. O. Adeyeye, M. E. Welland, and D. M. Tricker, Phys. Rev. Lett, **83**, 1042, (1999).
 [35] B. Van Waeyenberge, Nature, **444**, 461 (2006).
 [36] H. Hauser, J. Hochreiter, G. Stangl, R. Chabicovsky, M. Janiba and K. Riedling,, J. Magn. Mater, **215**, 788 (2000).
 [37] J. McCord, J. Westwood, IEEE Trans. Magn., **37**, 1755, (2005).
 [38] J. M. Kosterlitz and D. J. Thouless: J. Phys. C **6** 1181(1973).
 [39] V. L. Berezinskii, Sov. Phys. JETP **32**, 493(1970); Sov. Phys. JETP **34**, 610(1972).
 [40] J. V. José, ed., 40 Years of Berezinskii–Kosterlitz–Thouless Theory, World Scientific (2013), Chap. 1.
 [41] D. L. Huber, Phys. Lett. **68A**, 125(1978); Phys. Rev. B. **26**, 3758(1982).
 [42] F. G. Mertens, A. R. Bishop, G. M. Wysin and C. Kawabata, Phys. Rev. Lett, **59**, 117(1987); Phys. Rev. B. **39**, 591(1989).
 [43] M. E. Gouvêa, G. M. Wysin, A. R. Bishop, F. G. Mertens, Phys. Rev. B, **39**, 11840(1989).
 [44] A. R. Völkel, G. M. Wysin, A. R. Bishop and F. G. Mertens, Phys. Rev. B. **44**, 10066(1991).
 [45] G. M. Wysin and A. R. Bishop, Phys. Rev. B., **42**, 810 (1990).
 [46] P. W. Anderson, S. John, G. Baskaran, B. Doucot, and S. D. Liang, Princeton University Preprint, 1988.
 [47] R. Chaudhury, Indian J Phys, **66A**, 159 (1992)
 [48] S. Sarkar, S. K. Paul and R. Chaudhury, Eur. Phys. J. B, **85**, 380 (2012).
 [49] K. Harada and N. Kawashima, J. Phys. Soc. Jpn **67**, 2768 (1988).
 [50] M. Holschneider, S. Wessel, and W. Selke, Phys. Rev B **75**, 224417 (2007).
 [51] H. J. Mikeska, J. Phys. C: Solid St. Phys., **13**, 2913 (1980).
 [52] G. Shirane, S. M. Shapiro, and J. M. Tranquada, *Neutron Scattering with a Triple-Axis Spectrometer, Basic Techniques*, (Cambridge University Press) 2004, Chaps. : 1, 4.
 [53] F. Hippert, E. Geissler, Jean. L. Hodeau, E. L-Berna and Jean-R Regnard, *Neutron and X-Ray Spectroscopy, Grenoble Sciences*, Springer 2006, Chap: 11.
 [54] M. Takahashi, J. Phys. Soc. Jpn., **52**, 3592(1983).
 [55] R. C. Tolman, *The Principles of Statistical Mechanics*, (Dover Publication), 1976, Chap. XII .
 [56] M. T. Evans and C. G. Windsor, J. Phys. C., **6**, 495 (1973).
 [57] C. G. Windsor and J. Locke-Wheaton, J. Phys. C., **9**, 2749 (1973).
 [58] T. Thio, et.al, Phys. Rev. B., **38**, 905 (1988).
 [59] N. D. Mermin and H. Wagner, Phys. Rev. Letts. **17**, 1133 (1966); erratum: Phys. Rev. Letts. **17**, 1307 (1966).
 [60] F. J. Harris, Proceedings of The IEEE, **66**, 51(1978).

- [61] G. M. Jenkins and D. G. Watts, *Spectral Analysis and Its Applications*, (Holden-Day), 1968, Chap:6.
- [62] S. Sarkar, R. Chaudhury and S. K. Paul, Int. J. Mod. Phys. B, **29**, 1550209-1 - 1550209-22 (2015).
- [63] R. Chaudhury and B. S. Shastry, Phys. Rev. B. **37**, 5216(1988).
- [64] P. Böni and G. Shirane, Phys. Rev.B **33**, 3012 (1986).
- [65] R. Chaudhury, F. Demmel and T. Chatterji, arXiv:1104.4197v1.
- [66] R. Chaudhury, J. Magn. Magn. Mater. **307**, 99 (2006).
- [67] T. Chatterji, F. Demmel and R. Chaudhury, Physica B **385-386**, 428 (2006).
- [68] T. Huberman, et.al., Phys. Rev. B, **72**, 014413 (2005).
- [69] M. Hemmida, et.al., Phys. Rev. B, **80**, 054406 (2009).
- [70] A. R. Wildes, H. M. Rønnow, B. Roessli, M. J. Harris and, K. W. Godfrey,
- [71] Andrew R. Wildes, personal communication.
- [72] S. Chakravarty, B. Halperin and D. Nelson, Phys. Rev. B, **39**, 2344 (1989).
- [73] D.P. Arovas and A. Auerbach, Phys. Rev. B, **38**, 316-332, (1988).
- [74] L. P. Regnault and J. Rossat-Mignod, "Phase transitions in quasi-two-dimensional planar magnets" in Magnetic properties of layered transition metal compounds, Ed. by L. J. De Jongh, Kluwer Academic Publishers (1990).
- [75] F. D. M. Haldane, Phys. Rev. Lett., **50**, 1153(1983).
- [76] E. Fradkin, M. Stone, Phys. Rev. B., **38**, 7215, (1988); E. Fradkin, *Field Theories of Condensed Matter Systems*, (Addison-Wesley, CA, 1991).
- [77] F. D. M. Halden, Phys. Rev. Lett, **61**, 1029(1988).
- [78] R. Chaudhury and S. K. Paul, Phys. Rev. B., **60**, 6234(1999).
- [79] R. Chaudhury and S. K. Paul, Mod. Phys. Lett. B, **16**, 251-259(2002).
- [80] R. Chaudhury and S. K. Paul, Eur. Phys. J. B, **76**, 391-398(2010).
- [81] E. Vitali, M. Rossi, L. Reatto and, D. E. Galli, Phys. Rev. B, **82**, 174510 (2010).
- [82] M. A. Kastner, R. J. Birgeneau, G. Shirane and, Y. Endoh, Rev. Mod. Phys, **70**, No. 3, (1998).
- [83] Y. H. Chen, F. Wilczek, E. Witten and B. I. Halperin, Int. J. Mod. Phys. B, **3**, 1001 (1989).
- [84] C. M. Varma, Phys. Rev. Lett **115**, 186405 (2015).
- [85] C. M. Varma, Lijun Zhu, and Almut Schröder, Phys. Rev. B **92**, 155150 (2015).